THE UNIVERSITY
of EDINBURGH

Regulation of neural stem cell and glioblastoma stem cell quiescence by FOXG1 and Wnt/beta-catenin

Faye Louise Robertson

Supervisor: Professor Steven M Pollard

A thesis submitted for the degree of Doctor of Philosophy

MRC Centre for Regenerative Medicine
and Edinburgh Cancer Research UK Centre

University of Edinburgh

2020

Table of Contents

Abstract ..... *vi*

Lay Summary ..... *vii*

Acknowledgements ..... *viii*

Declaration of Originality ..... *ix*

Copyright Declaration ..... *ix*

List of abbreviations ..... *x*

List of Figures ..... *xiv*

Chapter 1: Introduction *1*

1.1 Overview **1**

1.2 Neural stem cell biology and quiescence **1**

1.2.1 Neural stem cells in the developing embryo, foetus and adult brain 1

1.2.2 Neural stem cells exist in the subventricular zone and resemble astrocytes 4

1.2.3 Adult NSCs exists in a variety of dormant, quiescent and proliferative states 7

1.2.4 Quiescence is an active state 11

1.2.5 BMP4 exposure induces a state of astrocytic differentiation or quiescence 12

1.2.6 NS cells can be isolated and cultured in adherent monolayer 14

1.3 The biology of glioblastoma **17**

1.3.1 Glioma is the most common intrinsic primary brain tumour 17

1.3.2 Glioma can be classified using molecular and histopathological features 17

1.3.3 GBM has a poor prognosis despite multi-modal treatment 19

1.3.4 GBM cells show genome instability and extensive mutation, particularly in RTK/PI3K, CDK4/RB and P53 pathways 22

1.3.5 GBM is a disease of stem cells 23

1.3.6 GBM stem cells have a neurodevelopmental transcriptional identity and are resistant to treatment 25

1.3.7 GBM stem cells cultured in adherent monolayer provide a tractable reductionist model to explore exit from quiescence 26

1.3.8 GBM stem cell quiescence is an important clinical problem 29

1.3.9 GBM stem cells demonstrate a spectrum of response to BMP4 31

1.4 FOXG1 ..... **33**

1.4.1 FOXG1 is a member of the Forkhead Box (Fox) superfamily of transcription factors 33

1.4.2 FOXG1 is overexpressed in GBM 36

1.4.3 FOXG1 overexpression has a role in 'de-differentiation', or activation, of BMP4-induced astrocytes/quiescent NSCs 39

1.4.4 Knockdown or knockout of FOXG1 reduces/abolishes tumorigenicity in human xenograft models of GBM 39

1.5 Wnt signaling **40**

1.5.1 The Wnt signaling pathway is highly conserved and has roles in diverse cell processes, particularly during development 40

1.5.2 Wnt signaling is active in the adult SVZ 44

1.5.3 Wnt signaling is implicated in cancer 44

1.5.4 Wnt signaling is active in GBM 45

1.5.5 FOXG1 binds TLEs, co-repressors of Tcf/Lef 48

1.6 Aims and hypotheses **49**

Chapter 2 ..... *51*

Methods **51**

2.1 Cell culture **51**
2.1.1 Self-renewal media 51
2.1.2 BMP4 media and BMP/FGF2 media for quiescence assays 51
2.1.3 Freezing media 51
2.1.4 Growth curves 52

2.2 Immunocytochemistry **52**

2.3 Western Immunoblotting **52**

2.4 Antibodies used **53**
2.4.1 Primary Antibodies 53
2.4.2 Secondary Antibodies 55

2.5 Colony forming assays **55**

2.6 EdU incorporation assays **56**

2.7 Taqman qRT-PCR **56**

2.8 Derivation of stable transgenic cell lines **58**
2.8.1 Cell lines used and generated in this thesis 58
2.8.2 Plasmid Preparation 59
2.8.3 Design and construction of CRISPR sgRNAs and PiggyBac plasmids for generation of NPE lines (by Ester Gangoso). 59
2.8.4 Cell transfection 61
2.8.5 Drug selection and clonal expansion 61
2.8.6 Gateway cloning 64
2.8.7 Specifics of creation of the inducible beta-catenin cell line 66
2.8.8 Specifics of creation of the Tcf/lef reporter cell line 68

2.9 Cell-based phenotypic screening **69**

2.10 RNAScope **69**

2.11 RPPA analysis **69**

2.12 Nanostring analysis **70**

2.13 Topflash assay **70**

2.14 TUNEL assay **71**

2.15 Flow cytometry **72**

2.16 Radiation experiments **72**

2.17 Mouse experiments **72**
2.17.1 Care of mice and transplantation 72
2.17.2 Administration of Dox and Tamoxifen 73
2.17.3 Mouse brain fixation, Histopathology and Immunohistochemistry 74
2.17.4 Generation of tumour-derived cell lines 74

2.18 Software and statistical analysis **75**

Chapter 3 ..... *76*

A cell-based phenotypic small molecule screen identifies a synergy between GSK3 inhibitors and FOXG1 overexpression in driving neural stem cell cell-cycle re-entry .. **76**

3.1 Introduction **76**

3.2 Optimization of phenotypic screening assay **78**

3.3 Phenotypic screening **82**
3.3.1 A phenotypic screen of stem cell pathway associated pharmacological agents identifies BIO synergising with FOXG1/SOX2 overexpression to trigger cell cycle re-entry 82
3.3.2 An independent GSK3 inhibitor, Chiron, phenocopies the BIO response 87
3.3.3 The promotion of cell cycle re-entry by BIO is seen in NSCs with FOXG1 overexpression alone 88
3.4 An additional assay, modelling NS quiescence, yields similar results **93**
3.5 The dox+chiron synergy depends on the presence of both at early time points but FOXG1 overexpression prevents deep quiescence **96**
3.5.1 The dox+chiron synergy depends on the presence of both at early time points 96
3.5.2 FOXG1 overexpression, as seen in human GBM, prevents deep quiescence 97
3.6 Conclusions **100**
Chapter 4 ..... ***101***
Canonical Wnt signaling cooperates with FOXG1 to drive exit from quiescence in NSCs **101**
4.1 Introduction **101**
4.2 Wnt3a can replace chiron in synergising with FOXG1 ..... **102**
4.3 Wnt inhibitors abrogate the synergy between GSK3i and elevated FOXG1 ..... **104**
4.4 Induction of beta-catenin confirms cooperation with FOXG1 in driving exit from NSC quiescence **108**
4.4.1 A tamoxifen-inducible constitutively active beta-catenin cell line shows that the synergy is effected by beta-catenin 108
4.4.2 Beta-catenin acts cell-autonomously to drive exit from quiescence 113
4.5 Elevated FOXG1 in qNSCs primes Wnt target genes for efficient reactivation and cell cycle re-entry **115**
4.5.1 Tcf/lef transcription is activated by FOXG1 upregulation 115
4.5.2 Reverse phase protein array reveals upregulation of Wnt target genes by FOXG1 and further upregulation by FOXG1+GSK3i 118
4.5.3 c-myc is a potentially important downstream target of the FOXG1/GSK3i synergy 121
4.5.4 Nanostring analysis suggests that FOXG1 may be activating Wnt target genes and repressing Wnt inhibitors 124
4.6 Conclusions and putative mechanisms of the FOXG1/Wnt synergy **127**
Chapter 5 ..... ***130***
Relevance of the FOXG1/Wnt synergy to in vivo and human cell line models **130**
5.1 Introduction **130**
5.2 RNAScope in human GBM samples confirms co-localisation of FOXG1 and beta-catenin **131**
5.3 FOXG1 overexpression and Wnt signaling drive accelerated relapse in a mouse model of GBM **134**
5.3.1 A cell line lacking key tumour suppressor genes and expressing a key oncogene was created from the F6BC1 line 134
5.3.2 Creation of a mouse GBM initiating model enabling activation of FOXG1 and/or beta catenin 135
5.3.3 In vivo induction of FOXG1 results in accelerated tumour growth and reduced survival time. 138
5.3.4 Upregulation of FOXG1 results in an increase in cytoplasmic beta-catenin in tumour cells 142

5.3.5 Induction of active beta-catenin results in non-significantly accelerated tumour growth 145

5.4 The synergy between FOXG1 over-expression and Wnt signaling is relevant to two human GBM cell lines, one adult and one paediatric **148**

5.4.1 The synergy is relevant to adult GSCs in a BMP4-induced quiescence model. 151

5.4.2 A paediatric GSC line is also responsive to chiron, only in the context of intact FOXG1 155

5.5 The Groucho binding domain of FOXG1 is required for cooperation with Wnt signaling **158**

5.6 The FOXG1/Wnt synergy is relevant to an additional, highly clinically-relevant, model of quiescence **161**

5.7 Conclusions **166**

Chapter 6: Discussion ***169***

6.1 A FOXG1/Wnt synergy drives exit from quiescence **169**

6.2 Implications for human GSCs **170**

6.3 Potential mechanisms of the interaction **171**

6.4 Implications of the in vivo findings and translational potential **173**

6.5 Concluding remarks and future directions **175**

References ***177***

Appendix 1: StemSelect compound library ***193***

Abstract

The balance of stem cell quiescence versus proliferation must be tightly regulated under normal homeostasis and becomes disrupted in cancers. The brain cancer glioblastoma is driven by cells with neural stem cell characteristics. These glioblastoma stem cells (GSCs) can reside in dormant, quiescent and proliferative states, yet the molecular transitions between these remain poorly understood. Quiescent GSCs are refractory to anti-mitotic cytotoxic therapies, and contribute to regrowth of the tumour; therefore elucidating molecular pathways that control GSC exit from quiescence may uncover new therapeutic strategies. The role of Wnt signaling in GBM has remained enigmatic. Here I show that the transcription factor FOXG1, which is frequently overexpressed in GSCs, cooperates with Wnt signaling to drive efficient exit from quiescence. However, Wnt signaling is dispensable once GSCs are fully proliferative. Using a phenotypic chemical screen (303 small molecule regulators of stem cell related pathways) I identified a potent synergy between glycogen synthase kinase 3 (GSK3) inhibitors and FOXG1 in driving exit from NSC quiescence. Pharmacological and genetic perturbations confirmed that this was due to activation of the Wnt/beta catenin pathway. The FOXG1/Wnt synergy is also relevant in vivo, and in human glioblastoma cell models. Mechanistically, these data suggest that the excessive FOXG1 both leads to an accumulation of beta-catenin and sequesters the Wnt/TCF co-repressor Groucho/TLE, thereby derepressing Wnt/beta catenin target genes and enabling their maximal activation. I conclude that FOXG1 and Wnt cooperate in the critical process of exiting the quiescent state. These findings suggest inhibition of Wnt signaling will have limited impact on the proliferative GSC compartment, but may be critical in preventing reactivation of the quiescent cells that drive regrowth of the tumour after chemo- and radiotherapy.

Lay Summary

Brain cancer is the leading cause of cancer death in children and young adults. Very little has changed in the treatment of malignant brain cancer (glioblastoma) in the last few decades, which means that the outlook for patients has remained dismal even as survival rates from other cancers has improved dramatically. Although glioblastoma (GBM) can be treated with surgery, radiotherapy and chemotherapy, it always comes back. Some tumour cells have stem cell properties, meaning that they can exist in a dormant state, not growing or dividing, but then go on to divide, reproducing themselves and regrowing the tumour. Our treatments target dividing cells and so do not destroy these stem cells.

I investigated what makes these dormant cells start dividing again. We already knew that a protein called FOXG1 - present in human GBMs at high levels - was involved. It is a transcription factor: a protein that controls which genes the cell switches on and off. We did not know quite how FOXG1 was helping cells to start dividing and we did not know which other factors were involved. I found that a signal, received by cells from the environment around them, co-operates with FOXG1 to wake up these dormant cells. This signal is called Wnt. I conducted experiments on stem cells in dishes, including actual GBM cells donated by patients. I also made GBM tumours in mice and showed the impact of FOXG1 and Wnt in this situation, which is closer to what actually happens in a patient's brain.

We cannot change the fact that human GBMs have high levels of FOXG1 but we can block the Wnt signal which co-operates with FOXG1. In this way, I hope we can keep more cells in a dormant state and come a step closer to improving the outlook for patients with GBM.

Acknowledgements

I would like to thank my supervisor, Professor Steve Pollard for his guidance and input. I have been very fortunate to be part of a lab led by such a dynamic and successful scientist. This environment also means being surrounded by wonderful post-doctoral researchers and students who have taken this hapless medic under their wing for the steep learning curve of my real scientific education. Special thanks to post-docs Eoghan O'Duibhir, Maria Angeles Marqués-Torrejón, Raul Bressan, Harry Bulstrode, Sabine Gogolok, Pooran Dewari. Carla Blin helped me practically and with advice, as did Vivien Grant who I also want to thank for the chat and encouragement. Many thanks to Neza Alfazema for her expertise in mouse work.

I gratefully acknowledge Cancer Research UK and the ECAT scheme for my fellowship. Thanks to Jo Ness from ECAT for support. Charlie Gourley, Gillian Morrison, Neil Carragher and Charles ffrench-Constant have been my advisory committee and I thank them for their extremely helpful guidance and suggestions.

Finally, thanks to my friends and family. The enthusiasm of my children, Clea and Tristan, for tales of the lab has been motivating. I won't forget Clea's bath time genome editing cancer cure hypothesis (aged 7) nor how cool Tristan looked in a giant lab coat. Thank-you, Anna, for all your love and support and for making everything and more fun. This thesis is dedicated to my parents, Rob and Isobel, who perhaps think I will never stop studying but have supported my decisions with love and unwavering confidence. They are probably right, as usual.

Declaration of Originality

I hereby declare that this thesis and the work presented in it was composed by and originated entirely from me and has not been submitted in any form for another degree or diploma at any other institution. Any information derived from the published or unpublished work of others has been acknowledged in the text and references are listed in the bibliography.

Faye Robertson

Edinburgh, October 2020

Copyright Declaration

List of abbreviations

BBB	Blood-brain barrier
BIO	Bromo-5-indirubin-3’-oxime
BMP	Bone morphogenetic protein
bp	Base pair
BSA	Bovine serum albumin
BSD	Blasticidin resistance gene
BrdU	5-bromo-2'-deoxyuridine
cAMP	Cyclic Adenine Monophosphate
Cas9	CRISPR associated protein 9
cDNA	Copy DNA
CNS	Central nervous system
CRISPR	Clustered regularly interspaced short palindromic repeats
crRNA	CRISPR RNA
CSF	Cerebrospinal fluid
Ct	Threshold cycle
CT	Computed tomography
DAPI	4’,6-diamidino-2-phenylindole dihydrochloride
dCt/ddCt	Delta Ct / delta delta Ct
DMEM	Dulbecco’s modified Eagle’s medium
DMSO	Dimethylsulfoxide
DNA	Deoxyribonucleic acid
dNTPs	Deoxynucleotide triphosphates
Dox	Doxycycline hyclate (1ug/ml)

ECM	Extracellular matrix
EdU	5-ethynyl-2-dexyuridine
EGF	Epidermal growth factor
EGFR	EGF receptor
FACS	Fluorescence activated cell sorting
FAP	Familial adenomatous polyposis
FGF	Fibroblast growth factor
FoxG1	Forkhead box G1
FoxO3	Forkhead box O3
4-OHT	4-hydroxytamoxifen
GAPDH	Glyceraldehyde-3-phosphate dehydrogenase
GBD	Groucho binding domain
GBM	Glioblastoma multiforme
GFAP	Glial fibrillary acidic protein
GFP	Green fluorescent protein
GLAST	Glutamate-aspartate transporter
GO	Gene ontology
gRNA	Guide RNA
GSC	Glioma neural stem cell
GSK3	Glycogen synthase kinase 3
GSK3i	GSK3 inhibition
Gy	Gray
ICC/IF	Immunocytochemistry/immunofluorescence
IDH	Isocitrate dehydrogenase
Ig	Immunoglobulin

KO	Knockout
MGMT	O-6-methylguanine-DNA-methyltransferase
MRI	Magnetic resonance imaging
mRNA	Messenger RNA
mTOR	Mammalian target of rapamycin
NF-1	Neurofibromatosis 1
NPC	Neural progenitor cell
NSC	Neural stem cell
NSG	NOD scid gamma
PBS(T)	Phosphate buffered saline (with Triton X-100)
PCR	Polymerase chain reaction
PDGFR	Platelet derived growth factor receptor
PI3K	Phosphoinositide 3-kinase
PTEN	Phosphatase and tensin homolog
qPCR	Quantitative PCR
Rb	Retinoblastoma
REMBRANDT	Repository of Molecular Brain Neoplasia Data
RNA	Ribonucleic acid
RNA-Seq	RNA sequencing
RPPA	Reverse phase protein array
RT-PCR	Reverse transcriptase PCR
RTK	Receptor tyrosine kinase
SDS PAGE	Sodium dodecylsulfate polyacrylamide gel electrophoresis
SVZ	Subventricular zone
Shh	Sonic hedgehog

shRNA	Short hairpin RNA
Tam	Tamoxifen (or 4-hydroxytamoxifen where specified)
TBS-T	Tris buffered saline with Tween-20
TCGA	The Cancer Genome Atlas
TMZ	Temozolomide
trRNA	Trans-activating CRISPR RNA
UTR	Untranslated region
WHO	World Health Organisation
WT	Wild-type

List of Figures

Figure 1. 1 Neural stem cells throughout development. 3
Figure 1. 2 Schematic of the cell types found in the adult SVZ. 6
Figure 1. 3 Marker expression across the spectrum of NSCs from quiescence to proliferation. 10
Figure 1. 4 BMP4 induced quiescence. 16
Figure 1. 5 A simplified schematic of the diagnosis of glioma based on histopathology and genetics. 18
Figure 1. 6 GBM overall survival curves. 21
Figure 1. 7 Sources of GBM tumour cells and their capture in vitro. 28
Figure 1. 8 Quiescence is one of several important challenges in understanding the biology of GBM. 30
Figure 1. 9 FOXG1 loss and overexpression. 35
Figure 1. 10 FOXG1 is overexpressed in GBM. 38
Figure 1. 11 Wnt signaling in GBM. 43
Figure 1. 12 Wnt signaling is active in GBM. 48

Figure 2. 1 Generation of tumorigenic lines lacking Pten and Nf-1 and expressing EGFRvIII. 63
Figure 2. 2 FOXG1 rescue plasmids. 65
Figure 2. 3 Creation of a cell line with tamoxifen-inducible constitutively active beta-catenin. 67
Figure 2. 4 Creation of the Tcf/lef mCherry cell line. 68

Figure 3. 1 Screen optimisation. 81
Figure 3. 2 A phenotypic screen identifies a synergy between a GSK3 inhibitor and FOXG1 overexpression in driving cell cycle re-entry. 86
Figure 3. 3 GSK3 inhibition and FOXG1 overexpression drive exit from quiescence with high efficiency. 91
Figure 3. 4 The effects of GSK3 inhibition are not dependent on SOX2 overexpression. 92
Figure 3. 5 BMP4+FGF2 exposure is an alternative model of quiescence to which the FOXG1/GSK3i synergy is relevant. 95
Figure 3. 6 The synergy depends on dox+chiron exposure simultaneously. 99

Figure 4. 1 A dose-dependent synergistic effect of FOXG1 overexpression and Wnt3a exposure in stimulating cell cycle re-entry of quiescent NSCs. 104
Figure 4. 2 The FOXG1/GSK3i synergy is abrogated by pharmacological Wnt inhibition. 108
Figure 4. 3 The inducible beta-catenin cell line confirms that the effects of chiron on qNSCs are through beta-catenin. 112
Figure 4. 4 Excision of the beta-catenin cassette confirms its role in the synergy and shows that the effect is cell-autonomous. 115
Figure 4. 5 A Tcf/lef reporter NSC line provides evidence that FOXG1 upregulates Tcf/lef activation. 117
Figure 4. 6 Reverse phase protein array analysis reveals a pattern of activation of Wnt target genes as major hits. 121

Figure 4. 7 An inhibitor of Myc/Max dimerization abrogates exit from quiescence with dox+chiron and has an additive effect with Wnt inhibition. *124*
Figure 4. 8 Nanostring and qPCR suggest activation of Wnt target genes by FOXG1. ..... *127*

Figure 5. 1 RNAScope confirms co-localisation of FOXG1 (red) and Beta-catenin (yellow) in human GBM. . *133*
Figure 5. 2 Schematic of the process of generation of tumorigenic lines lacking Pten and Nf-1 and expressing EGFRvIII. *135*
Figure 5. 3 ..... *138*
Figure 5. 4 FOXG1 upregulation in vivo results in reduced survival time in the NPE tumour model. *142*
Figure 5. 5 FOXG1 upregulation in vivo leads to increased beta-catenin accumulation in tumour cells. *145*
Figure 5. 6 Induction of active beta-catenin results in accelerated tumour growth. *148*
Figure 5. 7 Functional assays of GNS cell line G7 and G7 FOXG1-/- in various culture conditions. *150*
Figure 5. 8 Chiron drives cell cycle re-entry in adult GSCs in a FOXG1-dependent manner. *154*
Figure 5. 9 A paediatric GSC line is responsive to chiron only in the context of intact FOXG1. ..... *158*
Figure 5. 10 The synergy depends, in part, on the FOXG1 Groucho binding domain. *161*
Figure 5. 11 Irradiation of cells may provide a useful model of quiescence. *164*
Figure 5. 12 Chiron leads to increased exit from quiescence after irradiation, only in the context of intact FOXG1. ..... *166*

Figure 6. 1 Regulatory squelching. *173*

Chapter 1: Introduction

1.1 Overview

This thesis explores the molecular processes that control the transition from quiescence to active proliferation in neural stem cells (NSCs). This is a question of fundamental importance in understanding stem cell regulation but also has practical importance in the context of the brain cancer glioblastoma (GBM), as GBM stem cells have many similarities to normal NSCs. Four key topics are covered in this introduction. Firstly, I discuss regulation of neural stem cells in the developing and adult brain. Secondly, I cover GBM and the role of NSC-like cells in the disease. Thirdly, I explore FOXG1, a key forebrain transcription factor, which was an initial focus of this thesis due to its overexpression in GBM stem cells (GSCs). Finally, I discuss Wnt signaling, as we have uncovered this as a critical pathway that cooperates with FOXG1 to drive exit from quiescence.

1.2 Neural stem cell biology and quiescence

1.2.1 Neural stem cells in the developing embryo, foetus and adult brain

Neural stem cells are defined as cells with two key capabilities: self-renewal and multi-lineage differentiation (neurons and glia). During development, the first cells with these properties appear just prior to gastrulation and are the neuroepithelial cells of the early neural plate. These cells express the intermediate filament Nestin, CD133, Sox2 and epithelial markers such as tight junction proteins. They demonstrate apical-basal polarity (they are in contact with the

ventricle at their apical surface) and interkinetic nuclear migration, giving the neuroepithelium a pseudostratified appearance (Obernier et al., 2018). During neurulation, cells undergo symmetric division and subsequent asymmetric division to give rise to neurons (Götz and Huttner, 2005). Polarity is the determinant of symmetric versus asymmetric division in that divisions which split the apical plasma membrane will be symmetric, whereas those which leave it intact, allocated to one of the daughter cells, are asymmetric. Subsequently, the cells lose some neuroepithelial features – such as tight junctions – and gain astroglial features such as expression of GLAST and RC-2 expression. The resulting cells are termed radial glia and are the neural stem cells of the developing brain, giving rise to neurons, intermediate progenitors and astrocytes (Götz and Huttner, 2005). Radial glial cells retain contacts with the ventricle, express Nestin, are tripotent, and display both apical-basal polarity and interkinetic nuclear migration. A subgroup of these cells persist in the forebrain walls of the ventricle and are fated to become adult neural stem cells (Merkle et al., 2004).

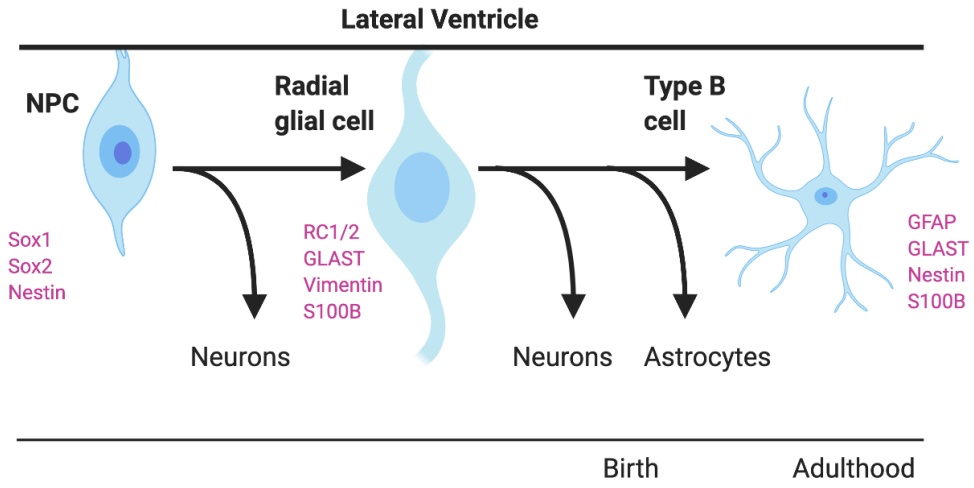

Figure 1. 1 Neural stem cells throughout development.

There is a continuum of cell states throughout development. Marker profile varies but cells share similar functional identities. The SVZ contains stem-like cells throughout adult life. NPC: neuroepithelial progenitor cell. Adapted from (Alvarez-Buylla et al., 2001).

1.2.2 Neural stem cells exist in the subventricular zone and resemble astrocytes

Neural stem cells reside in two regions in the adult brain: the subventricular zone (SVZ) and the subgranular zone of the dentate gyrus of the hippocampus (Gage and Temple, 2013; Ming and Song, 2005). Decades ago, it had been thought that multipotent stem cells existed only transiently during brain development. However, neurogenesis and gliogenesis continue throughout life in certain regions, and NSCs can be isolated in culture from the adult mammalian brain (Codega et al., 2014; Imura et al., 2003; Laywell et al., 2000; Lee et al., 2012; Reynolds and Weiss, 1992; Temple, 1989).

There are three major cell types within the adult SVZ: type A, B and C cells. Type B cells are GFAP positive cells, with ultrastructural and immunocytochemical features of astrocytes. These cells are largely quiescent or slowly proliferating and can be further subcategorised into type B1 and B2. B1 cells are in contact with the ependymal cells which line the walls of the lateral ventricle, extending a non-motile primary cilium into the CSF (Beckervordersandforth et al., 2010; Doetsch et al., 1999). At their basal surface, B1 cells are in contact with vessels, neuroblasts (around which they form a sheath) and the basal lamina. B2 cells are associated with the surrounding striatal parenchyma. Type B1 cells have been shown to be the source of type C cells, intermediate progenitors or transit-amplifying cells, which divide rapidly several times and generate type A cells, neuroblasts, which migrate through the rostral migratory stream to the olfactory bulb where they generate neurons (Doetsch et al., 1999; Ihrie and Alvarez-Buylla, 2011; Tong and Alvarez-Buylla, 2014).

Type B cells are therefore thought to be quiescent adult neural stem cells. They are descendants of foetal radial glia in the postnatal brain and express similar markers e.g. GLAST, GFAP,

nestin, vimentin, BLBP, connexin 30, CD15 and CD13 (Doetsch et al., 1997). They do not express S100ß, a marker of mature parenchymal astrocytes (Codega et al., 2014). Importantly, type B cells are not a uniform cell type. A subset of these cells is positive for Ascl1 and EGFR, markers associated with proliferative C cells, suggesting an activated fraction (Doetsch et al., 2002; Pastrana et al., 2009). This is poorly understood.

In humans, evidence has accumulated for the existence of NSCs in the adult brain, yet this still remains controversial in the hippocampus (Sorrels et al., 2018). In the 1990s, cells isolated from the SVZ and the hippocampus were shown to be capable of generating neurons and glia in vitro (Kukekov et al., 1999). Subsequently, Sanai et al. demonstrated the existence of a subventricular ribbon of astrocytes which proliferate faster in vitro than cortical astrocytes and which can generate multilineage progeny (Sanai et al., 2004). Some initial in vivo data came from post-mortem analysis of BrdU labelled neurons in the hippocampus of lung cancer patients who had received BrdU as a diagnostic tool (Eriksson et al., 1998). These fate mapping studies were also supported by proton nuclear magnetic resonance spectroscopy data, which has yielded evidence of proliferation in the adult hippocampus (Manganas et al., 2007). A study of post-mortem infant brains has shown migration of young neurons to the frontal lobe cortex, in keeping with the migratory process seen in the mouse (Paredes et al., 2016).

Recent clonal fate mapping studies have shown that neurogenesis in the adult mouse brain is supported by a symmetrically dividing NSC population, around a quarter of which remain in the niche, self-renewing, whilst the remaining three quarters generate differentiated progeny (Obernier et al., 2018).

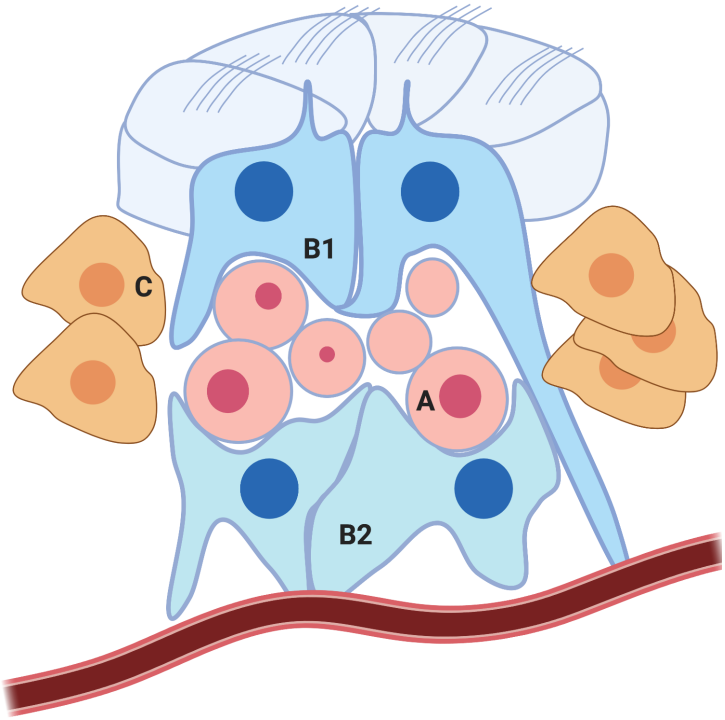

Figure 1. 2 Schematic of the cell types found in the adult SVZ.

B1 cells are in contact with the ventricle via primary cilia. At their basal surface, they contact the vessels. They give rise to C cells which give rise to A cells (migratory neuroblasts). B1 and B2 cells form a sheath around migratory neuroblasts. Adapted from (Ihrie and Alvarez-Buylla, 2011).

1.2.3 Adult NSCs exists in a variety of dormant, quiescent and proliferative states

These initial studies exploring fate mapping of NSCs and marker analysis, have suggested that there is considerable heterogeneity in the different cell types in the SVZ niche. This heterogeneity manifests itself in functional parameters such as state of NSC activation and capacity to generate different progeny. The majority of NSCs in the adult brain at any given time are found in G0, with only a small fraction actively cycling (Fuentealba et al., 2012; Temple, 2001). Codega et al. isolated and characterised two neural stem cell subpopulations from the adult SVZ, which they defined as quiescent and activated, based on cell cycle kinetics and label retaining assays. The quiescent subpopulation shared certain transcriptomic features with quiescent stem cells from other organs, such as skin and intestine (Codega et al., 2014).

In a study from the Martin-Villalba group, single cell RNA-seq was performed on cells isolated, based on expression of GLAST and CD133, from the SVZ of adult mice. This revealed a continuum of activation states that could be broadly categorised, using principal component analysis and unsupervised hierarchical clustering, into four groups based on level of activation: qNSC1 (dormant), qNSC2 (primed quiescent), aNSC1 and aNSC2 (active). Active NSCs were distinguished from quiescent NSCs on the basis of higher EGFR expression and the expression of a number of cell cycle genes. Clustering of the gene expression profiles of the cells further divided them into the four clusters, and pseudotemporal ordering placed them along a spectrum. The distinction between qNSC categories 1 and 2 was based on genes regulating protein synthesis, suggesting that activation of translation is an early event in the exit from quiescence, an intuitive conclusion. A further difference between these two groups was the expression of GLAST, which is higher in the qNSC1 – dormant – population (Llorens-Bobadilla et al., 2015). Parenchymal differentiated astrocytes express similar markers and molecular features to adult

quiescent NSCs, and these lie at the dormant extreme of this activation spectrum, overlapping somewhat with qNSCs.

Notably, qNSCs were characterised by expression of astrocyte-associated transcription factors, including: Sox9, Id2, Id3 and Id4, and unexpectedly did not express Nestin until the transition to the activated state. More recently, Artegiani et al performed single cell RNA-Seq on cells from the dentate gyrus and found that astrocytes did not cluster separately from the NSCs. They additionally demonstrated a spectrum of developmental states from quiescent NSC towards proliferating neural progenitor and were unable to divide cells into subgroups along this continuum, although progenitors were clearly distinct from NSCs (Artegiani et al., 2017).

The tetraspanin CD9 has been proposed as a potentially distinguishing marker between astrocytes and qNSCs (Llorens-Bobadilla et al., 2015) and, given the similarity between these populations such markers are urgently needed to dissect the biology of NSC activation. Indeed, it is not clear whether there is a fundamental transcriptional difference between these cell types or whether differentiated astrocytes may acquire neural stem cell characteristics upon exposure to the relevant niche. Further analysis of the epigenetic states may provide more insights into differences in potential.

Interestingly, there is evidence that quiescent cortical and spinal astrocytes can begin to proliferate and become reactive in response to injury (Götz et al., 2015). Post-stroke, astrocytes from the cortex are able to generate neurospheres and generate multilineage progeny in vitro, although they are more lineage restricted in vivo, generating only astrocytes and oligodendrocytes (Shimada et al., 2012). Similarly, lineage tracing studies showed that, following stab wound injury, a subset of astrocytes acquired stem-like properties of self-

renewal and multipotency (Buffo et al., 2008). It was established that these cells had not migrated to the cortex from the SVZ. It was further shown that a more permissive environment allowed multilineage differentiation, whereas a cortical microenvironment resulted in predominantly glial progeny (Buffo et al., 2008). Thus, the boundary between transcriptional state of differentiated astrocyte and quiescent neural stem cell remains blurred, and their distinct functional properties (i.e. multipotency versus unipotency) may be related to their distinct epigenetic states, or could be largely determined by the niche.

Mich et al. were also able to isolate two distinct quiescent and proliferative populations of cells from the adult mouse SVZ. The highly mitotic, EGFR expressing, GLAST expressing, PSA-NCAM negative cells (termed GEPCOT cells) were capable of generating neurospheres; the second population was quiescent, had higher levels of GLAST, lower EGFR and could not form neurospheres but, after temozolomide ablation of the GEPCOT cells, these cells repopulated the SVZ (Mich et al., 2014). This is consistent with findings that label-retaining cells survive treatment with antimitotic agents and go on to repopulate the SVZ and instigate neurogenesis and hence fulfil criteria of dormant or quiescent NSCs (Doetsch et al., 1999; Giachino and Taylor, 2009; Pastrana et al., 2009).

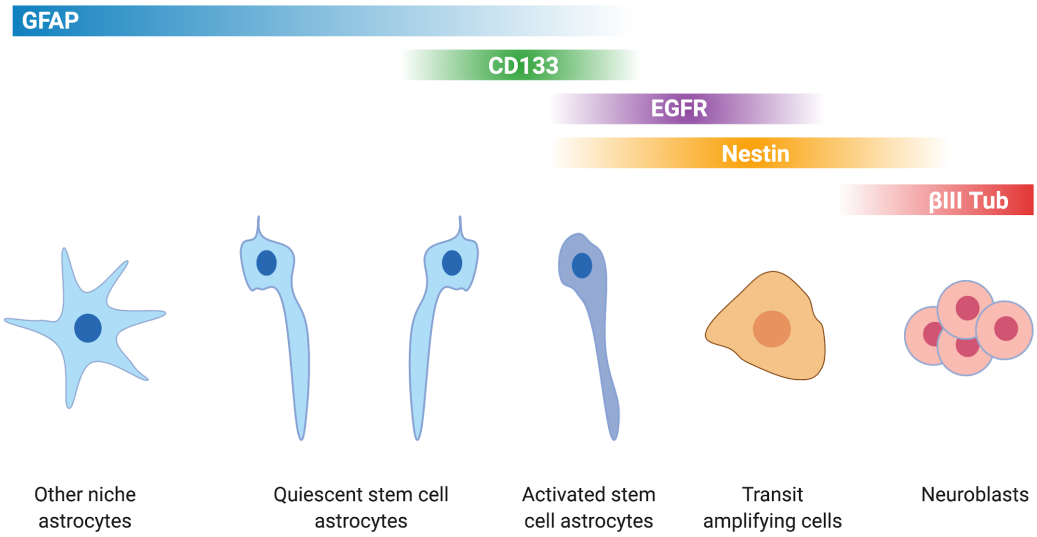

Figure 1. 3 Marker expression across the spectrum of NSCs from quiescence to proliferation.

After Codega et al 2014. Parenchymal astrocytes lie at the dormant extreme of the spectrum. GFAP is expressed by astrocytes and qNSCs. There are few clear distinct markers of the qNSC state and it seems to be a continuum of states. The transitions between these are poorly understood.

1.2.4 Quiescence is an active state

It should be noted that quiescence is an active state that must be maintained, in which proliferation and growth are reversibly arrested, and cellular physiological processes are altered, but in which the cell remains responsive to microenvironmental cues. Although the molecular basis of the control of quiescence remains poorly understood, a variety of genes and pathways have been implicated based on transcriptional profiling and some functional studies.

The transcriptome of quiescent NSCs is enriched in cell communication, response to stimulus and cell adhesion signatures, suggesting dynamic regulation and an interactive state. Functional G-protein coupled receptor activity has also been shown to be involved in the maintenance of quiescence (Codega et al., 2014). Martynoga et al., reported quiescence specific enhancers which are associated with high gene expression enriched for GREAT terms (McLean et al., 2010) such as “stem cell development” and “cell junction assembly”(Martynoga et al., 2013).

It is known that Bone Morphogenetic Protein (BMP) signaling has a role in regulating quiescence in vivo (Ables et al., 2010; Imayoshi et al., 2010; Mira et al., 2010). Receptors, ligands and targets of the BMP pathway are more highly expressed in quiescent, as compared with active, NSCs, suggesting autocrine regulation of quiescence by BMP (Llorens-Bobadilla et al., 2015). BMPs in vitro reduce proliferation of adult NSCs, without leading to differentiation (Mira et al., 2010). In vivo, BMP inhibition with Noggin leads to exit from quiescence in hippocampal stem cells, and inactivation of BMP signaling leads to proliferation and subsequent exhaustion of the stem cell pool (Mira et al., 2010). Thus, active maintenance of quiescence is essential for the maintenance of neurogenesis in the adult brain.

1.2.5 BMP4 exposure induces a state of astrocytic differentiation or quiescence

The bone morphogenetic proteins are a group of growth factors within the TGFβ superfamily. They act via phosphorylation of Smad proteins and have a diverse range of roles. In the developing embryo, BMPs have a key role in patterning (dorsoventral and left-right) as well as numerous other functions, including in formation of the primitive streak, mesoderm formation and cardiac development (Kishigami and Mishina, 2005; Wang et al., 2014). BMP-4 is involved in eye development, with defects leading to anophthalmia-microphthalmia and coloboma. In the CNS, BMPs have been shown to promote astroglial fate over oligodendroglial fate, in the SVZ during embryonic development and in adult brain niches; however, these studies assumed that GFAP is a marker of astroglial differentiation, whereas subsequent work revealed the radial glia-like identity and GFAP expression of quiescent neural stem cells (Gomes et al., 2003; Gross et al., 1996). This is especially relevant in view of the finding, discussed above, that BMPs regulate quiescence in adult hippocampal stem cells (Mira et al., 2010). Perhaps those early data also point to promotion of quiescence.

BMPs are also known to maintain quiescence in hair follicle (Oshimori and Fuchs, 2012), intestinal (Li and Clevers, 2010) and haematopoetic stem cells (Jankovic et al., 2007; Perry et al., 2007), through expression of Id1. Nam and Benezra showed that a population of GFAP positive astrocytic cells with stem cell properties express Id1 at high levels. These cells are quiescent, have type B1 morphology, and are capable of self-renewal and generation of neuroblasts (Nam and Benezra, 2009). BMP responsiveness, then, is a key feature of quiescent NSCs. More recently, BMP has been shown to regulate quiescence in GBM stem cells, a finding which will be discussed in more detail later in this chapter (Sachdeva et al., 2019; Carén et al., 2015; Piccirillo et al., 2006).

Treatment of dissociated neurospheres (from mouse embryonic NSCs) with bone morphogenetic protein 4 (BMP) results in upregulation of GFAP, down regulation of progenitor markers Sox1 and vimentin, acquisition of stellate astrocyte morphology and exit from cell cycle (Bonaguidi et al., 2005). This has been assumed to model astrocyte differentiation, but the lack of markers distinguishing astrocytes from quiescent neural stem cells proves problematic. Although cells treated with BMP for 6 days did not generate neurospheres and multi-lineage progeny in that study, they retain the capacity to do so upon exit from quiescence under certain conditions, such as the forced overexpression of FOXG1 and SOX2 (Bulstrode et al., 2017), analogous to the endogenous expression of these transcription factors in GBM-derived stem cells. Thus, it has been difficult to determine using the current panel of marker gene expression whether BMP treatment induces terminal astrocyte differentiation, or acquisition of a quiescent NS phenotype with GFAP positivity and astrocyte morphology. In GBM derived stem cells, BMP4 more clearly induces functional quiescence, as will be discussed in section 1.3.9, and there is some retention of expression of SOX2 (Carén et al., 2015).

While exposure of NSCs to BMP4 induces cell cycle arrest that can be overcome only by forced expression of GBM associated transcription factors, exposure to BMP4 in the presence of FGF2 provides an in vitro model of shallow, or primed, quiescence, with cells exhibiting reversible cell cycle arrest and upregulation of genes associated with quiescence, particularly those associated with ECM interaction and cell-cell adhesion (Martynoga et al., 2013). This shallow quiescent state is analogous to the state induced by exposure of GSCs to BMP4 (Carén et al., 2015). This thesis will describe BMP4 and BMP4+FGF2 models of quiescence in vitro, with respect to NSCs, NSCs modified to model human GSCs, and patient-derived GSCs.

1.2.6 NS cells can be isolated and cultured in adherent monolayer

NSCs can be isolated from the foetal or adult mouse SVZ and cultured in adherent monolayer in the presence of the growth factors EGF and FGF2. This adherent culture method has several advantages over more traditional 'neurosphere' or suspension culture, most notably in greater homogeneity of cultures and lack of spontaneous differentiation. This simplifies population based analysis as well as quantitative clonal analysis (Pollard et al., 2009). Cultured NSCs provide a tractable model to explore the molecular and cellular mechanisms controlling NSCs and, as discussed in the following section, enables comparison with tumour-derived GSCs (grown in the same conditions and phenotypically similar).

The mouse NSCs cultured in vitro and described here correspond closely to radial glia when cultured in EGF+FGF2 containing media (Uchida et al., 2000). Exposure of these NS cells at low density to BMP4, concomitant with removal of EGF and FGF-2, triggers rapid cell cycle exit and acquisition of astrocytic morphology, with upregulation of astrocyte markers GFAP and S100B and downregulation of NS cell markers Nestin and Sox2 (Conti et al., 2005). These cells do not re-enter cell cycle on re-exposure to growth factors and we have previously defined them functionally as terminally differentiated astrocytes (Bulstrode et al., 2017) although more recent studies by the Pollard lab suggest they more likely correspond to a dormant NSC state (Marqués-Torrejón et al., under revision).

By contrast, exposure to both BMP4 and FGF2, even for extended periods of 28 days, yields cells which also exit cell cycle, change marker profile as described above but which begin to divide again when returned to EGF-containing media (Martynoga et al., 2013). However, cells were plated at 350-650 cells/mm^2 by Martynoga et al, considerably higher than the density at which we found irreversible cell cycle arrest after BMP4 treatment. Here, we show data

regarding the importance of plating densities in these in vitro models of quiescence/differentiation. These suggest that, at higher density, BMP4 treatment alone (in the absence of FGF-2) may also induce quiescence rather than terminal differentiation, as cells are able to re-enter cycle on re-exposure to growth factors.

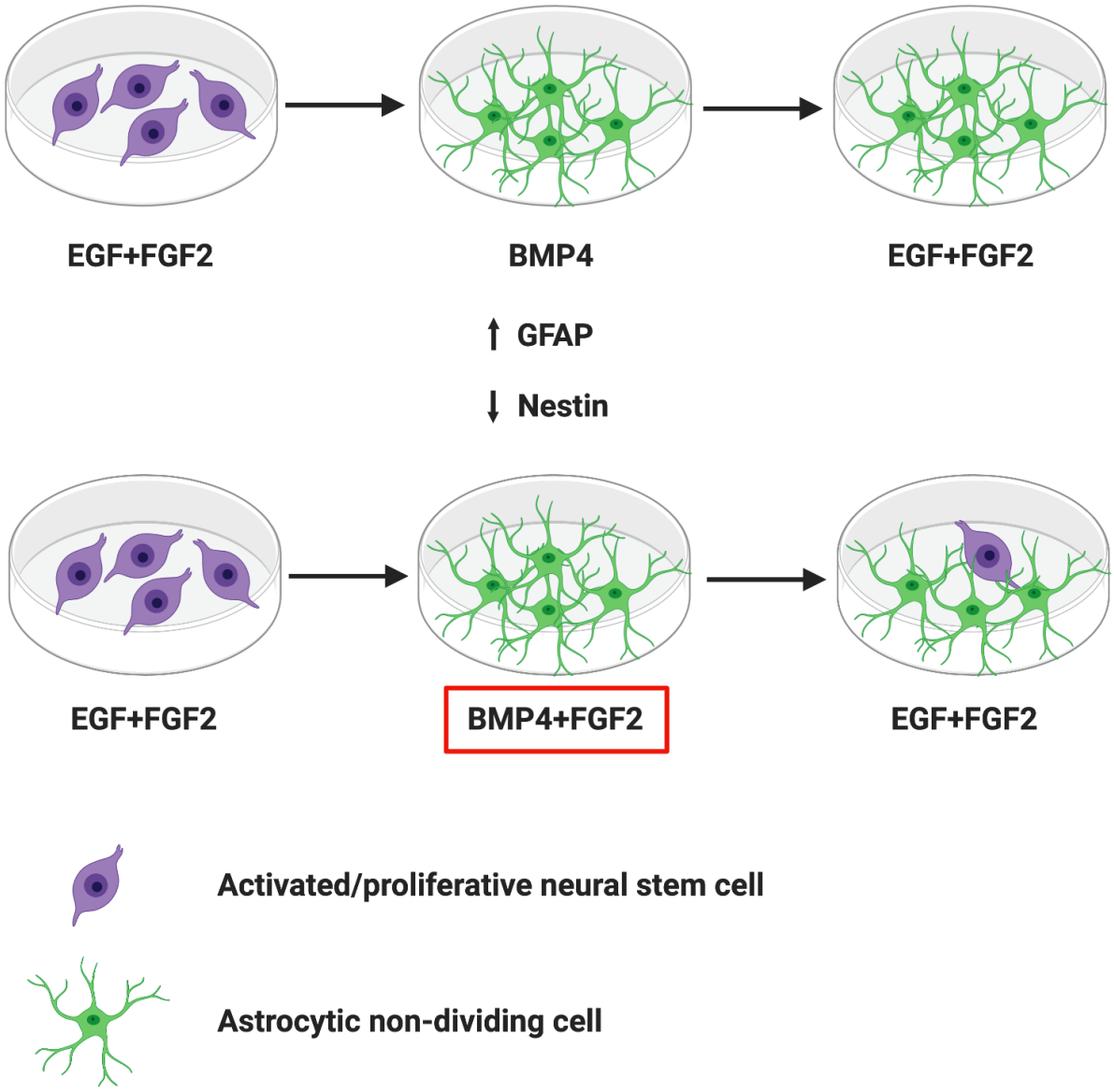

Figure 1. 4 BMP4 induced quiescence.

Exposure to BMP4, in the absence of EGF, triggers cell-cycle exit and a shift in marker expression to reflect a quiescent NSC or astrocytic identity. If FGF2 is also withdrawn, cells are less likely to re-enter cell cycle on re-exposure to growth factors. There is no clear distinction in marker profile between cells which will re-enter cell cycle and those which will not.

1.3 The biology of glioblastoma

1.3.1 Glioma is the most common intrinsic primary brain tumour

Glioma is the most common intrinsic primary brain tumour. The incidence is approximately 5 per 100,000 per year. The presenting features include seizures, focal neurological deficit, headaches and other symptoms of mass effect such as nausea or visual disturbance. CT and MRI are highly sensitive and specific but, where tissue can be obtained, diagnosis is made based on histopathological and molecular features. Classification according to the World Health Organisation (WHO) Classification of Tumours of the Central Nervous System has primarily been based on histopathology, but was updated in 2016 to reflect the increasing utility of molecular genetic markers.

1.3.2 Glioma can be classified using molecular and histopathological features

In the updated WHO classification, gliomas are categorised by predominant cell population as astrocytomas or oligodendrogliomas. The diagnosis of oligoastrocytoma, which describes tumours with mixed populations, is strongly discouraged in the updated classification, as genotype can often be used to determine category. Alongside this categorisation, IDH genotype, as determined by immunohistochemistry and/or sequencing, is used to aid classification (Figure 1.5). Tumours are also graded on a scale of I to IV: low grade tumours appear homogeneous and well-differentiated, whereas grade IV astrocytomas (GBMs) display nuclear atypia, extensive necrosis, and microvascular proliferation.

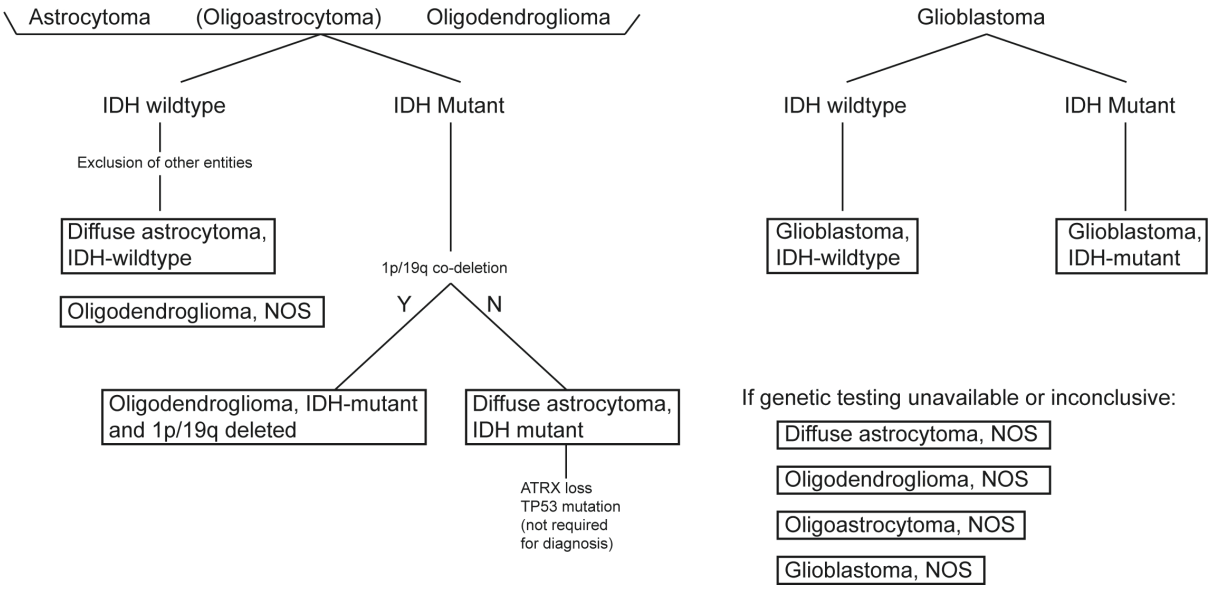

Figure 1. 5 A simplified schematic of the diagnosis of glioma based on histopathology and genetics.

Adapted from (Louis et al., 2016). NOS: not otherwise specified.

GBM, IDH-mutant (approximately 10% of cases) corresponds to the clinically-defined secondary GBM, which arises through transformation of a lower grade tumour. These tend to arise in younger patients and the median survival is longer, compared to IDH-wildtype GBM. The latter, which comprises around 90% of cases, has a median age at diagnosis of 64 years. There are a number of rarer distinct entities incorporated in the category of IDH-wildtype GBM: epithelioid GBM, gliosarcoma, giant cell GBM and GBM with a primitive neuronal component each have distinct histopathological and molecular features. In children, GBM is found in the hemispheres (paediatric high grade glioma) and brainstem (diffuse intrinsic pontine glioma) and has an extremely poor prognosis. Fortunately, these paediatric tumours are rare (Jones et al., 2012).

1.3.3 GBM has a poor prognosis despite multi-modal treatment

A combination of factors undermines effective therapies for GBM. Surgically, the tumour may be difficult to access due to its location in deep or eloquent brain areas. Even those tumours amenable to resection are impossible to remove fully due to widespread invasion beyond the margins of the visible mass. Early attempts at complete resection with hemispherectomy were unsuccessful due to transcollosal spread; however, this did sometimes offer improved survival over other options available in the 1920s, in that one of 5 patients survived three and a half years (the others died within days or months of complications or recurrence) (Dandy, 1928; Bell and Karnosh, 1949).

The utility of cytotoxic chemotherapy, and more recent targeted therapies, is limited by the blood-brain barrier (BBB) and lack of a single defined molecular target. Although disrupted in GBM, the BBB presents difficulties for drug delivery and the inherent resistance of the highly heterogeneous cell population within the tumour compounds these problems. Both

invasiveness and heterogeneity present challenges for successful radiotherapy treatment. Targeting all invasive cells, if that were possible, would lead to unacceptably high doses to normal brain tissue. As with chemotherapy, relatively resistant subclones within the heterogeneous population escape destruction by radiotherapy and cause relapse (Bao et al., 2006). Any future therapeutic approaches will need to tackle all of these inherent challenges.

Treatment is currently multi-modal, with the fittest patients undergoing maximal surgical debulking followed by concurrent chemoradiotherapy, 60Gy in 30 fractions with temozolomide, and further adjuvant chemotherapy, again with temozolomide. This so-called Stupp protocol, extends median survival to 14.6 months compared with 12.1 months for surgery and radiotherapy alone (Stupp et al., 2005). Survival benefit is greatest in those patients whose tumours display methylation of the promoter region of O-6-methylguanine-DNA methyltransferase, thus silencing transcription of the gene and translation into the protein which removes alkyl groups from the O^6 position of guanine – an important site of alkylation by temozolomide (Hegi et al., 2005).

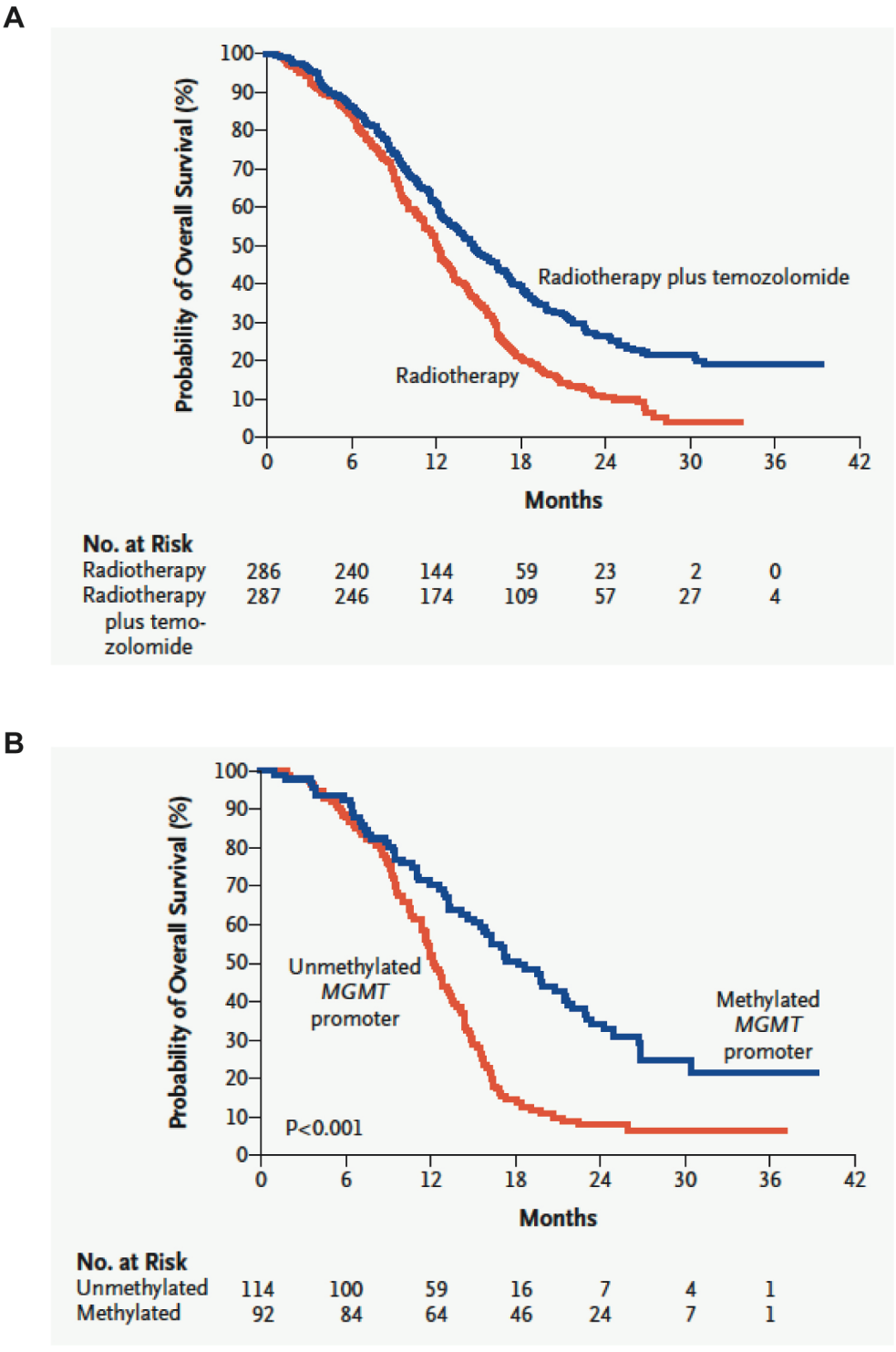

Figure 1. 6 GBM overall survival curves.

(A) Radiotherapy with concomitant temozolomide improves median survival as compared to radiotherapy alone. From (Stupp et al., 2005). (B) The MGMT methylation status, as measured on histology samples, has a significant impact on survival with treatment. From (Hegi et al., 2005).

1.3.4 GBM cells show genome instability and extensive mutation, particularly in RTK/PI3K, CDK4/RB and P53 pathways

Deep sequencing of large numbers of GBM samples, and classification of tumours accordingly, has been conducted as part of The Cancer Genome Atlas (TCGA) project (Verhaak et al., 2010). Three subtypes, based on tumour cell-intrinsic transcriptional signatures, were proposed – termed: classical, mesenchymal and proneural – with a fourth 'neural subtype' dismissed as normal neuronal contaminants (Wang et al., 2017). GBM is characterised by chromosome and genome instability. Individual tumours are highly heterogeneous and contain subclones with a range of driver and passenger mutations (Snuderl et al., 2011). Single cell analysis of GBM samples confirms this heterogeneity and shows that distinct subtype signatures co-exist within patient tumours (Patel et al., 2014; Darmanis et al., 2017). Currently, the classification into subtypes by TCGA project has not been adopted as a decision-making aid in clinical practice but can give prognostic information, with proneural subtypes showing a survival advantage but responding less well to chemotherapy, for example. There are, however, several core oncogenic pathways which are characteristically mutated in IDH-wildtype GBM. Gain of chromosome 7 and loss of chromosome 10 are prevalent, as are mutations in p53, Rb, and receptor tyrosine kinase (RTK)/Ras/phosphoinositide 3-kinase (PI3K) signaling. Common gain of function mutations involve the RTK receptors EGFR (26%), MET and PDGFR and their downstream effectors Ras, PI3K, mTOR and AKT. Loss-of-function mutations are frequently seen in TP53 (29%), Rb (9%), PTEN (31%) and NF-1 (11%) (Brennan et al., 2013). To date, knowledge of the existence and prevalence of these mutations has not translated into clinically useful targeting approaches. This is likely to relate both to the aforementioned heterogeneity within the tumour and to the emergence of new mutations at relapse. Additionally, there is significant redundancy in mutated pathways. For instance, Patel et al. found that, where EGFR

mutation/amplification was not seen, there was expression of other tyrosine kinase receptors, and therefore alternative pro-proliferative mechanisms (Patel et al., 2014).

1.3.5 GBM is a disease of stem cells

Cells with transcriptional and epigenetic features associated with neural stem cells can be isolated, in serum-free conditions, from GBMs, as from the normal brain (Uchida et al., 2000; Singh et al., 2003). These glioma stem cells (GSCs) are capable of self-renewal in adherent monolayer culture, generation of multilineage progeny and tumorigenesis on xenotransplantation (Pollard et al., 2009; Sun et al., 2008).

The discovery of a tumour-initiating population in human GBM represented a shift in our understanding of the aetiology and behaviour of GBM. These GSCs express markers normally restricted to neural stem and progenitor cells. Important studies showed that the subset of $CD133^+$ cells isolated from primary brain tumours proliferates in culture and can differentiate into cell phenotypes identical to the tumour in situ. The $CD133^+$ cells are capable of generating tumours, which recapitulate the phenotype of the original patient tumour, after transplantation of only 100 cells into immunocompromised mice (Singh et al., 2003, 2004). By contrast, transplantation of at least 10^5 $CD133^-$ cells is required for engraftment, but these did not generate tumours. These findings challenged the view of the astrocyte as the cell of origin in glioma and led to a focus on glioma stem cell biology for greater understanding of the cellular hierarchy within the tumour. The specific markers best used to isolate stem-like cells from tumours remain a subject of debate and may vary with tumour type, but it is clear that this subset of cells with features and transcriptional regulators of immature progenitor and stem cells exists within tumours. Whether or not they represent the cell of origin is perhaps less important than the fact that this cell state is universally observed across all GBMs, and is likely

responsible for driving relapse and tumour growth. Novel targets may be identified by comparing and contrasting mechanisms of normal NSC controls with GSCs.

Chen et al. have used a Nestin-ΔTK-GFP transgene which labels quiescent NSCs in the SVZ and a subset of tumour cells in GBM (Chen et al., 2012). It is these cells which repopulate the tumour after TMZ treatment and the consequent destruction of proliferative cells. Ablation of this population can prevent recurrence (Chen et al., 2012). More recently, in vivo genetic lineage tracing experiments also support the existence of a differentiation hierarchy within the tumour and show a subset of cells with higher clonogenic potential (Lan et al., 2017). Nomenclature has caused great discussions, and these cells have been given various names, including tumor/glioma propagating cells, tumor-initiating cells, cancer stem cells but all definitions should encompass the key functional features of tumorigenicity, plus features shared with somatic stem cells: self-renewal and differentiation capabilities (Lathia et al., 2015).

Capturing this functional state with marker profiles has proved challenging. And there are inherent challenges with reliance on the transplantation models. For example, CD133 is not universally expressed on all tumorigenic cells (Beier et al., 2007) and can vary with the cell cycle, so that slow cycling cells do not express it during G0/G1 but maintain functional stem cell properties (Sun et al., 2009). However, it is widely acknowledged that GBMs express core transcriptional and epigenetic pathways associated with immature neural stem and progenitor cells, and are not simply a proliferative astrocyte population. Exploring the ‘stemness’ pathways and self-renewal processes in NSCs therefore may identify new strategies to tackle GBM.

1.3.6 GBM stem cells have a neurodevelopmental transcriptional identity and are resistant to treatment

Work from the Bernstein laboratory has shown that, as well as surface markers suggestive of a neural stem cell identity, the tumour stem cell population, as compared with a 'differentiated glioma cell' (DGC) population, has a transcriptional programme in common with developmental NSCs/progenitor cells. In fact, forced overexpression of the neural stem cell transcription factors SOX2, ASCL1, SALL2 and POU3F2 in DGC cells is sufficient to drive reprogramming of differentiated GBM cells into a stem cell like state with associated tumourigenicity (Suvà et al., 2014). This transcriptional signature is found in a subset of cells in patient tumours (Patel et al., 2014). Mounting evidence confirms a key role for neurodevelopmental transcription factors in driving self-renewal in GSCs (Gallo et al., 2013; Lu et al., 2016; Singh et al., 2017).

As well as their increased clonogenicity, it is proposed that cancer stem cells are treatment resistant by virtue of often existing in quiescence, and therefore are better able to tolerate DNA damage repair response to radiotherapy (Bao et al., 2006). High levels of drug export proteins and lack of dependence on signaling pathways targeted by pharmacological agents also confers resistance (Stiles and Rowitch, 2008). Thus, a resistant, quiescent population survives multimodality treatment, but retains the capacity to self-renew and to generate proliferative progeny. Over a variable length of time, these cells re-enter the cell cycle and regenerate the tumour bulk, causing clinical relapse and, ultimately, the death of the patient. This project focuses on the switch, in these cells, from quiescence into proliferation, with a view to developing strategies to enforce quiescence and delay recurrence of the tumour after current standard of care treatment.

1.3.7 GBM stem cells cultured in adherent monolayer provide a tractable reductionist model to explore exit from quiescence

GSC lines can readily be derived from patient-derived tumour tissue. These in vitro models are well suited to reductionist questions regarding cell-intrinsic properties and to interrogation using genetic manipulations. Large cell numbers can be generated easily, allowing for large scale screening and molecular profiling (functional, genetic, transcriptomic, proteomic) and the production of rigorous data without the potentially confounding complexity of microenvironmental factors (Robertson et al., 2019). Clearly, studies in vitro using such cell lines must be complemented with in vivo data, testing the relevance of any findings to a more complex model. Additionally, care must be taken to ensure that cell lines are not subject to unacceptable divergence and genetic selection in culture from the original specimen, if disease-relevance is to be maintained. This latter problem affects glioma lines cultured in serum and passaged over many years, such as U87, which accumulate genetic and epigenetic changes due to the pressure exerted by their culture conditions and which generate, upon xenotransplantation, well-circumscribed tumours with poor resemblance to the initial glioma (Lee et al., 2006). Such lines have limited utility for studying the characteristics of stem cells within GBM and yet many studies progressing to phase 3 trials are based on pre-clinical work with such lines (Han et al., 2019). There is growing recognition that the field must move away from working with these ‘classic’ cell lines (Allen et al., 2016; Xie et al., 2015).

Patient-derived cell lines are now favoured by the field, and are cultured using serum-free, EGF/FGF2-containing media. These lines can be grown as neurospheres or in adherent monolayer on laminin. Lee et al. derived cells from human GBM and cultured them either in serum-free conditions with EGF/FGF2, or in conditions used for the culture of the widely used ‘classic’ cell lines (Lee et al., 2006). They showed that cells cultured in serum-free media have,

as discussed above, extensive similarities to normal NSCs. They retained genetic and transcriptomic features of the original tumour, without significant drift and recapitulated features of GBM when transplanted into immunocompromised mice (Lee et al., 2006). By contrast, cells cultured in serum lost the potential for multilineage differentiation and clonogenicity, acquiring a differentiated astrocytic phenotype, and drifted markedly from the original tumour genetically. Tumours generated from these cells had none of the hallmark histopathological features of GBM (Lee et al., 2006).

Adherent monolayer culture, as opposed to sphere culture, of patient-derived cell lines in serum-free conditions offers certain experimental advantages that support in vitro studies of GSC behaviour and allow comparison to the behaviour of genetically normal NSCs as discussed in section 1.2.6. The homogeneity afforded by adherent monolayer culture lends itself to reductionist approaches and imaging, screening, clonal selection and quantification are all more straightforward with monolayer culture as opposed to spheres (Conti et al., 2005; Pastrana et al., 2011). Furthermore, the Pollard lab and others have reported improved efficacy of monolayer culture for deriving lines from patient tumours (Pollard et al., 2009; Xie et al., 2015). The fact that such cells are tumorigenic when transplanted orthotopically into immunocompromised mice, allows for stepwise progression to a human, disease-relevant in vivo model system. Importantly, genetic disruptions in the parental tumour are retained across passages and into the in vivo model (deCarvalho et al., 2018).

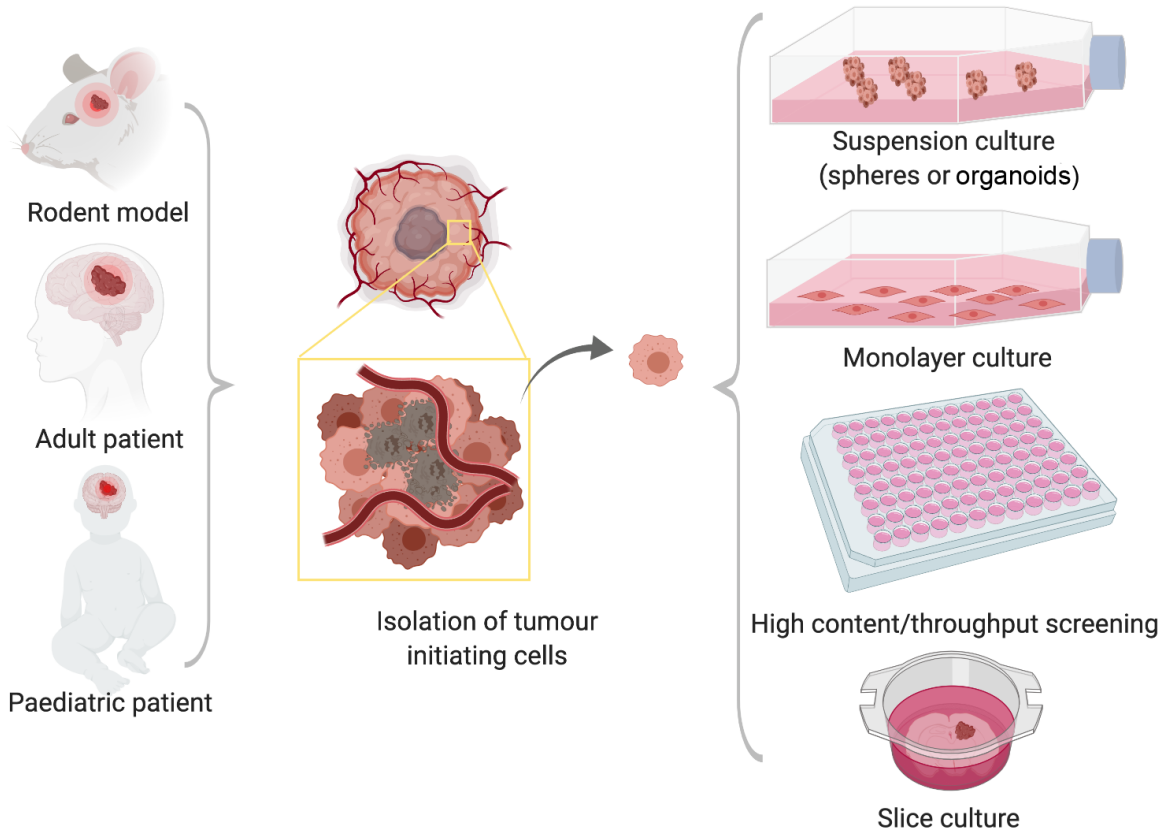

Figure 1. 7 Sources of GBM tumour cells and their capture in vitro.

Tumour tissue and tumour cell populations can be obtained from rodent models or patients (adult or paediatric). Tumour-initiating cells can be maintained in culture using neural-stem-cell culture conditions (serum-free media with growth factors EGF and FGF2). These can be expanded in suspension as spheres or organoids, or in an adherent monolayer. Clonal cell lines can be obtained, and cells plated in microtiter plates for arrayed genetic or chemical screens. Cells and tumour explants can also be engrafted on brain slice cultures to model tumour-host interactions. From (Robertson et al., 2019).

1.3.8 GBM stem cell quiescence is an important clinical problem

Analogous to the situation in the healthy adult SVZ, the majority of GSCs in vivo are in a quiescent, non-cycling state. Single cell RNA-Seq studies show the cycling fraction in the tumour to range between 1.4%-51% as assessed by cell cycle meta signature (with the majority of tumours lying toward the lower end of this spectrum) and 2.1%-13.6% as assessed by Ki67 staining (Darmanis et al., 2017; Neftel et al., 2019; Patel et al., 2014). Additionally, transcriptomic stemness signature anti-correlates with cell-cycle signature, suggesting that the stem cell component of the tumour is more quiescent than other cell types (Patel et al., 2014). If we interrogate GSCs in vitro, in conditions which support and promote proliferation, we may miss information relevant to the in vivo cell cycle state. However, it is clear that the quiescent stem cell fraction can generate rapidly proliferating progenitors/transit amplifying cells similarly to NSCs in the SVZ.

The study by Chen et al, described above, demonstrates a key principle for the treatment of GBM (Chen et al., 2012). Our current therapies target proliferating cells, but quiescent GSCs are left behind and, over time, re-enter the cell cycle and regenerate a heterogeneous tumour bulk, leading to recurrence (Chen et al., 2012). An additional therapeutic problem is that surgical management removes the tumour bulk (>90% debulking is the operative goal) but cannot target cells which have begun to infiltrate the surrounding parenchyma. These are the cells targeted by chemo- and radiotherapy, yet these cells are even less proliferative than cells in the tumour bulk: 1.6% versus 7.7% (Darmanis et al., 2017).

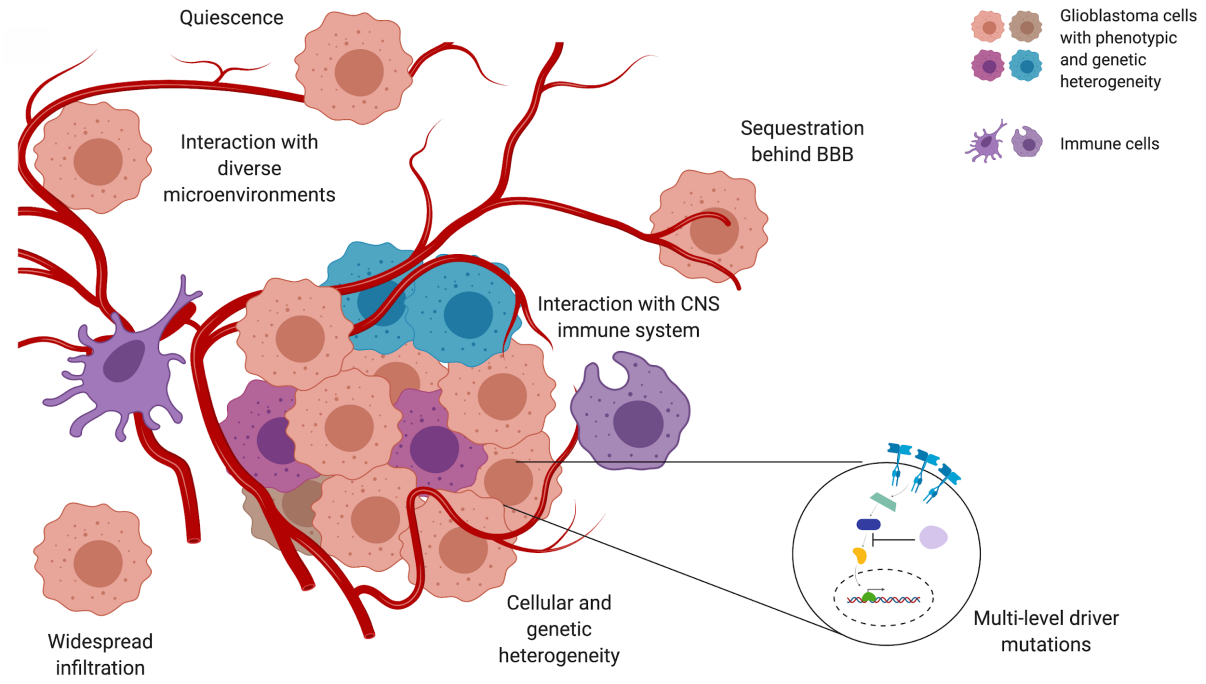

Figure 1. 8 Quiescence is one of several important challenges in understanding the biology of GBM.

GBM stem cells exist in various states (dormant/ quiescent, activated/quiescent or proliferative) that are influenced by diverse tumour microenvironments (TMEs). Complex niches, immune interactions and physical forces/mechanosignaling are all poorly understood areas of GBM biology. How these influence tumour cell signaling circuits and the subsequent transcriptional and epigenetic changes in GSC fate is an area of active research. Targeting both the quiescent and proliferative tumour populations will be vital for any successful therapeutic strategy. From (Robertson et al., 2019).

1.3.9 GBM stem cells demonstrate a spectrum of response to BMP4

As discussed briefly in section 1.2.5, bone morphogenetic proteins (BMPs) and their downstream targets, inhibitor of DNA-binding genes ID1-ID4, have been implicated in maintenance of quiescence in a number of stem cell types. For example, in the hair follicle, suppression of BMP signaling is necessary for stem cells to exit the quiescent telogen state and enter the activated anagen state (Oshimori and Fuchs, 2012). ID1 also has a major role in haematopoietic stem cell maintenance (Jankovic et al., 2007; Perry et al., 2007) and has been proposed as a marker of adult neural stem cells (Nam and Benezra, 2009; Niola et al., 2012). Indeed, in a GBM xenograft model, ID1 knockdown reduced cell invasion and led to prolonged survival (Anido et al., 2010; Soroceanu et al., 2013). However, *Id1* loss in a mouse model of GBM led to more rapid tumour growth, in keeping with the hypothesis that it marks quiescent GSCs (Barrett et al., 2012).

A key paper from 2006 reports striking effects of BMP4 on cells isolated from GBMs and sorted for CD133 expression, with the aim of isolating GSCs. BMP4 treatment reduced proliferation, without affecting death or apoptosis, and reduced CD133 positivity. Clonogenic index was reduced and cells acquired a flattened stellate morphology with increased GFAP immunoreactivity. Furthermore, BMP4 exposure for 48hrs rendered cells incapable of forming invasive tumours when transplanted into mice. Instead they formed small, well demarcated lesions with markedly improved survival of mice at 4 months (Piccirillo et al., 2006). However, the Pollard lab previously reported that, whilst 8 days of BMP4 treatment reduced proliferation in each of 6 human tumour-derived GSC lines, only 2 of the lines demonstrated efficient GFAP upregulation (Carén et al., 2015). Furthermore, in these lines, the apparent astrocyte differentiation was accompanied by delayed, or incomplete, reconfiguration of DNA methylation patterns, in contrast to the rapid epigenetic changes seen in association with

differentiation in haematopoetic cells. Importantly, there was incomplete silencing of cell cycle and DNA replication licensing genes in response to BMP4. Do these cells, therefore, acquire an astrocytic phenotype as part of the acquisition of a quiescent NS identity? Are they more akin to quiescent NSCs than terminally differentiated astrocytes?

Certainly, GSCs do not undergo terminal cell cycle arrest in response to BMP4: when returned to media containing EGF and FGF2, even after 54 days of BMP4, they immediately resume rapid proliferation. Furthermore, BMP4-treated GSCs could be transplanted into the brains of mice and were able to generate tumours. No survival advantage was demonstrated from BMP4 treatment (Carén et al., 2015). Interestingly, these experiments were conducted at high density and, as I will show, density has a significant impact on response to BMP. Work in this thesis will use low density for induction of quiescence in GSCs. More recently, Sachdeva et al. show that, whilst BMP exposure inhibits GSC proliferation, it does not alter stemness and cells remain able to self-renew upon return to growth factors and able to generate tumours on orthotopic transplantation (Sachdeva et al., 2019). The authors further show that ID1 is a marker of slow cycling, long term label retaining cells in GBM xenografts, potentially quiescent stem cells. Additionally, BMP pathway activation, marked by pSmad1 expression in vivo or induced by BMP exposure in vitro, leads to relative resistance to temozolomide and radiation. The plating density for in vitro assays in this study was lower than in the Carén paper, 150 cells/mm^2. BMP exposure, then, is a physiologically relevant method to induce quiescence in GSCs whilst maintaining stemness and the potential for reactivation and tumourigenesis.

The neurodevelopmental programme which is overexpressed/activated in GSCs may explain why, unlike NSCs; they are unable to terminally differentiate and remain primed to re-enter the cell cycle. Suva et al. reported four neurodevelopmental transcription factors (POU3F2,

SALL2, OLIG2, SOX2) which drive GBM propagation and stemness (Suvà et al., 2014) (although they only focussed on the 'proneural' subtype with limited cell lines). Others, including our lab, have shown the impact of other neurodevelopmental factors, such as ASCL-1 and FOXG1, in self-renewal and generation of progenitors (Bulstrode et al., 2017; Rheinbay et al., 2013; Verginelli et al., 2013).

1.4 FOXG1

1.4.1 FOXG1 is a member of the Forkhead Box (Fox) superfamily of transcription factors

The Fox superfamily of transcription factors share a forkhead box domain, a sequence of 80 to 100 amino acids which binds to DNA, also known as the winged helix domain. The name derives from the phenotype associated with mutation of the *forkhead* gene in *Drosophila*, in which foregut and hindgut are replaced by ectopic head structures (Weigel et al., 1989). There are 19 subfamilies, named FOXA-FOXS, on the basis of differences in domain structure. Function is further influenced by various post-translational modifications.

In mammals, FOXG1 expression is forebrain-specific and is involved in development of the telencephalon. It favours maintenance of the neural stem/progenitor cell state and promotes proliferation of these cells and limits terminal differentiation. Loss of *Foxg1* in the mouse embryo results in dramatic reduction of telencephalon size, putatively due to reduced proliferation and premature differentiation of the stem/progenitor cell pool (Xuan et al., 1995). Lengthening of the cell cycle is seen with *Foxg1* loss, in keeping with a more quiescent state in the stem cell population (Hanashima et al., 2002). Gain of function experiments in frogs resulted in expansion of the neural progenitor pool and, in chickens, in overgrowth of the neural

tube, in keeping with an exaggerated exit from quiescence of stem/progenitor cells (Ahlgren et al., 2003; Bourguignon et al., 1998). Additionally, FOXG1 has a role in specifying ventral identity in the developing telencephalon, responding to ventral signals Hedgehog and FGF8, and antagonising dorsal specification by Wnt signaling (Danesin et al., 2009; Martynoga et al., 2005). In humans, FOXG1 haploinsufficiency causes Rett syndrome, a neurodevelopmental disorder characterised by mental retardation, seizures, and stereotypic hand movements (Ariani et al., 2008).

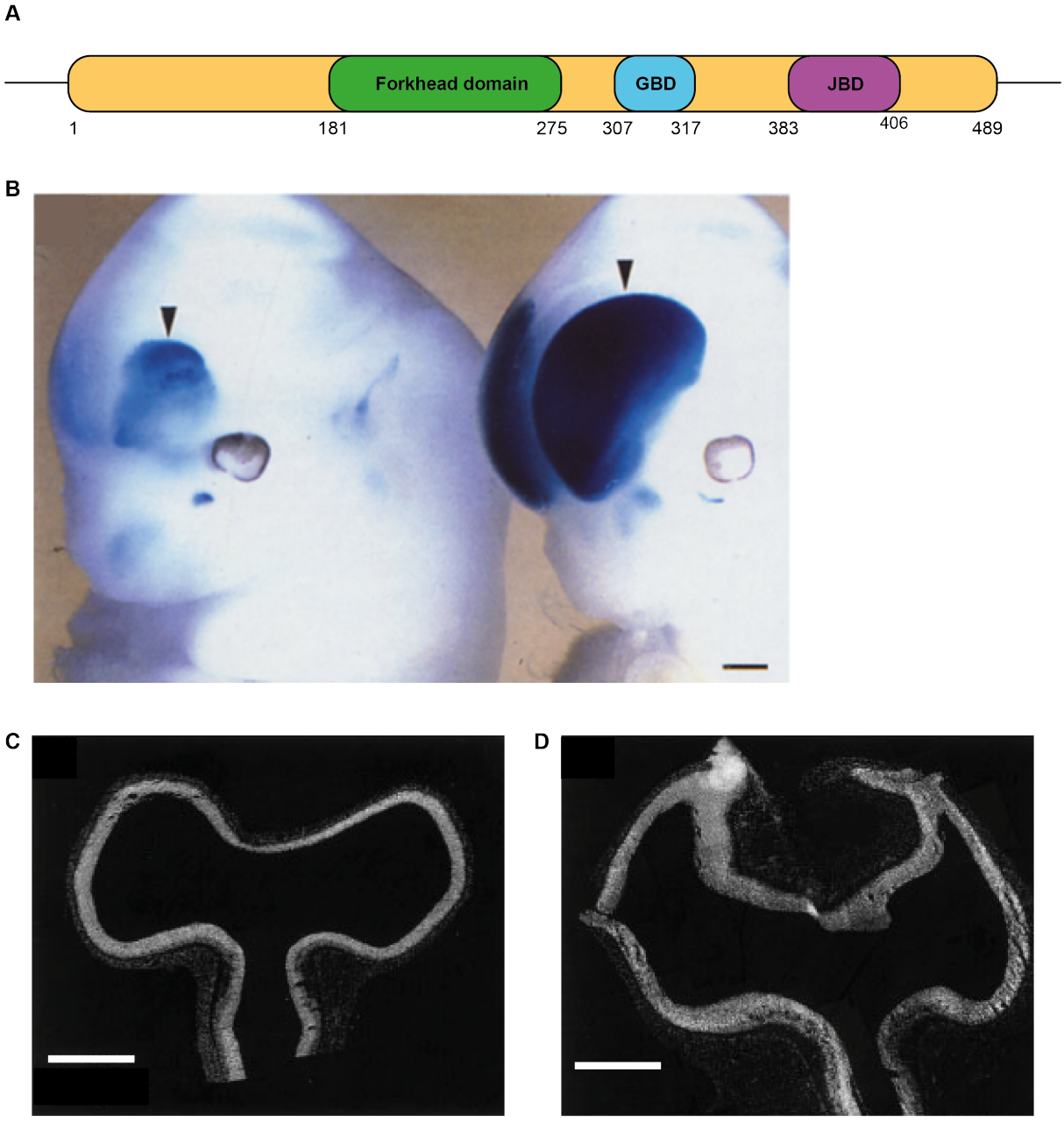

Figure 1. 9 FOXG1 loss and overexpression.

(A) FOXG1 is a single exon gene encoding a 489 amino acid protein with a forkhead domain and predicted Groucho binding and Jarid binding domains. (B) *Foxg1*-/- embryos have severe telencephalic hypoplasia which is lethal at birth. From (Xuan et al., 1995) scale bar 400 µm (C&D) In the chick embryo, *Foxg1* overexpression (D) leads to an increase in neural tube thickness as compared to control (C). From (Ahlgren et al., 2003) scale bars 500 µm.

FOXG1 is thought to act mainly as a transcriptional repressor, by direct and indirect means. The forkhead domain directly binds DNA on one side of the helix irrespective of nucleosome occupancy on the other side (and there is evidence of pioneer activity for FOXA1, which structurally resembles linker histones) (Zaret and Carroll, 2011). However, FOXG1 is also known to mediate transcriptional repression by recruitment of co-repressors of the Groucho/TLE and JARID families (Yao et al., 2001). Interestingly, the pro-proliferative effect of FOXG1 on neural progenitor cells is independent of its DNA binding, whereas the neuronal differentiation effects are uncoupled from this and are dependent on DNA binding (Hanashima et al., 2002).

Importantly, FOXG1 has been shown to be a necessary part of two transcription factor cocktails capable of reprogramming fibroblasts to neural precursor cells, capable of self-renewal and multipotency (Lujan et al., 2012; Raciti et al., 2013). Additionally, FOXG1 regulates neural stem cell fate specification in human embryonic stem cells (Ziller et al., 2015).

1.4.2 FOXG1 is overexpressed in GBM

Analysis of transcriptome data from 9783 Affymetrix gene expression array experiments in normal tissue and cancer, confirms high levels of FOXG1 expression in CNS tissue and in a number of cancers, most markedly in GBM (Kilpinen et al., 2008) (Figure 1.10A). Our group has previously published Tag-seq data demonstrating that FOXG1 is upregulated in three GSC lines as compared to two normal NSC lines. qRT-PCR validation in 16 GSC lines and comparison to 6 NSC lines confirms this high expression (Engström et al., 2012) (Figure 1.10B&C). Western blotting confirms that this finding is relevant at the protein level (Bulstrode et al., 2017). Furthermore, high FOXG1 mRNA levels predict a poorer overall survival

outcome in the Rembrandt dataset for glioma, whilst low levels predict a better outcome (Verginelli et al., 2013).

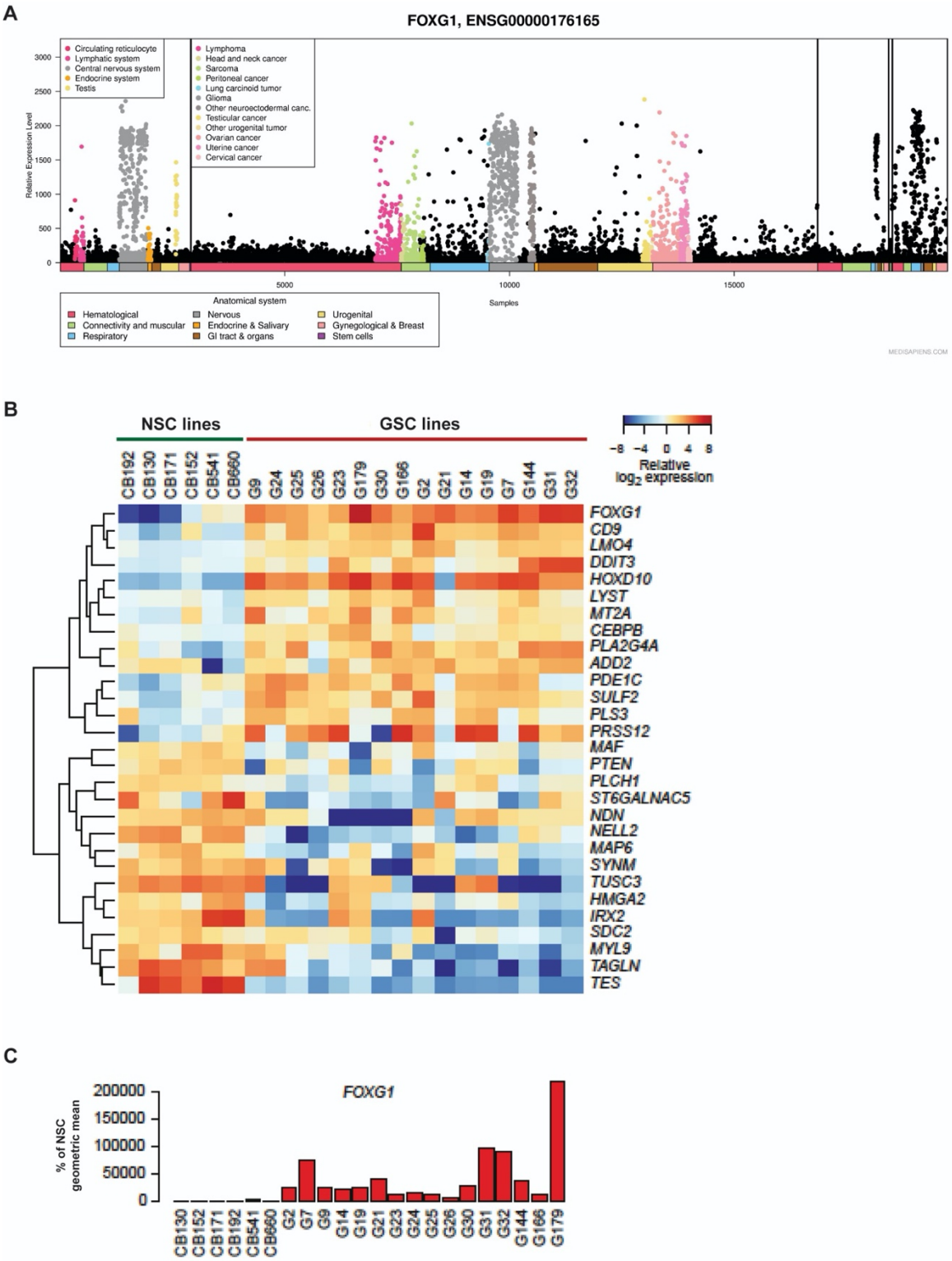

Figure 1. 10 FOXG1 is overexpressed in GBM.

(A) Affymetrix gene expression data for FOXG1 in normal tissue and tumours. From (Kilpinen et al., 2008). (B) TagSeq shows overexpression of FOXG1 in GSC lines as compared to non-malignant NSCs. (C) qRT-PCR confirms this overexpression. From (Engström et al., 2012).

1.4.3 FOXG1 overexpression has a role in 'de-differentiation', or activation, of BMP4-induced astrocytes/quiescent NSCs

Liu et al. have shown that the oncogenic effect of the ligand-independent, activated mutant form of EGFR (EGFRvIII), commonly found in GBM, particularly the classical subtype, is effected in part by FOXG1 upregulation (Liu et al., 2015). Our lab has previously published evidence that FOXG1 is not essential for proliferation of NSCs in vitro, when exposed to EGF/FGF2, but that its overexpression concomitantly with SOX2 drives cell cycle re-entry from quiescence and colony formation. FOXG1 overexpression alone also drives colony formation after BMP4 exposure but this occurs with low efficiency (Bulstrode et al., 2017). The acquisition of a Nestin-low, GFAP-high, post-mitotic state on BMP4 exposure could represent astrocytic differentiation but, as discussed above, could equally represent a quiescent neural stem cell-like state. Indeed, tumorigenic mouse cells and patient-derived GSCs are certainly in a reversible state of cell cycle arrest, more compatible with the latter definition, and this could be related to their high levels of FOXG1 expression.

1.4.4 Knockdown or knockout of FOXG1 reduces/abolishes tumorigenicity in human xenograft models of GBM

Work from the Stifani lab has shown that FOXG1 knockdown with shRNA effects a modest reduction in proliferation of GSCs grown as spheres in vitro and increases survival of mice after orthotopic transplantation (Verginelli et al., 2013). CRISPR-mediated FOXG1 knockout results in a failure of tumorigenesis on transplantation into immunocompromised mice, as compared with reliable tumour formation with the parental GSC line, with intact FOXG1 (Bulstrode et al., 2017). FOXG1 therefore seems important in facilitating entry into the cell cycle; however, it is dispensable in the presence of high levels of EGF and FGF2 in cycling cells. This may relate its ability to limit TGF-ß signaling and hence BMP induced cytostatic

effects via repression of FOXO3 expression and protein activity but we lack a strong understanding of the mechanisms involved (Bulstrode et al., 2017; Seoane et al., 2004).

1.5 Wnt signaling

1.5.1 The Wnt signaling pathway is highly conserved and has roles in diverse cell processes, particularly during development

Wnt proteins are secreted signaling proteins, all of which have a lipid modification: the addition of a palmitate by the palmitoyltransferase Porcupine (Nusse and Clevers, 2017). The first Wnt gene discovered was the mouse gene *Int-1* (subsequently *Wnt1*) in 1982 (Nusse and Varmus, 1982). *Wingless* in *Drosophila*, which controls segment polarity in larval development, was later shown to be a *Wnt1* homologue (Rijsewijk et al., 1987). Indeed, Wnt proteins are highly conserved, with orthologues identifiable throughout multiple phyla. Wnt signaling has crucial roles in cell proliferation, polarity and tissue organisation, with established roles in development (Nusse and Clevers, 2017). In central nervous system development, Wnt is implicated in NSC self-renewal and proliferation (Chenn and Walsh, 2002; Kalani et al., 2008).

The palmitate modification renders Wnt proteins hydrophobic and they remain tethered to the cell membrane or their cognate receptors. Wntless (Wls), a transmembrane protein, binds only modified Wnts and conveys them to the plasma membrane. It is poorly understood how they reach target cells: it has been proposed that they are secreted in vesicles with Wls acting as a chaperone. Thus, they act in the main over short distances, between touching cells, in spite of early hypotheses that they acted as long range, concentration-dependent morphogens in *Drosophila* (Langton et al., 2016; Sato et al., 2011; Strand and Micchelli, 2011). Wnt is

therefore a critical niche signaling factor for a variety of stem and progenitor cells through development and in the adult (Nusse and Clevers, 2017).

In mammals, there are 19 Wnt genes with distinct or partially overlapping loss-of-function phenotypes. There is, however, considerable cross-reactivity leading to the activation of one of three signaling cascades: the canonical Wnt signaling pathway, the non-canonical planar cell polarity pathway and the Wnt/Ca^{2+} pathway.

In canonical signaling, Wnts bind Frizzled receptors: 7 pass transmembrane domain proteins with a N-terminal cysteine rich domain. They also bind Lrp5/6 co-receptors, inducing complex formation with Frizzled, resulting in a conformational change which enables phosphorylation. The phosphorylated cytoplasmic Lrp tail then inhibits glycogen synthase kinase 3 (GSK3) and binds Axin (Mao et al., 2001). The beta-catenin destruction complex is a cytoplasmic agglomeration of molecules which co-operate to bind and phosphorylate beta-catenin. Axin is the scaffold of the complex, which also contains APC, WTX, CK1α/δ and GSK3α/β. When no Wnt ligand is bound, these latter serine-threonine kinases phosphorylate Axin-bound beta-catenin and the phosphorylated motif is recognised by β-TrCP, which ubiquitinates it, leading to its proteasomal destruction (Aberle et al., 1997). When the signaling pathway is activated by ligand binding, Axin recruitment to the phosphorylated tail of Lrp restricts both GSK3 mediated phosphorylation of beta-catenin and β-TrCP access to beta-catenin, resulting in cytoplasmic accumulation of unphosphorylated beta-catenin and its shuttling to the nucleus (Li et al., 2012). Here, in the absence of beta-catenin, Tcfs - transcriptional binding proteins - associate with TLE/Groucho co-repressors and transcription is inhibited (Cavallo et al., 1998; Roose et al., 1998). Beta-catenin displaces TLE/Groucho and recruits co-activators, including

CREB binding protein (CBP), transiently converting Tcfs to activators to initiate transcription at target genes (Hikasa et al., 2010; Lee et al., 2009). Figure 1.11 summarises Wnt signaling.

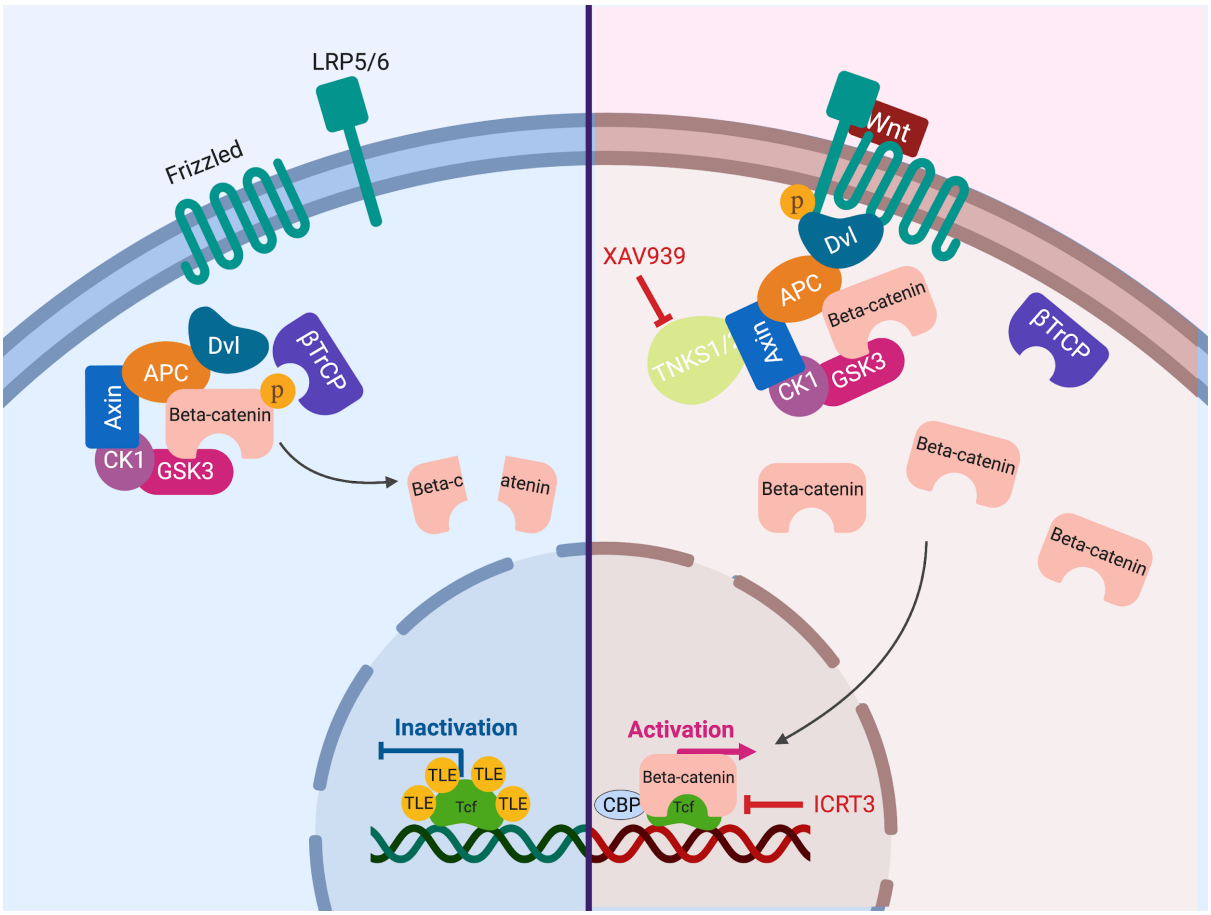

Figure 1. 11 Wnt signaling in GBM.

Schematic of the simplified Wnt signaling pathway in the 'Wnt off' and 'Wnt on' states showing the sites of action of two inhibitors, XAV939 and ICRT3.

1.5.2 Wnt signaling is active in the adult SVZ

Transgenic mouse studies, using mice with a Wnt activation reporter construct (Axin2-d2EGFP) have identified Wnt activated cells in the adult mouse SVZ (Adachi et al., 2007, Kalani et al., 2008). Proliferation of $Mash1^{+}$ cells could be induced in vivo with retrovirus mediated expression of stabilised beta-catenin, and inhibited by expression of the endogenous Wnt inhibitor DKK1, suggesting a role for Wnt in the regulation of adult neural stem cells in the niche (Adachi et al., 2007).

Wnt signaling is upregulated under conditions that promote symmetrical neural stem cell division, as in reconstitution of the VZ-SVZ after antimitotic treatment, and has therefore been suggested to function in maintaining the stem cell pool (Piccin and Morshead, 2011). A similar role has also been suggested for Wnt signaling in stem-like cells within brain tumors, with inhibition of Wnt signaling enhancing a differentiated phenotype in cultured tumor cells (Zheng et al., 2010). Wnt signaling may also occur in type C cells: elevated levels of beta-catenin result in increased progenitor proliferation within the VZ-SVZ and an increase in neurons in the olfactory bulb (Adachi et al., 2007).

1.5.3 Wnt signaling is implicated in cancer

The Wnt pathway has a role in the pathogenesis of various cancers, most notably in colorectal cancer where pathway mutations are common drivers. Germline loss of function mutations in one allele of the APC gene are responsible for the cancer predisposition syndrome Familial Adenomatous Polyposis (FAP), in which affected individuals develop large numbers of colonic polyps and have an 87% risk of colorectal cancer by age 45 (Soravia et al., 1998). Sporadic loss of the second allele results in a loss of the protein and destabilisation of the beta-catenin destruction complex, leading to accumulation and nuclear shuttling of beta-catenin. Most

sporadic cases of colorectal cancer contain loss of function mutations in both alleles of APC (Kinzler and Vogelstein, 1996). Mutations in genes encoding other Wnt pathway proteins are also seen; for example, 8% of tumours have mutations in R-spondins - potentiators of Wnt signaling (de Sousa E Melo and Vermeulen, 2016). Wnt pathway activation is not unique to colorectal cancer. Hyperactivation of the pathway is seen in hepatocellular carcinoma, due to AXIN1 and AXIN2 mutations (Satoh et al., 2000) and in some breast and ovarian cancers due to aberrant ligand production, rather than mutations (Bafico et al., 2004). Approximately 10% of medulloblastomas are defined as belonging to a Wnt active subtype due to the presence of activating mutations in beta-catenin (Kool et al., 2008). Activating mutations in beta-catenin have also been identified as the drivers of hair follicle tumours (Chan et al., 1999). Patients with active chronic myeloid leukaemia show high levels of Wnt activity, although no mutations have been identified (Jamieson et al., 2004).

1.5.4 Wnt signaling is active in GBM

Although Wnt pathway mutations are not common in GBM, in contrast to colorectal cancer (Paraf et al., 1997), beta-catenin is expressed in GBMs (Holland, 2000; Portela et al., 2019; Sareddy et al., 2009), as demonstrated by in situ RNA staining in the Ivy GBM Atlas Project (Figure 1.12A). Wnt pathway activation is associated with poorer prognosis in GBM (Holland, 2000; Liu et al., 2011; Sareddy et al., 2009). Several studies have focused on a role for Wnt in GSC stemness. Rheinbay et al show that ASCL1, a transcription factor upregulated in GSCs, particularly those of predominantly proneural type, has a role in maintaining tumorigenicity and is associated with increased Wnt activity. They further demonstrate that ASCL1 directly represses the Wnt inhibitor DKK1, suggesting the mechanism for its influence on the signaling pathway (Rheinbay et al., 2013). PLAGL2 has also been identified as an upregulator of Wnt pathway activity in GSCs and its activity leads to increased self-renewal and decreased

differentiation (Zheng et al., 2010). Depletion of beta-catenin in GSCs has been shown to reduce expression of stem cell markers and tumorigenicity and to cause G2/M arrest. Interestingly, the transcription factor FOXM1 forms a complex with beta-catenin and promotes cytoplasm to nuclear shuttling (Zhang et al., 2011). There is also evidence that pharmacological inhibition of Wnt leads to reduced clonogenicity in a range of patient-derived, serum-free and serum-exposed cell lines (Kahlert et al., 2015). An interesting study from Portela et al. proposes that GBM cells 'vampirize' Wnt from surrounding neurons, driving GBM cell proliferation and invasion, via JNK pathway activation, and simultaneous neuronal degeneration (Portela et al., 2019).

The Dirks lab have recently shown that, although Wnt signaling is widely active in GBM specimens and GSC cultures, there is a subset of GSCs, which have high ASCL1 expression, in which Wnt is important for self-renewal. They show that dual Wnt/Notch inhibition in these cells leads to increased neuronal differentiation (Rajakulendran et al., 2019). Further evidence that Wnt signaling is functionally important to the pathogenesis of GBM is demonstrated by Augustin et al who identify overexpression of Evi/Wntless, which is involved in Wnt ligand secretion, in GBM. They show that its depletion in GSCs leads to reduced cell proliferation, migration, apoptosis and tumorigenicity (Augustin et al., 2012). TCGA data reveal a weak but significant correlation between FOXG1 and beta-catenin, as well as Axin2, CyclinD1 and Myc, established Wnt target genes (Figure 1.12 C-F).

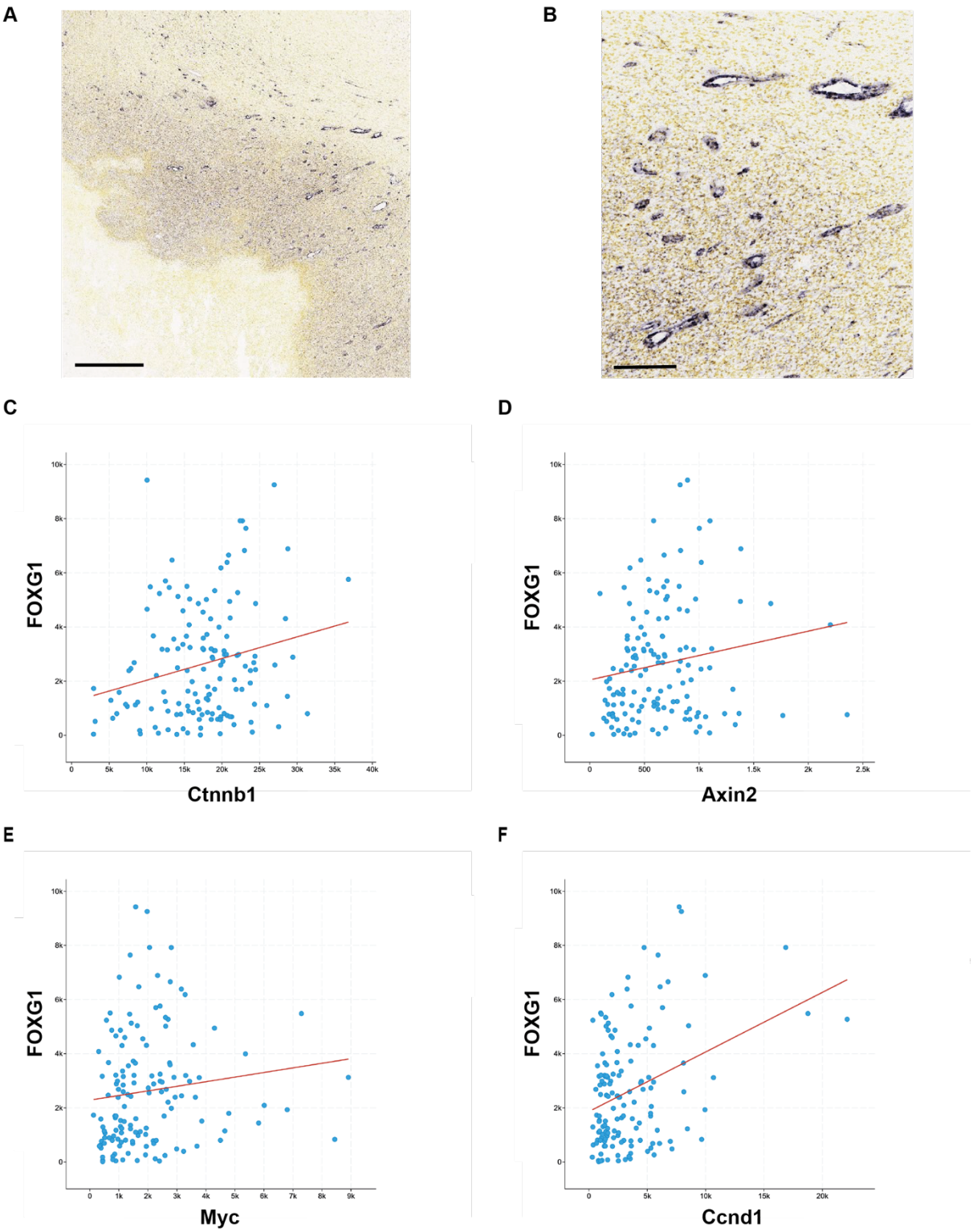
A
B
C
FOXG1
Ctnnb1
D
FOXG1
Axin2
E
FOXG1
Myc
F
FOXG1
Ccnd1

Figure 1. 12 Wnt signaling is active in GBM.

(A) In situ hybridisation for beta-catenin in an adult GBM specimen (Ivy GBM Atlas Project) - beta-catenin is seen in tumour tissue, most markedly in perivascular regions. Scale bar 800μm. (B) Expanded image to show perivascular beta-catenin. Scale bar 200μm. (C-F) TCGA data for mRNA expression of FOXG1 in GBM specimens, correlated to expression of CTNNB1 (Spearman 0.18, p=0.0293; Pearson 0.22 p=8.939e-3), AXIN2 (Spearman 0.20, p=0.0169; Pearson 0.17 p=0.0496), MYC (Spearman 0.25, p=3.110e-3; Pearson 0.12 p=0.141) and CCND1 (Spearman 0.23, p=6.769e-3; Pearson 0.35 p=2.297e-5). Data points represent each of 141 samples, of 543 analysed by Brennan et al. for TCGA, for which mRNA expression (RNA-Seq) data were available (Brennan et al., 2013). Plots, and associated statistical analyses, were created using the cBioPortal platform (Cerami et al., 2012; Gao et al., 2013).

1.5.5 FOXG1 binds TLEs, co-repressors of Tcf/Lef

As described above, TLEs (known as Groucho in *Drosophila*) are repressors of Tcf/Lef proteins, transcription activators downstream of Wnt signaling. FOXG1 is known to interact with TLEs, most likely via a C-terminal YWPMSPF motif (Buscarlet et al., 2008). FOXG1 and TLEs are known to be co-expressed in the neural progenitor cells of the developing telencephalon (Yao et al., 2001). Verginelli et al. showed that TLEs co-precipitate with FOXG1 when it is immunoprecipitated from cultured GSCs (Verginelli et al., 2013). Co-immunoprecipitation has also been shown from mouse embryonic telencephalon (Yao et al., 2001). TLE1 (but not TLE2) is expressed in GBM at higher levels than in normal brain and its expression co-localises with FOXG1. As with FOXG1, high TLE1 expression correlates with poor prognosis. Furthermore, TLE1 knockdown phenocopied the effects of FOXG1 knockdown in reducing GSC proliferation and tumorigenesis (Verginelli et al., 2013).

Deletion of the first 119 amino acids of FOXG1 (Foxg1 120-481), or the last 145 (Foxg1 1-336), does not abolish binding to TLE1, but a further deletion (Foxg1 120-275) does, suggesting that the relevant binding domain is found between AA 276 and 336. The interaction potentiates FOXG1-mediated transcriptional repression (Yao et al., 2001). There is another putative TLE interacting domain, in the FOXG1 protein, of direct interaction with TLEs: an N-terminal eh1 motif. This seems relevant to interactions with TLE2 in xenopus but most studies identify the C-terminal motif as the key binding site (Roth et al., 2010). Consistent with the characterisation of FOXG1 as predominantly a transcriptional repressor, Dali and colleagues found that more genes were upregulated than downregulated when they knocked down FOXG1 or TLE1 in GSCs. They identified CHAC1, a Notch inhibitor, as a FOXG1:TLE1 target, suggesting that FOXG1 overexpression may enhance Notch signaling (by repressing expression of this inhibitor of the pathway) (Dali et al., 2018).

1.6 Aims and hypotheses

Existing data show that increased expression of FOXG1 has a role in driving exit from quiescence in NSCs and GSCs and that it is overexpressed in GBM and associated with a poor prognosis. In vitro data indicate that although FOXG1 can support exit from quiescence this is a relatively inefficient process. We therefore predicted that additional pathways downstream or operating in parallel with FOXG1 cooperate to drive exit from quiescence. This project aimed to identify such pathways. Through small molecule screening I identified a putative activator of Wnt, and went on to validate this is through the canonical Wnt/beta-catenin pathway. The results chapters cover these areas:

1. GSK3 inhibition and FOXG1 act synergistically to drive exit from quiescence in NSCs
2. This synergistic effect is due to an interaction between FOXG1 and Wnt signaling
3. The FOXG1/Wnt synergistic effects are disease-relevant and operate in vivo
4. The FOXG1/Wnt cooperation is also observed in human GSCs
5. The synergy is dependent, in part, upon the FOXG1 Groucho/TLE binding domain.

Chapter 2

Methods

2.1 Cell culture

Cell lines were cultured at 37°C and 5% CO_2 and grown on uncoated tissue culture plastic. Dissociation was performed using Accutase (Sigma). Cells were passaged 1:6 to 1:8, or media changed as appropriate, every 3-4 days.

2.1.1 Self-renewal media

Mouse and human neural stem (NS) cells and GBM neural stem cells (GNS) were grown under serum-free conditions in DMEM F-12 supplemented with N2 and B27, penicillin-streptomycin, 1 μg/ml Laminin, 10 ng/ml EGF and 10 ng/ml FGF2. Dox media also contained doxycycline hyclate (1 μg/ml unless otherwise stated). Chiron was used at 3μM unless otherwise stated.

2.1.2 BMP4 media and BMP/FGF2 media for quiescence assays

BMP4 media composition was as for self-renewal media, except that the growth factors EGF and FGF2 were replaced with BMP4 10ng/ml (Peprotech). BMP/FGF2 media contained BMP4 10ng/ml and FGF2 10ng/ml but no EGF.

2.1.3 Freezing media

Freezing media comprised DMEM-F12, supplemented with 10% dimethylsulfoxide (DMSO).

2.1.4 Growth curves

Monitoring of growth kinetics was achieved with the Incucyte Zoom live cell imaging system (Essen Biosciences) and its built in software.

2.2 Immunocytochemistry

Cells were washed with PBS and fixed in 4% paraformaldehyde for 10 minutes at room temperature. The cells were washed and permeabilised in PBST (PBS with 0.1% Triton), then blocked for 30 minutes in blocking solution comprising PBST with 0.1% BSA and 3% goat serum. Overnight incubation was performed with primary antibodies suspended in blocking solution at the concentrations indicated. Residual primary antibody was removed with 3 rapid and 3 x 5-minute PBS washes, then secondary antibodies suspended in PBS at the concentrations indicated were applied and incubated for one hour. Wash steps were repeated as before, and the cells were incubated in 1:5000 DAPI (Sigma-Aldrich) for nuclear counter-staining. Images were obtained using the Nikon TiE, Leica DMi8 or the PerkinElmer Operetta high content imaging system and Harmony software.

2.3 Western Immunoblotting

Cells were dissociated with Accutase, pelleted, washed with PBS and lysed in buffer consisting of 150mM NaCl, 20mM TrisHCl, 1% NP40, 2mM EDTA, 1mM NaF, 0.1% SDS freshly supplemented with protease inhibitors as follows: AEB5F 1:200; Leupeptin 1:1000; Benzamidine 1:1000; DTT 1:2000. Lysates were incubated for 30 min at 4ºC and centrifuged at 13,000g for 15 min at 4ºC for supernatant collection. Following protein quantification using the Pierce Assay (ThermoFisher), samples were mixed with loading buffer containing 10% 2-

mercaptoethanol and denatured at 95ºC for 5 min. Electrophoresis was performed on polyacrylamide gels using BioRad system and Spectra Multicolor Broad Range Protein Ladder (Fermentas). Wet electroblotting was used for transfer of proteins onto Immobilon-P PVDF membrane (Millipore). Membranes were blocked using 5% milk powder in TBS-T for 1h at room temperature and incubated with primary antibody at appropriate dilutions at 4ºC overnight. Following washes with TBS-T at room temperature, membranes were then incubated with species-specific horseradish peroxidase-coupled secondary antibodies for 1 hour at room temperature and developed with a homemade ECL solution. Western blotting was conducted by Carla Blin unless otherwise stated.

2.4 Antibodies used

2.4.1 Primary Antibodies

Antigen	Host/Clone	Reactivity	Dilution	Supplier
Beta-catenin	Mouse IgG1	H,M	IF 1:500 WB 1:1000	BD
Phospho-EGFR (Y1068)	Rabbit IgG	H,M	WB 1:1000	CST
FoxG1	Mouse IgG2a (17B12)	H,M	IF 1:3; WB 1:15	Pollard lab
GAPDH	Mouse IgG1 (6C5)	H,M	WB 1:40000	ThermoFisher
FoxO3	Rabbit IgG (75D8)	H,M	IF 1:200 WB 1:1000	CST

Gfap	Chicken polyclonal	H,M	IF 1:100	Biolegend
Gfap	Mouse IgG1 (G-A-5)	H	IF 1:100, WB1:1000	Sigma G3893
GFP	Chicken polyclonal	Recombinant GFP	IF 1:500	Abcam 13970
Id1	Rabbit monoclonal	M	IF 1:100	BioCheck
Ki67	Rabbit IgG	H,M	IF 1:100	ThermoFisher
Nestin	mIgG1	M	IF 1:10	DSHB
Nmyc	mIgG1	H,M	IF 1:50	Santa-Cruz
Olig2	Rabbit polyclonal	H,M	IF 1:200	Millipore
Pten	Rabbit IgG (138G6)	H,M	WB 1:1000	CST
Sox2	mIgG2a	H,M	IF 1:50, WB 1:400	R&D
V5 tag	mIgG2b	-	IF 1:1000	eBioscience
Wif1	Rabbit IgG (EPR9385)	H,M	WB 1:2000	Abcam

Table 2.1 List of primary antibodies

2.4.2 Secondary Antibodies

Antigen	Host	Conjugation	Dilution	Supplier
Various IgG	Donkey	Alexa Dyes	IF 1:1000	Invitrogen
Rabbit IgG	Goat	HRP	WB 1:5000	Novex
Mouse IgG	Goat	HRP	WB 1:10000 to 1:40000	Novex

Table 2.2 List of secondary antibodies

2.5 Colony forming assays

Cells were plated at a density of 10 cells/mm^2 (10,000 cells per well of a 6 well plate), in NS cell media in the absence of EGF/FGF-2 and supplemented with BMP4 (10 ng/ml). After 24hrs, media was replaced fully with NS cell media containing EGF/FGF-2 with or without Dox. Media was then replaced every 3-4 days. Following 10-12 days, plates were fixed using 4% PFA for 10min at room temperature. Colonies were stained using methylene blue for 30 min. Plates were washed gently with deionised water and allowed to dry. Plates were then imaged on a Celigo Image Cytometer (Nexcelom Bioscience). Colonies were counted manually using the Cell Counter plugin on FIJI. Three technical replicates were averaged to give the mean number of colonies per biological replicate

2.6 EdU incorporation assays

EdU staining was performed using the Click-iT EdU Alexa Fluor 647 assay kit (Life Technologies) according to manufacturer's guidelines. Images were obtained using either the PerkinElmer Operetta high content imaging system and Harmony software. Columbus software was used to design a pathway for the quantification of positive and negative cells. Nuclei were identified and signal intensity determined. A threshold was set above which intensity cells were clearly positive. Where background intensity varied significantly between wells, a sliding parabola correction was applied.

2.7 Taqman qRT-PCR

RT-qPCR was performed using standard protocols. RNA was isolated and gDNA eliminated using the RNeasy Mini Kit (Qiagen, 74104). Reverse transcription was performed using SuperScript III (Invitrogen) and qPCR was performed using Taqman qPCR probes and Taqman Universal PCR Master Mix (Applied Biosystems) on the QuantStudio 7 Flex (Applied Biosystems) instrument. No RT and water controls were run on each plate to ensure the absence of contamination. Technical replicates were run to ensure pipetting accuracy. Data were analysed using the ddCt method; this method assumes 100% PCR efficiency which is guaranteed with TaqMan assays. Replicate Ct values were averaged and normalised to the housekeeping gene, Gapdh (to give dCt). These values were then normalised to a calibrator sample (to give ddCt).

The following TaqMan assays (Life Technologies) were used: Gapdh (Mm99999915_g1), Egfr (Mm00433023_m1, Hes5 (Mm00439311_g1), Tlx (Mm00455855_m1), mcm2 (Mm00484815_m1), Sox2 (Mm03053810_s1), Prom1 (Mm00726334_s1), Bmi1 (Mm03053308_g1), FoxG1 (Mm02059886_s1), FOXG1 (Hs01850784_s1), Foxo6

(Mm00809934_s1), Gfap (Mm99999915_g1), p21 (Mm04205640_g1), Nfix (Mm00477791_m1), Pdgfra (Mm00440701_m1), Ephr2 (Mm01215897_m1), FoxO3 (Mm00490673_m1), Id1 (Mm00775963_g1), Sox9 (Mm0083422_m1) Gli3 (Mm0049654_m1), Gli1 (Mm00492345_m1), Axin2 (Mm00443610_m1), Myc (Mm00487804_m1), Wif1 (Mm00442355_m1).

2.8 Derivation of stable transgenic cell lines

2.8.1 Cell lines used and generated in this thesis

Parent line	Name	Modifications/notes
ANS4		Derived from adult BL6 SVZ of mice
ANS4	F6	TRE_FOXG1_V5_IRES_BSD (Bulstrode et al., 2017)
F6	F6-Tcf/lef	Six copies of the TCF/Lef response elements together with the hsp68 minimal promoter from the TCF/Lef-LacZ reporter construct, inserted into the AseI/Nhe1sites of pCMV:H2B-mCherry. The plasmid used was a gift from Prof A-K Hadjantonakis.
F6	F6BC1	ERT2 Inducible active beta-catenin (point missense mutation in N-terminal degradation domain) flanked by LoxP sites. GFP reporter of recombination mediated excision.
F6BC1	F6BC1NPE	Excision of *Pten* and *Nf1*. Piggybac mediated overexpression of EGFRvIII.
F6BC1NPE	EM4C6	Clonal line derived after selection in NSG mouse
ANS4	FS3	TRE_FOXG1_V5_2A_SOX2_IRES_BSD (Bulstrode et al., 2017)
FS3	FOD3	TRE_FOXG1_V5_2A_SOX2_IRES_BSD; FOXO3-/- (Bulstrode et al., 2017)
ANS4	S15	TRE_SOX2_IRES_BSD
FF NS	FF	Foxg1fl/fl; GFP reporter of excision (Miyoshi and Fishell, 2012)
Hes5GFP NS	Hes5GFP	Derived from Hes5GFP mouse (Basak and Taylor, 2007)
G7	G7	Patient-derived GSC clonal line (Pollard et al., 2006)
G7	G7 FOXG1-/- (G7-A)	FOXG1 -/-. 23-bp frameshift insertion at the second allele; demonstrated loss of FOXG1 protein by immunoblotting (Bulstrode et al., 2017)
G7-A	G7-A-RWT	Endogenous FOXG1 -/-, rescue with CAG_FOXG1_HA_Hygro
G7-A	G7-A-RGBD	Endogenous FOXG1 -/-, rescue with CAG_FOXG1GBD-_HA_Hygro
GBM002	GBM002	Paediatric high grade GBM patient-derived GSC clonal line with H3.3 G34R allele (Mohammad et al., 2017)
GBM002	GBM002 FOXG1-/- (GBM002-W4)	FOXG1 -/-. Using sgRNA and targeting vectors as previously validated
GBM002-W4	GBM002-W4-RWT	Endogenous FOXG1 -/-, rescue with CAG_FOXG1_HA_Hygro
GBM002-W4	GBM002-W4-RGBD	Endogenous FOXG1 -/-, rescue with CAG_FOXG1GBD-_HA_Hygro

Table 2.3 List of cell lines used and created.

2.8.2 Plasmid Preparation

OneShot Top10 competent bacteria were transformed with plasmid constructs using a 30 second heat shock in a water bath at 42ºC, and grown on LB agar plates with appropriate antibiotic selection. Mini-prep and midi-prep were performed using the appropriate Qiagen kits according to manufacturers' instructions.

2.8.3 Design and construction of CRISPR sgRNAs and PiggyBac plasmids for generation of NPE lines (by Ester Gangoso).

For TSG knockout, two gRNAs were designed to remove or generate indels, these were introduced to the most disease relevant gene regions in the case of GBM drivers. CRISPR sgRNAs were designed using the Optimized CRISPR Design tool (http://crispr.mit.edu). Sequences are provided in Table 2.4. For construction of sgRNA-encoding plasmids, single-stranded oligonucleotides containing the guide sequence of the sgRNAs were annealed, phosphorylated and ligated into BsaI site of U6-*BsaI*-sgRNA backbone (kindly provided by S. Gerety, Sanger Institute) or U6-*BbsI*-CBh-Cas9-T2A-mCherry backbone (this was a gift from Ralf Kuehn, Addgene plasmid # 64324) (Chu et al., 2015).

Gene	Species	Name	Sequence
Pten	*M. musculus*	Pten_L	GGTTTGATAAGTTCTAGCTG
Pten	*M. musculus*	Pten_R	GTAAATACGTTCTTCATACC
Nf1	*M. musculus*	Nf1_L	TCATCATCACATCTTCGGAT
Nf1	*M. musculus*	Nf1_R	TCGGCTGCTTTGGAACAATC
Foxo3	*M. musculus*	Foxo3_gRNA1	CGCGTTCAGAATGAAGGCACGGG
Foxo3	*M. musculus*	Foxo3_gRNA2	CGCATGAAGCGGCTGTGCAGGG
FOXG1	*H. sapiens*	FOXG1_gRNA1	CCGCCCTGGACGGGGCTAA
FOXG1	*H. sapiens*	FOXG1_gRNA2	GCAAGGGCGAGCCGGGCGG

Table 2.4. List of the CRISPR gRNA sequences used for knockout gene targeting.

PiggyBac expression vectors were constructed via Gateway cloning with the exception of the EGFRvIII construct. The LUC-2A-GFP was PCR amplified from existing plasmids (gift from M. Pule, UCL). PCR products were cloned into Gateway pDONR^{TM}221 using BP cloning. The cassettes were then delivered into the intermediate targeting vectors via Gateway LR cloning. Plasmids were sequence verified. EGFRvIII was amplified from existing plasmids (gift from A. Medvinsky lab) incorporating BrsGI restriction sites to clone into a PB-CAG-Ires-Hygro (gift from Keisuke Kaji). Primers used for construction are provided in Table 2.5.

hEGFRvIII_Fwd	ATCACAAGTTTGTACAATGCGACCCTCCGGGACGGCC
hEGFRvIII_Rev	CACCACTTTGTACATCATGCTCCAATAAATTCACT
3FLAG-LUC-2A-GFP Fwd	GGGGACAAGTTTGTACAAAAAAGCAGGCTTCGCCACCATG GACTACAAAGA
3FLAG-LUC-2A-GFP Rev	GGGGACCACTTTGTACAAGAAAGCTGGGTTTTACTTGTACA GCTCGTCCA

Table 2.5. Primer sequences used for plasmid construction.

2.8.4 Cell transfection

NSCs were transfected using the DN 100 program of a 4D nucleofection system (Lonza). 1-2 x 10^6 cells were resuspended in 100µl of SG transfection solution (Lonza) containing a maximum of 3µg DNA. For CRISPR targeting, guide RNAs (x2), targeting vector (where appropriate) and Cas9 nickase were transfected in a 1:1:1:2 ratio. For inducible PiggyBac constructs, DNA comprised pBASE, pCAG-Tet3G and pDEST-TetOn vector in 1:1:2 ratios. For multiplex experiments, ratios were equal and the amount of DNA used was 4.2µg. Media was changed 6 hours after transfection. Cells were incubated for 48 hrs post-transfection prior to FACS sorting, where this was required. For random integration, 2 million cells were transfected with 1µg of linearised plasmid DNA.

2.8.5 Drug selection and clonal expansion.

Cells with stable integration of plasmids were selected for 5-7 days using 5µg/ml blasticidin, 100µg/ml hygromycin or 1µg/ml puromycin. Each of these antibiotics produced uniform cell death within 7 days in untransfected human NS and GNS. After 14 days, expression, or

inducible expression, was confirmed by immunofluorescence, qPCR and Western blot. An exception to this was inducible beta-catenin, which was confirmed by TOPflash assay. For NPE-Multiplex experiments, GFP and mCherry double positive cells were sorted and collected in tubes. These cells were expanded and maintained for 5 days with hygromycin and 6 days with blasticidin and transplanted orthotopically in the SVZ of NOD-SCID mice, without picking colonies. After tumour formation, a cell line was derived and individual colonies were picked into 2 x 24-well replica plates and expanded for cell banking and gDNA extraction. Loss of *Nf-1* and *Pten* and gain of EGFRvIII were confirmed in the resultant cell lines by Western blot.

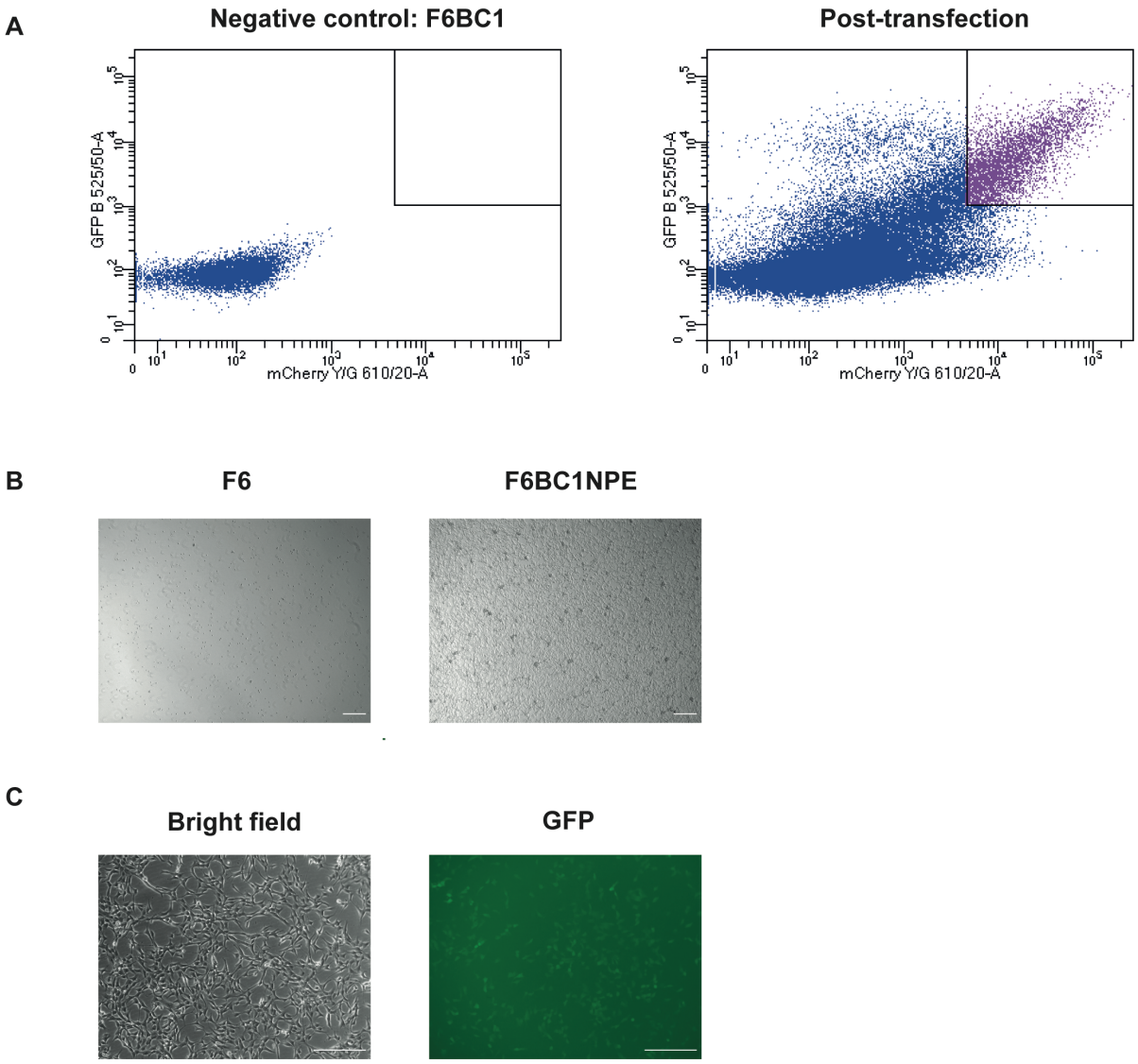

Figure 2. 1 Generation of tumorigenic lines lacking *Pten* and *Nf-1* and expressing EGFRvIII.

(A) FACS selection for GFP and mCherry double positive cells 48 hours post-transfection. (B) Resistance to puromycin confirms the persistence of the beta-catenin cassette. (C) GFP expression can be seen. Scale bars 150µm.

2.8.6 Gateway cloning

Gateway cloning was conducted according to standard protocols. For the creation of the FOXG1 rescue cell lines, DNA containing the sequence for FOXG1, or the same sequence without bases coding for AA 307-317: (YWPMSPFLSLH) with an HA tag, flanked by attL1&2 sites, was obtained from ThermoFisher (GeneArt) and midi-preps were performed. LR clonase was used to recombine entry clones into destination vector PB-CAG-DEST-pA-PGK-Hygro-PB, and resultant expression clones were verified by restriction digest (with AgeI, Figure 2.2C). Cells were transfected with this expression clone and a plasmid encoding hyPBase, using the Amaxa nucleofection system prior to selection in hygromycin.

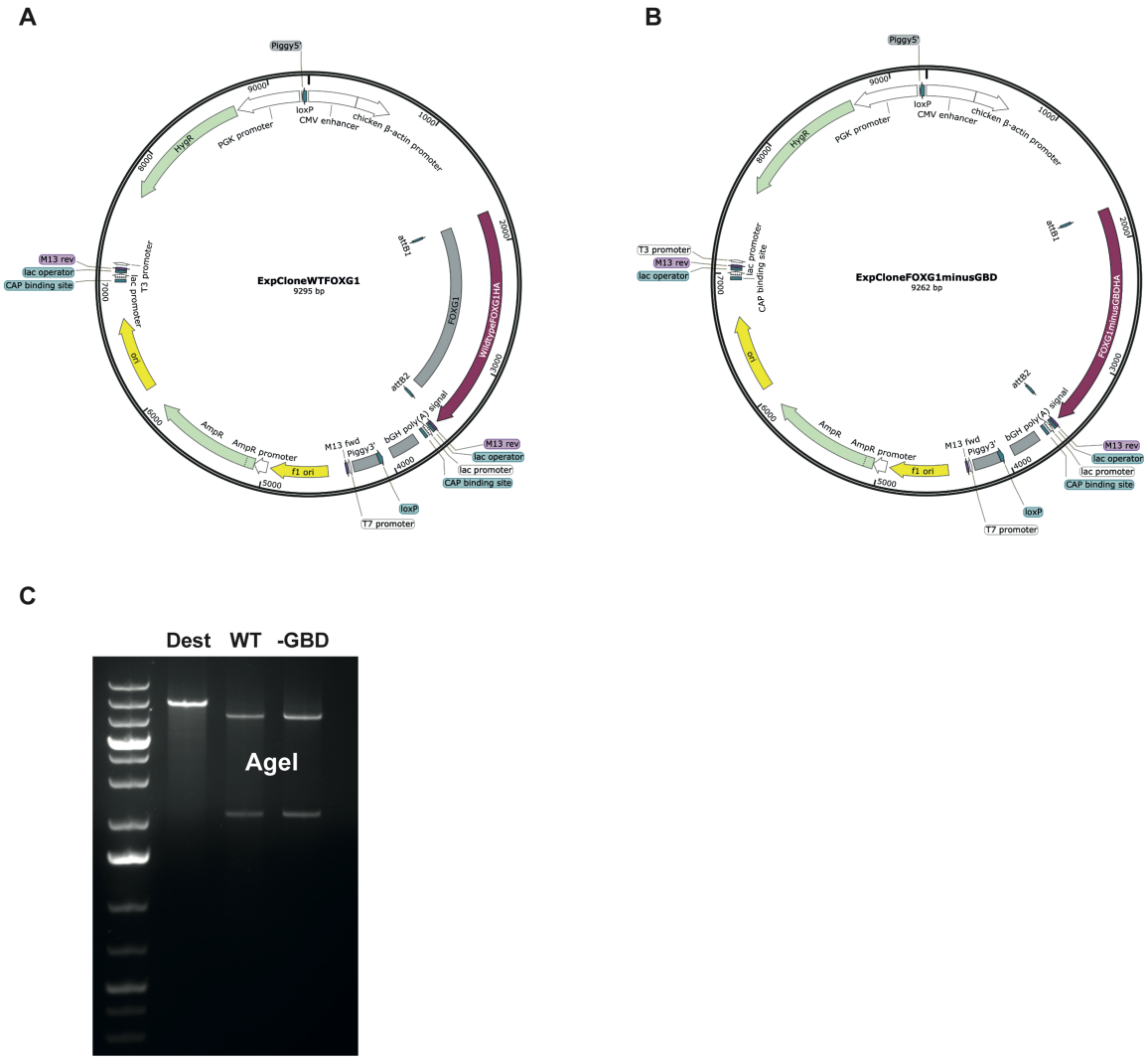

Figure 2. 2 FOXG1 rescue plasmids.

(A&B) Plasmid maps of expression vectors for FOXG1 and FOXG1 lacking the GBD, after LR recombination. (C) Restriction digest with AgeI confirmed expected bands in the destination vector and expression vectors.

2.8.7 Specifics of creation of the inducible beta-catenin cell line

Competent *E.coli* were transformed with the plasmid and ampicillin resistant colonies selected for midi-prep. The plasmid was then linearised by ScaI restriction digest and the resultant linear DNA was gel-extracted. Correct digestion was confirmed by restriction digests with NotI and BsaI, showing appropriately sized bands on a gel (Figure 2.3B). F6 cells were nucleofected with the linearised DNA for random stable integration and transfected cells expanded before exposure to puromycin. Surviving colonies were picked, expanded and then re-exposed these to puromycin over several passages to confirm resistance (Figure 2.3C). Functionality was confirmed for one of the clones using a TOPflash reporter assay (Molenaar et al., 1996), section 2.13. Transfection with a Cre-expressing plasmid resulted in GFP expression, a reporter of excision of the beta-catenin cassette, in ~50% of cells (Figure 2.3F). This was consistent over multiple transfection experiments using the Amaxa, DN100 programme, and 1μg of plasmid to transfect 2 million cells

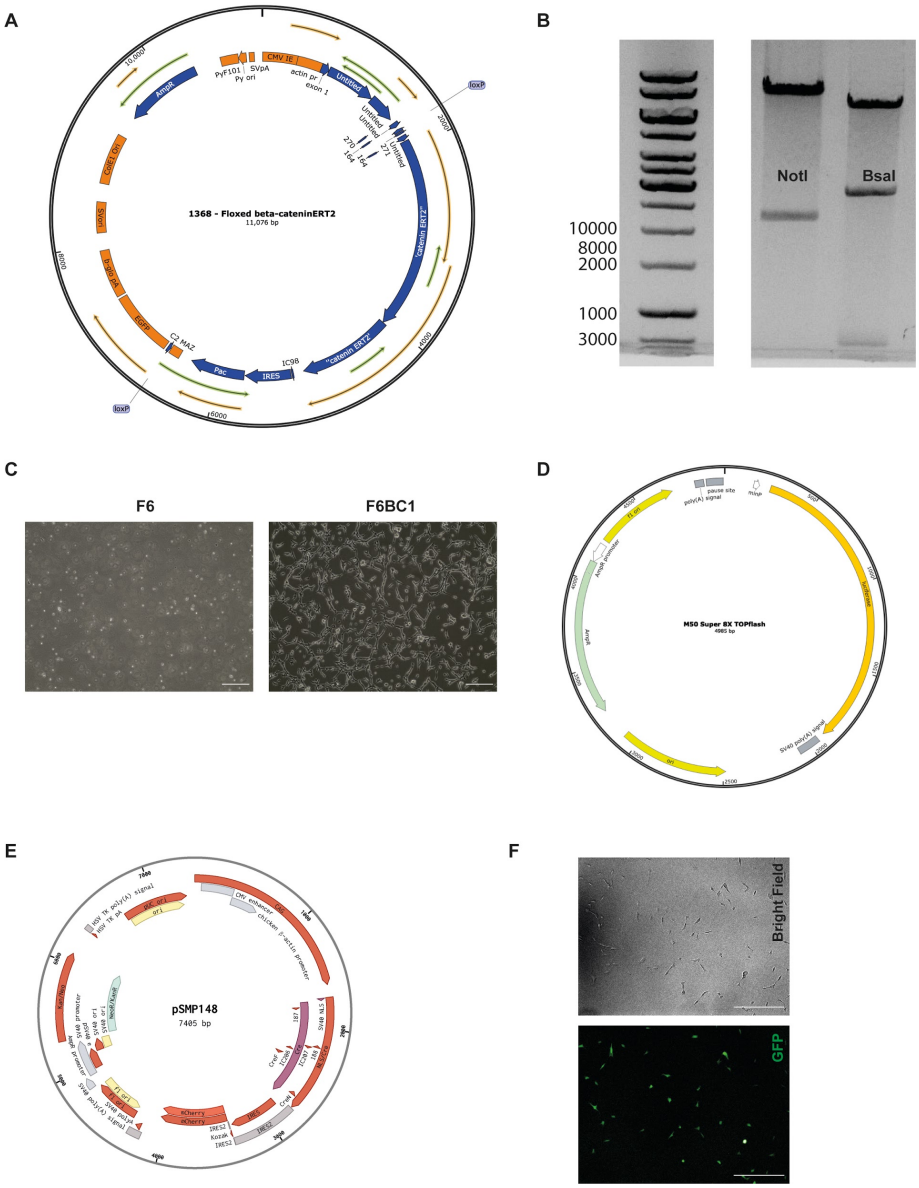

Figure 2. 3 Creation of a cell line with tamoxifen-inducible constitutively active beta-catenin.

(A) Floxed beta-catenin ERT2 plasmid. (B) Restriction digests of the linearised plasmid, with NotI and BsaI confirm bands of the expected sizes. (C) After transfection and clonal selection, a cell line (F6BC1) with stable integration of the cassette, survives in puromycin over several passages; the parental cell line does not survive in puromycin. Scale bars 150µm. (D) The TOPflash plasmid. (E) Cre-mCherry plasmid. (F) Transfection and recombination efficiency was around 50%. Brightfield and GFP images of live cells. Scale bars 150µm.

2.8.8 Specifics of creation of the Tcf/lef reporter cell line

A plasmid encoding mCherry under the control of 6 copies of the Tcf/Lef response elements together with the hsp68 minimal reporter, a gift from Prof A-K Hadjontanakis, (Figure 2.4A). was linearised with EcoRV. Restriction digest with BsaI confirmed the expected bands (Figure 2.4B). F6 cells were transfected with the linear DNA, using the Amaxa nucleofection system, and sorted for mCherry positive cells with FACS. In retrospect, the selection ought to have been done with G418 (geneticin, the neomycin variant), as this would select for all cells with the cassette whereas flow sorting selected those in which the protein was being expressed in baseline conditions.

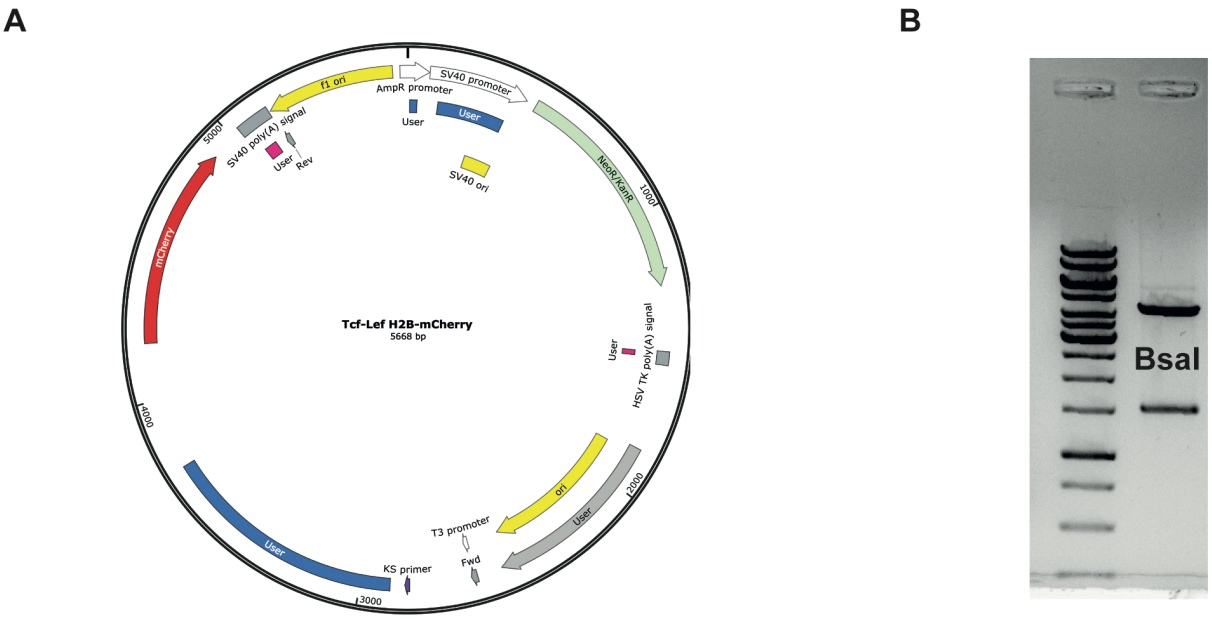

Figure 2. 4 Creation of the Tcf/lef mCherry cell line.

(A) Plasmid used. (B) Restriction digest with BsaI, after linearisation, confirming expected bands.

2.9 Cell-based phenotypic screening

F6 cells were plated in 96 well plates at 1000 cells/well (30 cells/mm^2) in BMP4 media using the Multidrop Combi liquid handler (ThermoFisher). At 24 hrs, media were changed and compounds from the StemSelect (Millipore) library added using the EpMotion (Eppendorf). At day 7, cells were fixed with 4% PFA, washed with 0.1% PBST, stained for 30 mins with HCS Cell Mask (ThermoFisher) and then with DAPI. Doxycycline concentration was 1µg/ml. DMSO concentration was 0.4%. The concentration of library compounds varied, depending on the library concentration: all compounds were used at 1:10000. All steps were performed using the Multidrop Combi. Imaging was conducted in PBS using the Operetta (PerkinElmer) and phenotypic data extracted using Columbus software. Data were analysed and hits called using Spotfire (Tibco) and Stratominer (Core Life Analytics).

2.10 RNAScope

RNAScope was conducted on 5µm slices of FFPE tissue prepared from human GBM samples obtained at the time of primary surgery by Paul Brennan. The RNAScope Multiplex Fluorescent Kit v2 Assay (ACD) was conducted in accordance with manufacturer's instructions. Slices were examined with an inverted fluorescence microscope (Leica).

2.11 RPPA analysis

Cell lysates were prepared and analysed as previously described (Teo et al., 2018). Briefly, medium was removed from the plates and cells were rinsed twice with PBS. Cells were lysed on ice for 20 minutes with occasional shaking every 5 minutes. Cell lysates were collected with a scraper and clarified by centrifugation at 18,000 rcf for 10 min at 4ºC. Clarified supernatants

in biological triplicate were adjusted to 2 mg/mL concentration and printed onto nitrocellulose-coated slides (Grace Bio-Labs) in a dilution series (four serial 2-fold dilutions) in technical triplicate using an Aushon 2470 arrayer (Aushon Biosystems). Slides were blocked, probed with validated primary antibodies and detected with DyLight 800-conjugated secondary antibodies (New England BioLabs). Slides were read using an InnoScan 710-IR scanner (Innopsys) and quantified using Mapix (Innopsys). Relative fluorescence intensities were normalised to respective FastGreen-stained spots (total protein), and data were computationally analysed as previously described in (Byron, 2017; Teo et al., 2018). Sixty antibodies were selected from an available 177. Triplicate analysis of two independent replicates was conducted. Clustering analysis was carried out using Cluster 3.0 and Java TreeView software, in accordance with (Byron, 2017).

2.12 Nanostring analysis

RNA was extracted from cells, and gDNA eliminated, using the RNeasy Mini Kit (Qiagen, 74104). The Nanostring PanCancer Pathways panel was used. Hybridization, purification and imaging on the nCounter system were conducted in accordance with manufacturers' protocols. Raw protein count data were processed by applying background thresholding and content normalization in NanoString nSolver 4.0.

2.13 Topflash assay

Cells were transfected with a Renilla luciferase plasmid and either the TOPflash plasmid, containing the TCF/LEF-Firefly luciferase expression construct (7 copies of the TCF/LEF transcriptional activator site upstream of firefly luciferase (Figure 2.3D) a gift from Randall Moon via Addgene) or the FOPflash control, in which the TCF/LEF sites are mutated and

cannot be activated by beta-catenin. Renilla activity was recorded as a control for transfection efficiency and results were normalised to Renilla activity prior to determining the ratio between TOPflash and FOPflash firefly luciferase activity. This assay is usually conducted with lipofection but NS cells are refractory to lipofection and so I employed nucleofection using the Amaxa system and optimised the plasmid quantities for this system. TOPflash and FOPflash plasmids were a gift from Randall Moon via Addgene. The backbone of the TOPflash plasmid (12456, M50 Super 8x TOPflash) is the pTA-Luc vector of Clontech, which provides a minimal TA viral promoter driving expression of the firefly luciferase gene. 7 TCF/LEF binding sites were cloned into the Mlu1 site of this vector (7 copies of: AGATCAAAGGgggta, with TCF/LEF binding site in CAP letters, and a spacer in lower case, separating each copy of the TCF/LEF site). In the FOPflash plasmid (12457, M51 Super 8x FOPflash) there are 6 mutated TCF/LEF binding sites that were cloned into the pGL3 vector (Promega), which contains a minimal promoter followed by a firefly luciferase open reading frame. This 134bp fragment was gene synthesized and cloned into the ASP718 and XMA-1 sites of the vector. The pGL4-hRLuc (renilla) plasmid (Promega) was used to control for transfection efficiency. The Promega Dual Luciferase Assay was conducted according to manufacturers' instructions.

2.14 TUNEL assay

The Click-IT TUNEL AlexaFluor 488 assay (ThermoFisher) was conducted according to manufacturers' instructions on cells fixed with 4% PFA and permeabilised with 0.1% PBST. Images were obtained using the Operetta and Columbus software was used to quantify positive cells. A positive control, supplied in the kit, was run and gave scores of >90% in each case.

2.15 Flow cytometry

The BD LSRFortessa (SORP) and BD Fusion Cell Sorter for analysis and sorting respectively. Cells were dissociated with Accutase, pelleted by centrifugation, washed with PBS and resuspended in FACS buffer (PBS + 2% BSA). DAPI was used to exclude non-viable cells from analysis. For mCherry quantification, clonal lines were expanded in EGF+FGF2, plated in BMP4 for 24 hrs, then EGF+FGF2 +/- dox for 48 hrs prior to flow analysis for mCherry. F6 cells not transfected with the TcfmCherry cassette were used as a negative control. Mouse NSCs expressing mCherry were used as a positive control. 100000 events were acquired. Gating was applied and populations quantified using BD FACSDiva software. For sorting after transfection of NPE cells, the bulk population of cells was sorted 48 hours after transfection. Untransfected F6BC1 cells were used as a negative control. No antibodies were used.

2.16 Radiation experiments

Cells were cultured in adherent monolayer and irradiated in a Gammacell 40 Exactor (Best Theratronics) or sham irradiated. When removed from the incubator, culture plates were sealed with Parafilm (Bemis) until returned.

2.17 Mouse experiments

2.17.1 Care of mice and transplantation

All treatments and procedures on mice were performed in accordance with protocols approved by Home Office UK guidelines under a project license to S.Pollard, (PC0395462) at the University of Edinburgh. Mice were maintained on a regular diet in a pathogen-free facility on a 12 hr light/dark cycle with unlimited access to food and water. Intracranial transplantation of

NSCs was performed using a stereotaxic frame to inject 200,000 cells (unless otherwise stated) in 2 µl into 6- to 8-week-old male NOD/SCID/GAMMA (NSG) mouse striatum, following administration of isoflourane general anesthesia and Rimadyl analgesic. Coordinates were 0.6mm anterior and 1.5mm lateral to the bregma and 2.4 mm deep. Cell preparation and procedures were done as previously described in (Pollard et al., 2009). Cell preparation was conducted by me. All transplantations were conducted by Neza Alfazema.

2.17.2 Administration of Dox and Tamoxifen

Mice were given doxycycline 2mg/ml in drinking water with 5% glucose, or 5% glucose alone. This dose of doxycycline was based on the dose most often used in mouse studies. There is evidence that lower doses may be as effective, but this evidence does not include data on activity within the brain (Redelsperger et al., 2016). Doxycycline is known to cross the BBB in humans and in mice, although the mouse data relates to intraperitoneally delivered doxycycline (Lucchetti et al.). There is no evidence of major toxicity from this dose of doxycycline, although mice are noted to drink less than controls, necessitating sweetening of the water with glucose, and on post-mortem analysis some mice are found to have moderate caecal distension and neutrophilic gastritis (Redelsperger et al., 2016). Where tamoxifen was administered, mice were given intraperitoneal tamoxifen 3mg (approx 100-120mg/kg) or sunflower oil vehicle. This dose was chosen based on a number of considerations. An average total dose of tamoxifen in recombination experiments is around 400mg/kg in divided doses (Valny et al., 2016). A schedule of divided doses appeared to cause unacceptable toxicity (weight loss, slow recovery from anaesthetic, unkempt coat) in mice. The concentration of the active metabolite, 4-hydroxytamoxifen, in the mouse brain does not rise with dose increases over 200mg/kg in two divided doses and there is a short (36 hour) window of effective concentrations (Valny et al., 2016). Practical considerations meant

that a single IP injection was felt to be a reasonable initial test dose. Monitoring of tumour growth in vivo was conducted using the IVIS Lumina LT Series III (PerkinElmer) instrument. IP injections and IVIS imaging were conducted by Neza Alfazema.

2.17.3 Mouse brain fixation, Histopathology and Immunohistochemistry

Brains were fixed in 4% PFA overnight at 4ºC, then rinsed several times with PBS and stored in PBS + 0.05% sodium azide. For histopathology procedures, brains were transferred into 70% ethanol media and then embedded in paraffin for processing. 10 µm coronal slices were prepared for hematoxylin and eosin (H&E) staining. For immunohistochemistry of fixed brain tissue, 50 µm vibratome (Leica VT1000S) slices were transferred into a 24-well plate. Slices were incubated at room temperature for 30 min in blocking solution (0.2% Triton X-100 and 3% Goat Serum). Primary antibodies were incubated overnight at 4ºC. After three washes with PBS, slices were incubated with appropriate Alexa Fluor secondary antibodies and DAPI (1:2000, Sigma) for 2 hours. Slices were washed three times and were mounted on a slide with FluoroSave™ Reagent (Calbiochem). Slices were examined with a confocal microscope (Leica TCS SP8).

2.17.4 Generation of tumour-derived cell lines

A piece of tumour was transferred into a 35 cm^2 well plate with 2 ml of Accutase. Tissue was minced into small pieces with scalpels and incubated 30 min at 37ºC. The Accutase with the tissue was transferred into a falcon before adding 6 ml of serum-free basal medium. Tissue was dissociated with a glass pipette very gently several times. After centrifugation for 5 min at 500 rcf, the cell pellet was resuspended in complete media and plated in a T25 flask. Cell debris was removed the following day and fresh media was added.

2.18 Software and statistical analysis

Screening data were analysed, and data visualisations created, with Spotfire (Tibco) and Stratominer (Core Life Analytics). RPPA data were assessed using Cluster 3.0 (University of Tokyo) and TreeView and graphs created in GraphPad Prism 8. nSolver software was used for Nanostring analysis. Some figures were created with BioRender.

Statistical analyses were performed in GraphPad Prism 8. Biological replicates were considered as different passage numbers of the same cell line plated in independent experiments. Mean and SEM are plotted unless otherwise stated. Statistical tests used are indicated in the figure legends.

Chapter 3

A cell-based phenotypic small molecule screen identifies a synergy between GSK3 inhibitors and FOXG1 overexpression in driving neural stem cell cell-cycle re-entry

3.1 Introduction

Our laboratory recently published evidence that elevated levels of FOXG1 and SOX2 enforce proliferative neural stem cell identity. Quiescent NSCs overexpressing these transcription factors can be activated and become rapidly proliferating. We identified the cell cycle regulator *Foxo3* and epigenetic modulators *Tet3* and *Dnmt1* as targets of FOXG1 (Bulstrode et al., 2017). However, other downstream effectors of these transcription factors remain unknown. Furthermore, the efficiency with which their overexpression drives cell-cycle re-entry is low: only ~1% of quiescent NSCs generate colonies after return to growth factors (EGF+FGF2) with induced FOXG1 overexpression, as opposed to ~12% of unmodified NSCs at low density in self-renewal conditions, suggesting that additional barriers remain (Figure 3.1C). I used a phenotypic screening approach to identify potential signaling pathways that may restrict exit from quiescence.

Phenotypic screening involves the use of libraries of small molecules, proteins or genetic perturbations to interrogate model systems for the extraction of data on functional biological endpoints (Carragher, 2009; Lee and Berg, 2013; Yarrow et al., 2003). In drug discovery, this contrasts with and complements the more popular 'target-based' approaches, which rely on pre-determined molecular targets.

Here, I use a phenotypic screening approach not for drug discovery but to elucidate relevant pathways which may antagonise, or co-operate with FOXG1/SOX2 overexpression to drive cells back into cycle and enforce the reacquisition of a proliferating NSC phenotype. We used our defined model of quiescence/differentiation and automated microscopy provided by the Operetta system (PerkinElmer) to screen a small molecule library of 303 known stem cell modulators (StemSelect, MerckMillipore) for compounds which would enhance or impede cell cycle re-entry. It is important to note that this screen was devised to take a reductionist approach to interrogate the role of FOXG1 in exit form quiescence, and to identify co-operating and antagonising pathways, rather than to discover compounds with a direct impact on quiescence, or indeed cell death, in malignant cells.

Previously we had used NSC colony formation assays to demonstrate the role of FOXG1 and SOX2 in cell cycle re-entry (Bulstrode et al., 2017). A clonal cell line (FS3), derived from mouse NS cells (ANS4) transfected with a stably integrating PiggyBac transposon plasmid carrying a tetracycline-inducible human *FOXG1-2A-SOX2* expression cassette, was used to model the acquisition of a quiescent state, on exposure to BMP-4. Human FOXG1 and SOX2 were used; these have ~97% homology with their mouse equivalents increasing to 100% homology in DNA binding domains. Addition of doxycycline (dox) to FS3 quiescent NSCs enables their exit from quiescence and colony formation in response to EGF and FGF-2. Details of this assay, including dose titration of doxycycline and confirmation of the reacquisition of a proliferative NSC state with upregulation of Nestin and downregulation of GFAP, have been published by our lab (Bulstrode et al., 2017). FOXG1 and SOX2 therefore support exit from the quiescent state. However, although efficiency of exit from quiescence is higher than with FOXG1 overexpression alone, >90% of cells do not respond, suggesting that other pathways must be present that are a barrier to cell cycle re-entry.

3.2 Optimization of phenotypic screening assay

It was necessary to move away from the colony assay in order to establish a 'screenable' assay compatible with the 96 well plate format, and an Operetta imaging-based assay. For this we therefore first established higher plating density (30 cells/mm^2 as opposed to 10 cells/mm^2) and reduced assay times (4-7 days). Quantitative data was obtained for absolute cell number as an indication of the frequency of cell cycle re-entry (Figure 3.1). Plating density was established by assessing cell cycle re-entry after BMP exposure and return to mitogens in unmodified adult mouse NSCs at serially reducing plating densities. Minimal EdU incorporation was seen below 50 cells/mm^2 (Figure 3.1H). A density of 30 cells/mm^2 allowed for the convenient plating of 1000 cells/well in the 96 well plate format.

To identify signaling pathways co-operating with, or facilitating, the effects of FOXG1 and SOX2, a line was used in which the cell cycle regulator *Foxo3* had been deleted from parental FS3 cells using CRISPR/Cas9-assisted gene targeting (Figure 3.1E) (Bressan et al., 2017). These cells (termed FOD3) have been shown to respond to BMP4 in a similar way to the parental line, with cell cycle exit and acquisition of an astrocytic quiescent NSC morphology and marker profile. Upon re-exposure to growth factors these cells cycle very slowly (doubling time ~ 6 days cf 24hrs for parental cells never exposed to BMP4) (Bulstrode et al., 2017). Thus, they enter a quiescent state but remain primed to re-enter cell cycle.

FOD3 cells at low density (30 cells/mm^2) were exposed to BMP4 for 24 hrs and then returned to media containing growth factors EGF+FGF2, with or without dox. Where dox was present, cell number, as assessed by DAPI staining and nuclei count, was significantly higher after 7 days. This difference was greater and more consistent in the FOD3 cell line than in a line with intact *Foxo3* (F6) (Figure 3.1D&F) and so this line provided a more 'screenable' assay. I plated

test plates and progressed from manual to automated media changes and then to automated cell seeding and media changes. For each test, cell number +/- dox was assessed and Z` and co-efficient of variation (CV) scores calculated. The Z` factor is a screening window co-efficient which is dimensionless and which assesses screen quality, taking into account the signal dynamic range and data variation in measurements (Zhang et al., 1999). Z` factors are meaningful in the range -1 to 1. A score of 0.5-1 represents an excellent assay, 0-0.5 is a 'doable' assay, 0 is a 'yes/no' type assay and <0 means screening is essentially impossible. Co-efficient of variation (CV) - the ratio of the standard deviation to the mean - is also a key measure in assessing screening assays and should be considered alongside Z` scores. Smaller CVs represent more precise and reproducible assays. There was an improvement, throughout assay development, to industry accepted Z` (0.58) and CV values (Iversen et al., 2006) (Figure 3.1G).

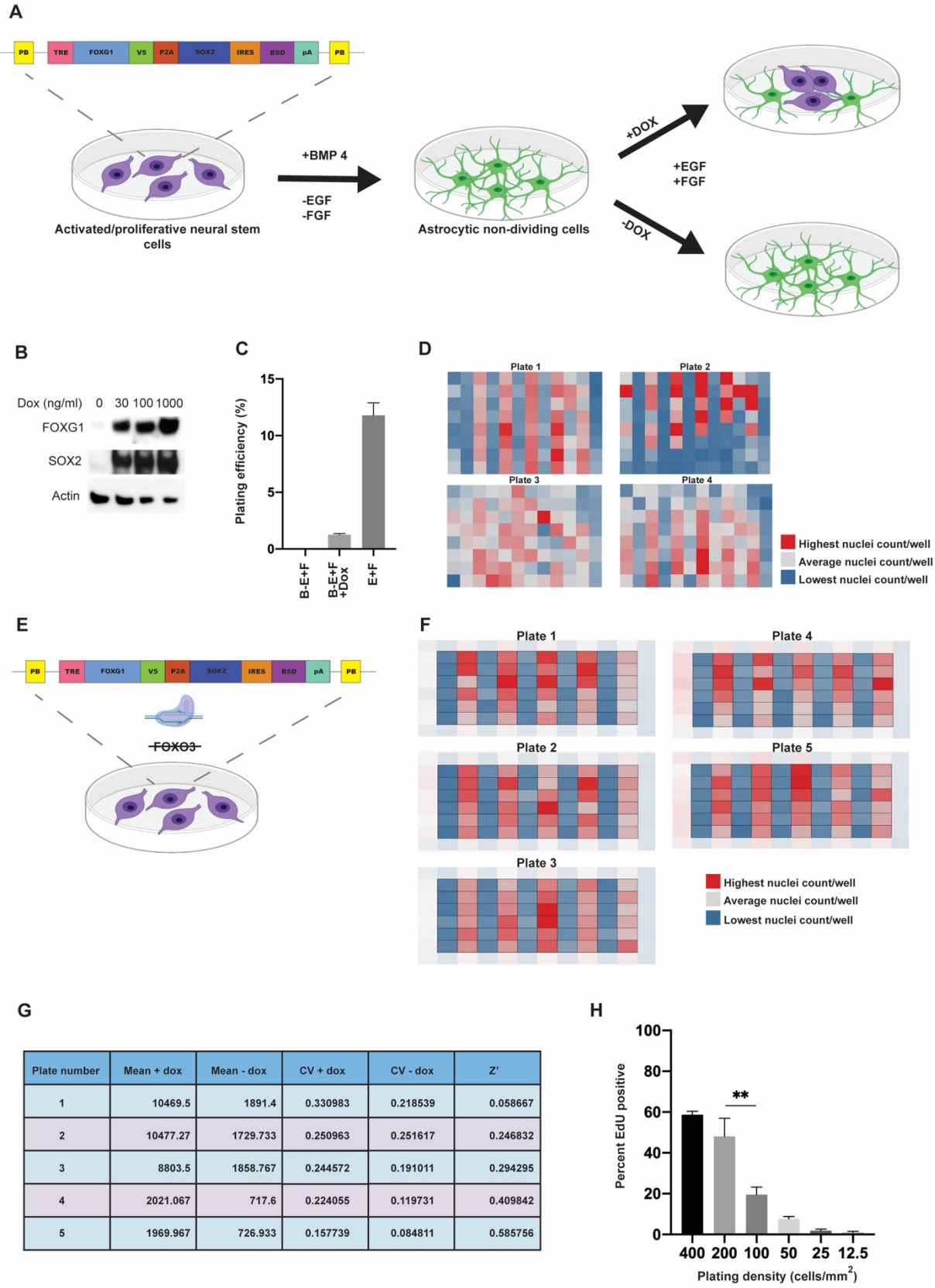

G

Plate number	Mean + dox	Mean - dox	CV + dox	CV - dox	Z'
1	10469.5	1891.4	0.330983	0.218539	0.058667
2	10477.27	1729.733	0.250963	0.251617	0.246832
3	8803.5	1858.767	0.244572	0.191011	0.294295
4	2021.067	717.6	0.224055	0.119731	0.409842
5	1969.967	726.933	0.157739	0.084811	0.585756

Figure 3. 1 Screen optimisation.

(A) Schematic representation of the in vitro assay which forms the basis of the screen. Withdrawal of growth factors and exposure to BMP4 drives cell cycle exit and acquisition of an astrocytic morphology. Re-exposure to EGF+FGF2 leads to low efficiency cell cycle re-entry in colony assays and therefore proliferation in wells, only where FOXG1 is upregulated by dox. (B) Western blot confirming expression of human FOXG1 and SOX2 in response to doxycycline in FS3 cells. (C) Quantification of colony forming efficiency (% of cells plated which give rise to colonies) for F6 cells plated in BMP4 and returned to EGF+FGF2 +/- FOXG1 overexpression with dox (B-E+F, B-E+F+Dox) as compared to F6 cells plated in EGF+FGF2 and never exposed to BMP4 (E+F). n=3. (D) Heatmaps of early attempts to develop a 'screenable' assay with F6 cells. All cells were plated, at 1000 cells per well, in BMP4 and, after 24 hours, returned to EGF+FGF2 +/- dox for 6 days. Alternate columns represent dox/no dox from left. Each square represents the nuclei count in a well of a 96 well plate. (Red: maximum nuclei count at end-point of assay; Blue: minimum count at end-point of assay). (E) *Foxo3* was excised from FS3 cells (with dox-inducible FOXG1 and SOX2 overexpression) to create FOD3 cells. (F) Heatmaps of FOD3 cells in the screening assay, conditions as in (D). (G) Cell numbers, CV and Z' scores for these plates. (H) Quantification of EdU incorporation at serially reducing plating density (plated in BMP4 and returned to mitogens). One-way ANOVA. n=4.

3.3 Phenotypic screening

3.3.1 A phenotypic screen of stem cell pathway associated pharmacological agents identifies BIO synergising with FOXG1/SOX2 overexpression to trigger cell cycle re-entry

The StemSelect library of 303 compounds (MerckMillipore) was tested to identify key signaling pathways antagonising or, conversely, co-operating with FOXG1/SOX2. Quiescent NSCs were screened in the presence of dox to search for agents that increased the efficiency of cell cycle re-entry. In parallel, we also identified pathways that block cell cycle re-entry. Full details of all compounds within the library are found in Appendix

The library was screened in triplicate, in 96 well format. Cells were plated in BMP4 for 24 hrs to drive cell cycle exit, then changed to media containing EGF+FGF2 + compounds +/- dox. Controls were wells with EGF+FGF2 and either DMSO or dox. Plates were fixed 7 days after the addition of compounds and nuclei were stained with DAPI. The PerkinElmer Operetta, with Harmony and Columbus analysis software, were used to obtain a total nuclei count for each well. We defined compounds producing mean nuclei counts greater than twice the plate median as significant hits (Figure 3.2B&C). Additional visual verification of morphology was used to confirm increased or decreased cell number for these hits (Figure 3.2D&E). A cytoplasmic stain – HCS CellMask (ThermoFisher) – was also used to assess cell morphology, distinguishing compounds resulting in retained astrocytic morphology from toxic compounds causing cell death (Figure 3.2D). In parallel, we also screened compounds in the absence of dox – to identify pathways that might be operating downstream of FOXG1/SOX2 (this was performed with Harry Bulstrode). Figure 3.2A summarises the approach to these two screens.

Forskolin, epinephrine and norepinephrine, all of which act via cAMP mediated signaling downstream of G protein coupled receptors were identified as agents that can mimic the effects of Dox. This suggests cAMP signaling may be a key downstream signaling pathway induced by FOXG1/SOX2 overexpression. However, these hits also were found in the presence of dox, suggesting this is a pathway that might act in parallel to FOXG1/SOX2. Further investigation of the impact of these compounds on exit from quiescence forms the basis of ongoing work and are not the focus of this thesis.

Strikingly, we identified 6-bromoindirubin-3'-oxime (BIO), as a compound that dramatically enhanced the effects of FOXG1/SOX2. This was only identified in the 'plus dox' screen. BIO is an inhibitor of glycogen synthase kinase 3. Initial validation experiments were conducted using independently sourced compounds, with FOD3 cells, over 3 biological replicates with a minimum of 6 technical replicates per condition. Again, the three cAMP mediators drove proliferation independently of FOXG1/SOX2 upregulation but BIO only increased cell number in the presence of dox, highlighting that the effect of BIO on cell cycle re-entry occurs only when FOXG1/SOX2 are upregulated (Figure 3.2F), suggesting some synergistic interaction. Tamoxifen did not validate as a hit, nor did its active metabolite produce any effect on exit from quiescence (Figure 3.2G). It is well recognised that screening can produce aberrant results and that careful validation is required. I conclude that the emergence of tamoxifen as a hit here is such an aberration. Further validation experiments with independent cell lines and with another GSK3 inhibitor are detailed below. BIO became the focus of work going forward, due to the clear synergy with FOXG1/SOX2 and resulting initial hypothesis that GSK inhibition, via activation of Wnt signaling, cooperates with FOXG1/SOX2 in driving proliferation of NSCs.

Compounds resulting in maintenance of a quiescent state, as determined by low cell number (at or below 1000 cells/well), cell area >750μm and visally confirmed astrocytic morphology, are detailed in Table 3.1. Again, these have formed the basis of ongoing work and are not discussed further here. Rapamycin is of particular interest in our work on PI3K/AKT signaling in GBM.

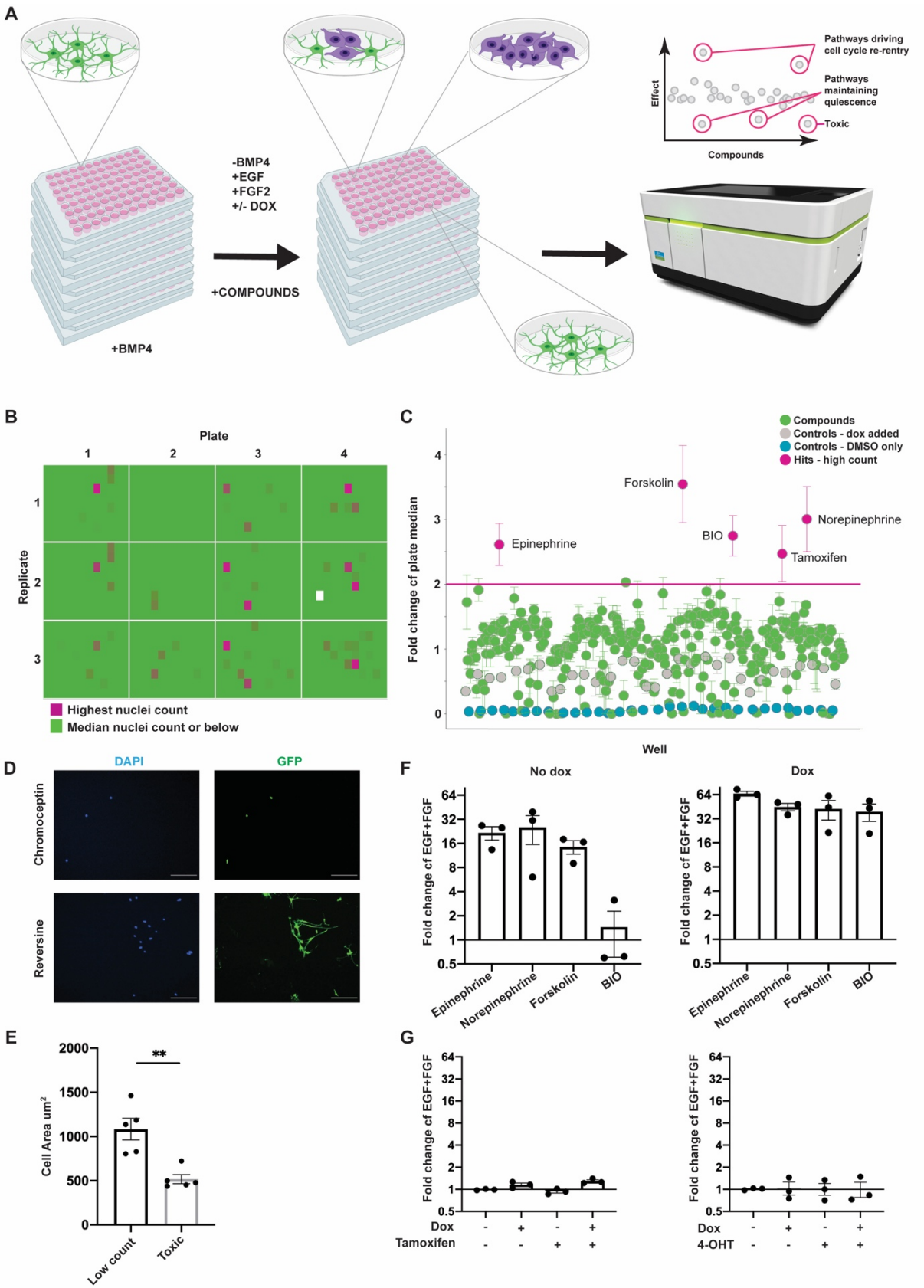
A
-BMP4
+EGF
+FGF2
+/- DOX
+COMPOUNDS
+BMP4
Pathways driving cell cycle re-entry
Pathways maintaining quiescence
Toxic
Effect
Compounds
B
Plate
1
2
3
4
Replicate
Highest nuclei count
Median nuclei count or below
C
Compounds
Controls - dox added
Controls - DMSO only
Hits - high count
Forskolin
Epinephrine
BIO
Norepinephrine
Tamoxifen
Fold change cf plate median
Well
D
DAPI
GFP
Chromoceptin
Reversine
E
Cell Area um2
**
Low count
Toxic
F
No dox
Dox
Fold change cf EGF+FGF
Epinephrine
Norepinephrine
Forskolin
BIO
G
Fold change cf EGF+FGF
Dox
Tamoxifen
4-OHT

Figure 3. 2 A phenotypic screen identifies a synergy between a GSK3 inhibitor and FOXG1 overexpression in driving cell cycle re-entry.

(A) Schematic of the screening process. (B) Heatmap of cell number per well, at screen end-point, across all 4 plates in triplicate, showing 5 clear potential hits. Shades of purple = cell count > median to highest, green = cell count ≤ median. (C) Scatter plot of cell counts normalised to plate median. Red line shows threshold for calling high count hits, 2x plate median. (D) Representative images of cells in conditions deemed to be toxic (Chromoceptin) and conditions accepted as maintaining cells in a non-proliferative/quiescent state (Reversine). Scale bars 150µm. Blue - DAPI, green - HCS CellMask. (E) Cell area (µm) for compounds accepted as low count hits (resulting in maintenance of quiescence) versus compounds deemed toxic. Mann-Whitney test. n=6. (F) Validation of the 4 high count hits. Concentration of all 4 compounds was 1µM. Fold change in cell number, as compared with the control (no dox, EGF+FGF2+DMSO). One-way ANOVA. Means of 3 biological replicates n=6. (G) Tamoxifen citrate, and its active metabolite 4-hydroxytamoxifen, failed to induce proliferation. One-way ANOVA. Means of 3 biological replicates n=15 each.

Compound	Mechanism
5-Aza-2′-Deoxycytidine	DNA methyltransferase inhibitor
PD166866	FGF Receptor Tyrosine Kinase Inhibitor
Fumidil B	Inhibitor of methionine amino-peptidase 2
Rapamycin	Inhibitor of mTORC1
Paclitaxel	Promotes assembly of microtubules and inhibits tubulin disassembly
Dexamethasone	Steroid
Reversine	De-differentiation inducing agent

Table 3.1 Compounds resulting in maintenance of quiescence.

3.3.2 An independent GSK3 inhibitor, Chiron, phenocopies the BIO response

To confirm that the effect of BIO seen in the screen was in fact due to GSK3 inhibition, rather than an off target effect, I first reproduced the results obtained with BIO using a different GSK3 inhibitor. CHIR99021 (chiron) is a well-established, highly potent and selective GSK3β inhibitor (An et al., 2012). We therefore tested chiron (Axon Medchem), in an identical assay to that described for screening and confirmed that this produces an equivalent increase in cell number to BIO (Figure 3.3A). This supports the hypothesis that GSK3 signaling inhibition can cooperate with FOXG1/SOX2 to drive exit from quiescence in NSCs.

We used chiron at doses commonly used in the literature to induce GSK3 inhibition (Silva et al., 2008; Bain et al., 2007; Naujok et al., 2014; Morrison et al., 2016). As chiron is widely

used at 3μM and has been shown to inhibit GSK3 at this concentration, I did not conduct confirmatory studies on GSK3 modulation. However, recognising that kinase inhibitors can have off-target effects and, indeed, that GSK3 has many substrates, I confirmed that the effects of chiron exposure could be phenocopied by Wnt activation, as would be expected with GSK3 inhibition (Chapter 4).

3.3.3 The promotion of cell cycle re-entry by BIO is seen in NSCs with FOXG1 overexpression alone

It remained possible that the lack of *Foxo3* in FOD3 cells was necessary for the effect of GSK3 inhibition, or that the requirement for FOXG1 or SOX2 alone would suffice. We therefore used the parental unmodified NSCs (called ANS4) and engineered inducible FOXG1 overexpression alone. A cassette expressing dox inducible human FOXG1 at high levels as a fusion protein with a V5 peptide tag was introduced to ANS4 cells, using the PiggyBac system, and clonal lines derived (Figure 3.3B). Activation of the FOXG1 overexpression cassette in the clonal line (F6) was confirmed by immunocytochemistry for V5 (Figure 3.3E). Notably, *Foxo3* is unmodified in these cells and SOX2 is not overexpressed, enabling us to ask specifically if the effect of chiron is dependent on FOXG1.

The F6 cells were exposed to BMP4 for 24 hrs and returned to growth factors, with and without dox, and BIO or chiron across a dose range. Both BIO and chiron drove cell cycle re-entry and proliferation, as measured by nuclei count at day 7, in the F6 cells only where FOXG1 overexpression was induced (Figure 3.3C&D). This was confirmed with EdU incorporation studies on chiron at 3μM, with and without dox (Figure 3.3F).

To exclude a synergistic effect of GSK3 inhibition with SOX2, a cell line with isolated doxycycline-inducible overexpression of SOX2, S15, generated in the same way as F6, was plated in BMP-4 media at 1000 cells per well in 96 well plates and, after 24 hours, exposed to chiron, in the presence or absence of doxycycline. Although SOX2 upregulation was confirmed in the context of dox exposure (Figure 3.4A), no effect of either dox or chiron was seen on cell cycle re-entry (Figure 3.4B). We conclude that GSK3 inhibition acts in synergy with FOXG1 overexpression to drive exit from quiescence.

NSC colony forming assays were also performed to confirm synergy. 10000 cells were plated in each well of a 6 well plate (10.5 cells/mm^2) in BMP-4 media. After 24 hrs, media were changed to media containing EGF+FGF2 +/- dox and/or chiron for 8-10 days. We noted significantly increased colony formation in the presence of dox plus chiron (Figure 3.3G) compared to each individually. The efficiency of cell cycle re-entry (based on colony formation), was higher in the presence of dox and chiron to that observed in controls with EGF/FGF-2 under normal proliferation (20-30% cf ~12%, figure 3.3H). In summary, we conclude that chiron cooperates with FOXG1 overexpression to enable maximally efficient cell cycle re-entry in NSCs.

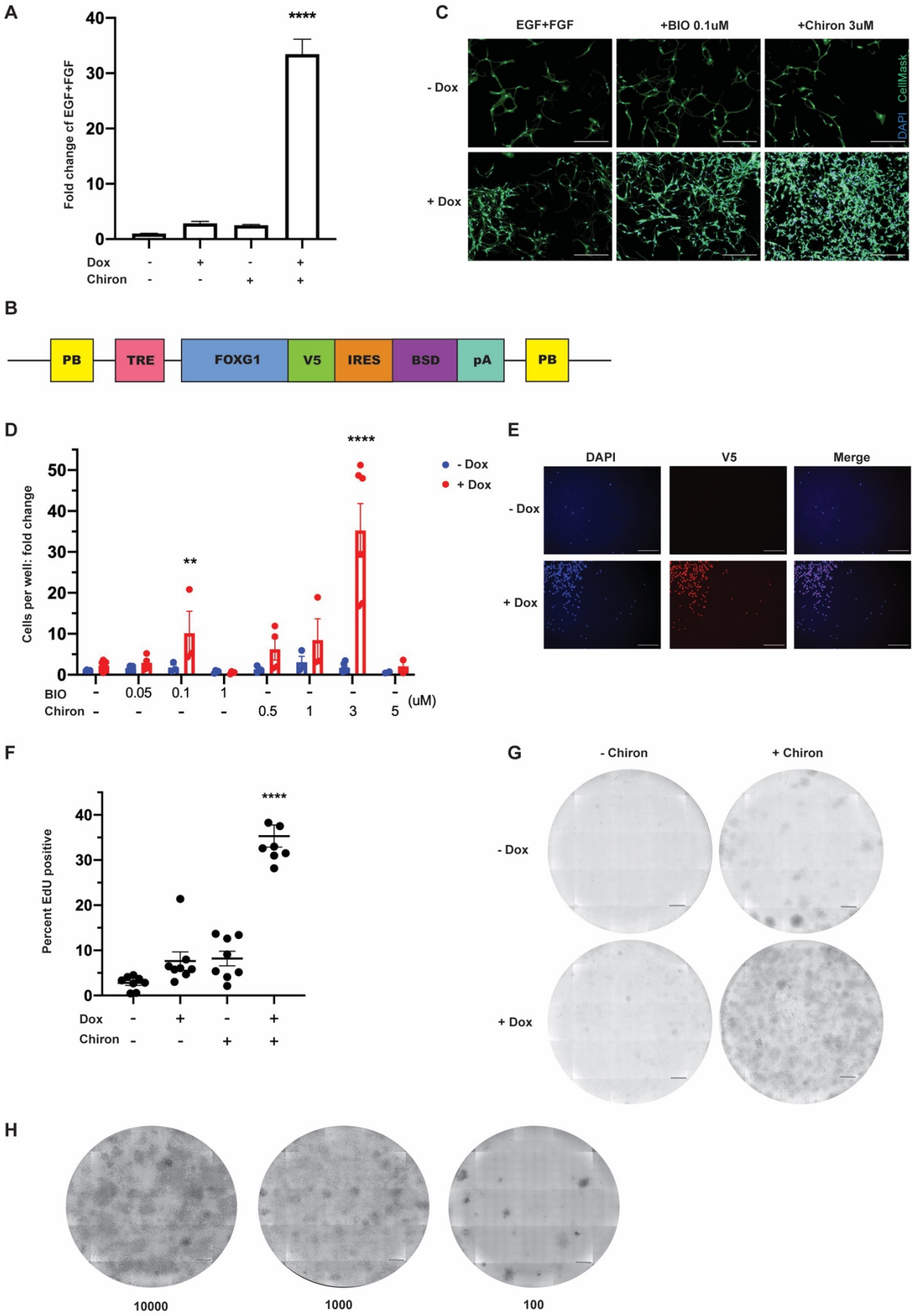
A
Fold change cf EGF+FGF
****
Dox
Chiron
C
EGF+FGF
+BIO 0.1uM
+Chiron 3uM
- Dox
+ Dox
DAPI CellMask
B
PB
TRE
FOXG1
V5
IRES
BSD
pA
PB
D
Cells per well: fold change
**
****
- Dox
+ Dox
BIO
Chiron
(uM)
E
DAPI
V5
Merge
- Dox
+ Dox
F
Percent EdU positive
****
Dox
Chiron
G
- Chiron
+ Chiron
- Dox
+ Dox
H
10000
1000
100

Figure 3. 3 GSK3 inhibition and FOXG1 overexpression drive exit from quiescence with high efficiency.

(A) Increase in FOD3 cell number seen after BMP4 exposure for 24hrs and return to EGF+FGF2 alone or with dox, chiron, or dox+chiron in combination for 6 days. One-way ANOVA. Significance in a comparison to EGF+FGF2 alone shown. Shapiro-Wilk test for normality. n=6. (B) Dox-inducible human FOXG1-V5 cassette. (C) Representative images of effects of dox, BIO, chiron and combinations in F6 cells. HCS CellMask (green), DAPI (blue). Scale bars 150μm. (D) Increase in F6 cell number after BMP4 exposure for 24 hrs and return to EGF+FGF2 alone or with varying doses of BIO and chiron, with/without dox for 6 days. Two-way ANOVA. Significance in a comparison to EGF+FGF2 alone shown. Shapiro-Wilk test for normality. Means of 6 biological replicates n=3-6 per condition. (E) Representative images of Staining for V5 in EGF+FGF2 or EGF+FGF2+dox confirm that dox exposure induces expression of the cassette. V5 (red), DAPI (blue). Scale bars 150μm. (F) Quantification of EdU incorporation by condition. Means of 8 biological replicates, n=15 per condition. Friedman test. Significance in a comparison to EGF+FGF2 alone shown. (G) Colony forming assays with BMP4 for 24 hours and return to mitogens for 10 days +/- dox/chiron. 10000 cells plated per well, 6 well plate. Scale bars 2mm. (H) Serial dilution colony assays 10000, 1000, 100 cells plated per well in BMP4 with return to EGF+FGF2+dox+chiron for 10 days. Scale bars 2mm.

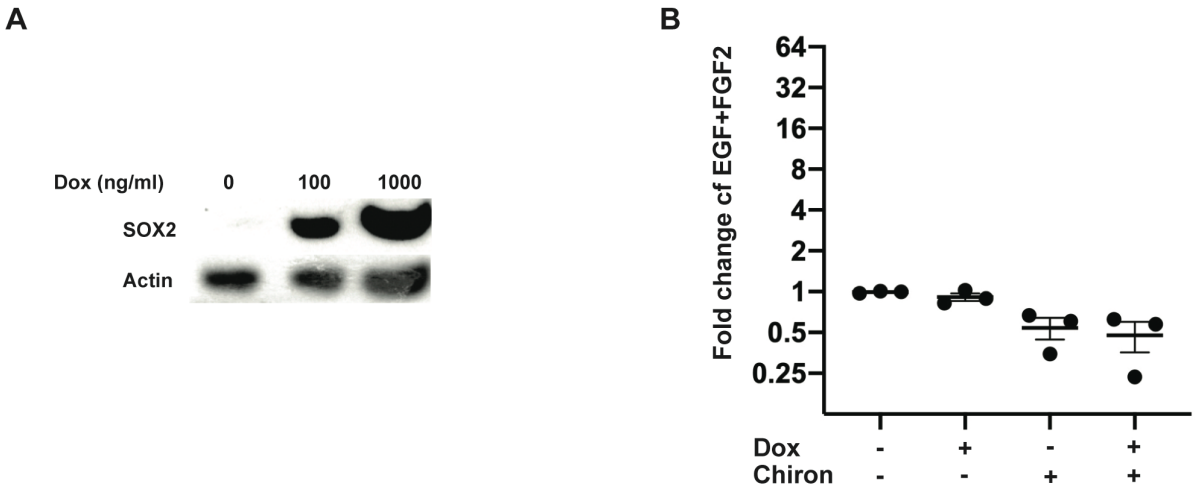

Figure 3. 4 The effects of GSK3 inhibition are not dependent on SOX2 overexpression.

(A) Western blot of SOX2 expression in S15 cells exposed to doxycycline. (B) Fold change in cell number (cf. EGF+FGF2) by condition after 24 hrs BMP4 and return to EGF+FGF2 for 6 days. One-way ANOVA (ns). Shapiro-Wilk test for normality. Means of 3 biological replicates.

3.4 An additional assay, modelling NS quiescence, yields similar results

The assay using exposure to BMP4 for 24 hrs to drive cells out of cycle was used for screening, based on work published by our group. As described above, exposure of mouse NSCs to BMP4, triggers rapid cell cycle exit, with acquisition of an astrocytic/quiescent NSC phenotype. When re-exposed to EGF and FGF, the cells will not re-enter cell cycle. However, although GSCs also respond to BMP, and can acquire an astrocytic phenotype, they remain predisposed to cell cycle re-entry. Although previous reports have suggested that BMP treatment is sufficient to induce astrocyte differentiation and loss of tumourigenic potential in GSCs, we have shown that GSCs fail to undergo terminal differentiation and remain vulnerable to cell cycle re-entry (Carén et al., 2015). They can be said to be, functionally, in a shallow, or primed, quiescent state. It is suggested that the consistently high levels of FOXG1 in GSCs contribute to this acquisition of a quiescent state as opposed to terminal differentiation.

The use of *Foxo3* deleted cells in the screen allowed for modelling of primed quiescent NSCs. However, an accepted in vitro model of quiescence is exposure to BMP4 without eliminating FGF2 (Martynoga et al., 2013). Work in our lab has characterised the shallow quiescent state induced by BMP4+FGF2 exposure (Marques-Torrejón, in press). Accordingly, I sought to establish whether the synergy between FOXG1 overexpression and GSK3 inhibition was relevant in this alternative assay of quiescence. The screen assay employed 24 hrs of BMP4 exposure, rather than 72 hrs (used by Maria Angeles Marques-Torrejón), but this resulted in an equivalent exit from cell cycle (Figure 3.5A). On re-exposure to EGF+FGF2 for 4 days, all 3 quiescence conditions lead to similar levels of cell cycle re-entry, with a clear equivalence between 24 hr BMP4 exposure and 72 hr BMP4+FGF2 exposure (Figure 3.5B). Colony forming assays reveal that 24hrs BMP4 leads to colony forming efficiency intermediate

between 72 hrs BMP4 and 72hrs BMP4+FGF2 (Figure 3.5C). I propose that BMP4 exposure for 24 or 72 hrs leads to a quiescent state, from which cells re-enter cell cycle with low efficiency; BMP4+FGF2 appears to give rise to a shallower quiescence from which cells are slightly more ready to re-enter cell cycle. The FOXG1/GSK3 inhibition synergy induces exit from quiescence in each assay (Figure 3.5D-F). Thus, GSK3 inhibition is sufficient, in the context of FOXG1 overexpression, as is seen in GBM, to overcome quiescence in two BMP-4 based assays that mirror dormant and primed quiescent NSCs.

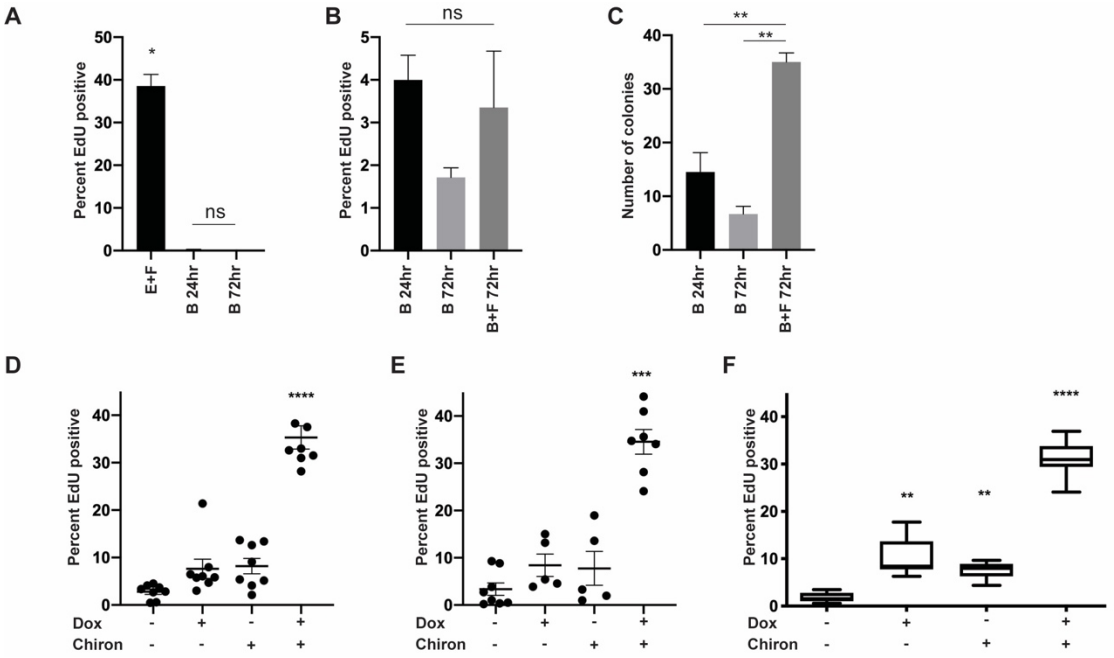

Figure 3. 5 BMP4+FGF2 exposure is an alternative model of quiescence to which the FOXG1/GSK3i synergy is relevant.

(A) Quantification EdU incorporation in F6 cells in EGF+FGF2 (E+F)/BMP4 24 hours (B 24hr)/BMP4 72 hours (B72hr), showing comparability between the 24hr exposure and the 72hr exposure studied by M.A. Marques- Torrejón (in press). Means of 3 replicates. Kruskal-Wallis test. (B) Quantification of EdU in F6 cells after exposure to BMP4 for 24hrs (B24hr) or 72hrs (B72hr) or to BMP4+FGF2 for 72hrs (B+F72hr) then to mitogens for 4 days, showing minimal EdU incorporation in all conditions. Means of 3 replicates. One-way ANOVA, Tukey's multiple comparison tests. (C) Colony formation in F6 cells after exposure to BMP4/BMP4+FGF2 and return to mitogens for 10 days. Means of 3-6 replicates. One-way ANOVA, Tukey's multiple comparison tests. (D) EdU incorporation after 24 hrs BMP4 then return to mitogens +/- dox/chiron for 4-6 days. (E) EdU incorporation after 72 hrs BMP4+FGF2 then return to mitogens +/- dox/chiron for 4-6 days. (D&E) Means of 8 biological replicates, n=15 per condition. (F) EdU incorporation after 72 hrs BMP4 then return to mitogens +/- dox/chiron for 4-6 days. Pilot experiment n=15 per condition. (D-F) Kruskal-Wallis test with Dunn's multiple comparison tests. Significance for comparisons to EGF+FGF2 alone shown.

3.5 The dox+chiron synergy depends on the presence of both at early time points but FOXG1 overexpression prevents deep quiescence

3.5.1 The dox+chiron synergy depends on the presence of both at early time points

The assay used to identify and confirm a synergy between FOXG1 overexpression and GSK3 inhibition in driving cell cycle re-entry is conducted over a week, admitting the possibility that one of the factors drives exit from quiescence and the other is simply pro-proliferative, affecting cells which are cycling i.e. the effects may act sequentially rather than in the same cell state. In order to investigate this possibility, I tested the impact of sequential administration of dox and chiron on cell cycle re-entry, using both BMP4 (24hrs) and BMP4+FGF2 (72hrs) induced quiescence and return to growth factors.

After induction of quiescence, cells were returned to media containing EGF+FGF2 +/- dox and/or chiron for 3 days and then switched to alternative media for a further 4 days (e.g. cells exposed to dox were switched to chiron or dox+chiron). The combination of dox+chiron is needed at early timepoints for maximal cell cycle re-entry. The addition of dox+chiron at later time points can partially recapitulate the effect but sequential use of dox or chiron is not so effective, suggesting a direct synergy driving exit from quiescence (Figure 3.6A&B). Furthermore, there is no increase in proliferation in non-quiescent cells (never driven out of cycle) with exposure to dox and/or chiron. There is, instead, a reduction in EdU incorporation with dox and dox+chiron and no significant impact with chiron alone, suggesting that the effect is indeed on exit from quiescence rather than on proliferating cells (Figure 3.6C). Additionally, growth curves of the mouse NSCs and human GSCs (Figure 3.6D and Chapter 5) confirm no

accelerated growth with chiron in proliferative conditions. We conclude that FOXG1 and GSK3 inhibition interact concurrently to drive exit from quiescence.

3.5.2 FOXG1 overexpression, as seen in human GBM, prevents deep quiescence

Overexpression of FOXG1 is universal across different patient-derived GSCs (Figure 1.10). The shallower quiescence seen in GSCs in response to BMP4 may be mediated by FOXG1 overexpression and the F6 cell line was created to model this. Previous work in the lab has shown that FOXG1 has a role to play in exit from quiescence, and the screen described here builds on those data to identify additional factors involved. To show that FOXG1 is indeed implicated in GSC refractoriness to the induction of deep quiescence, or terminal differentiation, I investigated the effect of FOXG1 overexpression during, rather than after, BMP4 exposure. I plated F6 cells in BMP4 or BMP4 plus dox, chiron or dox+chiron for 24 hrs then returned them to growth factors +/- dox and/or chiron for 6 days. Overexpression of FOXG1, with dox, during BMP4 exposure, results in cells being primed to exit quiescence and particularly primed to respond to GSK3 inhibition (Figure 3.6E). I hypothesise that GSCs may exist in a state of ‘primed quiescence’, vulnerable to proliferation cues, as a result of their high FOXG1 expression levels.

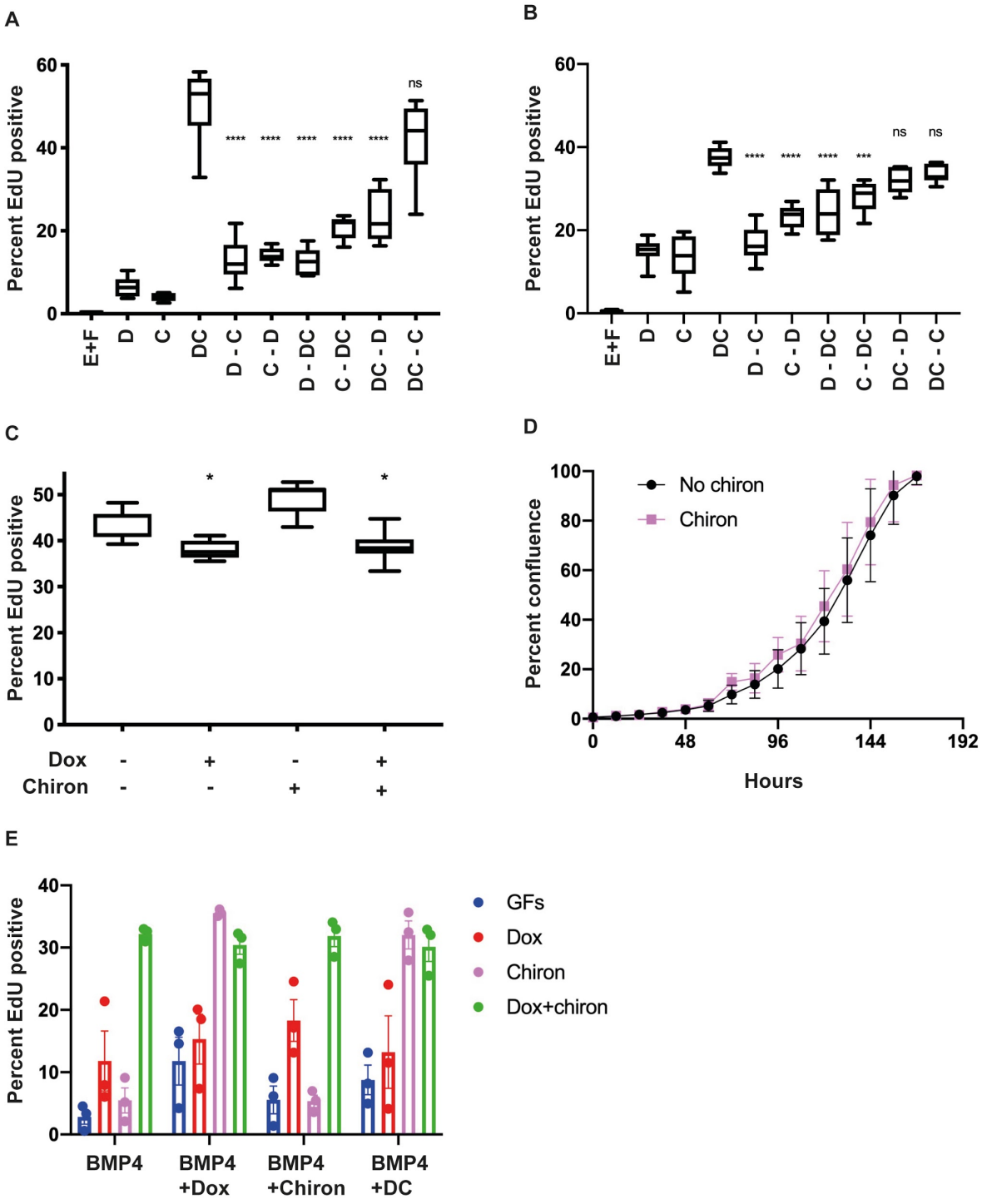
A
Percent EdU positive
60
40
20
0
E+F
D
C
DC
D - C
C - D
D - DC
C - DC
DC - D
DC - C
****
ns
B
Percent EdU positive
ns
ns
***
C
Percent EdU positive
50
40
30
20
10
0
*
Dox
Chiron
D
Percent confluence
100
80
60
40
20
0
No chiron
Chiron
0
48
96
144
192
Hours
E
Percent EdU positive
40
30
20
10
0
BMP4
BMP4 +Dox
BMP4 +Chiron
BMP4 +DC
GFs
Dox
Chiron
Dox+chiron

Figure 3. 6 The synergy depends on dox+chiron exposure simultaneously.

(A) EdU incorporation in F6 cells after BMP4 (24hrs) induced quiescence and return to EGF+FGF2 alone (E+F) or with dox 6 days (D), chiron 6 days (C), dox+chiron 6 days (DC), dox 3 days then chiron 3 days (D-C), chiron 3 days then dox 3 days (C-D), dox 3 days then dox+chiron 3 days (D-DC), chiron 3 days then dox+chiron 3 days (C-DC), dox+chiron 3 days then either dox 3 days (DC-D) or chiron 3 days (DC-C). One-way ANOVA with Dunnett's multiple comparison tests. Shapiro-Wilk test for normality. Significance in a comparison to DC shown. n=6. (B) EdU incorporation in F6 cells after BMP4+FGF2(72hrs) induced quiescence, x-axis labels as in (A). In A&B, cells were returned to growth factors plus dox and/or chiron for 3 days and then switched for a further 4 days. One-way ANOVA with Dunnett's multiple comparison tests. Shapiro-Wilk test for normality. Significance in a comparison to DC shown. n=6. (C) EdU incorporation in F6 cells never exposed to BMP4, showing no pro-proliferative effect of dox or chiron. Kruskal-Wallis test. n=10. Significance in a comparison to EGF+FGF2 alone shown. (D) Growth curve of F6 cells in EGF+FGF2 +/- chiron showing no pro-proliferative effect of chiron. n=6. (E) EdU incorporation in F6 cells after exposure to BMP4 +/- dox and or chiron, showing that dox during BMP4 exposure primes cells to exit quiescence in response to chiron. Data points represent the means of 3 biological replicates, n=3 per condition.

3.6 Conclusions

From the results presented in this chapter, I conclude that GSK3 inhibition synergises with increased FOXG1 and supports exit from quiescence in NSCs. This is likely to be relevant to human glioblastoma, as it is known that FOXG1 is overexpressed in patient-derived GSC lines. The efficiency of cell cycle re-entry seen with the combination of GSK3 inhibition and FOXG1 overexpression is dramatically higher than with FOXG1 overexpression alone. The mechanisms underlying this may explain why FOXG1 is selected to be highly expressed in GBM (where it is associated with poorer prognosis).

The cooperation between FOXG1 and GSK3i occurs in two related in vitro models of quiescence, which differ in depth of quiescence. The BMP4+FGF2 assay is largely used hereafter, due to its description in much of the literature as an assay of quiescence.

GSK3 is a kinase with functions in numerous intracellular pathways; most notably, it is part of the beta-catenin destruction complex and therefore critical to Wnt signaling. I therefore hypothesised that the GSK3i contribution to the synergy is effected by its role in Wnt signaling and explore this in the subsequent chapter.

Chapter 4

Canonical Wnt signaling cooperates with FOXG1 to drive exit from quiescence in NSCs

4.1 Introduction

In the previous chapter, I uncovered a potent synergy between GSK3 inhibition and FOXG1 overexpression in driving exit from quiescence in NSCs. Although the role of GSK3 in Wnt signaling is well established, it is also known to have pleotropic roles and can operate through multiple signaling pathways (Doble and Woodgett, 2003). In this chapter, I describe results testing the hypothesis that the effect of GSK3 inhibitors in quiescent NSCs is mediated by canonical Wnt/beta-catenin signaling. I use both pharmacological and genetic experimental approaches to explore this functionally.

Wnt pathway mutations are not frequently observed in GBM but they are a well known driver of tumorigenesis in other cancers, such colorectal cancer. GBMs, however, do have operational Wnt/beta-catenin, based on markers (Holland, 2000; Portela et al., 2019; Sareddy et al., 2009), and beta catenin is expressed, based on in-situ hybridisation for beta-catenin by the Ivy GBM Atlas Project (Introduction, Figure 1.12A&B). Interestingly, beta-catenin is most evident in perivascular regions, which is also the location of quiescent tumour stem cells, known to be rich in FOXG1 (Gilbertson and Rich, 2007). I hypothesise that FOXG1 interacts with Wnt to drive exit from quiescence and that this interaction could be relevant in the tumour niche.

4.2 Wnt3a can replace chiron in synergising with FOXG1

To verify that chiron's mechanism of action is through Wnt activation, rather than any other GSK3 effect, I first sought to phenocopy the effect using a ligand of canonical Wnt signaling. Wnt3a is a ligand of canonical Wnt signaling which is known to be overexpressed in GBM (Kaur et al., 2013).

I plated F6 cells at low density in BMP4/FGF2 media for 72 hrs or BMP4 media for 24 hrs. After this time period, media were replaced with media containing EGF, FGF2 +/- dox and/or Wnt 3a (R&D) at 100ng/ml or 200ng/ml. In the initial experiments, with BMP4, after 6 days, cells were fixed and stained with DAPI and HCS CellMask, for quantification of cell number. In subsequent experiments, investigating BMP4/FGF2 exposure, after 4 days a 2 hr EdU pulse was carried out and cells were fixed and stained for EdU quantification (Figure 4.1A). A dose-dependent proliferative effect, quantified by a >30-fold increased cell number and increased EdU incorporation from <5% to ~40%, was seen with Wnt3a in the context of FOXG1 overexpression with dox (Figure 4.1B-D). A much less marked effect, with EdU incorporation ⩽10%, was seen with Wnt3a alone.

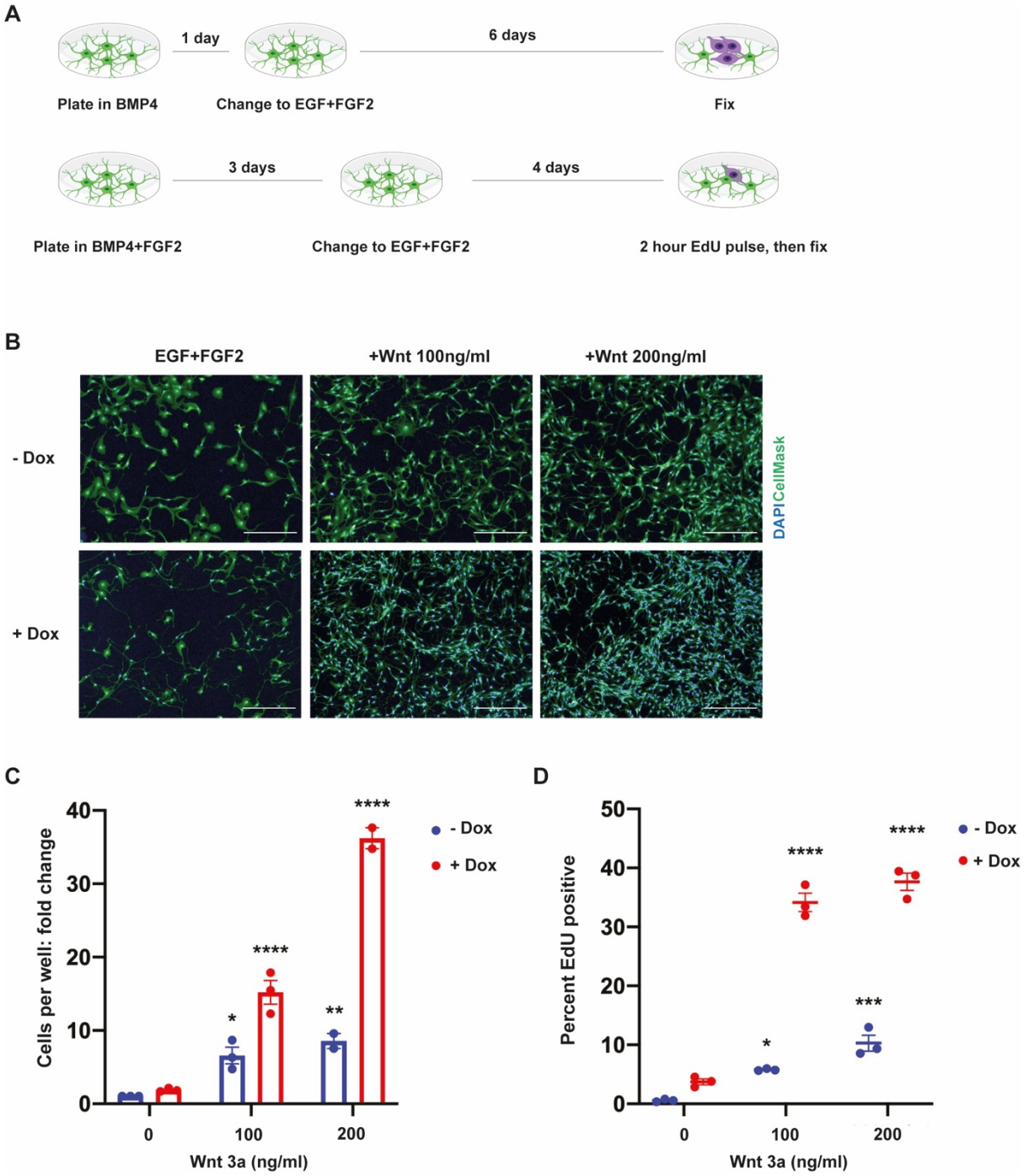
A
1 day
6 days
Plate in BMP4
Change to EGF+FGF2
Fix
3 days
4 days
Plate in BMP4+FGF2
Change to EGF+FGF2
2 hour EdU pulse, then fix
B
EGF+FGF2
+Wnt 100ng/ml
+Wnt 200ng/ml
- Dox
+ Dox
DAPI CellMask
C
Cells per well: fold change
40
30
20
10
0
0
100
200
Wnt 3a (ng/ml)
- Dox
+ Dox
*
****
**
****
D
Percent EdU positive
50
40
30
20
10
0
0
100
200
Wnt 3a (ng/ml)
- Dox
+ Dox
*
****
***
****

Figure 4. 1 A dose-dependent synergistic effect of FOXG1 overexpression and Wnt3a exposure in stimulating cell cycle re-entry of quiescent NSCs.

(A) Schematic of experiments to quantify cell count per well and EdU incorporation as functional assessments of exit from quiescence. (B) Representative images at assay endpoint. Scale bars 150µm. Blue - DAPI. Green – HCS CellMask. (C) Quantification of fold change in cell number (cf. EGF+FGF2) after exposure to BMP4 and return to growth factors for 6 days. The combination of Wnt3a exposure and FOXG1 overexpression drives exit from quiescence. (D) Quantification of EdU incorporation after BMP4+FGF2 exposure and return to growth factors for 4 days (at this time, cell number increases were minimal). C&D 2-way ANOVA with Shapiro Wilks test for normality. Data points represent means of 3 biological replicates, n=6 each. Significance shown for comparisons to EGF+FGF alone.

4.3 Wnt inhibitors abrogate the synergy between GSK3i and elevated FOXG1

I next sought further evidence for the role of the Wnt pathway in the FOXG1/chiron synergy by investigating the effect of Wnt inhibition at two different sites in the Wnt pathway. XAV939 is a tankyrase inhibitor. Tankyrases target Axin, a key component of the beta-catenin destruction complex, for degradation. Increased Axin stabilisation leads to more destruction of beta-catenin and reduced Wnt signaling (Kim, 2018). ICRT3 disrupts the interaction between beta-catenin and Tcf, leading to inhibition at the nuclear level, without upstream effects. It is one of thirty-four direct inhibitors of beta-catenin responsive transcription (CRT) and is known to inhibit canonical Wnt signaling potently and specifically, with much lesser effects on the non-canonical pathways (Gonsalves et al., 2011). Figure 1.11 shows the sites of action of these two inhibitors.

I selected doses with no impact on the growth of F6 cells in EGF+FGF2 conditions (Figure 4.2A). Wnt signaling is therefore not required for proliferation of NSCs. Subsequently, cells were plated in BMP4+FGF2 for 72 hrs and then changed to EGF+FGF2 media with doxycycline and chiron +/- a Wnt inhibitor. ICRT3 has been shown to have a nanomolar IC50 in some cell lines. However, the doses of ICRT3 used here are below those shown previously to have specific activity on beta-catenin transcriptional activity, and no impact on its cytoskeletal function, as in Gonsalves et al, in which 22 μM was used in an initial luciferase-assay based screen, and 6 μM in validation assays, with 25-75 μM used in assays demonstrating specificity to transcriptional activity and downregulation of Wnt target gene transcription (Gonsalves et al., 2011). The doses of XAV939 used here are in keeping with those shown to inhibit tankyrases 1 and 2 and to stabilise axin (Huang et al., 2009). They are below doses shown to reduce cell viability in GBM cell lines (https://www.cancerrxgene.org/).

Cell number after 6 days was significantly reduced, in a dose-dependent manner by each of the Wnt inhibitors (Figure 4.2B). Consistent with this, there was a reduction in EdU incorporation with the Wnt inhibitors (Figure 4.2E). This reduction was significant only at high doses of inhibitor, in contrast to the reduction in cell number. This may be because, by 6 days - when there is a significant impact on cell number - many cells are active, proliferative cells which incorporate EdU, and durably quiescent cells are markedly outnumbered. Imaging confirmed that cells retained an astrocytic morphology and that the reduction in cell number did not appear to relate to cell death (Figure 4.2C). TUNEL assays also confirmed no significant increase in apoptosis (Figure 4.2D).

Altogether, these data suggest that each of the two Wnt inhibitors can abrogate the effect of the dox/chiron combination on NSC cell cycle re-entry and that the effect of the FOXG1/GSK3i synergy is indeed Wnt dependent. Wnt signaling is therefore required for efficient exit from the quiescent NSC cell state and cooperates with FOXG1.

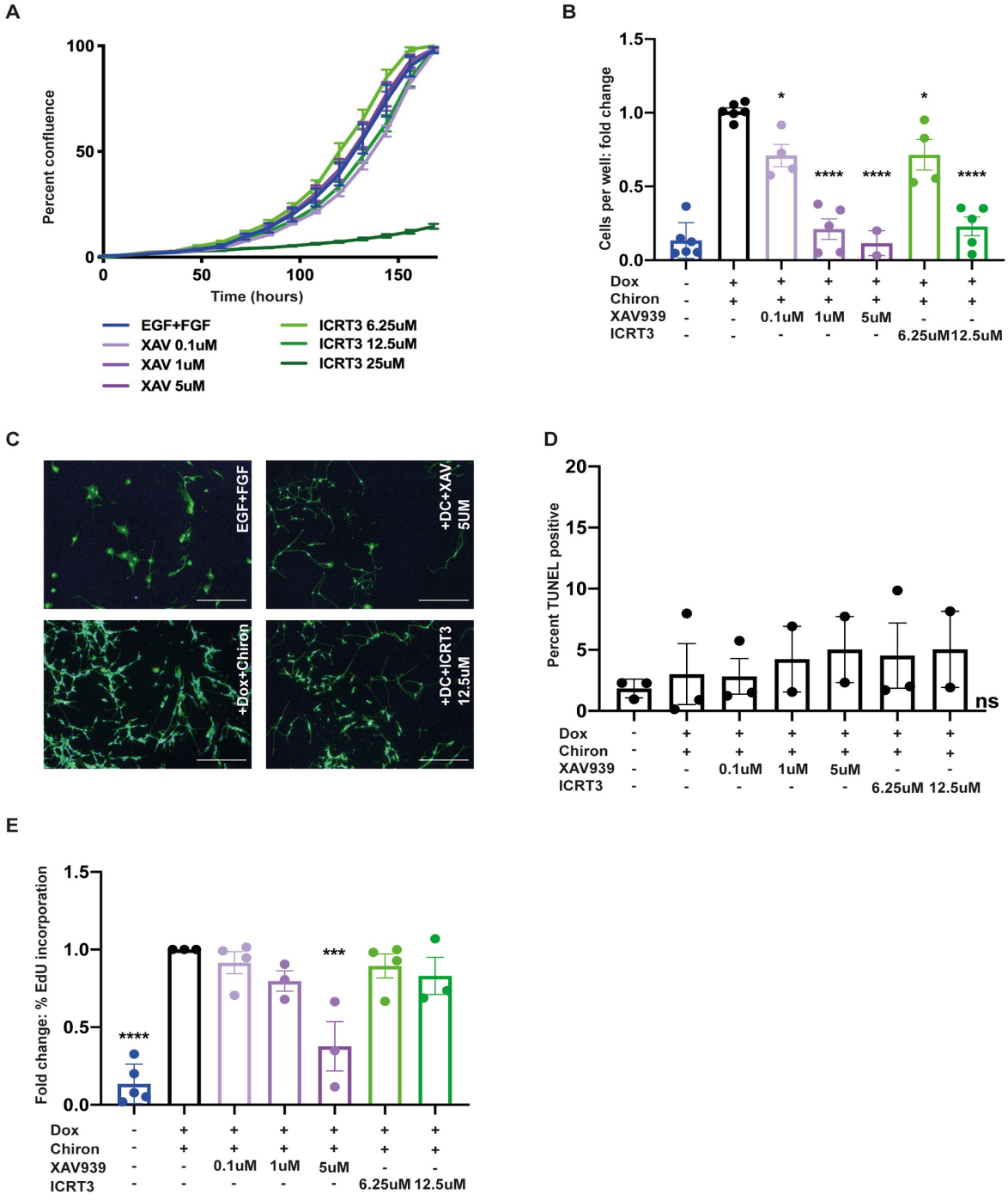
A
Percent confluence
Time (hours)
EGF+FGF
XAV 0.1uM
XAV 1uM
XAV 5uM
ICRT3 6.25uM
ICRT3 12.5uM
ICRT3 25uM
B
Cells per well: fold change
Dox
Chiron
XAV939
ICRT3
0.1uM
1uM
5uM
6.25uM
12.5uM
C
EGF+FGF
+DC+XAV 5UM
+Dox+Chiron
+DC+ICRT3 12.5uM
D
Percent TUNEL positive
ns
E
Fold change: % EdU incorporation

Figure 4. 2 The FOXG1/GSK3i synergy is abrogated by pharmacological Wnt inhibition.

(A) Growth curves showing that XAV939 has no effect on the proliferation of NSCs in EGF+FGF2 up to a dose of 5μM and ICRT3 has no effect on proliferation up to a dose of 12.5μM. n=6. (B) At these doses, the two Wnt inhibitors resulted in a significant reduction in cell number in the cell-cycle re-entry assay (BMP4+FGF2 72hrs, EGF+FGF2+dox+chiron +/- inhibitor for 6 days). Significance shown for comparisons to dox+chiron. (C) Representative images of cells exposed to each of the inhibitors at the assay endpoint. Scale bars 150μm. Green HCS CellMask; Blue DAPI. (D) TUNEL assay confirming no increase in apoptosis with the inhibitors. All non-significant in comparisons to EGF+FGF2 alone. (E) Fold change in EdU incorporation at the endpoint of the cell-cycle re-entry assay (6 days after return to mitogens). Significance shown for comparisons to dox+chiron. (B-E) One-way ANOVA. Shapiro-Wilk test for normality. Each data point represents the mean of a biological replicate with minimum 6 technical replicates.

4.4 Induction of beta-catenin confirms cooperation with FOXG1 in driving exit from NSC quiescence

4.4.1 A tamoxifen-inducible constitutively active beta-catenin cell line shows that the synergy is effected by beta-catenin

I next took a genetic approach to test if increased beta-catenin would synergise with FOXG1 in quiescent NSCs. I created a transgenic cell line with tamoxifen (tam) inducible activated beta-catenin, flanked by LoxP sites for Cre-mediated excision. The resultant beta-catenin protein has an altered N-terminal degradation domain, precluding its ubiquitination. F6 were

used as a parental line, so that I could simultaneously induce FOXG1 with dox. The beta-catenin cassette was a gift from Prof. Austin Smith and is depicted in Figure 4.3A (and the plasmid in Figure 2.3). Addition of tamoxifen leads to the expression of an active beta-catenin which shuttles to the nucleus. Cre-mediated recombination results in GFP expression under the control of the constitutively active beta-actin promoter, so that cells lacking the cassette can be identified. In section 4.4.2, I describe use of this function of the cassette to assess whether its effects are cell autonomous.

After clonal selection, transcriptional activation was confirmed for one of the clones using a TOPFlash reporter assay (Molenaar et al., 1996) (Figure 4.3B). Persistence of the dox-inducible FOXG1 cassette was validated using V5 immunocytochemistry (Figure 4.3C). This cell line was named F6BC1 and enables simultaneous activation of FOXG1 expression or beta-catenin using tam and dox.

This cell line was used to test the hypothesis that the effect of chiron in the synergy is through Wnt signaling, with beta-catenin as its downstream effector. If this is the case, tamoxifen should be able to replace chiron. To investigate this, I first tested response to dox+chiron by plating F6BC1 cells and F6 parental cells respectively in BMP4 media for 24 hrs or BMP4+FGF2 media for 72 hrs then changing the media for EGF/FGF2 media +/- dox and/or chiron. Results for cell number and EdU incorporation after BMP4 exposure for 24 hours and return to growth factors for 6 days were similar, although F6BC1 showed slightly increased cell cycle re-entry (Figure 4.3D), possibly due to some ‘leakiness’ of the cassette. In the BMP4+FGF2 experiment, cell number and EdU incorporation were quantified at 4 days and are therefore lower. They also show increased cell cycle re-entry in F6BC1 in keeping with

leaky expression of the beta-catenin cassette (Figure 4.3E). Overall, the response to dox+chiron is preserved in the F6BC1 cell line.

Next, I tested whether tam could substitute for chiron in driving exit from quiescence. The effect of dox+tam on EdU incorporation was similar to dox+chiron (Figure 4.3 F&G). These results suggest that beta-catenin is the major component through which FOXG1 is cooperating to drive exit from quiescence.

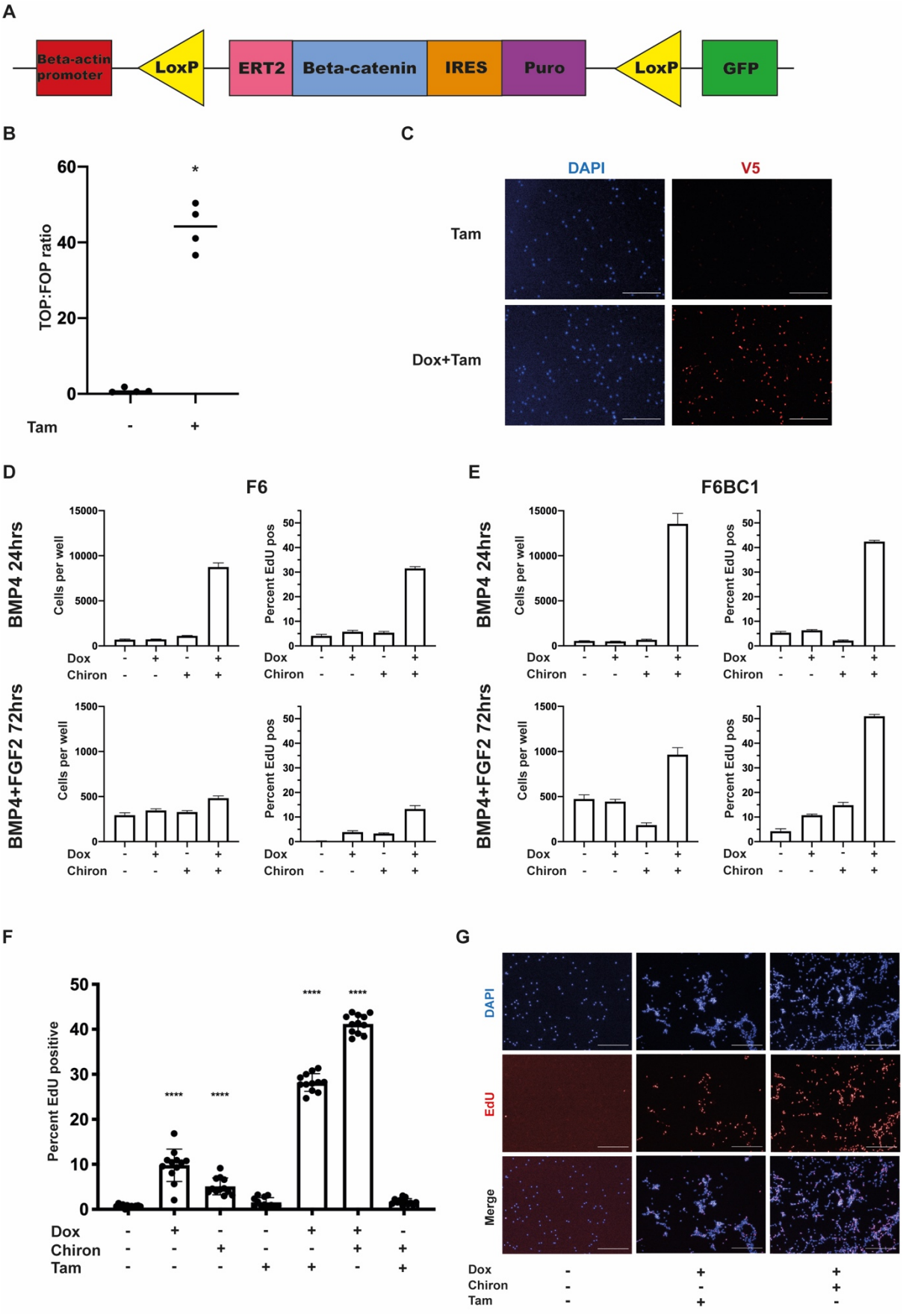
A
Beta-actin promoter
LoxP
ERT2
Beta-catenin
IRES
Puro
LoxP
GFP
B
TOP:FOP ratio
Tam
C
DAPI
V5
Tam
Dox+Tam
D
F6
BMP4 24hrs
BMP4+FGF2 72hrs
Cells per well
Percent EdU pos
Dox
Chiron
E
F6BC1
F
Percent EdU positive
Dox
Chiron
Tam
G
DAPI
EdU
Merge

Figure 4. 3 The inducible beta-catenin cell line confirms that the effects of chiron on qNSCs are through beta-catenin.

(A) Schematic of the functional cassette. (B) TOPflash assay confirms Tcf/lef activation in F6BC1 after exposure to the active metabolite of tamoxifen, 4-hydroxytamoxifen (Tam), for 48 hr. Two-tailed t-test. Shapiro-Wilk test for normality. Means of 4 biological replicates, 6 technical replicates each. (C) V5 staining (red) confirms that the inducible FOXG1 overexpression cassette is intact in the F6BC1 cell line and that it is not activated by tamoxifen in the absence of doxycycline. Blue - DAPI. Scale bars 150μm. (D) and (E) Responses of the parental line (F6) and the inducible beta-catenin line (F6BC1) to dox +/- chiron after induction of quiescence in each of the assays (note the earlier read-out point in the BMP4+FGF2 assay – 4 days cf 6 days for BMP4 assay - preventing direct comparison). n=15. (F) EdU incorporation by condition in F6BC1 cells, after BMP4+FGF2 exposure for 72 hr and return to mitogens for 4 days, shows similar – though less marked - response to dox+tam as to dox+chiron. One-way ANOVA with Dunnett's multiple comparison tests. Significance shown for comparisons to EGF+FGF2 alone. D'Agostino & Pearson test for normality. Chiron 3μM. Tam - 4-hydroxytamoxifen 1μM. n=12. (G) Representative images of F6BC1 cells at assay endpoint showing nuclear staining (DAPI, blue) and EdU incorporation (red). Scale bars 150μm.

4.4.2 Beta-catenin acts cell-autonomously to drive exit from quiescence

Next, further to confirm the role of beta-catenin and to investigate whether the effect is cell autonomous, I tested the hypothesis that excision of the active beta-catenin cassette would remove the functional activation response to tamoxifen. To this end, I transfected the F6BC1 cells with a Cre-containing plasmid (Figure 2.3E), which should excise the beta cassette. After transfection, approximately 50% of cells expressed GFP, a reporter of excision (Figure 2.3F) and this percentage was consistent. Following recovery, cells were subjected to the EdU assay as detailed above. The percentage of EdU positive cells in green and non-green populations in each condition was quantified.

Cells with the active beta-catenin cassette (non-green) respond to either tamoxifen or chiron, where FOXG1 is upregulated by dox. EdU incorporation in dox + tamoxifen is ~30%, as compared to ~1% in EGF+FGF2 alone (Figure 4.4B). In dox + chiron, where there are dual mechanisms of Wnt activation, EdU incorporation is >40%. Green cells (now lacking the beta-catenin cassette), within the same wells, no longer respond to dox + tamoxifen: EdU incorporation remains <10%. However, they retain a response to dox + chiron, which activates the cells' endogenous beta-catenin, with EdU incorporation >20%, similar to levels seen in non-green (cassette intact) cells in dox + tamoxifen (Figure 4.4B). These data suggest that the effect of beta-catenin is cell largely cell autonomous, although a slight, non-significant, increase in EdU incorporation is noted for green cells with dox+tamoxifen over tamoxifen or dox alone, suggesting there could be a very slight degree of 'rescue' from surrounding cells with the active cassette. Of note, the slightly increased EdU incorporation, in dox, of non-green cells (with the cassette intact) as compared to the green cells, suggests some 'leakiness' of the functionality of the cassette, as proposed in section 4.4.1.

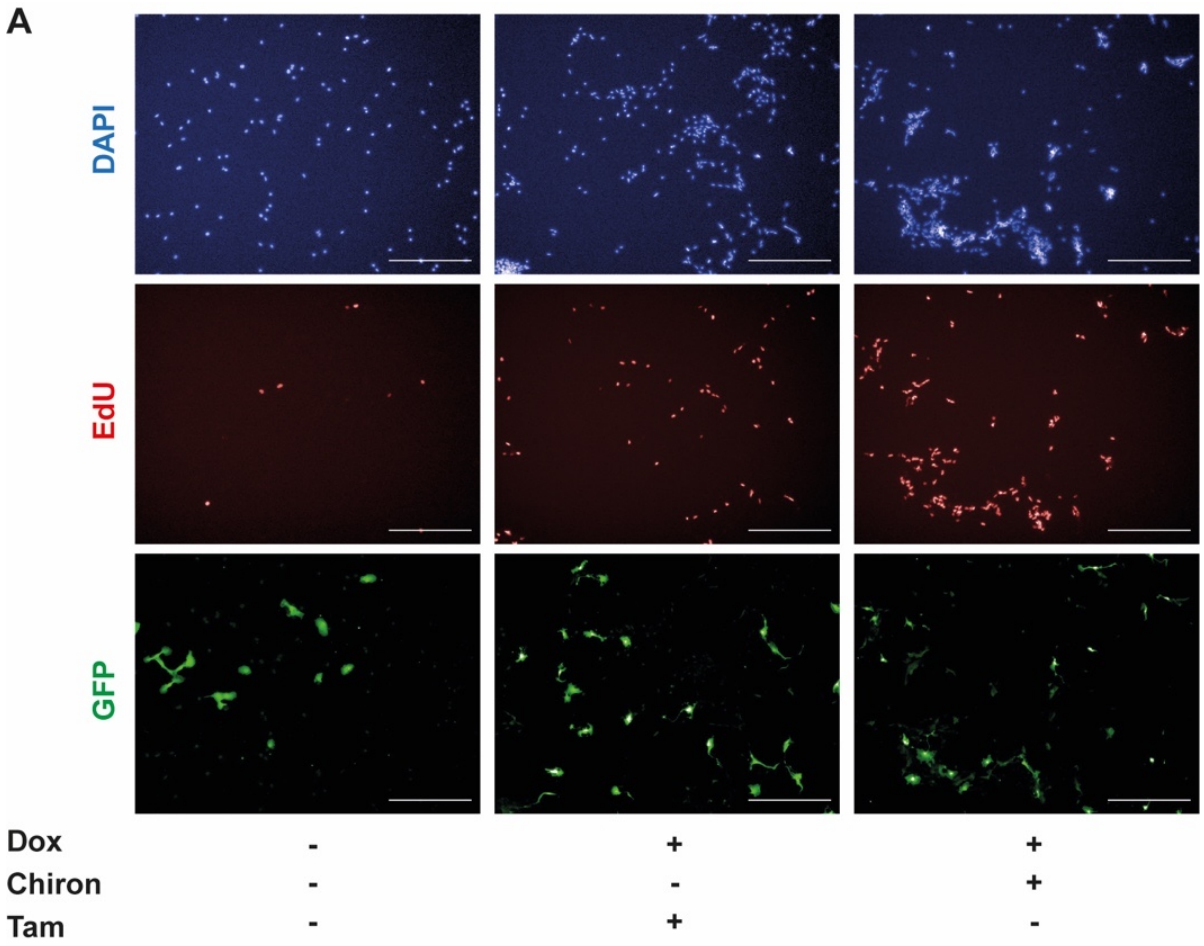
A
DAPI
EdU
GFP
Dox - + +
Chiron - - +
Tam - + -

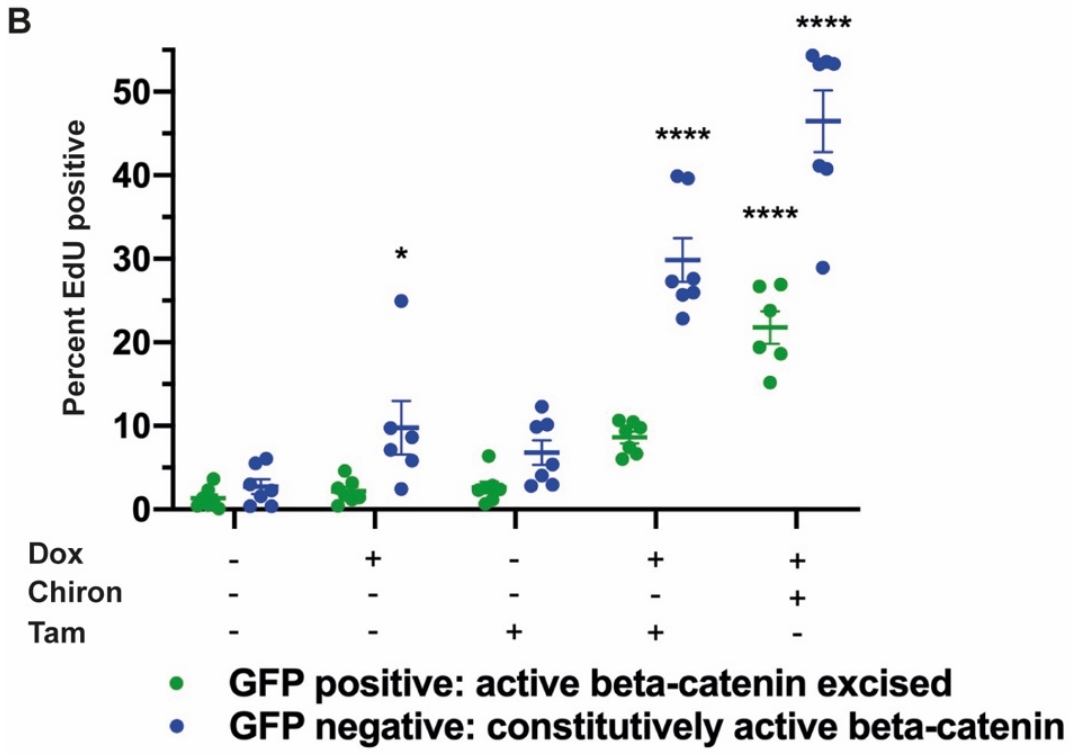
B
Percent EdU positive
0
10
20
30
40
50
*
****
****
****
Dox - + - + +
Chiron - - - - +
Tam - - + + -
GFP positive: active beta-catenin excised
GFP negative: constitutively active beta-catenin

Figure 4. 4 Excision of the beta-catenin cassette confirms its role in the synergy and shows that the effect is cell-autonomous.

(A) Representative images of F6BC1 cells, transfected with Cre-expressing plasmid, then plated in BMP4+FGF2 for 72hr and returned to mitogens for 4 days. DAPI, blue; EdU, red; GFP, green. (B) EdU incorporation by condition showing that cells with the cassette excised (green) retain response to dox+chiron but not to dox+tam. Tam 1μM as previously. Two-way ANOVA with Sidak's multiple comparison tests. Significance shown for comparisons to EGF+FGF2 alone. Data points represent means of 7 biological replicates with minimum n=6 each.

4.5 Elevated FOXG1 in qNSCs primes Wnt target genes for efficient reactivation and cell cycle re-entry

4.5.1 Tcf/lef transcription is activated by FOXG1 upregulation

To interrogate Wnt signaling in vitro and with a view to in vivo studies, I created a reporter line, expressing mCherry under the control of 6 copies of the Tcf/Lef response elements (plasmid gifted by Prof A-K Hadjontanakis). It was clear that the dox + chiron combination led to increased Tcf/lef activation (Figure 4.5B). However, the high basal activity of mCherry expression, likely related to selection by FACS for mCherry (see section 2.8.8), meant that the increase in activity with chiron addition was not easily quantifiable and clonal lines had limited utility for applications monitoring Wnt signaling with imaging based assays (Figure 4.5A).

Upregulation of FOXG1 alone leads to Tcf/lef activation and this was quantified by flow analysis (Figure 4.5C). Clonal lines were expanded in EGF+FGF2, plated in BMP4 for 24 hrs, then EGF+FGF2 +/- dox for 48 hrs prior to flow analysis for mCherry. mCherry expression

was increased in the presence of dox (FOXG1 upregulation). The proportion of cells with Tcf/lef activity was increased from 26% to 36%, and the proportion with high signal from 0 to 9% by the addition of dox (Figure 4.5C). These data suggest that FOXG1 drives Wnt target activation.

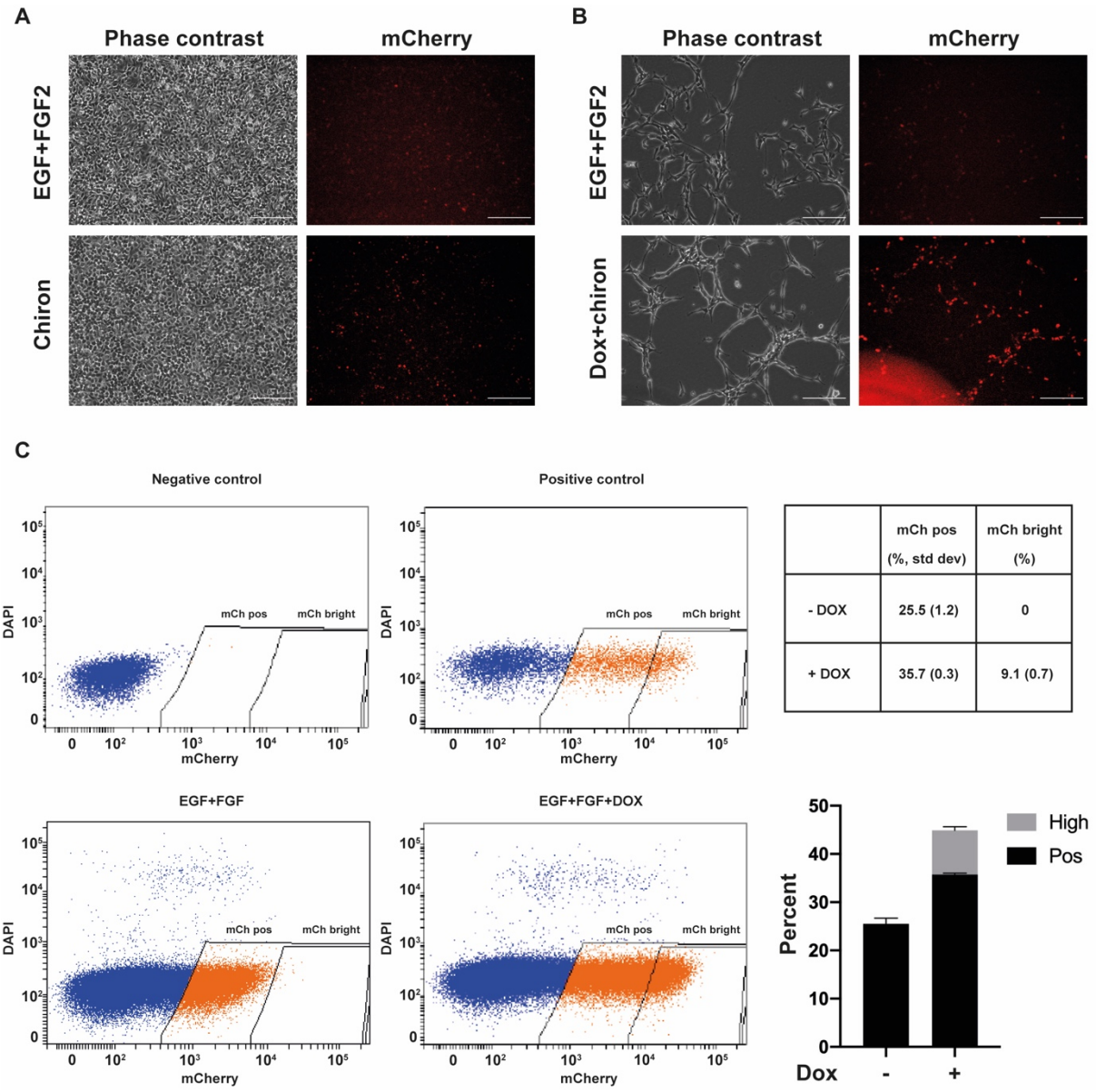

Figure 4. 5 A Tcf/lef reporter NSC line provides evidence that FOXG1 upregulates Tcf/lef activation.

(A) Representative images of reporter cells in EGF+FGF2 +/- chiron 3µM. (B) Representative images of reporter cells in EGF+FGF2 +/- dox+chiron. Red - mCherry. Scale bars 150µm. (C) FOXG1 overexpression with dox leads to increased Tcf/lef activation as measured by mCherry expression. Positive control: NSC line with constitutive mCherry expression. Negative control: F6.

4.5.2 Reverse phase protein array reveals upregulation of Wnt target genes by FOXG1 and further upregulation by FOXG1+GSK3i

Reverse phase protein array (RPPA) is a high throughput platform for sensitive and reproducible quantification of proteins, including post-translationally modified proteins, using validated, highly specific antibodies. Cell or tissue-derived protein samples are immobilised and printed on slides in multiple arrays, which are then probed with a single antibody. The picomole/femtomole sensitivity of the technology allows for robust quantification of even proteins with low expression levels (Byron et al., 2019; Creighton and Huang, 2015).

I collected protein lysates from cells which had been plated in BMP4+FGF2 for 72 hrs, then exposed to EGF+FGF2 +/- dox and/or chiron for 72 hrs. The 72 hr time point was chosen because increases in cell number and EdU incorporation are not yet seen at this point in the assay. Phospho-Plk1 was included in the antibody panel to identify any significant differences in mitotic activity between samples and none were seen (Figure 4.6C). Samples treated with dox+chiron clustered with those treated with dox, rather than those treated with chiron, which clustered with those exposed to neither dox nor chiron (Figure 4.6A). This initial suggestion that the mechanisms of the synergy are effected in part by FOXG1 and augmented by chiron, is further supported by detailed analysis of Wnt target genes within the dataset. The cluster most differentially upregulated in dox+chiron conditions contains c-myc, a known Wnt target (He et al., 1998), and two phosphorylated forms of Rb (Figure 4.6B). Unphosphorylated Rb levels are equivalent across the samples but that mono- and hyper-phosphorylated forms are increased in dox and further increased in dox+chiron conditions. This is likely to be explained by the upregulation, in the same pattern, of Cyclin D1, another Wnt target gene (Shtutman et al., 1999). Western blotting confirms upregulation of these Wnt targets in dox and dox+chiron (Figure 4.6D). There is also a slight upregulation in chiron, as would be expected. Rb

phosphorylation is seen at the G1/S transition and may indicate progression toward cell cycle re-entry but, at this stage in the assay, cells are not seen to divide, EdU incorporation is <10% in all conditions and phosphoPlk1 (a mitotic marker) is not significantly elevated in any condition relative to any other. The pattern of upregulation of Cyclin D1 is consistent with that of other Wnt targets, suggesting a Wnt-driven mechanism.

Non-phosphorylated beta-catenin was not upregulated but there was an unexpected increase in phosphorylated beta-catenin at this timepoint suggesting a possible recent surge in active beta-catenin (Figure 4.6E).

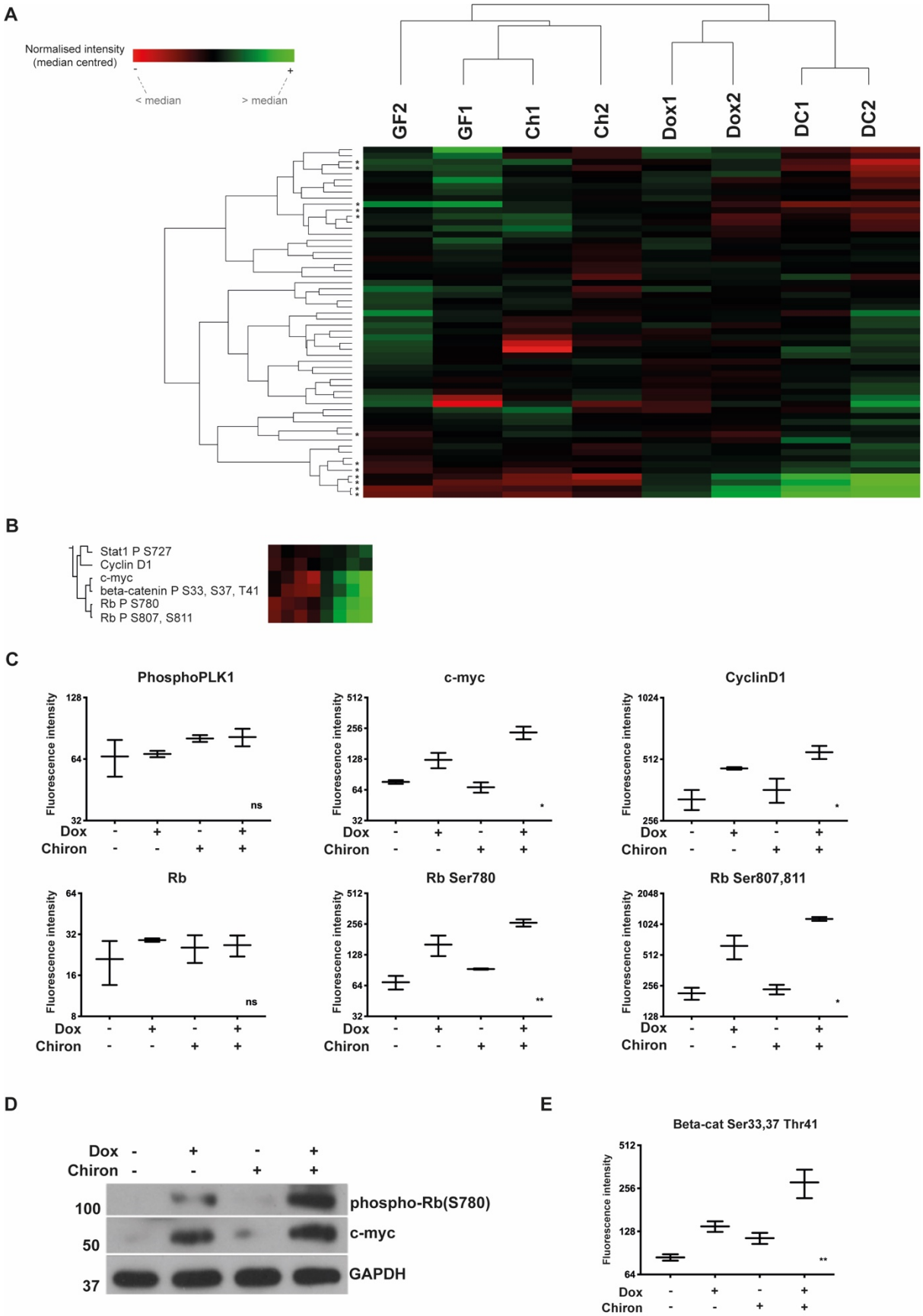
A
Normalised intensity
(median centred)
< median
> median
GF2
GF1
Ch1
Ch2
Dox1
Dox2
DC1
DC2
B
Stat1 P S727
Cyclin D1
c-myc
beta-catenin P S33, S37, T41
Rb P S780
Rb P S807, S811
C
PhosphoPLK1
c-myc
CyclinD1
Rb
Rb Ser780
Rb Ser807,811
Fluorescence intensity
Dox
Chiron
ns
D
phospho-Rb(S780)
c-myc
GAPDH
100
50
37
E
Beta-cat Ser33,37 Thr41

Figure 4. 6 Reverse phase protein array analysis reveals a pattern of activation of Wnt target genes as major hits.

(A) Hierarchical clustering shows that cells exposed to dox, rather than chiron, cluster with those exposed to dox+chiron although the top upregulated proteins are Wnt targets, or the products of Wnt targets. To examine changes to signaling pathways in different cell types, total cell lysates were subjected to RPPA analysis (technical-triplicate analysis of biological duplicates) using a panel of antibodies covering signaling pathways linked to cancer phenotypes. Normalized RPPA data were median-subtracted protein/phosphoprotein- and sample-wise and hierarchically clustered on the basis of uncentered Pearson correlation, computing distances using an average-linkage matrix. Asterisks mark proteins demonstrating significant differences between EGF+FGF and Dox+Chiron conditions (T-Tests with Holm-Sidak post-hoc correction) (B) Details of the major significant cluster. Other significant proteins, as marked by asterisks from top to bottom are: Akt P S473, Akt P T308, Src (family) P Y416, Src, PKC-alpha P T638, Akt. Investigation of these forms the basis of ongoing work and will not be further discussed here. (C) Detailed quantification of the relative abundance of relevant proteins, including mitotic marker phosphoPLK1. Data plotted are the medians of 4 serially diluted dots from 3 technical replicates of duplicate samples. Kruskal-Wallis test. (D) Confirmatory Western blot for the top hits. (E) Relative levels of phosphorylated beta-catenin in the four conditions. Kruskal-Wallis test.

4.5.3 c-myc is a potentially important downstream target of the FOXG1/GSK3i synergy

Upregulation of c-myc by dox and further upregulation by dox+chiron is potentially a driver of the phenotypic changes seen, including exit from quiescence. *Myc* is a target of Wnt

signaling (He et al., 1998) but the protein is also a direct target of GSK3, which phosphorylates c-myc, targeting it for degradation (Morrison et al, 2016; Doble and Woodgett, 2003). The transcriptional activity of *Myc* is exerted via dimerisation with a partner protein, Max. Myc/Max acts mainly as a transcriptional activator but can also act as a repressor in association with Miz1 (Walz et al, 2014). To show the potential functional relevance of c-myc induction to exit from quiescence, I used an inhibitor of Myc/Max dimerisation, 10058-F4 to confirm that Myc has an impact on exit from quiescence. This inhibitor had been used previously by members of the lab and shown to inhibit Myc/Max dimerisation, as has been published by other groups (Müller et al, 2014; Zirath et al, 2013). It should be noted that the doses I used are below those shown to give complete inhibition of Myc/Max dimerisation, as those higher doses resulted in growth inhibition of cells in proliferative conditions, suggesting that Myc activity is essential for proliferation. Instead, I selected doses with no impact on proliferation in EGF+FGF2, to investigate impact of a degree of inhibition on exit from quiescence (Figure 4.7A). F6 cells were plated in BMP4+FGF2 and, after 72 hours, changed to EGF+FGF with dox+chiron +/- 10058-F4. Myc/Max inhibition results in a reduction of cell cycle re-entry, as measured by a reduction in cell number (Figue 4.7B). This is not due to increased apoptosis (Figure 4.7E). I investigated the combination of Myc/Max inhibition with Wnt inhibition and confirmed an additive effect on inhibition of exit from quiescence, as could be expected from the double hit of Wnt inhibition (with its resultant effect on myc among other targets) and Myc/Max inhibition (Figure 4.7C&D). This preliminary work on the role of Myc in the dox/chiron synergy will require further studies.

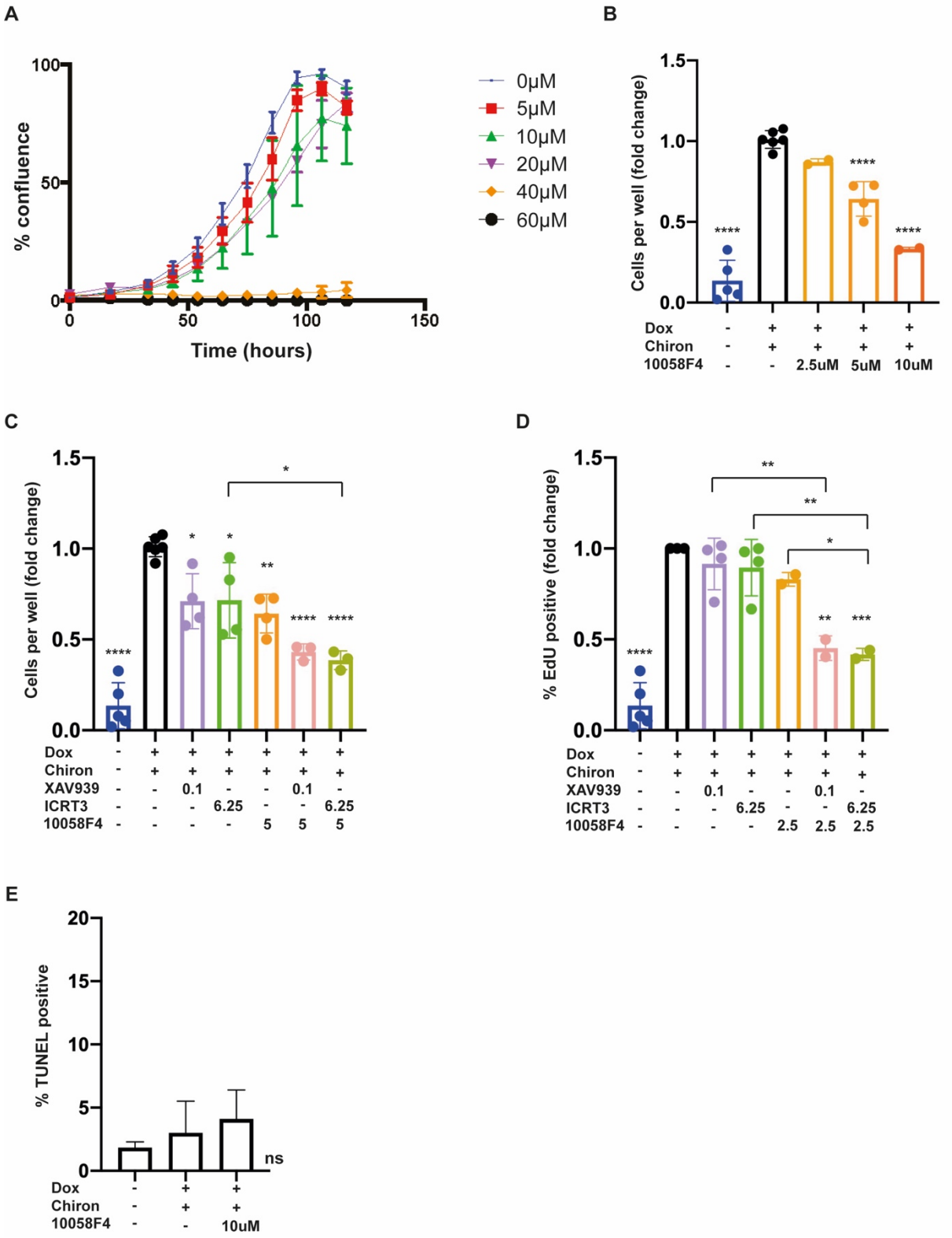
A
% confluence
Time (hours)
0μM
5μM
10μM
20μM
40μM
60μM
B
Cells per well (fold change)
Dox
Chiron
10058F4
2.5uM
5uM
10uM
C
Cells per well (fold change)
Dox
Chiron
XAV939
ICRT3
10058F4
D
% EdU positive (fold change)
Dox
Chiron
XAV939
ICRT3
10058F4
E
% TUNEL positive
ns
Dox
Chiron
10058F4
10uM

Figure 4. 7 An inhibitor of Myc/Max dimerization abrogates exit from quiescence with dox+chiron and has an additive effect with Wnt inhibition.

(A) Growth curve for FS3 cells in proliferative conditions (EGF+FGF2) exposed to different concentrations of 10058-F4. n=3. Graph by Harry Bulstrode. (B) 10058-F4 reduces cell cycle re-entry in F6 cells exposed to BMP4+FGF2 for 72 hours and returned to EGF+FGF2 with dox+chiron +/- 10058-F4 for 6 days at the concentrations shown. One-way ANOVA. n=3-6. An additive effect of Wnt inhibitors (XAV939/ICRT3) and 10058-F4 is shown and can be measured in terms of cell number at 6 days (C) or EdU incorporation at 6 days (D). (C&D) One-way ANOVA. n=3-6. Significance shown or comparisons to dox+chiron. Concentrations in μM. (E) TUNEL assay confirms no significant increase in apoptosis with the highest dose of 10058-F4 used. One-way ANOVA. n=3.

4.5.4 Nanostring analysis suggests that FOXG1 may be activating Wnt target genes and repressing Wnt inhibitors

To assess the impact of FOXG1 overexpression on Wnt target genes and other pathways associated with cancer, I conducted Nanostring analysis on RNA extracted from F6 cells driven into a quiescent state (with BMP4+FGF2) and returned to growth factors +/- dox and/or chiron for 48 hrs. Three biological replicates were analysed. Nanostring quantifies mRNA expression levels in cell or tissue samples using molecular barcoding of specific probes. nSolver software was used to QC check the data and normalise them to internal controls and reference genes before displaying them as relative counts. Differential expression was assessed using the built-in statistical analysis software within nSolver, as described in Wang et al, 2016.

Two hundred and twenty-nine genes were significantly differentially expressed between the dox+chiron condition and the EGF+FGF2 alone condition. The most differentially expressed gene identified in the Nanostring analysis was the Wnt inhibitor *Wif1*, which is significantly downregulated by dox, chiron and, most dramatically, dox+chiron. This result was confirmed by qPCR (Figure 4.8C). *Wif1* is known to be downregulated by Hedgehog pathway (Shh) activity (Ng et al., 2014) and it is known that GSK3 inhibition can increase Shh activity but this would not explain the impact of FOXG1 on *Wif1*. However, *FoxO6* is a positive regulator of Shh activity (Sun et al., 2018) and its expression is increased markedly by FOXG1 overexpression and further increased by the FOXG1/GSK3i combination (Figure 4.8B). This interaction has not been explored further in this thesis and is the subject of ongoing work in the lab. *Wif1* downregulation by FOXG1 could partially contribute to the greater impact of chiron in the context of FOXG1 upregulation. The most differentially upregulated Wnt target genes were *Frzd9*, *Nkd1*, *Axin2* and *Myc*. As expected, *Axin2* expression was upregulated in chiron and dox+chiron conditions but significant upregulation was also seen with dox alone, in keeping with the evidence from the protein data that FOXG1 upregulates Wnt targets (Figure 4.8A). This was confirmed by qPCR for *Axin2* (Figure 4.8C). Consistently, upregulation of Wnt targets *Nkd1* (Koch et al., 2005; Yan et al., 2001) and *Myc* (Xu et al., 2016) were all seen with dox, chiron and, more markedly, dox+chiron (Figure 4.7A&C). Human FOXG1 was present in only the dox and dox+chiron samples, as expected; expression levels were equivalent in each (Figure 4.8B). However, in summary, we find that an unbiased approach yields clear evidence that FOXG1 upregulates Wnt target genes and that their activation is further augmented by chiron. This corroborates evidence from the protein data presented in section 4.5.2.

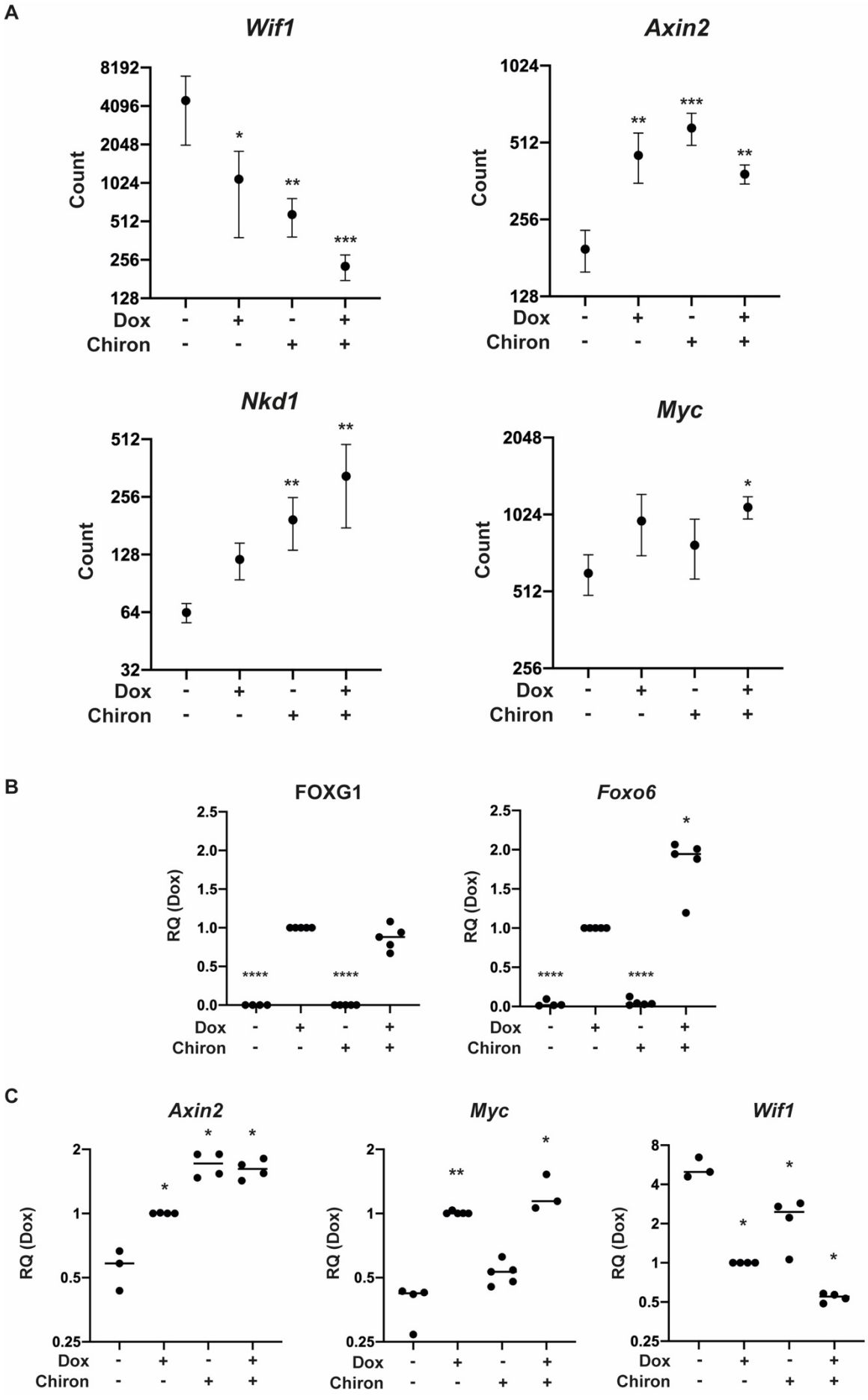
A
Wif1
Axin2
Nkd1
Myc
Count
Dox
Chiron
B
FOXG1
Foxo6
RQ (Dox)
C
Axin2
Myc
Wif1
RQ (Dox)
Dox
Chiron

Figure 4. 8 Nanostring and qPCR suggest activation of Wnt target genes by FOXG1.

(A) The most differentially expressed gene in the NanoString dataset is the Wnt inhibitor, *Wif1*, which is downregulated in dox, chiron and dox+chiron as compared to EGF+FGF2 alone. NanoString was conducted on RNA extracted from F6 cells after 72 hours in BMP4+FGF2 followed by 48 hours in EGF+FGF2 +/- dox and/or chiron. Statistics using nSolver Advanced Analysis software as per Wang et al, 2016. Significance shown is for comparison to EGF+FGF2 alone. n=3. (B&C) qPCR in F6 cells after 72 hours in BMP4+FGF2, then 72 hours in EGF+FGF2 +/- dox and/or chiron. (B) Human FOXG1 is elevated to similar levels in dox and dox+chiron, as expected. *FoxO6* expression is upregulated by dox and further by dox+chiron. Mixed effects ANOVA with Dunnett's multiple comparison tests. Significance shown is for comparison to the dox condition. Each data point (n=4-5) represents the mean of 3 replicates. (C) qPCR confirms NanoString results for *Wif1*, *Axin2* and *Myc* at this slightly later timepoint. Mixed effects ANOVA with Dunnett's multiple comparison tests. Significance shown is for comparison to the EGF+FGF2 condition. Each data point (n=3-6) represents the mean of 3 replicates.

4.6 Conclusions and putative mechanisms of the FOXG1/Wnt synergy

In this chapter, I have shown that the effect of chiron (an additional GSK3 inhibitor to that originally identified in the screen) in this synergy is due to its modulation of Wnt activity, as its contribution can be phenocopied by Wnt3a and by an inducible active beta-catenin inserted into the genome of the cells. I have shown that the synergy may be abrogated by two Wnt inhibitors, each acting at a different point in the signaling pathway (at the destruction complex and at the transcriptional level). The protein and mRNA data hint at a mechanism whereby

FOXG1 alone activates Wnt target genes but a greater activation is achieved by the combination of FOXG1 and GSK3 inhibition. There are two next steps: to establish whether this synergy is relevant to GBM models and to identify the mechanism(s) of the synergy. Chapter 5 will deal mainly with the former question but will go some way to addressing the latter, which will also form the basis for ongoing work beyond this thesis.

The data showing an increase in beta-catenin marked for ubiquitination at the 3 day time point might suggest that the effects on Wnt target genes by FOXG1 are effected through an earlier increase in beta-catenin activity, possibly due to repression of Wif1. The fact that the synergy can be abrogated by two inhibitors acting at different points in the pathway suggests that the effect is not entirely due to a nuclear mechanism. However, there is also evidence that the effect is largely cell-autonomous, which would suggest that altered levels of an extracellular Wnt inhibitor are an unlikely mechanism in isolation.

It is clear from the RPPA and Nanostring data that Wnt target genes are primed by FOXG1 and further activated by the addition of chiron. If upregulated during BMP4 exposure, FOXG1 primes cells to respond to chiron. However, once cells are in a quiescent state, concurrent upregulation of FOXG1 and chiron exposure are required for maximal cell cycle re-entry - sequential administration does not produce an equivalent effect. This could be due to separate effects of both FOXG1 and Wnt on target genes, or to a more direct interaction.

A potential mechanism is suggested by the structure of FOXG1, which, as discussed in Chapter 1, has a Groucho binding domain at which it recruits TLE1, the mammalian equivalent of the *Drosophila* protein Groucho. This interaction is best known in the context of transcriptional co-repression, with FOXG1's repressive effects being augmented by its recruitment of TLE1

(Yao et al., 2001). However, TLE1 is a repressor at Tcf/lef sites and, if it were competitively sequestered from these sites by FOXG1, this could facilitate activation by beta-catenin. The addition of chiron would then further activate transcription. Were this hypothesis to prove correct, a FOXG1 protein lacking the Groucho domain would be expected to fail to reproduce the synergy with chiron. These potential mechanisms will be explored in Chapter 5, although its main focus will be on the synergy in GBM models in vitro and in vivo.

Chapter 5

Relevance of the FOXG1/Wnt synergy to in vivo and human cell line models

5.1 Introduction

Having shown the impact of the Wnt/FOXG1 interaction on exit from quiescence in an in vitro model system, I next sought to confirm its relevance to an in vivo model of GBM.

GBM research is in the fortunate position of having an unparalleled range of preclinical models available for the study of the disease (Robertson et al., 2019). Historically, techniques such as transposase integration, plasmid transfection and viral transduction have been used to deliver oncogenes or short hairpin RNAs to effect in vitro genetic knockdown (Bachoo et al., 2002; Ding et al., 2005; Funato et al., 2014). With the advent and development of increasingly sophisticated genetic modification technology, notably CRISPR, in vitro editing can be used to generate models or reporters of any aspect of the disease (Bressan et al., 2017; Dewari et al., 2018). However, in vitro models cannot recapitulate the complexity of the disease and, for consideration of microenvironmental factors, animal models are necessary. Transplantation of either patient-derived tumour cells or engineered tumour-initiating cells provides a straightforward, tractable and low-cost option for interrogating tumour biology and identifying potential therapeutic targets. Importantly, orthotopic transplantation allows for the correct tissue/microenvironment context for the tumour. Accordingly, I used CRISPR and transposase techniques developed in the Pollard lab to engineer key GBM driver mutations into the F6BC1 parental cells and then used the resultant line in an orthotopic transplant model to examine the

effects of FOXG1 overexpression and Wnt pathway activation on tumour progression and exit from quiescence.

The question of relevance to human disease is crucial in the use of any mouse model. As discussed in section 4.1, whilst Wnt pathway mutations are rare in GBM, Wnt signaling is active in tumours and the areas of highest beta-catenin expression correlate with the location of FOXG1 overexpressing GSCs.

5.2 RNAScope in human GBM samples confirms co-localisation of FOXG1 and beta-catenin

I aimed to confirm the co-localisation of beta-catenin and FOXG1 in human GBM. Immunohistochemistry for beta-catenin in vitro and in vivo can be challenging and there are several situations in which beta-catenin is known to be active and nuclear localised, but cannot be easily detected in the nucleus using IHC (Riggleman et al., 1990; Tolwinski and Wieschaus, 2004). In vitro, I was able to detect beta-catenin in the cytoplasm and the nucleus but it was difficult to detect and quantify a clear difference in nuclear-cytoplasmic shuttling. In vivo, it was more difficult to stain for nuclear beta-catenin. Others have used an antibody for active beta-catenin (Rajakulendran et al., 2019). We opted to use RNAScope to determine if the subset of GSCs in quiescence expresses beta-catenin. RNAScope is an in-situ hybridisation technique for the detection and quantification of mRNA in formalin-fixed, paraffin embedded (FFPE) tissue (Wang et al., 2012). Oligonucleotide probes, specific to target RNA sequences, are hybridized in pairs to RNA targets. Subsequently, signal amplification molecules are hybridized to specific probes and label probes (conjugated to a fluorophore or enzyme

depending on choice of fluorescent or chromogenic assay) are then detected by microscopy (Figure 5.1A).

Our laboratory has established a large resource of patient-derived GSC lines and matched clinical specimens (gcgr.org.uk). We therefore performed RNAScope for FOXG1 and beta-catenin on FFPE samples from primary GBM specimens (Figure 5.1B). Figure 5.1C shows the co-localisation of FOXG1 with beta-catenin in a human GBM sample, donated by an adult patient, suggesting that beta-catenin and FOXG1 are indeed co-expressed in GBM. Quantification of this co-expression and assessment of its structural location within the tumour will be conducted when additional samples have been stained.

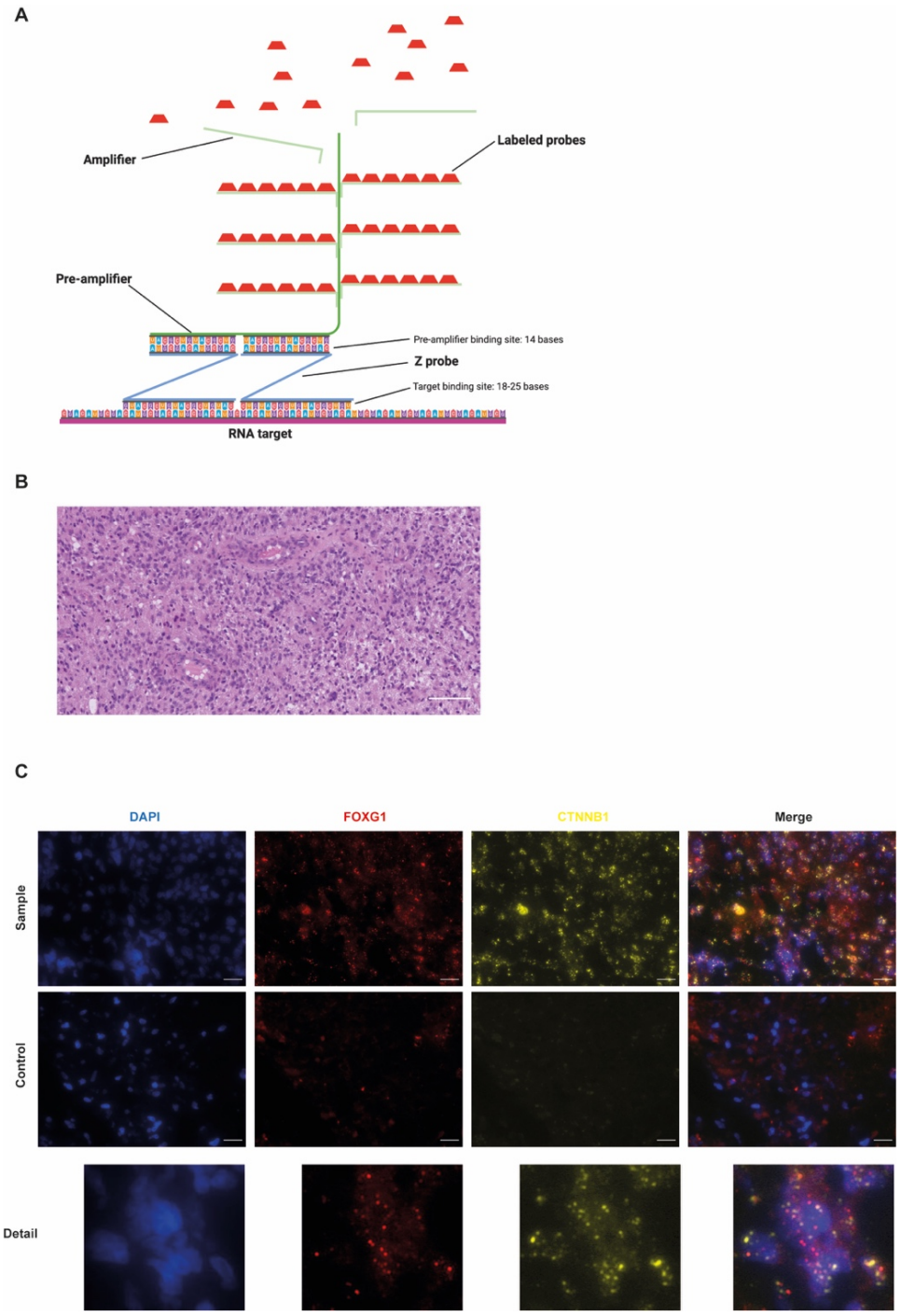

Figure 5. 1 RNAScope confirms co-localisation of FOXG1 (red) and Beta-catenin (yellow) in human GBM.

(A) Schematic of the RNAScope technology. (B) Haematoxylin and eosin stain of patient sample G313, reviewed by NHS consultant pathologist and determined to show diagnostic features of glioblastoma. Magnification 20x. Scale bar 100µm. (C) Representative images of RNAScope in human GBM from the GCGR resource. Scale bars 50µm. Magnification 40x.

5.3 FOXG1 overexpression and Wnt signaling drive accelerated relapse in a mouse model of GBM

5.3.1 A cell line lacking key tumour suppressor genes and expressing a key oncogene was created from the F6BC1 line

I used a single multiplex transfection system (Gangoso, Bradley and Southgate, under review) to excise *Nf-1* and *Pten* using CRISPR-Cas9 from the F6BC1 cells and to introduce EGFRvIII, as well as GFP and luciferase, using the PiggyBac transposase. EGFRvIII is among the most common gain-of-function mutations seen in GBM. Loss-of-function mutations are commonly seen in *Pten* and *Nf-1* together (Brennan et al., 2013; Huse et al., 2011; Olar and Aldape, 2014; Verhaak et al., 2010). Luciferase enables live tracking of tumour development with the IVIS imaging platform, while GFP allows identification of tumour cells in the brain post-mortem. Figure 5.2 shows a schematic of the approach. A single transfection introduces plasmids which encode the sgRNAs for Cas9 mediated excision of *Pten* and *Nf-1* along with a plasmid encoding GFP-Luciferase-Blasticidin resistance cassette with PiggyBac sites, a PiggyBac EGFRvIII plasmid and a plasmid encoding pBase (the PiggyBac transposase). The plasmids encoding the guides for *Nf-1* also encode Cas9mCherry, allowing for initial sorting for transfected cells prior to antibiotic selection (Figure 2.1). This new cell line was termed F6BC1NPE, in reference to *Nf-1*, *Pten*, EGFRvIII.

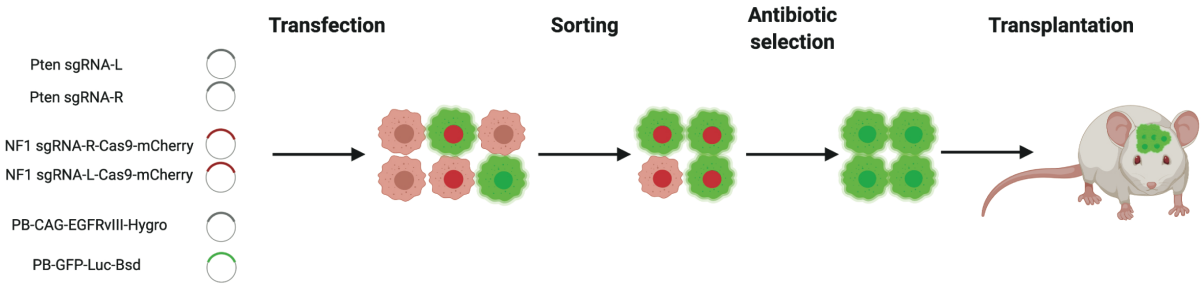

Figure 5. 2 Schematic of the process of generation of tumorigenic lines lacking *Pten* and *Nf-1* and expressing EGFRvIII.

A single transfection was conducted for all plasmids. Sorting for GFP and mCherry 48 hours after transfection allows selection of a population of successfully transfected cells. Sequential antibiotic selection with hygromycin and blasticidin further selects cells containing the EGFRvIII and GFP-Luc cassettes. Correctly targeted cells are tumorigenic on transplantation into the brains of NOD-SCID mice.

5.3.2 Creation of a mouse GBM initiating model enabling activation of FOXG1 and/or beta catenin

To select cells correctly targeted, and therefore most tumorigenic, F6BC1NPE bulk population cells were transplanted into the brains of adult NSG mice – thereby using the mouse to select for the transformed subpopulation. Mice were culled if they displayed motor deficits, lack of grooming or severe weight loss. GFP positive tumours were evident in all mice (Figure 5.3B). The first mouse became symptomatic and was culled after 32 days and all mice were dead by 42 days (Figure 5.3A). H&E staining confirmed that these tumours were histologically similar to human GBM (Figure 5.3D). Staining for beta-catenin and Ki67 confirmed that these were proliferative tumours, positive for beta-catenin, particularly in perivascular areas (Figure 5.3C&E).

Cells were isolated from tumour tissue by disrupting the tissue (by pipetting) and plating homogenised material in stem cell culture media. Clones were picked and expanded and protein was collected from these for Western blotting. This confirmed selection of correctly targeted cells by the process of tumourigenesis in the mouse (Figure 5.3F). Each clone derived from mouse tumours shows complete absence of *Nf-1* and *Pten* and the presence of EGFRvIII. EM4C6 was used for subsequent transplantation experiments and was subjected to puromycin selection to confirm the ongoing presence of the beta-catenin cassette and V5 staining in doxycycline, to confirm the ongoing presence of the FOXG1 cassette.

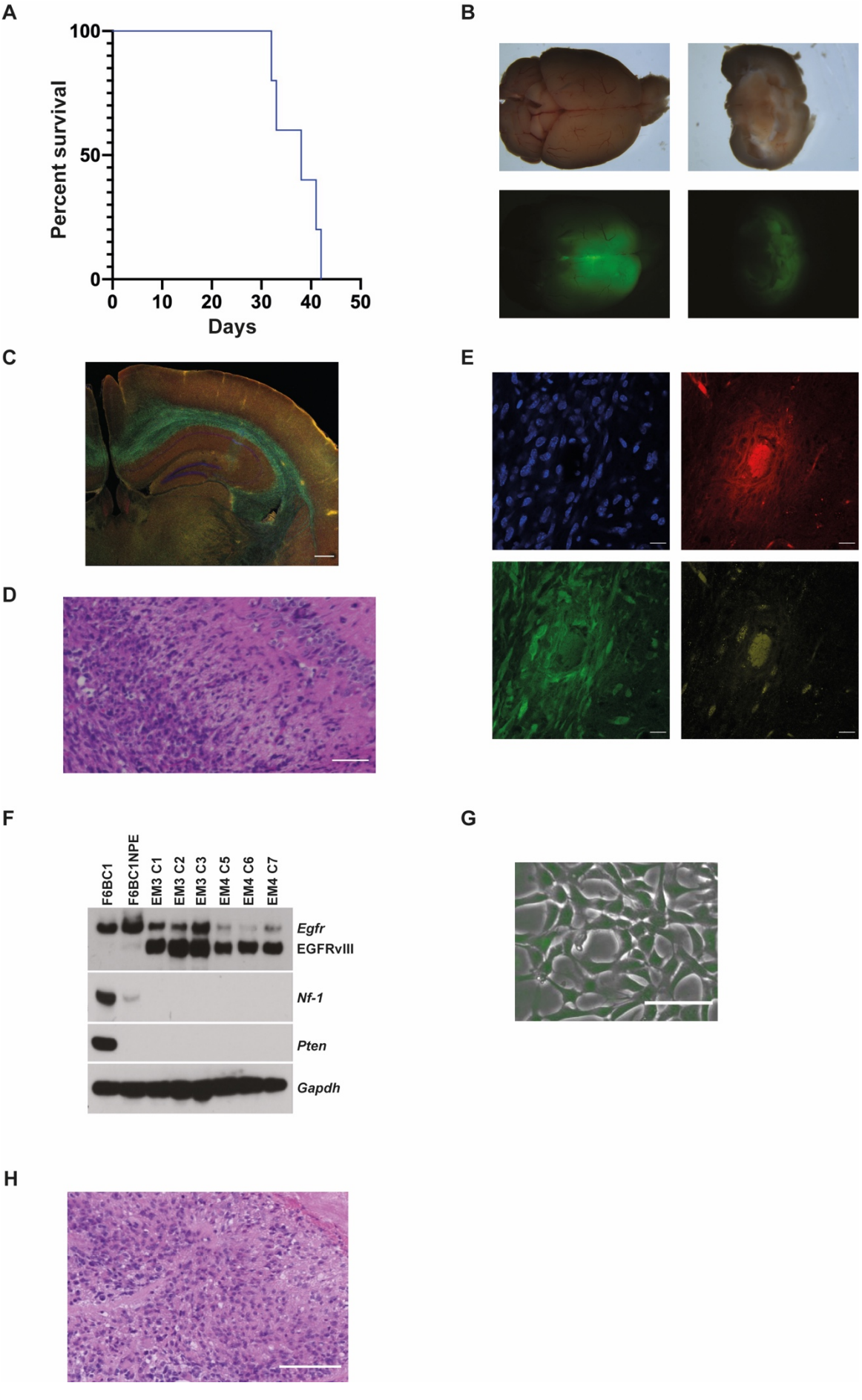
A
100
50
0
Percent survival
0
10
20
30
40
50
Days
B
C
D
E
F
F6BC1
F6BC1NPE
EM3 C1
EM3 C2
EM3 C3
EM4 C5
EM4 C6
EM4 C7
Egfr
EGFRvIII
Nf-1
Pten
Gapdh
G
H

Figure 5. 3 **F6BC1NPE cells are tumorigenic.**

(A) Survival curve for the 5 mice transplanted with the F6BC1NPE cells. (B) GFP positive tumours formed. (C) Tumours were infiltrative, including along white matter tracts. Grey - DAPI, Green - GFP, Red - beta-catenin, Yellow - Ki67. Scale bar 250μm. (D) Tumours show characteristic histological features of human GBM, including necrosis, palisading, apoptosis and mitotic figures (haematoxylin and eosin). Scale bar 100μm. (E) Images of a perivascular zone. Colours as in C. Scale bars 15μm. (F) Western blot of protein extracts from the parental F6BC1 population, the bulk F6BC1NPE population post-transfection, prior to transplantation, and 6 clones, derived from tumours formed in 2 mice. (G) Representative merged brightfield and GFP image of F6BC1NPE cells in culture media containing puromycin. Scale 50μm. (H) Human GBM for comparison with (D) showing similar characteristic features of GBM. Scale bar 100μm.

5.3.3 In vivo induction of FOXG1 results in accelerated tumour growth and reduced survival time.

It is known that elevated FOXG1 levels correlate with poor prognosis in GBM and that FOXG1 knockdown delays tumour growth in xenotransplant models (Verginelli et al., 2013). It has also been shown that knockout of FOXG1 abolishes the tumorigenicity of human GSCs (Bulstrode et al., 2017). However, there is no direct evidence that increased FOXG1 is sufficient to drive accelerated tumour growth. This inducible human FOXG1 overexpression system was therefore first used to test this directly. In view of the rapid course of the tumours generated by the parental F6BC1NPE cells, EM4C6 cells were transplanted in reduced numbers (50000 per mouse) into the SVZ of 12 mice, to give a longer period for monitoring of tumour growth so that, when tumours of roughly equivalent size were identified by IVIS

imaging, mice could be randomised to receive doxycycline 2mg/ml in drinking water with 5% glucose, or 5% glucose alone.

Similar luciferase signal was seen in 9 of the mice after 27 days (Figure 5.4A), 5 were randomised to receive dox and 4 to receive glucose alone from the following day. The mice were monitored by clinical assessment and IVIS imaging and were culled when they showed symptoms (defined in advance as any symptoms suggestive of illness or loss of ≥20% body weight). After culling, brains were collected and imaged to confirm the presence of an infiltrative tumour in each case (Figure 5.4B). Importantly, activation of the dox-inducible FOXG1 cassette was confirmed by V5 staining, which establishes the utility of this model for the assessment of the impact of FOXG1 upregulation (Figure 5.4C). In this pilot experiment, doxycycline treated mice had accelerated tumour growth and reduced survival time (Figure 5.4D).

This initial experiment tested the effect of FOXG1 upregulation on an established tumour, with an established proliferative population. We hypothesised that upregulation would have a greater effect earlier after engraftment, a situation analogous to the putative clinical context in which relapse occurs, when a small residual stem-cell population persists and begins to cycle. To test this, 50000 cells were transplanted orthotopically into the brains of each of 12 mice. Mice were randomised by cage to receive dox/glucose or glucose alone from day 10 after transplantation, prior to IVIS signal development. Again, mice were monitored clinically and by weekly IVIS imaging and culled when they became symptomatic. A significant difference in survival was seen between the two groups, with the dox group having a median survival of 40 days, compared to 51.5 days in the glucose alone group (Figure 5.4E). These data show that FOXG1 upregulation results in more aggressive tumours which kill the host more rapidly, in

keeping with human REMBRANDT data showing an anti-correlation of prognosis to FOXG1 expression (Verginelli et al., 2013).

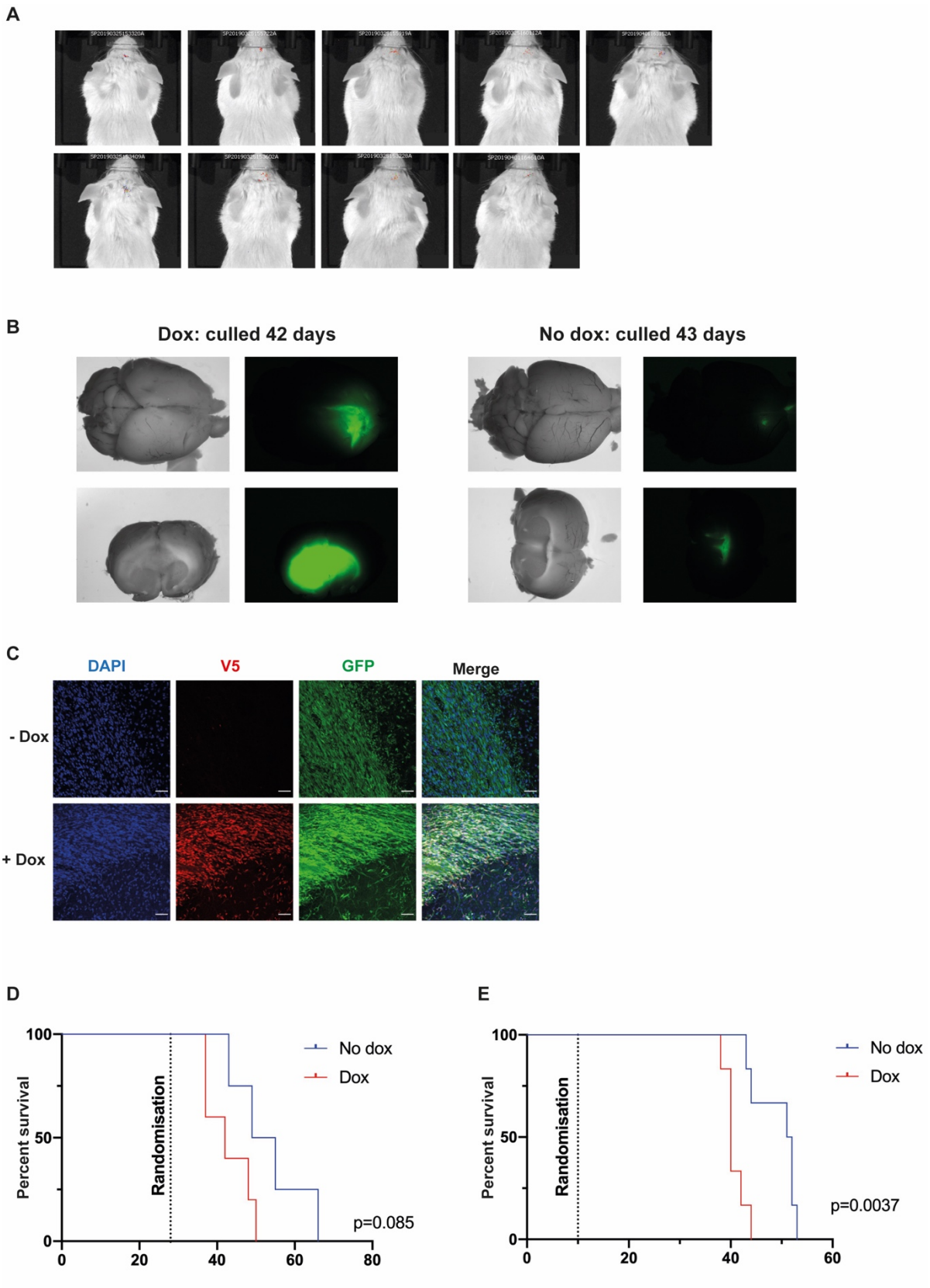
A
B
Dox: culled 42 days
No dox: culled 43 days
C
DAPI
V5
GFP
Merge
- Dox
+ Dox
D
Percent survival
Randomisation
No dox
Dox
p=0.085
E
Percent survival
Randomisation
No dox
Dox
p=0.0037

Figure 5. 4 FOXG1 upregulation in vivo results in reduced survival time in the NPE tumour model.

(A) IVIS imaging showing the emergence of early tumours at 27 days. (B) Representative images of GFP positive tumours seen at the time of culling in mice given dox+glucose (Dox) or glucose alone (No dox). (C) Representative images showing GFP positive tumour cells which express V5 in the context of dox administration. Blue - DAPI, Red - V5, Green - GFP. Scale bars 50μm. (D) Survival curve for mice randomised to dox+glucose or glucose alone at 28 days. Log-rank (Mantel-Cox) test. (E) There was a significance reduction in survival of mice randomised, at 10 days, to dox+glucose as compared to glucose alone. Log-rank (Mantel-Cox) test.

5.3.4 Upregulation of FOXG1 results in an increase in cytoplasmic beta-catenin in tumour cells

Wnt signaling is active in human GBM and is likely to be active in the microenvironment in these mouse tumours. I stained vibratome slices of mouse brains from mice given dox or glucose alone, for beta-catenin, to establish whether FOXG1 upregulation alone, in vivo, is sufficient to drive increased Wnt signaling, in keeping with the RPPA and Nanostring data. Beta-catenin was increased in the tumours of mice which had been exposed to dox, suggesting an increase in Wnt signaling in these mice (Figure 5.5A). In keeping with the pattern of expression seen in human GBM, beta-catenin expression is most prominent in perivascular areas (Figure 5.5) Notably, staining was seen in the cytoplasm of tumour cells but not the nucleus. Identifying an increase in nuclear beta-catenin is notoriously problematic and future staining may make use of an antibody specific to activated beta-catenin. The antibody used here does not distinguish between active and inactive, or differentially phosphorylated, forms of beta-catenin. RPPA data showed an increase in phosphorylated beta-catenin, marked for

ubiquitination, in dox and, particularly, dox+chiron conditions in vitro, suggesting a recent surge in activity. A plausible explanation for increased beta-catenin in the tumours of mice given dox is the repression of Wif1, as seen in the NanoString dataset. Increased Wif1 would lead to activation of Wnt signaling and increased levels of beta-catenin in tumour cells.

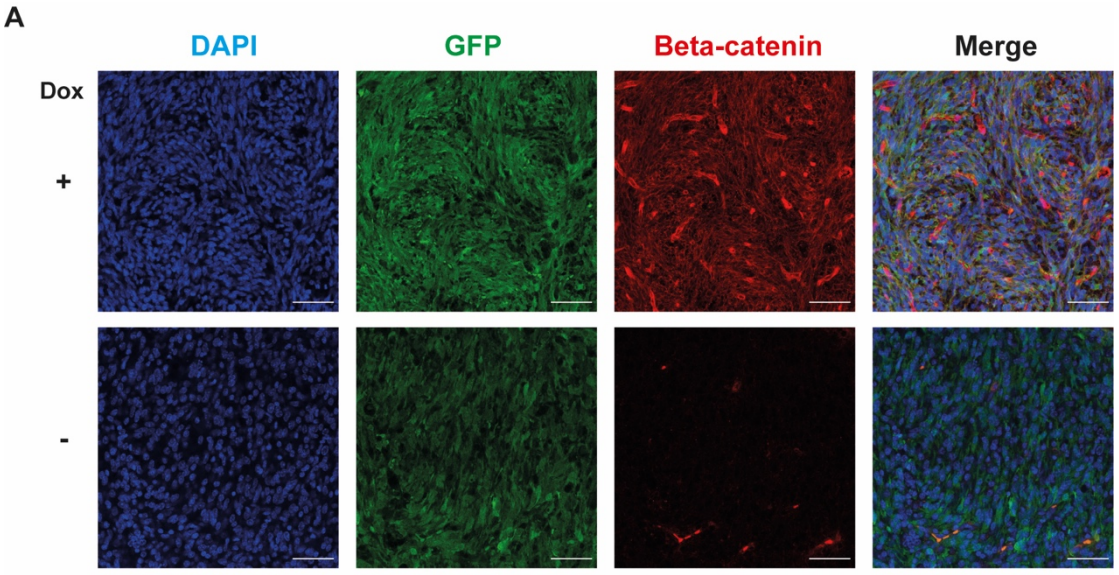
A
DAPI
GFP
Beta-catenin
Merge
Dox
+
-

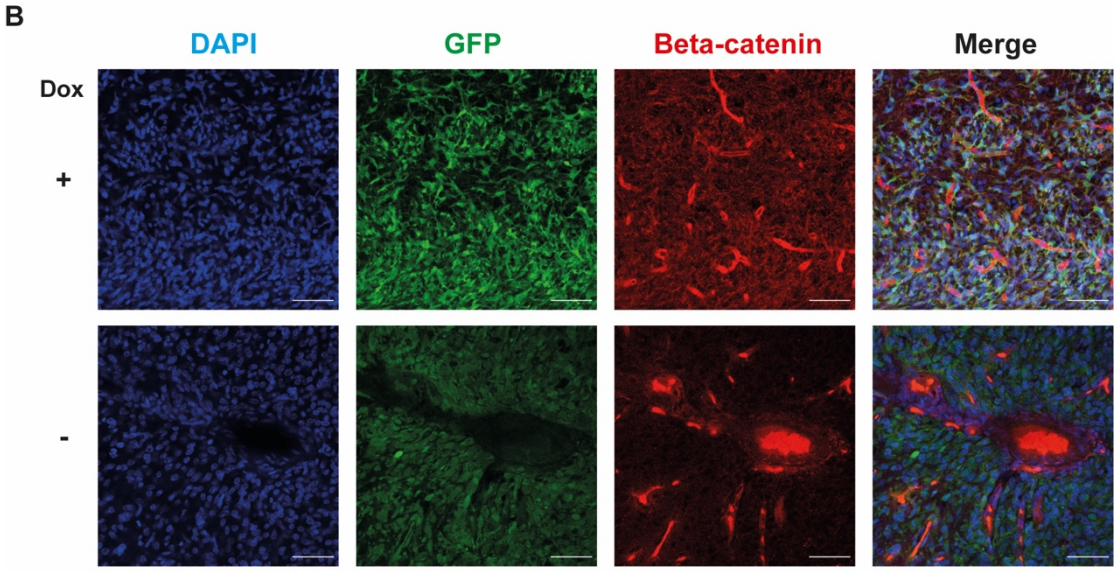
B
DAPI
GFP
Beta-catenin
Merge
Dox
+
-

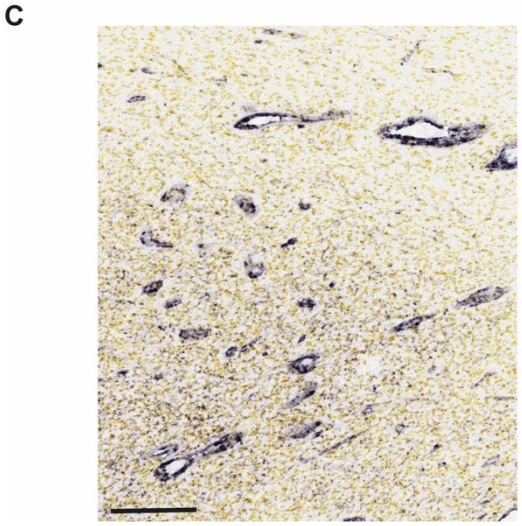
C

Figure 5. 5 FOXG1 upregulation in vivo leads to increased beta-catenin accumulation in tumour cells.

(A&B) show different areas of tumours from mice given dox or not given dox. Blue - DAPI, green - GFP, red - beta-catenin. Scale bars 50μm. Autofluorescence is seen in erythrocytes within the vessels. Tumour cells are GFP positive. (C) In situ hybridisation for beta-catenin in an adult GBM specimen (Ivy GBM Atlas Project) - beta-catenin is seen in tumour tissue, most markedly in perivascular regions. Scale bar 200μm.

5.3.5 Induction of active beta-catenin results in non-significantly accelerated tumour growth

The obvious next step was to test whether the addition of tamoxifen to doxycycline could accelerate tumour growth and reduce survival time by super-activation of Wnt. However, as detailed previously, Wnt signaling is active in GBM (Liu et al., 2011; Sareddy et al., 2009) and so we might expect that FOXG1's effect on exit from quiescence is achieved by interaction with endogenous Wnt and requires no additional Wnt activation. The rapid progression of these tumours with doxycycline treatment was a further reason to suspect that there may be little scope for an additional effect of tamoxifen and this led to a slight change in approach. Cells were plated in BMP4 media (without EGF or FGF2) to induce a less proliferative state prior to transplantation of 200000 cells into the brains of each of 11 mice. The growth rate of these NPE cells (EM4C6) reduces in BMP4 media and EdU incorporation is reduced but division is not completely abolished and cells remain primed to re-enter cell-cycle upon return to EGF/FGF2 media (Figure 5.6B), in a situation analogous to human patient-derived GSCs (Carén et al., 2015). Mice were started on doxycycline the day after transplantation and one group (5 mice) were given intraperitoneal tamoxifen 3mg (approx. 100-120mg/kg) on day 2,

while the other group received vehicle alone. We aimed to deliver a transient pulse of Wnt activity, at a time when FOXG1 levels had become elevated but shortly after transplantation, while cells had yet to escape from quiescence. A schematic of the experiment is shown in Figure 5.6A. Tumours, as measured by IVIS signal, developed more rapidly in mice given tamoxifen (Figure 5.6C). There was a quantifiable trend, not quite reaching significance, toward increased tumour size and growth in this group (Figure 5.6D). There was also a trend towards shorter survival time in the group given both dox and tamoxifen, although this was minimal and not significant (Figure 5.6E).

There are a number of possible reasons for the failure to reach significance. Firstly, the numbers of mice are small. Secondly, although many cells were rendered non-dividing by BMP4 treatment prior to transplantation, the high cell number transplanted allowed for an aggressive clinical course with short survival time and therefore less opportunity for differences to become apparent. Thirdly, the dose of tamoxifen was deliberately cautious and low (see Chapter 2) and may not have provided a high enough or sustained enough intracerebral concentration of the active metabolite. Finally, and most importantly, there is likely to be sufficient endogenous Wnt in the microenvironment that the signaling pathway is active even in the absence of tamoxifen induced active beta-catenin within cells, blunting the comparison.

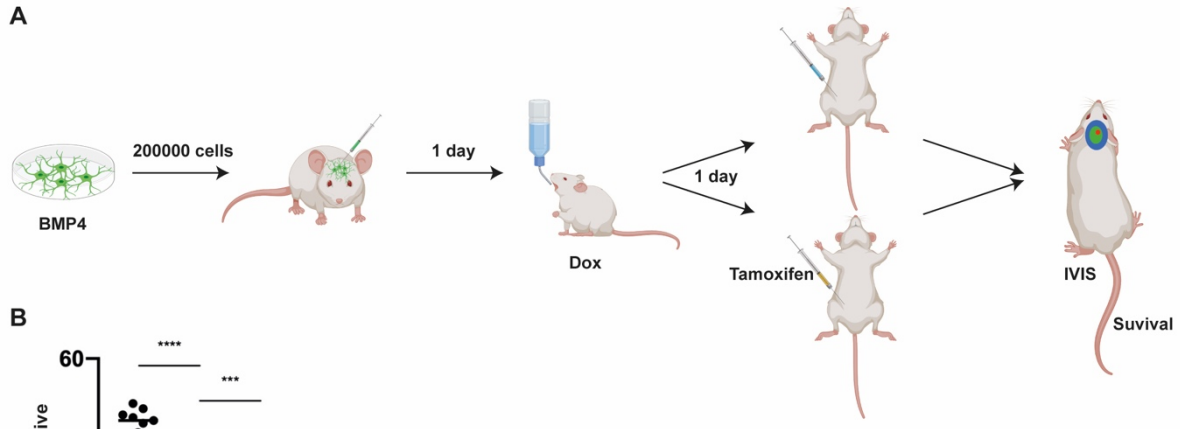
A
200000 cells
BMP4
1 day
Dox
1 day
Tamoxifen
IVIS
Suvival

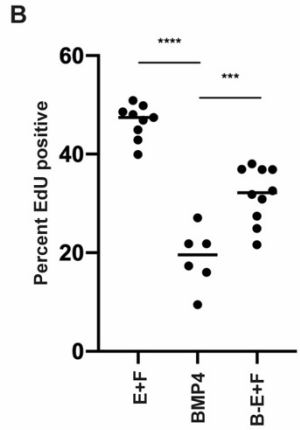
B
****
***
Percent EdU positive
60
40
20
0
E+F
BMP4
B-E+F

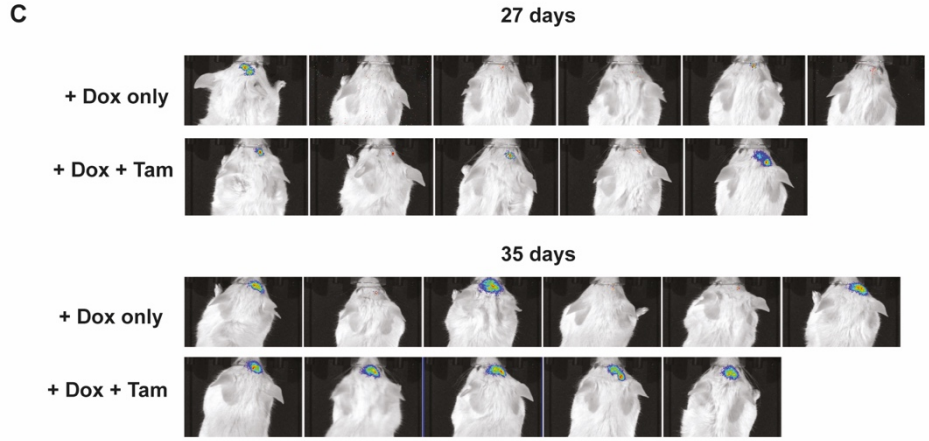
C
27 days
+ Dox only
+ Dox + Tam
35 days
+ Dox only
+ Dox + Tam

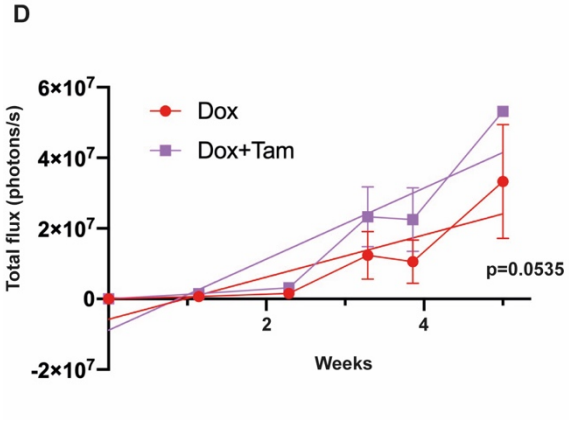
D
Total flux (photons/s)
6×10^7
4×10^7
2×10^7
0
-2×10^7
Dox
Dox+Tam
p=0.0535
2
4
Weeks

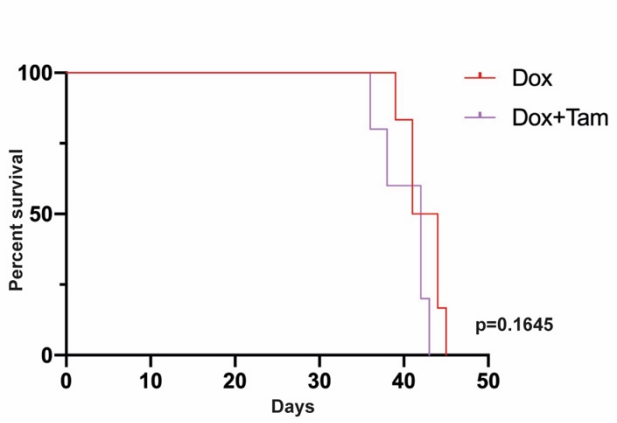
E
Percent survival
100
50
0
Dox
Dox+Tam
p=0.1645
0
10
20
30
40
50
Days

Figure 5. 6 Induction of active beta-catenin results in accelerated tumour growth.

(A) Schematic of the experiment to evaluate the impact of tamoxifen on tumour growth. (B) EdU incorporation of EM4C6 cells in proliferative conditions (E+F), BMP4 (B) and on return to proliferative conditions after BMP4 exposure (B-E+F) showing that these transformed cells retain some response to BMP4. One-way ANOVA with Tukey's multiple comparison tests. Shapiro-Wilk test for normality. (C) IVIS images from days 27 and 35. (D) Quantification of IVIS signal in the two groups over time shows non-significant trend toward faster growth in the group given dox+tam as compared to dox alone. Linear regression analysis. (E) Survival curve for mice given dox alone and mice given dox+tamoxifen. Log-rank (Mantel-Cox) test.

5.4 The synergy between FOXG1 over-expression and Wnt signaling is relevant to two human GBM cell lines, one adult and one paediatric

Results in the previous chapters and sections have been obtained using mouse cell based models, engineered to mimic human GBM. However, in spite of their physiological and genetic similarities to the human, mice cannot fully recapitulate all the conditions and complexities of the human disease. I aimed to demonstrate direct relevance of the synergy between FOXG1 and Wnt signaling in human GSCs. BMP4 signaling is known to trigger cell-cycle exit in NSCs (Bonaguidi et al., 2005) and in human GSCs in vitro and in vivo, reducing their tumorigenicity (Piccirillo et al., 2006). This has been proposed to represent astrocyte differentiation. However, previous work in the Pollard lab has shown that, although human GSCs acquire an astrocytic morphology, they do not acquire the DNA methylation changes of differentiated astrocytes and remain primed to re-enter cell cycle, suggesting a quiescent NSC phenotype rather than that of

a differentiated astrocyte (Carén et al., 2015). Furthermore, the response to BMP4 is variable across human cell lines.

I selected G7, which exhibit a typical reduction in cycling on exposure to BMP4 but remain primed to re-enter a proliferative state and which are known to be high in FOXG1 (Engström et al., 2012), to investigate the effect of the FOXG1/chiron interaction on human GSCs. The Pollard lab have previously characterised G7 in terms of FOXG1 and SOX2 expression, response to BMP4 and chromatin accessibility (Engström et al., 2012; Carén et al., 2015; Bulstrode et al., 2017). The lab had existing data characterising the response of G7 and a G7 FOXG1 knockout cell line to BMP4, which showed that these cells could be driven out of cycle with BMP4 and that excision of FOXG1 did not alter their growth kinetics (Figure 5.7, Harry Bulstrode). My data show that, while loss of FOXG1 does result in a slightly more pronounced response to BMP4 (Figure 5.8D), FOXG1 is not necessary to drive increased cell cycle re-entry after exposure to BMP4 (Figure 5.8E), in keeping with the mouse NSC data presented in Chapter 3.

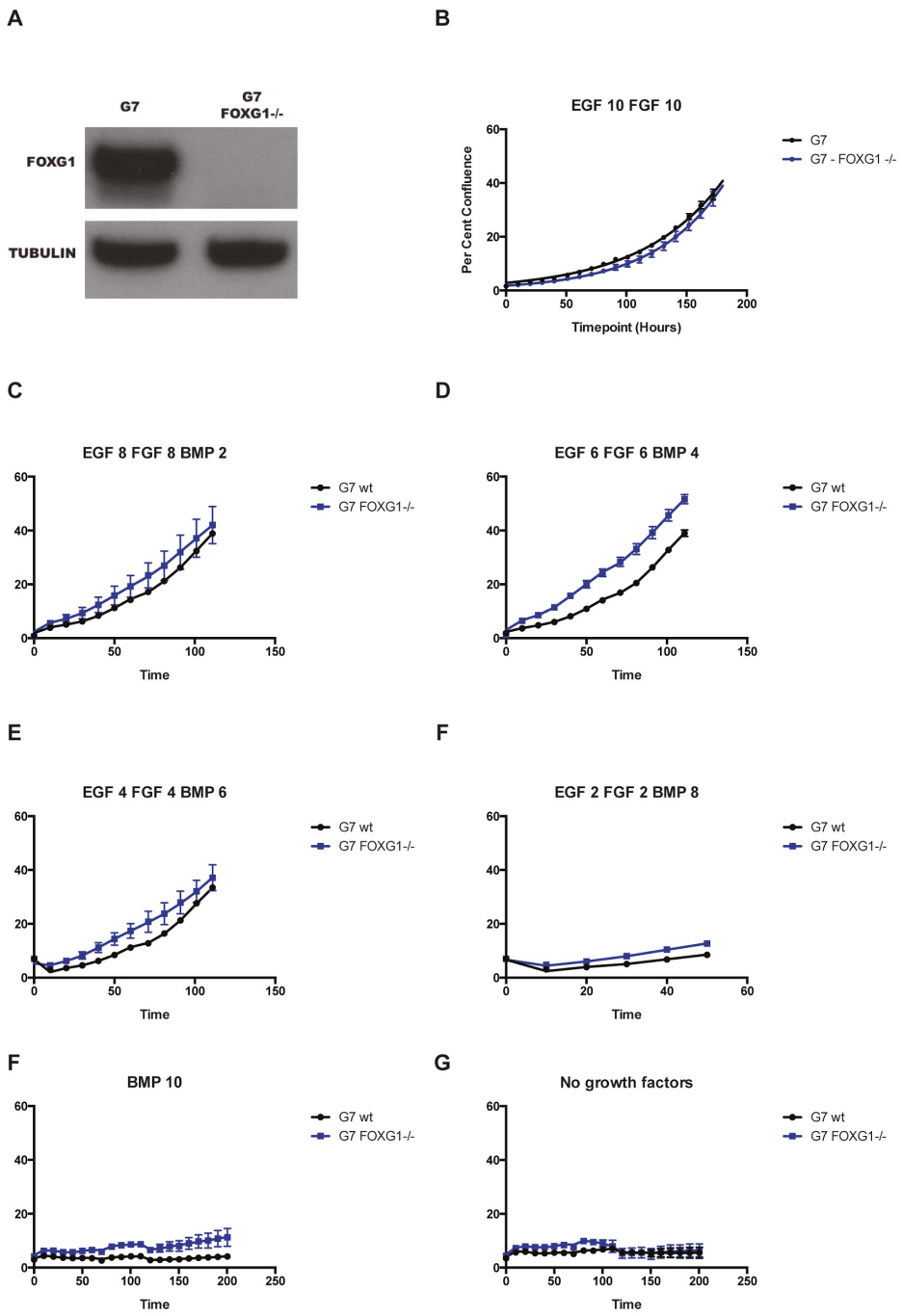

Figure 5. 7 Functional assays of GNS cell line G7 and G7 FOXG1-/- in various culture conditions.

(A) G7 FOXG1-/- clone A1 demonstrates absent expression of the protein (B-G) A range of combinations of EGF/FGF and BMP supplementation fail to elicit differences in proliferation between wild type and FOXG1-/- derivatives. Values refer to ng/ml of EGF, FGF2 and BMP4. Figure by Harry Bulstrode.

5.4.1 The synergy is relevant to adult GSCs in a BMP4-induced quiescence model.

I hypothesised that the high endogenous levels of FOXG1 in G7 would be sufficient to synergise with chiron in driving increased exit from quiescence. Importantly, I first showed that chiron has no effect on the growth rate of G7 cells in proliferative conditions, ie. in EGF+FGF2 media, never exposed to BMP4 (Figure 5.8A). To test the effect of chiron on quiescent cells specifically, I plated G7 at low density (30 cells/mm^2) in BMP4 for 8 days (in accordance with the schedule used in (Carén et al., 2015)) and then re-exposed them to EGF+FGF2 media +/- chiron 3μM for 6 days. Those cells exposed to chiron grew faster and reacquired, more quickly, a proliferative NSC morphology. Cell number per well in chiron was at least double that in EGF+FGF2 alone, and cell area approximately half (Figure 5.8B), in keeping with the visible reacquisition of a proliferative NSC morphology (Figure 5.8C). Of note, doxycycline had no effect on cell number or morphology, consistent with the fact that its effect in the F6 mouse NSCs was to upregulate FOXG1 expression only.

Next, I tested the dose response to chiron in G7 and G7 FOXG1 null cells, again using an 8 day BMP exposure. It could be expected that the effect of chiron would be abolished by excision of FOXG1, if its effects are due to a synergy with FOXG1. BMP4 for 8 days reduces EdU incorporation, after a 6 hr incubation, from around 30% to around 10% but does not completely abolish it. The effect is more dramatic in FOXG1 null cells, with levels reducing to <10% (Figure 5.8D) but response to return to EGF/FGF2 media for 4 days is equivalent for the FOXG1 intact and null cells (Figure 5.8E) showing that FOXG1 is not necessary for cell cycle re-entry.

The effect of chiron on cell cycle re-entry, or exit from quiescence, is seen only in the presence of FOXG1 and a dose-dependent relationship can be demonstrated, up to 5μM (Figure 5.8E). I varied the duration of exposure to EGF/FGF2 +/- chiron and the duration of EdU pulse to show that this effect is consistent. It can be represented as a fold change in EdU incorporation with chiron as compared to EGF+FGF2 alone. Chiron results in an average 2.5 fold increase in EdU incorporation in cells with intact FOXG1 but no difference in EdU incorporation where FOXG1 has been excised (Figure 5.8F). These data suggest that, just as in the mouse NSC quiescence-to-proliferation model, this cooperation between FOXG1 and Wnt is operating in human GBM stem cells.

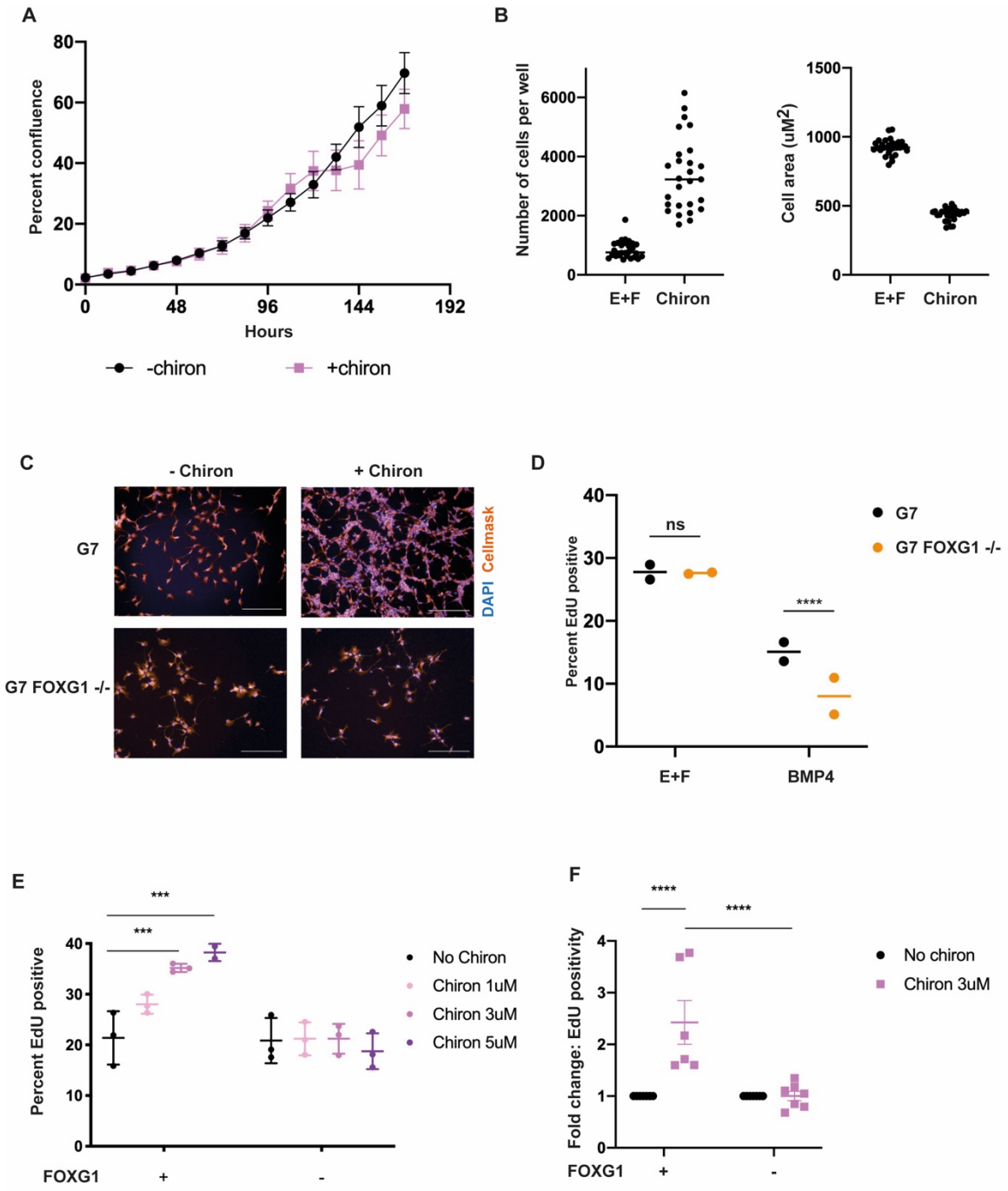
A
Percent confluence
80
60
40
20
0
0
48
96
144
192
Hours
-chiron
+chiron
B
Number of cells per well
6000
4000
2000
0
E+F
Chiron
Cell area (uM2)
1500
1000
500
0
E+F
Chiron
C
- Chiron
+ Chiron
G7
G7 FOXG1 -/-
DAPI Cellmask
D
Percent EdU positive
40
30
20
10
0
ns
****
E+F
BMP4
G7
G7 FOXG1 -/-
E
***
***
Percent EdU positive
40
30
20
10
0
FOXG1
+
-
No Chiron
Chiron 1uM
Chiron 3uM
Chiron 5uM
F
****
****
Fold change: EdU positivity
4
3
2
1
0
FOXG1
+
-
No chiron
Chiron 3uM

Figure 5. 8 Chiron drives cell cycle re-entry in adult GSCs in a FOXG1-dependent manner.

(A) Chiron has no effect on the rate of growth of G7 cells in proliferative conditions. (B&C) After BMP4 exposure for 8 days and return to mitogens for 4 days, however, chiron drives increased proliferation and reacquisition of a proliferative NS morphology, as quantified here by cell area and demonstrated in representative images. Blue - DAPI, Red - HCS CellMask. Scale bars 150μm. Cells were stained with HCS CellMask, a cytoplasmic stain to allow visualisation of morphology and assessment of morphological parameters. Data points represent technical replicates in a pilot experiment. (D) FOXG1 knockout has no impact on EdU incorporation in proliferative conditions but does confer increased sensitivity to BMP4 in terms of cell cycle exit. 8 day exposure to BMP4, 6hr EdU pulse. Mixed-effects analysis with Sidak's multiple comparison tests. Data points represent means of biological duplicates with 3-6 replicates each. (E) Chiron drives exit from quiescence in a dose-dependent manner, only in the context of intact FOXG1. 8 day exposure to BMP4, return to mitogens for 4 days. Two-way ANOVA with Sidak's multiple comparison tests. Data points represent means of 3 biological replicates with 6-15 replicates each. (F) The effect of chiron is consistent across experiments with varied time intervals and plating densities, as expressed by fold change. Mixed-effects ANOVA. Data points represent means of 6 biological replicates with 6-15 replicates each.

5.4.2 A paediatric GSC line is also responsive to chiron, only in the context of intact FOXG1

GBM is one of the most common childhood cancers. Paediatric GBM is clinically and histologically similar to the adult disease but the emergence of differences in genetic and molecular profiles has shown that paediatric and adult GBM are biologically distinct (Jones et al., 2012). In spite of these differences, elevated FOXG1 expression is seen in paediatric GBM. Schwartzentruber et al identified two single nucleotide variant mutations in the H3F3A gene which encodes the histone H3.3. The mutations (K27M and G34R - in one case G34V) were found in a third of paediatric GBMs (Schwartzentruber et al., 2012). A further paper from the same group showed that the two mutations gave rise to tumours in different anatomical sites and with differentially regulated transcription factors (OLIG1, OLIG2 and FOXG1). G34 mutant tumours were found in the cerebral cortex and showed high levels of FOXG1 expression, whereas K27 mutants were found in midline locations and demonstrated hypermethylation and consequent lower levels of FOXG1 (Sturm et al., 2012).

To assess further the relevance of the FOXG1/Wnt synergy to human GBM, I tested the effect in a paediatric GBM derived cell line, GBM002, known to express FOXG1 at high levels (Mohammad et al., 2017). First, as for the adult line, I ensured that chiron had no effect on the cells in proliferative conditions (Figure 5.9A). A FOXG1 null cell line was created from this parental line by Raul Bressan. Western blotting confirmed the loss of the protein in the knockout line (Figure 5.9B). Next, I exposed the cells to BMP4, in the absence of growth factors, for 8 days and returned them to EGF/FG2 +/- chiron for 4-6 days. I found a small but significant effect of chiron on exit from quiescence in the context of intact FOXG1. No effect of chiron was seen in the FOXG1 knockout cells (Figure 5.9C). These data can be represented as fold change as compared to EdU positivity in cells returned to EGF+FGF2 alone, to account

for variability between plates due to plating density/minor variations in timescales (Figure 5.9D). As with the adult line, the FOXG1 knockout showed an increased sensitivity to BMP4 but no difference in EdU incorporation after return to growth factors, suggesting, again, that FOXG1 is not necessary for cell cycle re-entry (Figure 5.9E). These data suggest, however, that FOXG1 is necessary for the response to chiron and that the FOXG1/Wnt is relevant to this paediatric in vitro model.

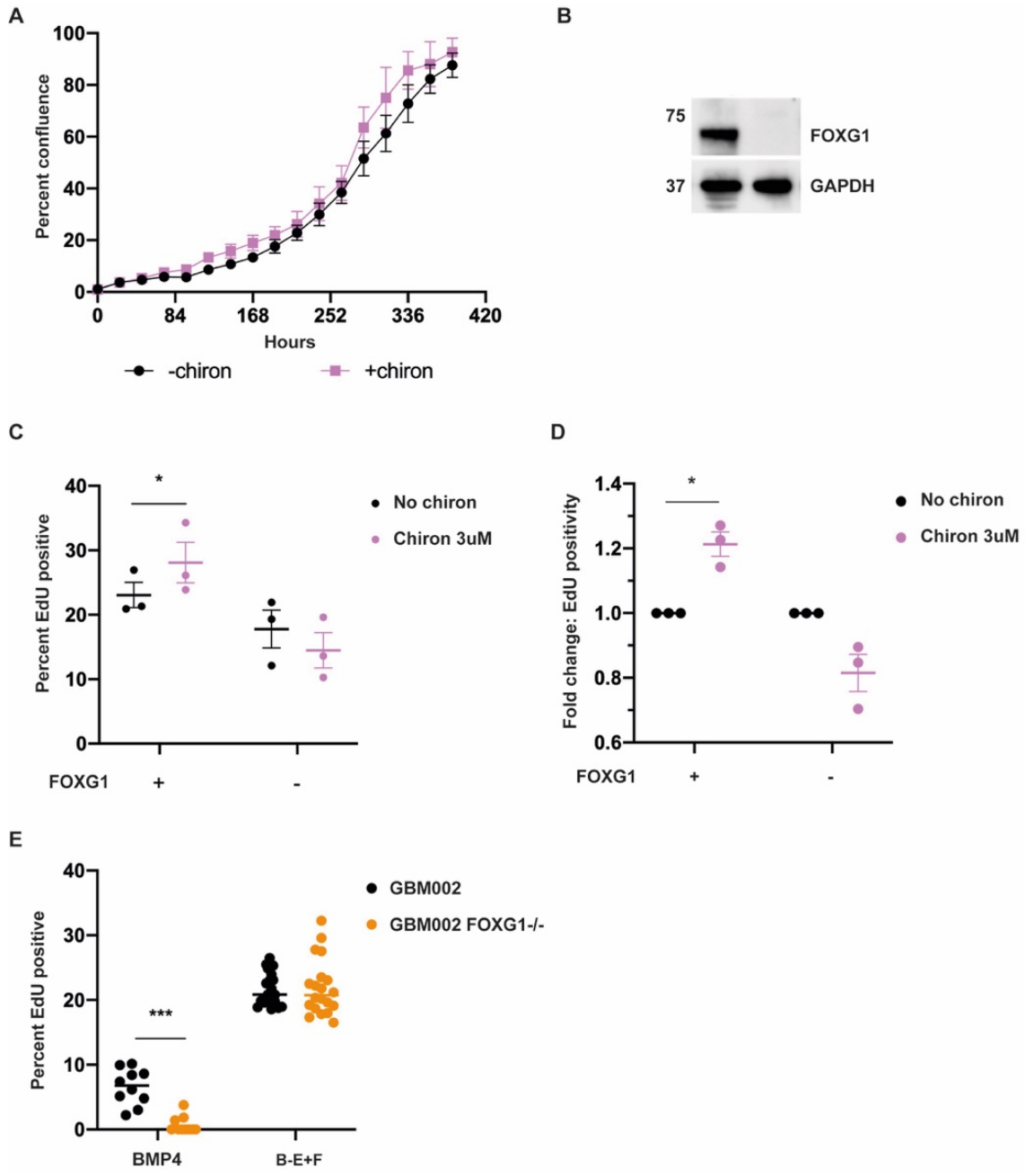
A
Percent confluence
100
80
60
40
20
0
0
84
168
252
336
420
Hours
-chiron
+chiron
B
75
37
FOXG1
GAPDH
C
Percent EdU positive
40
30
20
10
0
*
No chiron
Chiron 3uM
FOXG1
+
-
D
Fold change: EdU positivity
1.4
1.2
1.0
0.8
0.6
*
No chiron
Chiron 3uM
FOXG1
+
-
E
Percent EdU positive
40
30
20
10
0
***
GBM002
GBM002 FOXG1-/-
BMP4
B-E+F

Figure 5. 9 A paediatric GSC line is responsive to chiron only in the context of intact FOXG1.

(A) Chiron has no impact on the growth of GBM002 cells in proliferative conditions. (B) Western blotting confirms FOXG1 knockout. (C) Chiron 3μM results in increased cell cycle re-entry where FOXG1 is intact, but not in the knockout. n=3 biological replicates with 15 technical replicates each. Exposure to BMP4 for 8 days, return to mitogens +/- chiron for 4-6 days. (D) Representation of these data as fold change over cells returned to EGF+FGF2 without chiron. (E) The knockout exhibits increased cell cycle exit in response to BMP4 but identical return to cell cycle, as compared with the FOXG1-intact cell line. Data points represent replicates in a pilot experiment. (C-E) Two-way ANOVA with Sidak's multiple comparison tests. B-E+F: cells plated in BMP4 for 8 days and then returned to media containing EGF+FGF2 for 4 days.

5.5 The Groucho binding domain of FOXG1 is required for cooperation with Wnt signaling

A potential mechanism for the FOXG1/Wnt synergy is suggested by the structure of FOXG1, which has a Groucho binding domain. As mentioned in Chapter 1, the mammalian equivalent of Groucho is TLE, which FOXG1 is known to recruit in the context of transcriptional repression (Yao et al., 2001). TLEs are also involved in Wnt signaling as co-repressors of Tcf/lef transcriptional activation (Cavallo et al., 1998; Lee et al., 2009). Could elevated FOXG1 sequester TLE from Tcf, facilitating transcriptional activation by beta-catenin? If so, FOXG1 lacking the Groucho binding domain (GBD) would fail to synergise with chiron in driving exit from quiescence.

I first confirmed rescued FOXG1 expression in G7 FOXG1 null cells, using a gateway cloning approach to deliver sequences coding for wild-type FOXG1 or for FOXG1 minus the GBD, tagged with HA, via PiggyBac for stable integration (Figure 5.10A). After creation of clonal lines, the presence of FOXG1 was confirmed by Western blotting (Figure 5.10B) and immunocytochemistry for FOXG1 and HA (Figure 5.10C&D). EdU incorporation assays were conducted after exposure to BMP4 for 8 days and return to EGF+FGF +/- chiron for 4-6 days, as in previous assays. A greater increase in proliferating fraction was seen in the cells rescued with wild-type FOXG1 as compared to cells rescued with Groucho-domain-null FOXG1, suggesting that the Groucho binding domain has a role in the interaction of FOXG1 with chiron (Figure 5.10E). Loss of the GBD does not abolish the effect of chiron entirely, suggesting that the GBD-mediated effect is not the only mechanism of the synergy, which fits with findings in Chapter 4 and section 5.3.4 of this chapter, that point to repression of the Wnt inhibitor Wif1 and increased beta-catenin where FOXG1 is upregulated. Further work with these lines, and an expansion of this strategy to other human GSC lines, could determine whether Wnt target gene activation is reduced in the absence of the GBD.

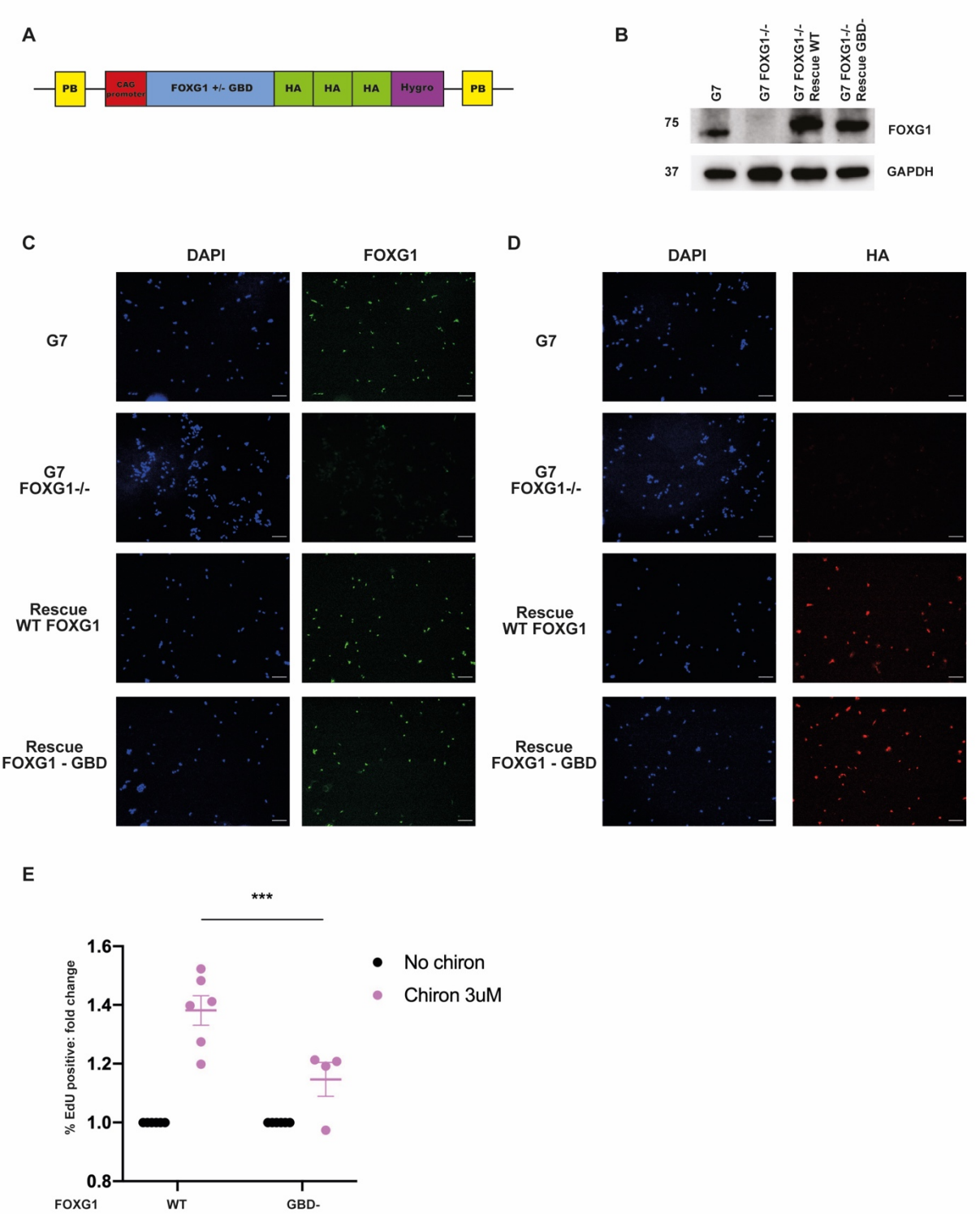
A
PB
CAG promoter
FOXG1 +/- GBD
HA
HA
HA
Hygro
PB
B
G7
G7 FOXG1-/-
G7 FOXG1-/- Rescue WT
G7 FOXG1-/- Rescue GBD-
75
FOXG1
37
GAPDH
C
DAPI
FOXG1
G7
G7 FOXG1-/-
Rescue WT FOXG1
Rescue FOXG1 - GBD
D
DAPI
HA
G7
G7 FOXG1-/-
Rescue WT FOXG1
Rescue FOXG1 - GBD
E
***
% EdU positive: fold change
1.6
1.4
1.2
1.0
0.8
FOXG1
WT
GBD-
No chiron
Chiron 3uM

Figure 5. 10 The synergy depends, in part, on the FOXG1 Groucho binding domain.

(A) Schematic of the cassette used to rescue FOXG1 expression in the knockout cells. (B) Western blotting confirms re-introduction of FOXG1. (C&D) Immunocytochemistry for FOXG1 and HA in the parental G7, the G7 FOXG1 knockout and the two rescue lines confirms integration and expression of the cassette. Blue - DAPI, green - FOXG1, red - HA. Scale bars 150μm. (E) Rescued cell lines have a reinstated response to chiron after exposure to BMP4 for 8 days and return to mitogens +/- chiron for 4-6 days. This is significantly reduced where the GBD is missing. Expressed as fold change relative to EGF+FGF2 alone (no chiron). Two-way ANOVA with Sidak's multiple comparison tests. Data points are means of biological replicates with n=15.

5.6 The FOXG1/Wnt synergy is relevant to an additional, highly clinically-relevant, model of quiescence

Having established the relevance of the synergy to this well established in vitro model of quiescence, I next sought to investigate its effect in another model of quiescence, arguably more relevant to the clinical reality of post-treatment quiescence and reactivation at relapse. I used radiation to induce cell cycle exit. It has been reported that ionising radiation induces cellular senescence, a state of irreversible cell cycle exit (Tabasso et al., 2019), but I found that cells could be driven into a non-dividing state, with minimal EdU incorporation, and the population could then recover, suggesting that some cells are in a reversible state of cell cycle arrest (Figure 5.11A). Regardless, if chiron has a FOXG1-dependent effect on cell proliferation post-irradiation, this would suggest additional clinical relevance.

Doses of 6Gy and over led to a flattening of the growth curve when delivered to mouse NSCs plated at 30 cells/mm^2 in EGF+FGF2 media (Figure 5.11A). EdU incorporation (2 hr pulse) is reduced <5% 3 days after an 8 Gy dose - as compared with 45% in cells given sham irradiation (Figure 5.11B). G7 GSCs can be driven out of cycle in a manner comparable with BMP4-induced quiescence, at 72 hr (Figure 5.11C&D) and irradiated cells upregulate gammaH2AX, a marker of double strand DNA breaks (Kuo and Yang, 2008) consistent with the expected effect of ionising radiation (Figure 5.11E&F). A pilot experiment with G7 cells, using a 6Gy dose, suggested that chiron had an impact on EdU incorporation at 72 hr post-irradiation and that this translated into a difference in cell number at 196 hr. This effect was not seen in the G7 FOXG1 knockout line (Figure 5.11G&H). However, it was apparent from these data that these human cells take longer than 72 hrs to reach a state of quiescence: EdU incorporation at 72 hrs was still over 20%. Accordingly, future experiments were conducted after longer time intervals from irradiation.

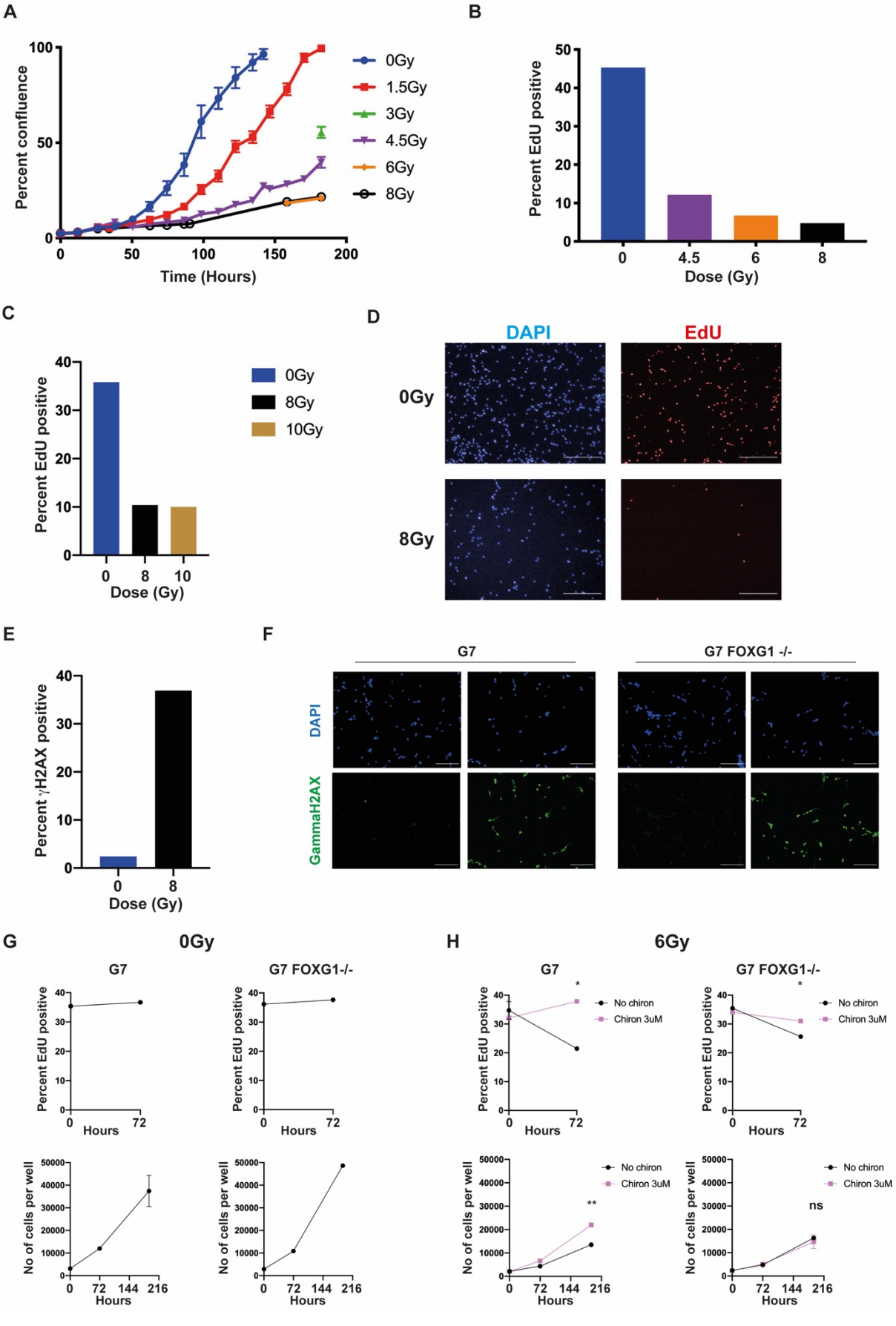
A
Percent confluence
Time (Hours)
0Gy
1.5Gy
3Gy
4.5Gy
6Gy
8Gy
B
Percent EdU positive
Dose (Gy)
C
Percent EdU positive
Dose (Gy)
0Gy
8Gy
10Gy
D
DAPI
EdU
0Gy
8Gy
E
Percent γH2AX positive
Dose (Gy)
F
G7
G7 FOXG1 -/-
DAPI
GammaH2AX
G
0Gy
G7
G7 FOXG1-/-
Percent EdU positive
Hours
No of cells per well
H
6Gy
No chiron
Chiron 3uM
ns

Figure 5. 11 Irradiation of cells may provide a useful model of quiescence.

(A) Growth curves showing the response of mouse NSCs (F6) to ionising radiation. (B) EdU incorporation of mouse NSCs 72 hours post-irradiation/sham irradiation. (C) EdU incorporation of human GSCs (G7) 72 hours after irradiation/sham irradiation. (D) Representative images of EdU incorporation in G7 at 72 hours. Blue - DAPI, red - EdU. Scale bars 150μm. (E) γH2AX incorporation in G7 cells irradiated with 8Gy/sham irradiated. (F) Representative images of γH2AX staining in these cells. Scale bars 150μm. (G) EdU incorporation and cell number in G7 cells after sham irradiation at hour 0. (H) The corresponding data for G7 and G7 FOXG1 -/- cells after irradiation with 6Gy at hour 0. Linear regression analysis. Data points represent means of duplicates.

I irradiated GBM002 cells, and their FOXG1 null counterparts, plated at 30 cells/mm^2, and observed that, by 14 days post-irradiation with 8Gy, cell number was static and cells had acquired an astrocytic morphology. EdU incorporation was around 10% in both the parental GBM002 and the corresponding FOXG1 null cell line, similar to levels reached with BMP4 exposure (Figure 5.12A&B). As previously discussed, human tumour cells do not achieve a complete, uniform exit of all cells from the cell cycle but rather some cells become slow cycling, primed to become activated and proliferative. Chiron, 3μM, was added to half of the wells for each cell line and DMSO to the other half and further EdU pulses and cell counts conducted at 21 and 28 days. Cells with intact FOXG1 exposed to chiron grew faster than those in EGF/FGF2 alone (Figure 5.12B). This effect was not seen where FOXG1 had been excised.

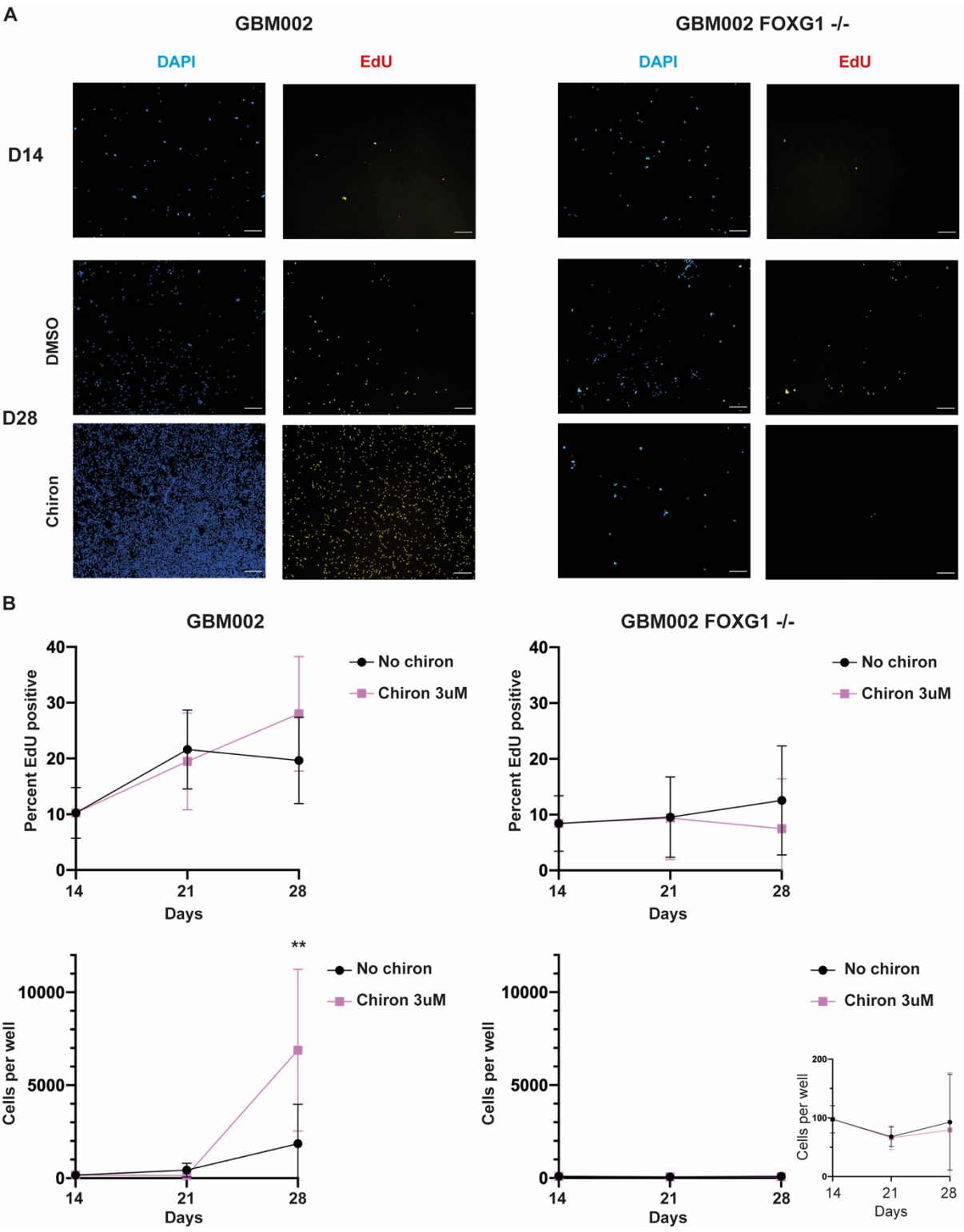
A
GBM002
GBM002 FOXG1 -/-
DAPI
EdU
DAPI
EdU
D14
DMSO
D28
Chiron
B
GBM002
GBM002 FOXG1 -/-
Percent EdU positive
No chiron
Chiron 3uM
Days
Cells per well
**
No chiron
Chiron 3uM
Days

Figure 5. 12 Chiron leads to increased exit from quiescence after irradiation, only in the context of intact FOXG1.

(A) Representative images of EdU incorporation in GBM002 and GBM002 FOXG1 knockout cells at 14 days post-irradiation and at 28 days post-irradiation +/- chiron. Blue - DAPI, yellow - EdU. Scale bars 150μm. (B) EdU incorporation and cell number at days 14, 21 and 28 post-irradiation. Data points represent means of 6-12 replicates. Linear regression analysis. Inset shows FOXG1-/- cell number on smaller scale.

These data suggest that the FOXG1/Wnt synergy is not only relevant to BMP4-induced quiescence but may also facilitate exit from quiescence after exposure to ionising radiation. As FOXG1 is overexpressed in GSCs and radiotherapy forms the mainstay of post-operative treatment for GBM, this poses the question of whether Wnt inhibition could be a therapeutic strategy to prevent relapse after chemo-radiotherapy. The question of chemotherapy/radiation-induced quiescence will form a key part of my future work.

5.7 Conclusions

This chapter has provided evidence of the relevance of the synergy between FOXG1 and Wnt to an in vivo model of GBM, to a human GSC model and to the post-irradiation context. These data build on the mechanisms identified in Chapters 3 and 4, and suggest cooperative mechanisms between FOXG1 and Wnt could drive relapse of GBM tumour by supporting exit from quiescence. Targeting Wnt signaling may therefore be unlikely to have value in established GBMs as it would not affect the proliferative GSCs; however, targeting the quiescent cells after standard of care to prevent relapse may be highly relevant.

The in vivo data show the interaction between FOXG1 and Wnt translating to accelerated tumour growth. They also hint at a potential impact of the tumour microenvironment in that FOXG1 upregulation alone is sufficient to increase intracellular beta-catenin levels and drive accelerated tumour growth, possibly in connection with the presence of Wnt ligands in the microenvironment. This CRISPR-based model of tumorigenesis, using cells with tuneable FOXG1 and beta-catenin, will be exploited in future experiments aimed at prolonging the time to recurrence in GBM with Wnt inhibition after brain irradiation +/- temozolomide. Only by modeling the clinical treatment received by patients can we hope to identify effective therapeutics.

It was crucial to show that the synergy is relevant to human GBM and I have done this in two cell lines. It is additionally valuable to demonstrate relevance to both adult and paediatric GBM. The use of GSCs gave me an opportunity to interrogate the hypothesis that the GBD plays a role in the interaction and I have shown some preliminary evidence of its importance.

Going forward, I hope to focus on the radiobiology of fractionated radiotherapy to GSCs. There are many unanswered questions. Can we demonstrate the acquisition of quiescence following fractionated radiotherapy? Are quiescent GSCs responsible for relapse after treatment? Currently, due to the lack of validated markers of the quiescent state, it is difficult to identify quiescent cells and to interrogate their specific responses. Functional lineage tracing studies, such as those conducted by the Parada group (Chen et al., 2012) give perhaps the closest clues that quiescent cells are likely to be responsible, after anti-mitotic treatments, for regeneration of the tumour. Further questions arise as a result of this hypothesis: is Wnt activity upregulated

in these cells and can it be blocked? Crucially, can Wnt inhibition form part of a therapeutic strategy to delay relapse?

Chapter 6: Discussion

Understanding mechanisms of NSC and GSC quiescence has been the focus of these thesis. Previous work identified a role for FOXG1 in exit from quiescence but the impact of FOXG1 alone on cell cycle re-entry was limited and little was known about co-operating pathways. It remained clear that other pathways were rate-limiting in enabling exit from quiescence. I reveal a key cooperation between FOXG1 and Wnt signaling in driving exit from NSCs and GSCs.

These data suggest a key role for the canonical Wnt signaling pathway in driving the exit from the quiescent NSC state and this is consistent with many in vivo studies of the role of Wnt in stem cell biology. In normal physiology, the activation of Wnt may increase output from the endogenous quiescent NSCs in the niche. Targeting the Wnt pathway may be predicted to limit the relapse of tumour regrowth by quiescent GSCs.

6.1 A FOXG1/Wnt synergy drives exit from quiescence

Using cell based phenotypic screening of small molecules, I discovered that GSK3 inhibition enhances the effect of increased FOXG1 in driving exit from quiescence. This suggested a synergy between Wnt/beta-catenin signaling and FOXG1 which removes barriers to efficient cell cycle re-entry of quiescent NSCs and GSCs.

Our group has previously shown that FOXG1 overexpression has no impact on proliferative NSCs/GSCs. Similarly, addition of GSK3 inhibition has no effect on proliferative cells, suggesting the effect is on exit from quiescence. Surprisingly, pathways driving self-renewal of proliferative cells are therefore distinct from those required to exit the quiescent state back into cycle. Indeed, FOXG1 and GSK3 inhibition are required simultaneously, at early

timepoints, to drive maximally efficient cell cycle re-entry, indicating a direct synergy on exit from quiescence.

My initial goal was to confirm that the GSK3 inhibitors were operating through Wnt signaling, rather than other GSK3-related signaling pathways. It is known that Wnt signaling has key roles in the development of the CNS, including in the proliferation of NPCs (Kim et al., 2009) and in spatial patterning (Patapoutian and Reichardt, 2000; Saint-Jeannet, 2013). Similarly, there is evidence for Wnt-mediated self-renewal of neural stem/progenitor cells in the adult brain (Kalani et al., 2008; Wexler et al., 2009). This was therefore the clear candidate. I showed that chiron could be replaced by Wnt3a and that the synergistic effect with FOXG1 could be abrogated by two Wnt inhibitors. I then showed that the introduction of a cassette encoding inducible active beta-catenin phenocopied the effects of GSK3 inhibition. All of these data confirm that canonical Wnt/beta-catenin are working with FOXG1 to drive cell cycle re-entry of quiescent NSCs.

6.2 Implications for human GSCs

The differential response of NSCs and GSCs to BMP4 exposure raises several questions. NSCs are driven out of cycle, into a deep quiescent state indistinguishable from terminal astrocyte differentiation. GSCs, however, enter a shallow, or primed quiescence, in which they remain vulnerable to cell cycle re-entry. The universal overexpression of FOXG1 in these cells is thought to account for their resistance to deep quiescence and I showed that forced overexpression of FOXG1 leaves NSCs primed to respond to proliferation cues, in the form of Wnt activation. The Dirks lab has published evidence of a subpopulation of GSCs which exhibit high levels of beta-catenin signaling (Rajakulendran et al., 2019). Could these be the

cells with the greatest readiness to exit quiescence? Or is microenvironmental Wnt signaling sufficient to drive cell cycle re-entry in any FOXG1 expressing GSC? It is known that adult neural progenitors secrete functional Wnt that self-stimulates low-level canonical Wnt signaling (Wexler et al., 2009). FOXG1 and beta-catenin co-localise in human GBM as I confirm using RNAScope, in keeping with the hypothesis that the synergistic interaction between them is relevant in the human context. Evidence from a Tcf/lef reporter NSC line, in Chapter 4, shows that there are cells with detectable Wnt target activity on return to mitogens after BMP exposure and that FOXG1 upregulation leads to high level upregulation in some cells. It could be expected that the endogenous high levels of FOXG1 in GSCs would have the same effect. Elevated FOXG1 therefore primes NSCs and GSCs for responsiveness to Wnt signaling. MYC and other established downstream targets likely play a critical role in driving cells back into full proliferation.

A striking effect of chiron was seen on human GSCs, both adult and paediatric, and this effect was clearly abolished with the knockout of FOXG1. It was essential to demonstrate relevance of the FOXG1/Wnt synergy to human GSCs and to demonstrate that the expression levels of FOXG1 seen in human GSCs are sufficient to contribute to the synergy. The human cells were then the ideal model to interrogate Groucho binding domain effects, but it was necessary to return to mouse cells for in vivo modeling as tunable FOXG1 was required: human FOXG1 knockout cells are not tumorigenic (Bulstrode et al, 2017).

6.3 Potential mechanisms of the interaction

What is the mechanism of the interaction? There are two possibilities suggested by the data here, and these are not mutually exclusive. Firstly, FOXG1 represses transcription of the Wnt

inhibitor Wif1 and there is evidence, in vivo, of increased beta-catenin accumulation in the context of FOXG1 overexpression. However, there are several clues that this is not the only mechanism. Firstly, insertion of a cassette expressing constitutively active beta-catenin phenocopies the effect of GSK3 inhibition/Wnt ligand exposure. It drives exit from quiescence only when FOXG1 is overexpressed, and, when the cassette is excised from a proportion of cells, the effect cannot be rescued by adjacent cells with the intact cassette. This suggests that there is a cell-autonomous, direct nuclear interaction which cannot be phenocopied by increased microenvironmental Wnt signaling alone. The requirement for FOXG1 and Wnt activation simultaneously to drive maximal cell cycle re-entry would further suggest this.

The direct nuclear interaction is suggested by the structure of the FOXG1 protein and its Groucho/TLE binding domain. Although FOXG1 has been thought to be primarily a transcriptional repressor, it clearly also serves as an activator of some genes. Dali et al identify 216 differentially regulated genes following FOXG1 knockdown, 11% of which are activation targets of FOXG1 (Dali et al., 2018). They focused only on genes which have proximal FOXG1 binding sites and demonstrate direct FOXG1 binding on ChIP-seq. However, FOXG1 is known to have repressive mechanisms independent of DNA binding (Hanashima et al., 2002; Seoane et al., 2004) and may therefore also have DNA-independent activating mechanisms. I suggest a novel mechanism of Wnt target gene activation in which sequestration of the co-repressor TLE1 by FOXG1 leads to derepression of beta-catenin targets, facilitating their maximal activation (Figure 6.1). Such a mechanism has been proposed by Cahill et al, although not with specific reference to FOXG1, and termed ‘regulatory squelching’ (Cahill et al., 1994). Data presented in Chapter 5 show that excision of the FOXG1 Groucho binding domain attenuates, but does not completely abolish, the response to chiron. These data are in keeping with the co-existence of the two mechanisms suggested here.

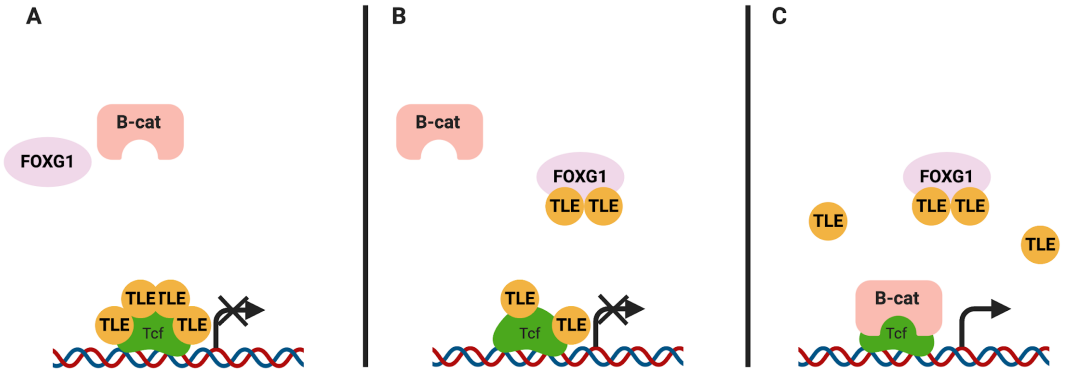

Figure 6. 1 Regulatory squelching.

(A) TLEs act as transcriptional co-repressors at Tcf sites. (B) FOXG1 sequesters TLE via its Groucho binding domain. (C) This facilitates displacement of remaining TLE by beta-catenin, enabling maximal activation.

6.4 Implications of the in vivo findings and translational potential

The finding, in our mouse model of GBM, that FOXG1 overexpression drives accelerated tumour growth and reduced survival is the exciting corollary of the finding, published by the Pollard lab, that FOXG1 excision abolishes tumour growth in a GBM xenograft model (Bulstrode et al, 2017). That the cells show beta-catenin accumulation and that further acceleration is seen with the induction of active beta-catenin suggest that the FOXG1/Wnt synergy is active. RNAScope analysis of Wnt target expression in the tumours, to address the hypothesis that FOXG1 upregulates these targets in vivo, is ongoing (Robertson, in preparation). Certainly, there is in vitro evidence, presented in Chapter 4, that Wnt targets are upregulated, at the mRNA and protein levels, by FOXG1 alone and further by the FOXG1/Wnt combination.

Could Wnt inhibition be useful in the clinical treatment of GBM? The most attractive feature of this strategy is the potentially large therapeutic window created by the synergy with FOXG1, which is abundant in GSCs but not in the normal surrounding brain tissue/NSCs. However, Wnt inhibition will not be a single agent therapeutic for several reasons. Firstly, Wnt activation is not necessary for proliferating GSCs and Wnt inhibition is not cytostatic in proliferative conditions. Therefore, Wnt inhibition is a strategy best suited to the adjuvant setting, for the prevention of relapse, due to its effects on quiescent GSCs. Secondly, the marked molecular redundancy seen in GBM will never allow for a single target for treatment and a cocktail of concurrent and sequential agents and approaches seems likely to be necessary. Thirdly, and in keeping with this, the proportion of human GSCs re-entering cell cycle even in the absence of Wnt activation suggests that there are additional mechanisms which need simultaneously to be overcome. However, as discussed above, it may also suggest that the endogenous Wnt activity of the cells is sufficient to facilitate some interaction with FOXG1.

Future studies will build on these findings to interrogate the impact of adjuvant Wnt inhibition in this mouse model of GBM after treatment which closely mirrors that received by patients. Temozolomide (TMZ) is frequently used as a stand in for treatment in animal models of GBM but, in the clinical setting, TMZ adds a small benefit to the mainstay of post-surgical treatment: radiotherapy. I have demonstrated some initial relevance to radiotherapy-induced quiescence but the next step will be to characterise in detail the response of GSCs to ionising radiation, and to identify the putative quiescent population before introducing a Wnt inhibitor to mice treated with radiotherapy. My use of the NPE mouse tumour model system is the first outside the context in which it was developed, for the generation of isogenic tumours in mice to interrogate the immune response (Gangoso, Southgate, Bradley et al, under revision). It will be

of great utility in diverse preclinical studies, testing potential therapeutic strategies, of which I hope Wnt inhibitor studies will be among the first. The next key experiment will be to treat mice with a FOXG1-inducible NPE tumour with radiotherapy, using a linear accelerator developed for use with mice, and assess their response to post-treatment Wnt inhibition. Although I used NSG mice, there is scope, in future work, to use isogenic mice and therefore account for the impact of the tumour microenvironment in a host with intact immunity.

Given the maximal efficiency of cell cycle re-entry with the FOXG1/Wnt combination, it is tempting to consider a radically different approach to the treatment of GBM, one which would create a role for Wnt modulation up front in the management of patients. If the problem is resistance to anti-mitotic treatment, due to quiescence, the solution would seem to be to abolish the quiescent subpopulation prior to chemoradiotherapy. Post-surgical Wnt activation has the potential to drive cell cycle re-entry in all quiescent, FOXG1-high GSCs, leaving them vulnerable to destruction by radiotherapy and chemotherapy. Clearly, the ethics of this approach are fraught with difficulty but, should such an approach cure 100% of mice, it might be difficult to ignore.

6.5 Concluding remarks and future directions

Future work, as described above, will focus on characterising the response of GSCs to ionising radiation and evaluating the impact of adjuvant Wnt inhibition (after radiotherapy treatment) on recurrence. Additional work on the mechanism of the interaction will include assessment of Wnt target gene activation with FOXG1 upregulation in vivo, using RNAScope analysis of tissue from mice given dox or no dox. I will also conduct analysis of Wnt target gene activation in cells with wild-type FOXG1 and cell with FOXG1 lacking the Groucho binding domain, to

assess further the necessity of the GBD to the response to chiron. Targeting Wnt signaling to prevent relapse after standard of care is the translational hypothesis that has emerged from these studies.

References

Aberle, H., Bauer, A., Stappert, J., Kispert, A., and Kemler, R. (1997). beta-catenin is a target for the ubiquitin-proteasome pathway. EMBO J. *16*, 3797–3804.

Ables, J.L., Decarolis, N.A., Johnson, M.A., Rivera, P.D., Gao, Z., Cooper, D.C., Radtke, F., Hsieh, J., and Eisch, A.J. (2010). Notch1 is required for maintenance of the reservoir of adult hippocampal stem cells. J. Neurosci. *30*, 10484–10492.

Adachi, K., Mirzadeh, Z., Sakaguchi, M., Yamashita, T., Nikolcheva, T., Gotoh, Y., Peltz, G., Gong, L., Kawase, T., Alvarez-Buylla, A., et al. (2007). β-Catenin Signaling Promotes Proliferation of Progenitor Cells in the Adult Mouse Subventricular Zone. Stem Cells *25*, 2827–2836.

Ahlgren, S., Vogt, P., and Bronner-Fraser, M. (2003). Excess FoxG1 causes overgrowth of the neural tube. J. Neurobiol. *57*, 337–349.

Allen, M., Bjerke, M., Edlund, H., Nelander, S., and Westermark, B. (2016). Origin of the U87MG glioma cell line: Good news and bad news. Sci. Transl. Med. *8*, 354re3.

Alvarez-Buylla, A., García-Verdugo, J.M., and Tramontin, A.D. (2001). A unified hypothesis on the lineage of neural stem cells. Nat. Rev. Neurosci. *2*, 287–293.

An, W.F., Germain, A.R., Bishop, J.A., Nag, P.P., Metkar, S., Ketterman, J., Walk, M., Weiwer, M., Liu, X., Patnaik, D., et al. (2012). Discovery of Potent and Highly Selective Inhibitors of GSK3b. In Probe Reports from the NIH Molecular Libraries Program, (Bethesda (MD): National Center for Biotechnology Information (US)),.

Anido, J., Sáez-Borderías, A., Gonzàlez-Juncà, A., Rodón, L., Folch, G., Carmona, M.A., Prieto-Sánchez, R.M., Barba, I., Martínez-Sáez, E., Prudkin, L., et al. (2010). TGF-β Receptor Inhibitors Target the CD44(high)/Id1(high) Glioma-Initiating Cell Population in Human Glioblastoma. Cancer Cell *18*, 655–668.

Ariani, F., Hayek, G., Rondinella, D., Artuso, R., Mencarelli, M.A., Spanhol-Rosseto, A., Pollazzon, M., Buoni, S., Spiga, O., Ricciardi, S., et al. (2008). FOXG1 is responsible for the congenital variant of Rett syndrome. Am. J. Hum. Genet. *83*, 89–93.

Artegiani, B., Lyubimova, A., Muraro, M., van Es, J.H., van Oudenaarden, A., and Clevers, H. (2017). A Single-Cell RNA Sequencing Study Reveals Cellular and Molecular Dynamics of the Hippocampal Neurogenic Niche. Cell Rep. *21*, 3271–3284.

Augustin, I., Goidts, V., Bongers, A., Kerr, G., Vollert, G., Radlwimmer, B., Hartmann, C., Herold-Mende, C., Reifenberger, G., von Deimling, A., et al. (2012). The Wnt secretion protein Evi/Gpr177 promotes glioma tumourigenesis. EMBO Mol. Med. *4*, 38–51.

Bachoo, R.M., Maher, E.A., Ligon, K.L., Sharpless, N.E., Chan, S.S., You, M.J., Tang, Y., DeFrances, J., Stover, E., Weissleder, R., et al. (2002). Epidermal growth factor receptor and Ink4a/Arf: convergent mechanisms governing terminal differentiation and transformation along the neural stem cell to astrocyte axis. Cancer Cell *1*, 269–277.

Bafico, A., Liu, G., Goldin, L., Harris, V., and Aaronson, S.A. (2004). An autocrine mechanism for constitutive Wnt pathway activation in human cancer cells. Cancer Cell *6*, 497–506.

Bain, J., Plater, L., Elliott, M., Shpiro, N., Hastie, J., McLauchlan, H., Klevernic, I., Arthur, J.S.C., Alessi, D.R., Cohen, P. (2007). The selectivity of protein kinase inhibitors: a further update. Biochem J. *408*, 297-315.

Bao, S., Wu, Q., McLendon, R.E., Hao, Y., Shi, Q., Hjelmeland, A.B., Dewhirst, M.W., Bigner, D.D., and Rich, J.N. (2006). Glioma stem cells promote radioresistance by preferential activation of the DNA damage response. Nature *444*, 756–760.

Barrett, L.E., Granot, Z., Coker, C., Iavarone, A., Hambardzumyan, D., Holland, E.C., Nam, H.-S., and Benezra, R. (2012). Self-renewal does not predict tumor growth potential in mouse models of high-grade glioma. Cancer Cell *21*, 11–24.

Basak, O., and Taylor, V. (2007). Identification of self-replicating multipotent progenitors in the embryonic nervous system by high Notch activity and Hes5 expression. Eur. J. Neurosci. *25*, 1006–1022.

Beckervordersandforth, R., Tripathi, P., Ninkovic, J., Bayam, E., Lepier, A., Stempfhuber, B., Kirchhoff, F., Hirrlinger, J., Haslinger, A., Lie, D.C., et al. (2010). In vivo fate mapping and expression analysis reveals molecular hallmarks of prospectively isolated adult neural stem cells. Cell Stem Cell *7*, 744–758.

Beier, D., Hau, P., Proescholdt, M., Lohmeier, A., Wischhusen, J., Oefner, P.J., Aigner, L., Brawanski, A., Bogdahn, U., and Beier, C.P. (2007). CD133(+) and CD133(-) glioblastoma-derived cancer stem cells show differential growth characteristics and molecular profiles. Cancer Res. *67*, 4010–4015.

Bell, E., Jr, and Karnosh, L.J. (1949). Cerebral hemispherectomy; report of a case 10 years after operation. J. Neurosurg. *6*, 285–293.

Bonaguidi, M.A., McGuire, T., Hu, M., Kan, L., Samanta, J., and Kessler, J.A. (2005). LIF and BMP signaling generate separate and discrete types of GFAP-expressing cells. Development *132*, 5503–5514.

Bourguignon, C., Li, J., and Papalopulu, N. (1998). XBF-1, a winged helix transcription factor with dual activity, has a role in positioning neurogenesis in Xenopus competent ectoderm. Development *125*, 4889–4900.

Brennan, C.W., Verhaak, R.G.W., McKenna, A., Campos, B., Noushmehr, H., Salama, S.R., Zheng, S., Chakravarty, D., Sanborn, J.Z., Berman, S.H., et al. (2013). The somatic genomic landscape of glioblastoma. Cell *155*, 462–477.

Bressan, R.B., Dewari, P.S., Kalantzaki, M., Gangoso, E., Matjusaitis, M., Garcia-Diaz, C., Blin, C., Grant, V., Bulstrode, H., Gogolok, S., et al. (2017). Efficient CRISPR/Cas9-assisted gene targeting enables rapid and precise genetic manipulation of mammalian neural stem cells. Development *144*, 635–648.

Buffo, A., Rite, I., Tripathi, P., Lepier, A., Colak, D., Horn, A.-P., Mori, T., and Götz, M. (2008). Origin and progeny of reactive gliosis: A source of multipotent cells in the injured

brain. Proc. Natl. Acad. Sci. U. S. A. *105*, 3581–3586.

Bulstrode, H., Johnstone, E., Marques-Torrejon, M.A., Ferguson, K.M., Bressan, R.B., Blin, C., Grant, V., Gogolok, S., Gangoso, E., Gagrica, S., et al. (2017). Elevated FOXG1 and SOX2 in glioblastoma enforces neural stem cell identity through transcriptional control of cell cycle and epigenetic regulators. Genes Dev. *31*, 757–773.

Buscarlet, M., Perin, A., Laing, A., Brickman, J.M., and Stifani, S. (2008). Inhibition of cortical neuron differentiation by Groucho/TLE1 requires interaction with WRPW, but not Eh1, repressor peptides. J. Biol. Chem. *283*, 24881–24888.

Byron, A. (2017). Clustering and Network Analysis of Reverse Phase Protein Array Data. Methods Mol. Biol. *1606*, 171–191.

Byron, A., Bernhardt, S., Ouine, B., Cartier, A., Macleod, K.G., Carragher, N.O., Sibut, V., Korf, U., Serrels, B., and de Koning, L. (2019). Integrative analysis of multi-platform reverse-phase protein array data for the pharmacodynamic assessment of response to targeted therapies.

Cahill, M.A., Ernst, W.H., Janknecht, R., and Nordheim, A. (1994). Regulatory squelching. FEBS Lett. *344*, 105–108.

Carén, H., Stricker, S.H., Bulstrode, H., Gagrica, S., Johnstone, E., Bartlett, T.E., Feber, A., Wilson, G., Teschendorff, A.E., Bertone, P., et al. (2015). Glioblastoma Stem Cells Respond to Differentiation Cues but Fail to Undergo Commitment and Terminal Cell-Cycle Arrest. Stem Cell Reports *5*, 829–842.

Carragher, N.O. (2009). Profiling distinct mechanisms of tumour invasion for drug discovery: imaging adhesion, signaling and matrix turnover. Clin. Exp. Metastasis *26*, 381–397.

Cavallo, R.A., Cox, R.T., Moline, M.M., Roose, J., Polevoy, G.A., Clevers, H., Peifer, M., and Bejsovec, A. (1998). Drosophila Tcf and Groucho interact to repress Wingless signaling activity. Nature *395*, 604–608.

Cerami, E., Gao, J., Dogrusoz, U., Gross, B.E., Sumer, S.O., Aksoy, B.A., Jacobsen, A., Byrne, C.J., Heuer, M.L., Larsson, E., Antipin, Y., Reva, B., Goldberg, A.P., Sander, C., Schultz, N. (2012). The cBio Cancer Genomics Portal: An open platform for exploring multidimensional cancer genomics data. Cancer Discov. *2(5)*, 401-404.

Chan, E.F., Gat, U., McNiff, J.M., and Fuchs, E. (1999). A common human skin tumour is caused by activating mutations in beta-catenin. Nat. Genet. *21*, 410–413.

Chen, J., Li, Y., Yu, T.-S., McKay, R.M., Burns, D.K., Kernie, S.G., and Parada, L.F. (2012). A restricted cell population propagates glioblastoma growth after chemotherapy. Nature *488*, 522–526.

Chenn, A., and Walsh, C.A. (2002). Regulation of cerebral cortical size by control of cell cycle exit in neural precursors. Science *297*, 365–369.

Chu, V.T., Weber, T., Wefers, B., Wurst, W., Sander, S., Rajewsky, K., and Kühn, R. (2015). Increasing the efficiency of homology-directed repair for CRISPR-Cas9-induced precise gene editing in mammalian cells. Nat. Biotechnol. *33*, 543–548.

Codega, P., Silva-Vargas, V., Paul, A., Maldonado-Soto, A.R., Deleo, A.M., Pastrana, E., and Doetsch, F. (2014). Prospective identification and purification of quiescent adult neural stem cells from their in vivo niche. Neuron *82*, 545–559.

Conti, L., Pollard, S.M., Gorba, T., Reitano, E., Toselli, M., Biella, G., Sun, Y., Sanzone, S., Ying, Q.-L., Cattaneo, E., et al. (2005). Niche-independent symmetrical self-renewal of a mammalian tissue stem cell. PLoS Biol. *3*, e283.

Creighton, C.J., and Huang, S. (2015). Reverse phase protein arrays in signaling pathways: a data integration perspective. Drug Des. Devel. Ther. *9*, 3519–3527.

Dali, R., Verginelli, F., Pramatarova, A., Sladek, R., and Stifani, S. (2018). Characterization of a FOXG1:TLE1 transcriptional network in glioblastoma-initiating cells. Mol. Oncol. *12*, 775–787.

Dandy, W.E. (1928). Removal of right cerebral hemisphere for certain tumors with hemiplegia: preliminary report. J. Am. Med. Assoc. *90*, The 823–825.

Danesin, C., Peres, J.N., Johansson, M., Snowden, V., Cording, A., Papalopulu, N., and Houart, C. (2009). Integration of telencephalic Wnt and hedgehog signaling center activities by Foxg1. Dev. Cell *16*, 576–587.

Darmanis, S., Sloan, S.A., Croote, D., Mignardi, M., Chernikova, S., Samghababi, P., Zhang, Y., Neff, N., Kowarsky, M., Caneda, C., et al. (2017). Single-Cell RNA-Seq Analysis of Infiltrating Neoplastic Cells at the Migrating Front of Human Glioblastoma. Cell Rep. *21*, 1399–1410.

deCarvalho, A.C., Kim, H., Poisson, L.M., Winn, M.E., Mueller, C., Cherba, D., Koeman, J., Seth, S., Protopopov, A., Felicella, M., et al. (2018). Discordant inheritance of chromosomal and extrachromosomal DNA elements contributes to dynamic disease evolution in glioblastoma. Nat. Genet. *50*, 708–717.

Dewari, P.S., Southgate, B., Mccarten, K., Monogarov, G., O'Duibhir, E., Quinn, N., Tyrer, A., Leitner, M.-C., Plumb, C., Kalantzaki, M., et al. (2018). An efficient and scalable pipeline for epitope tagging in mammalian stem cells using Cas9 ribonucleoprotein. Elife *7*.

Ding, S., Wu, X., Li, G., Han, M., Zhuang, Y., and Xu, T. (2005). Efficient transposition of the piggyBac (PB) transposon in mammalian cells and mice. Cell *122*, 473–483.

Doble, B.W., and Woodgett, J.R. (2003). GSK-3: tricks of the trade for a multi-tasking kinase. J. Cell Sci. *116*, 1175–1186.

Doetsch, F., García-Verdugo, J.M., and Alvarez-Buylla, A. (1997). Cellular composition and three-dimensional organization of the subventricular germinal zone in the adult mammalian brain. J. Neurosci. *17*, 5046–5061.

Doetsch, F., Caillé, I., Lim, D.A., García-Verdugo, J.M., and Alvarez-Buylla, A. (1999). Subventricular zone astrocytes are neural stem cells in the adult mammalian brain. Cell *97*, 703–716.

Doetsch, F., Petreanu, L., Caille, I., Garcia-Verdugo, J.M., and Alvarez-Buylla, A. (2002). EGF converts transit-amplifying neurogenic precursors in the adult brain into multipotent

stem cells. Neuron *36*, 1021–1034.

Engström, P.G., Tommei, D., Stricker, S.H., Ender, C., Pollard, S.M., and Bertone, P. (2012). Digital transcriptome profiling of normal and glioblastoma-derived neural stem cells identifies genes associated with patient survival. Genome Med. *4*, 76.

Eriksson, P.S., Perfilieva, E., Björk-Eriksson, T., Alborn, A.M., Nordborg, C., Peterson, D.A., and Gage, F.H. (1998). Neurogenesis in the adult human hippocampus. Nat. Med. *4*, 1313–1317.

Fuentealba, L.C., Obernier, K., and Alvarez-Buylla, A. (2012). Adult neural stem cells bridge their niche. Cell Stem Cell *10*, 698–708.

Funato, K., Major, T., Lewis, P.W., Allis, C.D., and Tabar, V. (2014). Use of human embryonic stem cells to model pediatric gliomas with H3.3K27M histone mutation. Science *346*, 1529–1533.

Gage, F.H., and Temple, S. (2013). Neural stem cells: generating and regenerating the brain. Neuron *80*, 588–601.

Gallo, M., Ho, J., Coutinho, F.J., Vanner, R., Lee, L., Head, R., Ling, E.K.M., Clarke, I.D., and Dirks, P.B. (2013). A tumorigenic MLL-homeobox network in human glioblastoma stem cells. Cancer Res. *73*, 417–427.

Gao, J., Aksoy, B.A., Dogrusoz, U., Dresdner, G., Gross, B.E., Sumer, S.O., Sun, Y., Jacobsen, A., Sinha, R., Larsson, E., Cerami, E., Sander, C., Schultz, N. (2013). Integrative analysis of complex cancer genomics and clinial profiles using the cBioPortal. Sci Signal. *6(269)*, pl1.

Giachino, C., and Taylor, V. (2009). Lineage analysis of quiescent regenerative stem cells in the adult brain by genetic labelling reveals spatially restricted neurogenic niches in the olfactory bulb. Eur. J. Neurosci. *30*, 9–24.

Gilbertson, R.J., and Rich, J.N. (2007). Making a tumour's bed: glioblastoma stem cells and the vascular niche. Nat. Rev. Cancer *7*, 733–736.

Gomes, W.A., Mehler, M.F., and Kessler, J.A. (2003). Transgenic overexpression of BMP4 increases astroglial and decreases oligodendroglial lineage commitment. Dev. Biol. *255*, 164–177.

Gonsalves, F.C., Klein, K., Carson, B.B., Katz, S., Ekas, L.A., Evans, S., Nagourney, R., Cardozo, T., Brown, A.M.C., and DasGupta, R. (2011). An RNAi-based chemical genetic screen identifies three small-molecule inhibitors of the Wnt/wingless signaling pathway. Proc. Natl. Acad. Sci. U. S. A. *108*, 5954–5963.

Götz, M., and Huttner, W.B. (2005). The cell biology of neurogenesis. Nat. Rev. Mol. Cell Biol. *6*, 777–788.

Götz, M., Sirko, S., Beckers, J., and Irmler, M. (2015). Reactive astrocytes as neural stem or progenitor cells: In vivo lineage, In vitro potential, and Genome-wide expression analysis. Glia *63*, 1452–1468.

Gross, R.E., Mehler, M.F., Mabie, P.C., Zang, Z., Santschi, L., and Kessler, J.A. (1996). Bone morphogenetic proteins promote astroglial lineage commitment by mammalian subventricular zone progenitor cells. Neuron *17*, 595–606.

Han, D., Yu, T., Dong, N., Wang, B., Sun, F., and Jiang, D. (2019). Napabucasin, a novel STAT3 inhibitor suppresses proliferation, invasion and stemness of glioblastoma cells. J. Exp. Clin. Cancer Res. *38*, 289.

Hanashima, C., Shen, L., Li, S.C., and Lai, E. (2002). Brain factor-1 controls the proliferation and differentiation of neocortical progenitor cells through independent mechanisms. J. Neurosci. *22*, 6526–6536.

He, T.C., Sparks, A.B., Rago, C., Hermeking, H., Zawel, L., da Costa, L.T., Morin, P.J., Vogelstein, B., and Kinzler, K.W. (1998). Identification of c-MYC as a target of the APC pathway. Science *281*, 1509–1512.

Hegi, M.E., Diserens, A.-C., Gorlia, T., Hamou, M.-F., de Tribolet, N., Weller, M., Kros, J.M., Hainfellner, J.A., Mason, W., Mariani, L., et al. (2005). MGMT gene silencing and benefit from temozolomide in glioblastoma. N. Engl. J. Med. *352*, 997–1003.

Hikasa, H., Ezan, J., Itoh, K., Li, X., Klymkowsky, M.W., and Sokol, S.Y. (2010). Regulation of TCF3 by Wnt-dependent phosphorylation during vertebrate axis specification. Dev. Cell *19*, 521–532.

Holland, E.C. (2000). Glioblastoma multiforme: the terminator. Proc. Natl. Acad. Sci. U. S. A. *97*, 6242–6244.

Huang, S.A., Mishina Y.M., Liu, S., Cheung, A., Stegmeier, F., Michaud, G.A., Charlat, O., Wiellette, E., Zhang, Y., Wiessner, S., Hild, M., Shi, X., Wilson, C.J., Mickanin, C., Myer, V., Fazal, A., Tomlinson, R., Serluca, F., Shao, W., Cheng, H., Shultz, M., Rau, C., Schirle, M., Schlegel, J., Ghidelli, S., Fawell, S., Lu, C., Curtis, D., Kirschner, M.W., Lengauer, C., Finan, P.M., Tallarico, J.A., Bouwmeester, T., Porter, J.A., Bauer, A., Cong, F. (2009). Tankyrase inhibition stabilizes axin and antagonizes Wnt signalling. Nature. *461*, 614-620.

Huse, J.T., Phillips, H.S., and Brennan, C.W. (2011). Molecular subclassification of diffuse gliomas: seeing order in the chaos. Glia *59*, 1190–1199.

Ihrie, R.A., and Alvarez-Buylla, A. (2011). Lake-front property: a unique germinal niche by the lateral ventricles of the adult brain. Neuron *70*, 674–686.

Imayoshi, I., Sakamoto, M., Yamaguchi, M., Mori, K., and Kageyama, R. (2010). Essential roles of Notch signaling in maintenance of neural stem cells in developing and adult brains. J. Neurosci. *30*, 3489–3498.

Imura, T., Kornblum, H.I., and Sofroniew, M.V. (2003). The predominant neural stem cell isolated from postnatal and adult forebrain but not early embryonic forebrain expresses GFAP. J. Neurosci. *23*, 2824–2832.

Iversen, P.W., Eastwood, B.J., Sittampalam, G.S., and Cox, K.L. (2006). A comparison of assay performance measures in screening assays: signal window, Z' factor, and assay variability ratio. J. Biomol. Screen. *11*, 247–252.

Jamieson, C.H.M., Ailles, L.E., Dylla, S.J., Muijtjens, M., Jones, C., Zehnder, J.L., Gotlib, J., Li, K., Manz, M.G., Keating, A., et al. (2004). Granulocyte-macrophage progenitors as candidate leukemic stem cells in blast-crisis CML. N. Engl. J. Med. *351*, 657–667.

Jankovic, V., Ciarrocchi, A., Boccuni, P., DeBlasio, T., Benezra, R., and Nimer, S.D. (2007). Id1 restrains myeloid commitment, maintaining the self-renewal capacity of hematopoietic stem cells. Proc. Natl. Acad. Sci. U. S. A. *104*, 1260–1265.

Jones, C., Perryman, L., and Hargrave, D. (2012). Paediatric and adult malignant glioma: close relatives or distant cousins? Nat. Rev. Clin. Oncol. *9*, 400–413.

Kahlert, U.D., Suwala, A.K., Koch, K., Natsumeda, M., Orr, B.A., Hayashi, M., Maciaczyk, J., and Eberhart, C.G. (2015). Pharmacologic Wnt Inhibition Reduces Proliferation, Survival, and Clonogenicity of Glioblastoma Cells. J. Neuropathol. Exp. Neurol. *74*, 889–900.

Kalani, M.Y.S., Cheshier, S.H., Cord, B.J., Bababeygy, S.R., Vogel, H., Weissman, I.L., Palmer, T.D., and Nusse, R. (2008). Wnt-mediated self-renewal of neural stem/progenitor cells. Proc. Natl. Acad. Sci. U. S. A. *105*, 16970–16975.

Kaur, N., Chettiar, S., Rathod, S., Rath, P., Muzumdar, D., Shaikh, M.L., and Shiras, A. (2013). Wnt3a mediated activation of Wnt/β-catenin signaling promotes tumor progression in glioblastoma. Mol. Cell. Neurosci. *54*, 44–57.

Kilpinen, S., Autio, R., Ojala, K., Iljin, K., Bucher, E., Sara, H., Pisto, T., Saarela, M., Skotheim, R.I., Björkman, M., et al. (2008). Systematic bioinformatic analysis of expression levels of 17,330 human genes across 9,783 samples from 175 types of healthy and pathological tissues. Genome Biol. *9*, R139.

Kim, M.K. (2018). Novel insight into the function of tankyrase. Oncol. Lett. *16*, 6895–6902.

Kim, W.-Y., Wang, X., Wu, Y., Doble, B.W., Patel, S., Woodgett, J.R., and Snider, W.D. (2009). GSK-3 is a master regulator of neural progenitor homeostasis. Nat. Neurosci. *12*, 1390–1397.

Kinzler, K.W., and Vogelstein, B. (1996). Lessons from hereditary colorectal cancer. Cell *87*, 159–170.

Kishigami, S., and Mishina, Y. (2005). BMP signaling and early embryonic patterning. Cytokine Growth Factor Rev. *16*, 265–278.

Koch, A., Waha, A., Hartmann, W., Hrychyk, A., Schüller, U., Waha, A., Wharton, K.A., Jr, Fuchs, S.Y., von Schweinitz, D., and Pietsch, T. (2005). Elevated expression of Wnt antagonists is a common event in hepatoblastomas. Clin. Cancer Res. *11*, 4295–4304.

Kool, M., Koster, J., Bunt, J., Hasselt, N.E., Lakeman, A., van Sluis, P., Troost, D., Meeteren, N.S., Caron, H.N., Cloos, J., et al. (2008). Integrated genomics identifies five medulloblastoma subtypes with distinct genetic profiles, pathway signatures and clinicopathological features. PLoS One *3*, e3088.

Kukekov, V.G., Laywell, E.D., Suslov, O., Davies, K., Scheffler, B., Thomas, L.B., O'Brien, T.F., Kusakabe, M., and Steindler, D.A. (1999). Multipotent stem/progenitor cells with similar properties arise from two neurogenic regions of adult human brain. Exp. Neurol. *156*,

333–344.

Kuo, L.J., and Yang, L.-X. (2008). Gamma-H2AX - a novel biomarker for DNA double-strand breaks. In Vivo *22*, 305–309.

Lan, X., Jörg, D.J., Cavalli, F.M.G., Richards, L.M., Nguyen, L.V., Vanner, R.J., Guilhamon, P., Lee, L., Kushida, M.M., Pellacani, D., et al. (2017). Fate mapping of human glioblastoma reveals an invariant stem cell hierarchy. Nature *549*, 227–232.

Langton, P.F., Kakugawa, S., and Vincent, J.-P. (2016). Making, Exporting, and Modulating Wnts. Trends Cell Biol. *26*, 756–765.

Lathia, J.D., Mack, S.C., Mulkearns-Hubert, E.E., Valentim, C.L.L., and Rich, J.N. (2015). Cancer stem cells in glioblastoma. Genes Dev. *29*, 1203–1217.

Laywell, E.D., Rakic, P., Kukekov, V.G., Holland, E.C., and Steindler, D.A. (2000). Identification of a multipotent astrocytic stem cell in the immature and adult mouse brain. Proc. Natl. Acad. Sci. U. S. A. *97*, 13883–13888.

Lee, J.A., and Berg, E.L. (2013). Neoclassic drug discovery: the case for lead generation using phenotypic and functional approaches. J. Biomol. Screen. *18*, 1143–1155.

Lee, C., Hu, J., Ralls, S., Kitamura, T., Loh, Y.P., Yang, Y., Mukouyama, Y.-S., and Ahn, S. (2012). The molecular profiles of neural stem cell niche in the adult subventricular zone. PLoS One *7*, e50501.

Lee, J., Kotliarova, S., Kotliarov, Y., Li, A., Su, Q., Donin, N.M., Pastorino, S., Purow, B.W., Christopher, N., Zhang, W., et al. (2006). Tumor stem cells derived from glioblastomas cultured in bFGF and EGF more closely mirror the phenotype and genotype of primary tumors than do serum-cultured cell lines. Cancer Cell *9*, 391–403.

Lee, W., Swarup, S., Chen, J., Ishitani, T., and Verheyen, E.M. (2009). Homeodomain-interacting protein kinases (Hipks) promote Wnt/Wg signaling through stabilization of beta-catenin/Arm and stimulation of target gene expression. Development *136*, 241–251.

Li, L., and Clevers, H. (2010). Coexistence of quiescent and active adult stem cells in mammals. Science *327*, 542–545.

Li, V.S.W., Ng, S.S., Boersema, P.J., Low, T.Y., Karthaus, W.R., Gerlach, J.P., Mohammed, S., Heck, A.J.R., Maurice, M.M., Mahmoudi, T., et al. (2012). Wnt signaling through inhibition of β-catenin degradation in an intact Axin1 complex. Cell *149*, 1245–1256.

Liu, C., Tu, Y., Sun, X., Jiang, J., Jin, X., Bo, X., Li, Z., Bian, A., Wang, X., Liu, D., et al. (2011). Wnt/beta-Catenin pathway in human glioma: expression pattern and clinical/prognostic correlations. Clin. Exp. Med. *11*, 105–112.

Liu, F., Hon, G.C., Villa, G.R., Turner, K.M., Ikegami, S., Yang, H., Ye, Z., Li, B., Kuan, S., Lee, A.Y., et al. (2015). EGFR Mutation Promotes Glioblastoma through Epigenome and Transcription Factor Network Remodeling. Mol. Cell *60*, 307–318.

Llorens-Bobadilla, E., Zhao, S., Baser, A., Saiz-Castro, G., Zwadlo, K., and Martin-Villalba, A. (2015). Single-Cell Transcriptomics Reveals a Population of Dormant Neural Stem Cells

that Become Activated upon Brain Injury. Cell Stem Cell *17*, 329–340.

Louis, D.N., Perry, A., Reifenberger, G., von Deimling, A., Figarella-Branger, D., Cavenee, W.K., Ohgaki, H., Wiestler, O.D., Kleihues, P., and Ellison, D.W. (2016). The 2016 World Health Organization Classification of Tumors of the Central Nervous System: a summary. Acta Neuropathol. *131*, 803–820.

Lu, F., Chen, Y., Zhao, C., Wang, H., He, D., Xu, L., Wang, J., He, X., Deng, Y., Lu, E.E., et al. (2016). Olig2-Dependent Reciprocal Shift in PDGF and EGF Receptor Signaling Regulates Tumor Phenotype and Mitotic Growth in Malignant Glioma. Cancer Cell *29*, 669–683.

Lucchetti, J., Fracasso, C., Balducci, C., Passoni, A., Forloni, G., Salmona, M., and Gobbi, M. Plasma and brain concentrations of doxycycline after single and repeated doses in wild-type and APP23 mice.

Lujan, E., Chanda, S., Ahlenius, H., Südhof, T.C., and Wernig, M. (2012). Direct conversion of mouse fibroblasts to self-renewing, tripotent neural precursor cells. Proc. Natl. Acad. Sci. U. S. A. *109*, 2527–2532.

Manganas, L.N., Zhang, X., Li, Y., Hazel, R.D., Smith, S.D., Wagshul, M.E., Henn, F., Benveniste, H., Djuric, P.M., Enikolopov, G., et al. (2007). Magnetic resonance spectroscopy identifies neural progenitor cells in the live human brain. Science *318*, 980–985.

Mao, J., Wang, J., Liu, B., Pan, W., Farr, G.H., 3rd, Flynn, C., Yuan, H., Takada, S., Kimelman, D., Li, L., et al. (2001). Low-density lipoprotein receptor-related protein-5 binds to Axin and regulates the canonical Wnt signaling pathway. Mol. Cell *7*, 801–809.

Martynoga, B., Morrison, H., Price, D.J., and Mason, J.O. (2005). Foxg1 is required for specification of ventral telencephalon and region-specific regulation of dorsal telencephalic precursor proliferation and apoptosis. Dev. Biol. *283*, 113–127.

Martynoga, B., Mateo, J.L., Zhou, B., Andersen, J., Achimastou, A., Urbán, N., van den Berg, D., Georgopoulou, D., Hadjur, S., Wittbrodt, J., et al. (2013). Epigenomic enhancer annotation reveals a key role for NFIX in neural stem cell quiescence. Genes Dev. *27*, 1769–1786.

McLean, C.Y., Bristor, D., Hiller, M., Clarke, S.L., Schaar, B.T., Lowe, C.B., Wenger, A.M., and Bejerano, G. (2010). GREAT improves functional interpretation of cis-regulatory regions. Nat. Biotechnol. *28*, 495–501.

Merkle, F.T., Tramontin, A.D., García-Verdugo, J.M., and Alvarez-Buylla, A. (2004). Radial glia give rise to adult neural stem cells in the subventricular zone. Proc. Natl. Acad. Sci. U. S. A. *101*, 17528–17532.

Mich, J.K., Signer, R.A., Nakada, D., Pineda, A., Burgess, R.J., Vue, T.Y., Johnson, J.E., and Morrison, S.J. (2014). Prospective identification of functionally distinct stem cells and neurosphere-initiating cells in adult mouse forebrain. Elife *3*, e02669.

Ming, G.-L., and Song, H. (2005). Adult neurogenesis in the mammalian central nervous system. Annu. Rev. Neurosci. *28*, 223–250.

Mira, H., Andreu, Z., Suh, H., Lie, D.C., Jessberger, S., Consiglio, A., San Emeterio, J., Hortigüela, R., Marqués-Torrejón, M.A., Nakashima, K., et al. (2010). Signaling through BMPR-IA regulates quiescence and long-term activity of neural stem cells in the adult hippocampus. Cell Stem Cell *7*, 78–89.

Miyoshi, G., and Fishell, G. (2012). Dynamic FoxG1 expression coordinates the integration of multipolar pyramidal neuron precursors into the cortical plate. Neuron *74*, 1045–1058.

Mohammad, F., Weissmann, S., Leblanc, B., Pandey, D.P., Højfeldt, J.W., Comet, I., Zheng, C., Johansen, J.V., Rapin, N., Porse, B.T., et al. (2017). EZH2 is a potential therapeutic target for H3K27M-mutant pediatric gliomas. Nat. Med. *23*, 483–492.

Molenaar, M., van de Wetering, M., Oosterwegel, M., Peterson-Maduro, J., Godsave, S., Korinek, V., Roose, J., Destrée, O., and Clevers, H. (1996). XTcf-3 transcription factor mediates beta-catenin-induced axis formation in Xenopus embryos. Cell *86*, 391–399.

Morrison, G., Scognamiglio, R., Trumpp, A., Smith, A. (2016). Convergence of c-myc and beta-catenin on Tcf7l1 enable endoderm specification. EMBO J. *35*, 356-368.

Müller, I., Larsson, K., Frenzel, A., Oliynyk, G., Zirath, H., Prochownik, E.V., Westwood, N.J., Henriksson, M.A. (2014) Targeting of the MYCN protein with small molecule c-myc inhibitors. PLoS One *9*, e97285.

Nam, H.-S., and Benezra, R. (2009). High levels of Id1 expression define B1 type adult neural stem cells. Cell Stem Cell *5*, 515–526.

Naujok, O., Lentes, J., Diekmann, U., Davenport, C., Lenzen, S. (2014). Cytotoxicity and activation of the Wnt/beta-catenin pathway in mouse embryonic stem cells treated with four GSK3 inhibitors. BMC Research Notes *7*, 273.

Neftel, C., Laffy, J., Filbin, M.G., Hara, T., Shore, M.E., Rahme, G.J., Richman, A.R., Silverbush, D., Shaw, M.L., Hebert, C.M., et al. (2019). An Integrative Model of Cellular States, Plasticity, and Genetics for Glioblastoma. Cell *178*, 835–849.e21.

Ng, R.C.-L., Matsumaru, D., Ho, A.S.-H., Garcia-Barceló, M.-M., Yuan, Z.-W., Smith, D., Kodjabachian, L., Tam, P.K.-H., Yamada, G., and Lui, V.C.-H. (2014). Dysregulation of Wnt inhibitory factor 1 (Wif1) expression resulted in aberrant Wnt-β-catenin signaling and cell death of the cloaca endoderm, and anorectal malformations. Cell Death Differ. *21*, 978–989.

Niola, F., Zhao, X., Singh, D., Castano, A., Sullivan, R., Lauria, M., Nam, H.-S., Zhuang, Y., Benezra, R., Di Bernardo, D., et al. (2012). Id proteins synchronize stemness and anchorage to the niche of neural stem cells. Nat. Cell Biol. *14*, 477–487.

Nusse, R., and Clevers, H. (2017). Wnt/β-Catenin Signaling, Disease, and Emerging Therapeutic Modalities. Cell *169*, 985–999.

Nusse, R., and Varmus, H.E. (1982). Many tumors induced by the mouse mammary tumor virus contain a provirus integrated in the same region of the host genome. Cell *31*, 99–109.

Obernier, K., Cebrian-Silla, A., Thomson, M., Parraguez, J.I., Anderson, R., Guinto, C., Rodas Rodriguez, J., Garcia-Verdugo, J.-M., and Alvarez-Buylla, A. (2018). Adult Neurogenesis Is Sustained by Symmetric Self-Renewal and Differentiation. Cell Stem Cell

22, 221–234.e8.

Olar, A., and Aldape, K.D. (2014). Using the molecular classification of glioblastoma to inform personalized treatment. J. Pathol. *232*, 165–177.

Oshimori, N., and Fuchs, E. (2012). Paracrine TGF-β signaling counterbalances BMP-mediated repression in hair follicle stem cell activation. Cell Stem Cell *10*, 63–75.

Paraf, F., Jothy, S., and Van Meir, E.G. (1997). Brain tumor-polyposis syndrome: two genetic diseases? J. Clin. Oncol. *15*, 2744–2758.

Paredes, M.F., James, D., Gil-Perotin, S., Kim, H., Cotter, J.A., Ng, C., Sandoval, K., Rowitch, D.H., Xu, D., McQuillen, P.S., et al. (2016). Extensive migration of young neurons into the infant human frontal lobe. Science *354*.

Pastrana, E., Cheng, L.-C., and Doetsch, F. (2009). Simultaneous prospective purification of adult subventricular zone neural stem cells and their progeny. Proc. Natl. Acad. Sci. U. S. A. *106*, 6387–6392.

Pastrana, E., Silva-Vargas, V., and Doetsch, F. (2011). Eyes wide open: a critical review of sphere-formation as an assay for stem cells. Cell Stem Cell *8*, 486–498.

Patapoutian, A., and Reichardt, L.F. (2000). Roles of Wnt proteins in neural development and maintenance. Curr. Opin. Neurobiol. *10*, 392–399.

Patel, A.P., Tirosh, I., Trombetta, J.J., Shalek, A.K., Gillespie, S.M., Wakimoto, H., Cahill, D.P., Nahed, B.V., Curry, W.T., Martuza, R.L., et al. (2014). Single-cell RNA-seq highlights intratumoral heterogeneity in primary glioblastoma. Science *344*, 1396–1401.

Perry, S.S., Zhao, Y., Nie, L., Cochrane, S.W., Huang, Z., and Sun, X.-H. (2007). Id1, but not Id3, directs long-term repopulating hematopoietic stem-cell maintenance. Blood *110*, 2351–2360.

Piccin, D., and Morshead, C.M. (2011). Wnt signaling regulates symmetry of division of neural stem cells in the adult brain and in response to injury. Stem Cells *29*, 528–538.

Piccirillo, S.G.M., Reynolds, B.A., Zanetti, N., Lamorte, G., Binda, E., Broggi, G., Brem, H., Olivi, A., Dimeco, F., and Vescovi, A.L. (2006). Bone morphogenetic proteins inhibit the tumorigenic potential of human brain tumour-initiating cells. Nature *444*, 761–765.

Pollard, S.M., Conti, L., Sun, Y., Goffredo, D., and Smith, A. (2006). Adherent neural stem (NS) cells from fetal and adult forebrain. Cereb. Cortex *16 Suppl 1*, i112–i120.

Pollard, S.M., Yoshikawa, K., Clarke, I.D., Danovi, D., Stricker, S., Russell, R., Bayani, J., Head, R., Lee, M., Bernstein, M., et al. (2009). Glioma stem cell lines expanded in adherent culture have tumor-specific phenotypes and are suitable for chemical and genetic screens. Cell Stem Cell *4*, 568–580.

Portela, M., Venkataramani, V., Fahey-Lozano, N., Seco, E., Losada-Perez, M., Winkler, F., and Casas-Tintó, S. (2019). Glioblastoma cells vampirize WNT from neurons and trigger a JNK/MMP signaling loop that enhances glioblastoma progression and neurodegeneration. PLoS Biol. *17*, e3000545.

Raciti, M., Granzotto, M., Duc, M.D., Fimiani, C., Cellot, G., Cherubini, E., and Mallamaci, A. (2013). Reprogramming fibroblasts to neural-precursor-like cells by structured overexpression of pallial patterning genes. Mol. Cell. Neurosci. *57*, 42–53.

Rajakulendran, N., Rowland, K.J., Selvadurai, H.J., Ahmadi, M., Park, N.I., Naumenko, S., Dolma, S., Ward, R.J., So, M., Lee, L., et al. (2019). Wnt and Notch signaling govern self-renewal and differentiation in a subset of human glioblastoma stem cells. Genes Dev. *33*, 498–510.

Redelsperger, I.M., Taldone, T., Riedel, E.R., Lepherd, M.L., Lipman, N.S., and Wolf, F.R. (2016). Stability of Doxycycline in Feed and Water and Minimal Effective Doses in Tetracycline-Inducible Systems. J. Am. Assoc. Lab. Anim. Sci. *55*, 467–474.

Reynolds, B.A., and Weiss, S. (1992). Generation of neurons and astrocytes from isolated cells of the adult mammalian central nervous system. Science *255*, 1707–1710.

Rheinbay, E., Suvà, M.L., Gillespie, S.M., Wakimoto, H., Patel, A.P., Shahid, M., Oksuz, O., Rabkin, S.D., Martuza, R.L., Rivera, M.N., et al. (2013). An aberrant transcription factor network essential for Wnt signaling and stem cell maintenance in glioblastoma. Cell Rep. *3*, 1567–1579.

Riggleman, B., Schedl, P., and Wieschaus, E. (1990). Spatial expression of the Drosophila segment polarity gene armadillo is posttranscriptionally regulated by wingless. Cell *63*, 549–560.

Rijsewijk, F., Schuermann, M., Wagenaar, E., Parren, P., Weigel, D., and Nusse, R. (1987). The Drosophila homolog of the mouse mammary oncogene int-1 is identical to the segment polarity gene wingless. Cell *50*, 649–657.

Robertson, F.L., Marqués-Torrejón, M.-A., Morrison, G.M., and Pollard, S.M. (2019). Experimental models and tools to tackle glioblastoma. Dis. Model. Mech. *12*.

Roose, J., Molenaar, M., Peterson, J., Hurenkamp, J., Brantjes, H., Moerer, P., van de Wetering, M., Destrée, O., and Clevers, H. (1998). The Xenopus Wnt effector XTcf-3 interacts with Groucho-related transcriptional repressors. Nature *395*, 608–612.

Roth, M., Bonev, B., Lindsay, J., Lea, R., Panagiotaki, N., Houart, C., and Papalopulu, N. (2010). FoxG1 and TLE2 act cooperatively to regulate ventral telencephalon formation. Development *137*, 1553–1562.

Sachdeva, R., Wu, M., Johnson, K., Kim, H., Celebre, A., Shahzad, U., Graham, M.S., Kessler, J.A., Chuang, J.H., Karamchandani, J., et al. (2019). BMP signaling mediates glioma stem cell quiescence and confers treatment resistance in glioblastoma. Sci. Rep. *9*, 14569.

Saint-Jeannet, J.-P. (2013). Patterning the Vertebrate Neural Plate by Wnt Signaling (Landes Bioscience).

Sanai, N., Tramontin, A.D., Quiñones-Hinojosa, A., Barbaro, N.M., Gupta, N., Kunwar, S., Lawton, M.T., McDermott, M.W., Parsa, A.T., Manuel-García Verdugo, J., et al. (2004). Unique astrocyte ribbon in adult human brain contains neural stem cells but lacks chain migration. Nature *427*, 740–744.

Sareddy, G.R., Panigrahi, M., Challa, S., Mahadevan, A., and Babu, P.P. (2009). Activation of Wnt/beta-catenin/Tcf signaling pathway in human astrocytomas. Neurochem. Int. *55*, 307–317.

Sato, T., van Es, J.H., Snippert, H.J., Stange, D.E., Vries, R.G., van den Born, M., Barker, N., Shroyer, N.F., van de Wetering, M., and Clevers, H. (2011). Paneth cells constitute the niche for Lgr5 stem cells in intestinal crypts. Nature *469*, 415–418.

Satoh, S., Daigo, Y., Furukawa, Y., Kato, T., Miwa, N., Nishiwaki, T., Kawasoe, T., Ishiguro, H., Fujita, M., Tokino, T., et al. (2000). AXIN1 mutations in hepatocellular carcinomas, and growth suppression in cancer cells by virus-mediated transfer of AXIN1. Nat. Genet. *24*, 245–250.

Schwartzentruber, J., Korshunov, A., Liu, X.-Y., Jones, D.T.W., Pfaff, E., Jacob, K., Sturm, D., Fontebasso, A.M., Quang, D.-A.K., Tönjes, M., et al. (2012). Driver mutations in histone H3.3 and chromatin remodelling genes in paediatric glioblastoma. Nature *482*, 226–231.

Seoane, J., Le, H.-V., Shen, L., Anderson, S.A., and Massagué, J. (2004). Integration of Smad and forkhead pathways in the control of neuroepithelial and glioblastoma cell proliferation. Cell *117*, 211–223.

Shimada, I.S., LeComte, M.D., Granger, J.C., Quinlan, N.J., and Spees, J.L. (2012). Self-renewal and differentiation of reactive astrocyte-derived neural stem/progenitor cells isolated from the cortical peri-infarct area after stroke. J. Neurosci. *32*, 7926–7940.

Shtutman, M., Zhurinsky, J., Simcha, I., Albanese, C., D'Amico, M., Pestell, R., and Ben-Ze'ev, A. (1999). The cyclin D1 gene is a target of the beta-catenin/LEF-1 pathway. Proc. Natl. Acad. Sci. U. S. A. *96*, 5522–5527.

Silva, J., Barrandon, O., Nichols, J., Kawaguchi, J., Theunissen, T.W., Smith, A. Promotion of reprogramming to ground state pluripotency by signal inhibition. PLOS Biology *6(10)*, e253.

Singh, D.K., Kollipara, R.K., Vemireddy, V., Yang, X.-L., Sun, Y., Regmi, N., Klingler, S., Hatanpaa, K.J., Raisanen, J., Cho, S.K., et al. (2017). Oncogenes Activate an Autonomous Transcriptional Regulatory Circuit That Drives Glioblastoma. Cell Rep. *18*, 961–976.

Singh, S.K., Clarke, I.D., Terasaki, M., Bonn, V.E., Hawkins, C., Squire, J., and Dirks, P.B. (2003). Identification of a cancer stem cell in human brain tumors. Cancer Res. *63*, 5821–5828.

Singh, S.K., Hawkins, C., Clarke, I.D., Squire, J.A., Bayani, J., Hide, T., Henkelman, R.M., Cusimano, M.D., and Dirks, P.B. (2004). Identification of human brain tumour initiating cells. Nature *432*, 396–401.

Snuderl, M., Fazlollahi, L., Le, L.P., Nitta, M., Zhelyazkova, B.H., Davidson, C.J., Akhavanfard, S., Cahill, D.P., Aldape, K.D., Betensky, R.A., et al. (2011). Mosaic amplification of multiple receptor tyrosine kinase genes in glioblastoma. Cancer Cell *20*, 810–817.

Soravia, C., Berk, T., Madlensky, L., Mitri, A., Cheng, H., Gallinger, S., Cohen, Z., and Bapat, B. (1998). Genotype-phenotype correlations in attenuated adenomatous polyposis coli.

Am. J. Hum. Genet. *62*, 1290–1301.

Soroceanu, L., Murase, R., Limbad, C., Singer, E., Allison, J., Adrados, I., Kawamura, R., Pakdel, A., Fukuyo, Y., Nguyen, D., et al. (2013). Id-1 is a key transcriptional regulator of glioblastoma aggressiveness and a novel therapeutic target. Cancer Res. *73*, 1559–1569.

Sorrells SF, Paredes MF, Cebrian-Silla A, et al. Human hippocampal neurogenesis drops sharply in children to undetectable levels in adults. *Nature*. 2018;555(7696):377-381.

de Sousa E Melo, F., and Vermeulen, L. (2016). Wnt Signaling in Cancer Stem Cell Biology. Cancers *8*.

Stiles, C.D., and Rowitch, D.H. (2008). Glioma stem cells: a midterm exam. Neuron *58*, 832–846.

Strand, M., and Micchelli, C.A. (2011). Quiescent gastric stem cells maintain the adult Drosophila stomach. Proc. Natl. Acad. Sci. U. S. A. *108*, 17696–17701.

Stupp, R., Mason, W.P., van den Bent, M.J., Weller, M., Fisher, B., Taphoorn, M.J.B., Belanger, K., Brandes, A.A., Marosi, C., Bogdahn, U., et al. (2005). Radiotherapy plus concomitant and adjuvant temozolomide for glioblastoma. N. Engl. J. Med. *352*, 987–996.

Sturm, D., Witt, H., Hovestadt, V., Khuong-Quang, D.-A., Jones, D.T.W., Konermann, C., Pfaff, E., Tönjes, M., Sill, M., Bender, S., et al. (2012). Hotspot mutations in H3F3A and IDH1 define distinct epigenetic and biological subgroups of glioblastoma. Cancer Cell *22*, 425–437.

Sun, Y., Pollard, S., Conti, L., Toselli, M., Biella, G., Parkin, G., Willatt, L., Falk, A., Cattaneo, E., and Smith, A. (2008). Long-term tripotent differentiation capacity of human neural stem (NS) cells in adherent culture. Mol. Cell. Neurosci. *38*, 245–258.

Sun, Y., Kong, W., Falk, A., Hu, J., Zhou, L., Pollard, S., and Smith, A. (2009). CD133 (Prominin) negative human neural stem cells are clonogenic and tripotent. PLoS One *4*, e5498.

Sun, Z., da Fontoura, C.S.G., Moreno, M., Holton, N.E., Sweat, M., Sweat, Y., Lee, M.K., Arbon, J., Bidlack, F.B., Thedens, D.R., et al. (2018). FoxO6 regulates Hippo signaling and growth of the craniofacial complex. PLoS Genet. *14*, e1007675.

Suvà, M.L., Rheinbay, E., Gillespie, S.M., Patel, A.P., Wakimoto, H., Rabkin, S.D., Riggi, N., Chi, A.S., Cahill, D.P., Nahed, B.V., et al. (2014). Reconstructing and reprogramming the tumor-propagating potential of glioblastoma stem-like cells. Cell *157*, 580–594.

Tabasso, A.F.S., Jones, D.J.L., Jones G.D.D., Macip, S (2019). Radiotherapy-induced senescence and its effects on responses to treatment. Clinical Oncology *31*, 283-289.

Temple, S. (1989). Division and differentiation of isolated CNS blast cells in microculture. Nature *340*, 471–473.

Temple, S. (2001). The development of neural stem cells. Nature *414*, 112–117.

Teo, K., Gómez-Cuadrado, L., Tenhagen, M., Byron, A., Rätze, M., van Amersfoort, M.,

Renes, J., Strengman, E., Mandoli, A., Singh, A.A., et al. (2018). E-cadherin loss induces targetable autocrine activation of growth factor signaling in lobular breast cancer. Sci. Rep. *8*, 15454.

Tolwinski, N.S., and Wieschaus, E. (2004). A nuclear function for armadillo/beta-catenin. PLoS Biol. *2*, E95.

Tong, C.K., and Alvarez-Buylla, A. (2014). SnapShot: adult neurogenesis in the V-SVZ. Neuron *81*, 220–220.e1.

Uchida, N., Buck, D.W., He, D., Reitsma, M.J., Masek, M., Phan, T.V., Tsukamoto, A.S., Gage, F.H., and Weissman, I.L. (2000). Direct isolation of human central nervous system stem cells. Proc. Natl. Acad. Sci. U. S. A. *97*, 14720–14725.

Valny, M., Honsa, P., Kirdajova, D., Kamenik, Z., and Anderova, M. (2016). Tamoxifen in the Mouse Brain: Implications for Fate-Mapping Studies Using the Tamoxifen-Inducible Cre-loxP System. Front. Cell. Neurosci. *10*, 243.

Verginelli, F., Perin, A., Dali, R., Fung, K.H., Lo, R., Longatti, P., Guiot, M.-C., Del Maestro, R.F., Rossi, S., di Porzio, U., et al. (2013). Transcription factors FOXG1 and Groucho/TLE promote glioblastoma growth. Nat. Commun. *4*, 2956.

Verhaak, R.G.W., Hoadley, K.A., Purdom, E., Wang, V., Qi, Y., Wilkerson, M.D., Miller, C.R., Ding, L., Golub, T., Mesirov, J.P., et al. (2010). Integrated genomic analysis identifies clinically relevant subtypes of glioblastoma characterized by abnormalities in PDGFRA, IDH1, EGFR, and NF1. Cancer Cell *17*, 98–110.

Walz, S., Lorenzin, F., Morton, J., Wiese, K.E., von Eyss, B., Herold, S., Rycak, L., Dumay-Odelot, H., Karim, S., Bartkuhn, M., Roels, F., Wüstefeld, T., Fischer, M., Teichmann, M., Zender, L., Wei, C-L., Sansom, O., Wolf, E., Eilers, M. (2014). Activation and repression by oncogenic MYC shape tumour-specific gene expression profiles. Nature *511*, 483-487.

Wang, F., Flanagan, J., Su, N., Wang, L.-C., Bui, S., Nielson, A., Wu, X., Vo, H.-T., Ma, X.-J., and Luo, Y. (2012). RNAscope: A Novel in Situ RNA Analysis Platform for Formalin-Fixed, Paraffin-Embedded Tissues. J. Mol. Diagn. *14*, 22–29.

Wang, Q., Hu, B., Hu, X., Kim, H., Squatrito, M., Scarpace, L., deCarvalho, A.C., Lyu, S., Li, P., Li, Y., et al. (2017). Tumor Evolution of Glioma-Intrinsic Gene Expression Subtypes Associates with Immunological Changes in the Microenvironment. Cancer Cell *32*, 42–56.e6.

Wang, H., Horbinski, C., Wu, H., Liu, Y., Sheng, S., Liu, J., Weiss, H., Stromberg, A.J., Wang, C. (2016). NanoStringDiff: a novel statistical method for differential expression analysis based on NanoString nCounter data. Nucleic Acids Res. *44*, e151.

Wang, R.N., Green, J., Wang, Z., Deng, Y., Qiao, M., Peabody, M., Zhang, Q., Ye, J., Yan, Z., Denduluri, S., et al. (2014). Bone Morphogenetic Protein (BMP) signaling in development and human diseases. Genes Dis *1*, 87–105.

Weigel, D., Jürgens, G., Küttner, F., Seifert, E., and Jäckle, H. (1989). The homeotic gene fork head encodes a nuclear protein and is expressed in the terminal regions of the Drosophila embryo. Cell *57*, 645–658.

Wexler, E.M., Paucer, A., Kornblum, H.I., Palmer, T.D., and Geschwind, D.H. (2009). Endogenous Wnt signaling maintains neural progenitor cell potency. Stem Cells *27*, 1130–1141.

Xie, Y., Bergström, T., Jiang, Y., Johansson, P., Marinescu, V.D., Lindberg, N., Segerman, A., Wicher, G., Niklasson, M., Baskaran, S., et al. (2015). The Human Glioblastoma Cell Culture Resource: Validated Cell Models Representing All Molecular Subtypes. EBioMedicine *2*, 1351–1363.

Xu, J., Chen, Y., Huo, D., Khramtsov, A., Khramtsova, G., Zhang, C., Goss, K.H., and Olopade, O.I. (2016). β-catenin regulates c-Myc and CDKN1A expression in breast cancer cells. Mol. Carcinog. *55*, 431–439.

Xuan, S., Baptista, C.A., Balas, G., Tao, W., Soares, V.C., and Lai, E. (1995). Winged helix transcription factor BF-1 is essential for the development of the cerebral hemispheres. Neuron *14*, 1141–1152.

Yan, D., Wallingford, J.B., Sun, T.Q., Nelson, A.M., Sakanaka, C., Reinhard, C., Harland, R.M., Fantl, W.J., and Williams, L.T. (2001). Cell autonomous regulation of multiple Dishevelled-dependent pathways by mammalian Nkd. Proc. Natl. Acad. Sci. U. S. A. *98*, 3802–3807.

Yao, J., Lai, E., and Stifani, S. (2001). The winged-helix protein brain factor 1 interacts with groucho and hes proteins to repress transcription. Mol. Cell. Biol. *21*, 1962–1972.

Yarrow, J.C., Feng, Y., Perlman, Z.E., Kirchhausen, T., and Mitchison, T.J. (2003). Phenotypic screening of small molecule libraries by high throughput cell imaging. Comb. Chem. High Throughput Screen. *6*, 279–286.

Zaret, K.S., and Carroll, J.S. (2011). Pioneer transcription factors: establishing competence for gene expression. Genes Dev. *25*, 2227–2241.

Zhang, J.-H., Chung, T.D.Y., and Oldenburg, K.R. (1999). A Simple Statistical Parameter for Use in Evaluation and Validation of High Throughput Screening Assays. J. Biomol. Screen. *4*, 67–73.

Zhang, N., Wei, P., Gong, A., Chiu, W.-T., Lee, H.-T., Colman, H., Huang, H., Xue, J., Liu, M., Wang, Y., et al. (2011). FoxM1 promotes β-catenin nuclear localization and controls Wnt target-gene expression and glioma tumorigenesis. Cancer Cell *20*, 427–442.

Zheng, H., Ying, H., Wiedemeyer, R., Yan, H., Quayle, S.N., Ivanova, E.V., Paik, J.-H., Zhang, H., Xiao, Y., Perry, S.R., et al. (2010). PLAGL2 regulates Wnt signaling to impede differentiation in neural stem cells and gliomas. Cancer Cell *17*, 497–509.

Ziller, M.J., Edri, R., Yaffe, Y., Donaghey, J., Pop, R., Mallard, W., Issner, R., Gifford, C.A., Goren, A., Xing, J., et al. (2015). Dissecting neural differentiation regulatory networks through epigenetic footprinting. Nature *518*, 355–359.

Zirath, H., Frenzel, A., Oliynyk, G., Segerström, L., Westermark, U.K., Larsson, K., Munksgaard Persson, M., Hultenby, K., Lehtiö, J., Einvik, C., Pålman, S., Kogner, P., Jakobsson, P-J., Henriksson MA. (2013). MYC inhibition induces metabolic changes leading to accumulation of lipid droplets in tumor cells. Proc Natl Acad Sci. *110*, 10258-10263.

Appendix 1: StemSelect compound library

Adenosine
17β-Estradiol
Inosine
Ouabain, Octahydrate
2-APB
A77 1726
Luciferase Inhibitor I
Luciferase Inhibitor II
AICA-Riboside
Amiloride, Hydrochloride
PARP Inhibitor I, 3-ABA
Anacardic Acid
Apicidin, Fusarium sp.
Apigenin
Apoptosis Activator VI, CD437/AHPN
βARK1 Inhibitor
5-Aza-2′-Deoxycytidine
Betulinic Acid
BTS
CA 1001
CaMKP Inhibitor
Castanospermine, Castanospermum australe
Cell Sheet Migration Inhibitor, Locostatin
Clioquinol
Cryptotanshinone
Corticosterone
COX-1 Inhibitor IV, TFAP
CXCR4 Antagonist I, AMD3100
Daidzein
Deferoxamine Mesylate
5′-Deoxy-5′-methylthioadenosine
BHQ
Diclofenac Sodium
1,1-Dimethylbiguanide, Hydrochloride
Diminutol
E2F Inhibitor, HLM006474
Ellagic Acid, Dihydrate
L-(–)-Epinephrine-(+)-bitartrate
Fasentin
PD166866
sFRP-1 Inhibitor
Fumadil B
Genistein
Glucokinase Activator, Cpd A
Glyburide
Glycogen Phosphorylase Inhibitor
GSK-3 Inhibitor IX
GSK-3β Inhibitor XII, TWS119
GW1929
Histone Acetyltransferase Activator, CTB
Histone Deacetylase Inhibitor VI, HNHA
Honokiol
Iron Chelator, Dp44mT
ITSA1
Kainic Acid, Natural
Kaempferol
Lithium Chloride, Molecular Biology Grade
Minocycline, Hydrochloride
Mn-cpx 3
(+)-MK 801 Maleate
Mycophenolic Acid
Muristerone A, Ipomoea spp.
Myricetin
Ras-Net (Elk-3) Pathway Inhibitor, XRP44X
Nicotinamide
Nicotinic Acid
NAADP Receptor Modulator
Nifedipine
Nigericin, Sodium Salt, Streptomyces hygroscopicus
L-(–)-Norepinephrine-(+)-bitartrate
NSC 721648
Okadaic Acid, Prorocentrum sp.
Oncrasin-1
p53 Activator III, RITA
Pterostilbene, Pterocarpus marsupium
2,4,6-Trimethyl-N-(m-3-trifluoromethylphenyl)benzenesulfonamide
PRL-3 Inhibitor
Quercetin, Dihydrate
Quinacrine, Dihydrochloride
Rapamycin
Resveratrol
Ribavirin
Riluzole
γ-Secretase Inhibitor VI
γ-Secretase Inhibitor IX
SIRT1/2 Inhibitor VIII, Salermide
Sodium 4-Phenylbutyrate
Sodium Salicylate

SMER28
Suramin, Sodium Salt
Tamoxifen Citrate
Paclitaxel, Taxus sp.
Tetrahydrouridine
TNF-α Inhibitor
UCH-L1 Inhibitor
UCH-L1 Inhibitor II
UCH-L3 Inhibitor
Vacuolin-1
Valinomycin, Streptomyces fulvissimus
Valproic Acid, Sodium Salt
(±)-Verapamil, Hydrochloride
IWR-1-endo
WY-14643
Y-27632
Calpeptin
NF-κB Activation Inhibitor V, 5HPP-33
ACA
Acetyl-11-keto-β-Boswellic Acid, Boswellia serrata
Adenylyl Cyclase Type V Inhibitor, NKY80
AICA-Riboside, 5′-Phosphate
AMPK Activator
Angiogenesis Inhibitor
Anisomycin, Streptomyces griseolus
Apocynin
Apoptosis Inhibitor
Apoptosis Inhibitor II, NS3694
Aristolochic Acid
AhR Antagonist
Autophagy Inhibitor, 3-MA
AY 9944
B-Cell Immunosuppressant
Baicalein
Bax Channel Blocker
BAY 41-2272
(±)-Bay K 8644
Bisindolylmaleimide V
(±)-Blebbistatin
CRAC Channel Inhibitor, BTP2
2,3-Butanedione 2-Monoxime
Caffeine
Calmidazolium Chloride
ALLN
Cardiogenol C
Keratinocyte Differentiation Inducer
β-Catenin/Tcf Inhibitor, FH535
Celastrol, Celastrus scandens
CBFβ Inhibitor
CFTR Inhibitor-172
CFTR-F508del Corrector, KM11060
CGP-37157
Chetomin, Chaetomium sp.
CCR4 Antagonist
CCR2 Antagonist
Chromeceptin
Clotrimazole
Colchicine, Colchicum autumnale
C5a Receptor Antagonist, W-54011
COX-1 Inhibitor, FR122047
COX-2 Inhibitor II
Curcumin, Curcuma longa L.
Cyclopamine, V. californicum
Cyclopiazonic Acid, Penicillium cyclopium
Cyclosporin A, Tolypocladium inflatum
DNA Methyltransferase Inhibitor
DNA Base Excision Repair Pathway Inhibitor
Dexamethasone
Dynamin Inhibitor I, Dynasore
E-4031
EHNA, Hydrochloride
(–)-Epigallocatechin Gallate
Epigenetic Multiple Ligand
eIF-2α Inhibitor, Salubrinal
eIF-2α Inhibitor II, Sal003
Erastin
Exo1
Flurbiprofen
Fluvastatin, Sodium Salt
Forskolin
Fumonisin B1, Fusarium moniliforme
Glucagon Receptor Antagonist II
Glucocorticoid Receptor Modulator, CpdA
NS-398
GM 6001
Z-Guggulsterone
GPR30 Agonist, G-1
GPR40 Agonist
Gβγ Modulator II, Gallein
GPR109b Agonist
Hdm2 E3 Ligase Inhibitor
Heat Shock Protein Inhibitor I
Hh Signaling Antagonist VII, JK184
Hh/Gli Antagonist, GANT58
Hh/Gli Antagonist, GANT61
Hedgehog Antagonist VIII

Histone Deacetylase Inhibitor III
Histone Deacetylase Inhibitor IV
Histone Lysine Methyltransferase Inhibitor
HSP90 Inhibitor, CCT018159
4-Hydroxyphenylretinamide
HIF-1 Inhibitor
Indomethacin
Integrin αMβ2 Ligand
IL-2Rα Antagonist
3-Isobutyl-1-methylxanthine
IQ-1
KB-R7943
(Z-LL)2 Ketone
L-165,041
Latrunculin A, Latrunculia magnifica
Licochalcone-A, Synthetic
Luteolin
LXRα/β Agonist
LY 231617
MCI-186
MDM2 Antagonist, Nutlin-3, Racemic
Manumycin A, Streptomyces parvulus
Marimastat
Melatonin
2-Methoxyestradiol
Mevastatin, Sodium Salt
MG-132
MIF Antagonist, ISO-1
Mifepristone
Mitochondrial Division Inhibitor, mdivi-1
Monastrol
c-Myc Inhibitor
Myoseverin
Myriocin, Mycelia sterilia
Nemadipine-A
NFAT Activation Inhibitor III
Neurodazine
Neuronal Differentiation Inducer III
Neuropathiazol
NF-κB Activation Inhibitor II, JSH-23
NF-κB Activation Inhibitor III
NF-κB Activation Inhibitor IV
Nifuroxazide
Nimodipine
Nocodazole
PARP Inhibitor VI, NU1025
Pifithrin-α, Cyclic-
Pifithrin-μ
Parthenolide, Tanacetum parthenium
Pentoxifylline
Phorbol-12-myristate-13-acetate
Piceatannol
PIH
PARP Inhibitor VIII, PJ34
PARP Inhibitor XI, DR2313
PARP Inhibitor XII
PPIase-Parvulin Inhibitor
Protein Methyltransferase Inhibitor, AMI-5
PTP1B Inhibitor
PTP Inhibitor V, PHPS1
Purmorphamine
Reversine
trans-Retinoic Acid
ATRA-BA Hybrid
RNA Polymerase III Inhibitor
SANT-1
SB 225002
SB 328437
SC-560
SCH-202676
SecinH3
Scriptaid
β-Secretase Inhibitor IV
γ-Secretase Inhibitor XXI, Compound E
SHP1/2 PTPase Inhibitor, NSC-87877
SIRT1 Inhibitor III
SIRT1/2 Inhibitor IV, Cambinol
SIRT2 Inhibitor, AGK2
SIRT1 Inhibitor IV, (S)-35
Smoothened Agonist, SAG
Simvastatin, Sodium Salt
SKF-96365, Hydrochloride
Na+/H+ Exchanger Isoform-1 Inhibitor
S1P1 Receptor Agonist, SEW2871
SQ 22536
Stem-Cell Factor/c-Kit Inhibitor, ISCK03
STAT1 Enhancer, 2-NP
STAT3 Inhibitor III, WP1066
JAK2 Inhibitor III, SD-1029
STAT3 Inhibitor VII
STAT5 Inhibitor
SMC Proliferation Inhibitor-2w
Sulindac Sulfide
T0070907
T113242
T0901317
Tenovin-1
Telomerase Inhibitor IX
Thapsigargin

TAS-301
Thyroid Hormone Receptor Antagonist, 1-850
TJU103
Tobramycin, Free Base
Toll-Like Receptor 7 Ligand II
Tranilast
Triptolide, Tripterygium wilfordii
Trichostatin A, Streptomyces sp.
Trolox
TTNPB
TNF-α Antagonist III, R-7050
VEGF Inducer, GS4012
VEGFR2/Flt3/c-Kit Inhibitor
Veratridine
Wiskostatin
Withaferin A, Withania somnifera
2-Amino-4-(3,4-(methylenedioxy)benzylamino)-6-(3-methoxyphenyl)pyrimidine
Zaprinast
YC-1
Zebularine